

Lawrence Berkeley National Laboratory

Recent Work

Title

Bonding and Reactivity of Unsaturated Hydrocarbons on Transition Metal Surfaces: Spectroscopic and Kinetic Studies of Platinum and Rhodium Single Crystal Surfaces

Permalink

<https://escholarship.org/uc/item/9d85175q>

Author

Bent, B.E.

Publication Date

1986-11-01



Lawrence Berkeley Laboratory

UNIVERSITY OF CALIFORNIA

Materials & Molecular Research Division

RECEIVED
LAWRENCE
BERKELEY LABORATORY

JAN 22 1987

LIBRARY AND
DOCUMENTS SECTION

BONDING AND REACTIVITY OF UNSATURATED HYDROCARBONS
ON TRANSITION METAL SURFACES: SPECTROSCOPIC AND
KINETIC STUDIES OF PLATINUM AND RHODIUM SINGLE
CRYSTAL SURFACES

B.E. Bent
(Ph.D. Thesis)

November 1986

TWO-WEEK LOAN COPY
*This is a Library Circulating Copy
which may be borrowed for two weeks.*



LBL-22026
c.2

DISCLAIMER

This document was prepared as an account of work sponsored by the United States Government. While this document is believed to contain correct information, neither the United States Government nor any agency thereof, nor the Regents of the University of California, nor any of their employees, makes any warranty, express or implied, or assumes any legal responsibility for the accuracy, completeness, or usefulness of any information, apparatus, product, or process disclosed, or represents that its use would not infringe privately owned rights. Reference herein to any specific commercial product, process, or service by its trade name, trademark, manufacturer, or otherwise, does not necessarily constitute or imply its endorsement, recommendation, or favoring by the United States Government or any agency thereof, or the Regents of the University of California. The views and opinions of authors expressed herein do not necessarily state or reflect those of the United States Government or any agency thereof or the Regents of the University of California.

LBL-22026

BONDING AND REACTIVITY OF UNSATURATED HYDROCARBONS ON
TRANSITION METAL SURFACES: SPECTROSCOPIC AND
KINETIC STUDIES OF PLATINUM AND RHODIUM
SINGLE CRYSTAL SURFACES

Brian Edward Bent

(Ph.D. Thesis)

Materials and Molecular Research Division
Lawrence Berkeley Laboratory
and Department of Chemistry
University of California
Berkeley, CA 94720

The United States Department of Energy has the right to use this thesis for any purpose whatsoever including the right to reproduce all or any part thereof.

This work was supported by the U.S. Department of Energy under Contract No. DE-AC03-76SF00098.

**Bonding and Reactivity of Unsaturated Hydrocarbons
on Transition Metal Surfaces:
Spectroscopic and Kinetic Studies
of Platinum and Rhodium Single Crystal Surfaces**

Copyright © 1986

Brian Edward Bent

CONTENTS		<u>Page</u>
ABSTRACT		vii
ACKNOWLEDGEMENTS		ix
1. INTRODUCTION AND OVERVIEW.		1
REFERENCES		11
2. EXPERIMENTAL METHODS		13
2.1 Apparatus		13
2.2 Materials and Sample Preparation.		21
2.2.1 Single Crystals.		21
2.2.2 Crystal Cleaning		22
2.2.3 Reagents		26
2.2.4 Gas Dosing		28
2.3 Catalytic Reaction Procedure.		30
2.4 Surface Analysis Techniques:		
Principles, Applications and Procedures		33
2.4.1 Auger Electron Spectroscopy (AES).		33
2.4.2 Thermal Desorption Spectroscopy (TDS).		36
2.4.3 Low-Energy Electron Diffraction (LEED)		39
2.4.4 High-Resolution Electron Energy Loss Spectroscopy (HREELS)		44
REFERENCES		54

	<u>Page</u>
3. IDENTIFICATION OF SURFACE HYDROCARBON SPECIES:	
HREELS, LEED AND TDS STUDIES ON Rh(111), Rh(100) AND Pt(111).	60
3.1 Interpretation of HREEL Spectra: Ethylidyne (CCH ₃) on Rh(111).	60
3.1.1 Background	60
3.1.2 Interpretation of the HREEL Spectra.	61
3.2 Ethylidyne Adsorbed on Rh(111) and Rh(100) in the Temperature Range of 200–400 K	74
3.2.1 Background	74
3.2.2 Ethylidyne on Rh(111).	75
3.2.3 Ethylidyne + Carbon Monoxide on Rh(100).	86
3.2.4 Comparison of Ethylidyne Bonding on Transition Metal Surfaces and in Metal Clusters.	99
3.3 Propylidyne Adsorbed on Pt(111) (T = 270–430 K) and on Rh(111) (T = 200–270 K).	109
3.3.1 Background	103
3.3.2 Results and Discussion	110
3.4 Molecular Ethylene Adsorbed on Rh(111) and Rh(100) in the Temperature Range of 80–200 K.	118
3.4.1 Background	118
3.4.2 Low-Energy Electron Diffraction (LEED)	120
3.4.3 Thermal Desorption Spectroscopy (TDS).	121

	<u>Page</u>
3.4.4 High-Resolution Electron Energy Loss Spectroscopy (HREELS)	124
3.4.5 Appendix	140
3.5 C _x H Fragments on Rh(111) and Rh(100) Formed by Thermal Decomposition of Alkenes, Alkynes, Dienes and Aromatics between 400 and 800 K.	148
3.5.1 Background	148
3.5.2 Results and Interpretation	149
REFERENCES	181
4. STOICHIOMETRIC REACTIONS OF UNSATURATED HYDROCARBONS WITH TRANSITION METAL SURFACES: EXPERIMENTAL STUDIES ON Rh(111), Rh(100) and Pt(111).	189
4.1 Thermal Fragmentation of Ethylene on Rh(111) and Rh(100) in the temperature Range of 80-800 K.	189
4.1.1 Background	189
4.1.2 Ethylene on Rh(111).	190
4.1.3 Ethylene on Rh(100).	195
4.1.4 Ethylene Thermal Fragmentation on Transition Metal Surfaces: Formation of Ethylidyne	201
4.2 Hydrogenation and H,D-Exchange Studies of Ethylidyne on Pt(111) and Rh(111) in UHV and at 1 atm Pressure	218
4.2.1 Background	218
4.2.2 Results and Discussion	219

	<u>Page</u>
4.3 Thermal Fragmentation of Propylene, Propadiene and Methylacetylene on Rh(111) in the Temperature Range of 80–800 K: Comparison to Pt(111)	238
4.3.1 Background	238
4.3.2 Results and Interpretation	239
4.3.3 Discussion	260
4.4 Bonding and Reactivity of Unsaturated Hydrocarbons on Transition Metal Surfaces.	268
4.4.1 Background	268
4.4.2 Structure and Bonding.	269
4.4.3 C–H Bond Chemistry	283
REFERENCES	292
5. SURFACE SCIENCE STUDIES OF ETHYLENE HYDROGENATION.	304
5.1 Catalytic Hydrogenation of Ethylene over Pt(111) and Rh(111) Single Crystal Surfaces	304
5.1.1 Background	304
5.1.2 Results and Interpretation	306
5.1.3 Discussion	318
5.2 Effects of Surface Modification on Catalytic Ethylene Hydrogenation over Rh(111) Surfaces.	324
5.2.1 Background	324
5.2.2 Results and Interpretation	324
5.2.3 Discussion	333
REFERENCES	338

BONDING AND REACTIVITY OF UNSATURATED HYDROCARBONS
ON TRANSITION METAL SURFACES: SPECTROSCOPIC AND KINETIC STUDIES
OF PLATINUM AND RHODIUM SINGLE CRYSTAL SURFACES

Brian Edward Bent

Materials and Molecular Research Division
Lawrence Berkeley Laboratory
and Department of Chemistry
University of California
Berkeley, CA 94720

ABSTRACT

The surface chemistry of small, unsaturated hydrocarbons on platinum and rhodium single crystal surfaces has been investigated. Using a high pressure/low pressure apparatus capable of catalysis at atmospheric pressures and surface analysis in ultra-high vacuum, adsorbed hydrocarbon species have been identified by high-resolution electron energy loss spectroscopy (HREELS), low-energy electron diffraction (LEED) and thermal desorption spectroscopy (TDS).

Among the surface fragments identified are ethylidyne (CCH_3) on Rh(111) and Rh(100), propylidyne (CCH_2CH_3) on Rh(111) and Pt(111), vinylidene (CCH_2) on Rh(100), acetylide (CCH) on Rh(111) and Rh(100), and polymeric C_xH species on Rh(111) and Rh(100). All these species are stable in discrete temperature ranges; the higher the temperature, the more highly dehydrogenated the fragment. The vibrational spectra for molecularly adsorbed ethylene on metal surfaces are extensively discussed and used to predict carbon-carbon bond lengths for adsorbed ethylene.

The effects of metal atomic number and surface geometry on hydrocarbon reactivity have been investigated. Similar fragments are found in ethylene decomposition on Rh(111) and Rh(100), but the sequence as a function of temperature is coverage dependent on Rh(100) and independent of coverage on Rh(111). Different decomposition pathways for propylene are found on Pt(111) and Rh(111); the differences are correlated with the relative rates of propylidyne decomposition and hydrogen desorption on these surfaces. The analogy between hydrocarbon chemistry on metal surfaces and in metal clusters is stressed. Mechanisms are proposed for the conversion of ethylene to ethylidyne, ethylidyne H,D-exchange, and ethylidyne decomposition.

Studies of the structure and role of the adsorbed carbonaceous overlayer on Pt(111) and Rh(111) surfaces active in the catalytic hydrogenation of ethylene are also reported. It is shown that an irreversibly adsorbed deposit (bonding as ethylidyne species in ultra-high vacuum) covers the active catalysts. Isotope labelling and controlled catalyst poisoning implicate these ethylidyne species as a protective monolayer that inhibits adsorption of poisons but permits adsorption and dissociation of hydrogen.

ACKNOWLEDGEMENTS

I am grateful to be able to acknowledge the contributions of so many people to this thesis. I feel quite fortunate to have been able to work with Professor Gabor Somorjai. It's been an experience I wouldn't trade. Gabor's enthusiasm, encouragement, scientific insights and timely social advice surpassed by high expectations.

Gabor has also established a congenial and productive research group, and I thank all those who have been a part of it these past four years. I am particularly grateful to Bruce Koel and John Crowell for teaching me how to do surface science research and for involving me in their work. They have initiated and contributed to all the Rh(111) projects in Chapters 3 and 4. I have enjoyed collaborating with Mathew Mate on the Rh(111)/C₂ and C₃ hydrocarbon experiments and with Chi-Tzu Kao and Al Slavin on the Rh(100) experiments. Combining the ideas of two physicists (Mathew and Al) and two chemists (myself and Chi-Tzu) has been, I feel, especially fruitful. I thank Francisco Zaera and David Godbey for complimentary experiments and enlightening discussions about ethylene hydrogenation, and Bruno Marchon, Hiroko Ohtani, and Don Chin for collaborating on many interesting experiments not reported in this thesis. The results of Michel Van Hove's LEED calculations are frequently cited and add much to this thesis. Jose, Greg, David G., David K., Ken, Peter and Istvan have been especially helpful in proof reading, editing, and putting this thesis together. Special thanks to Brian Naasz for numerous

stimulating conversations and advice about science and life over lunches and dinners at The House.

The skillful and generous assistance of many people made the experimental work and production of this thesis possible. Dan Columb, Keith Franck and Richard Whiteman solved the many experimental problems that I couldn't, Winnie Hepler expertly prepared all the single crystal surfaces, Marilyn Wong sped confusing orders through the photo lab, Ann Kahn and Brigid Tung handled the campus bureaucracy, and June DeLaVergne and the word processing staff skillfully typed this manuscript.

I am especially grateful to those who have contributed indirectly to this thesis, most of all, my parents and Libby for their love, support and advice, even when I failed to write. Ken Laughlin's friendship, roommatesmanship, and contagious zest for sports have made life in Berkeley unusually enjoyable. I am particularly thankful for Roberta Wong's love and support throughout the last 3 years, especially during my innumerable grouchy moods while writing this thesis.

CHAPTER 1
INTRODUCTION AND OVERVIEW

Transition metal surfaces readily catalyze the breaking and making of carbon-carbon and carbon-hydrogen bonds. In fact these surfaces are so active in making and breaking bonds that almost any hydrocarbon can be synthesized from almost any carbon- and hydrogen-containing starting materials like coal, methane, carbon monoxide and hydrogen. The challenge is to control which hydrocarbon is made and to make it using the cheapest possible catalysts and starting materials. In the long run, meeting this challenge requires understanding on a molecular level how transition metal catalysts make and break C-H and C-C bonds. That is the motivation for this thesis.

Our present understanding of how heterogeneous catalysts make and break bonds is limited by our knowledge of how molecules bond to surfaces. However, over the last 25 years, ultra-high vacuum (UHV) technology and surface sensitive spectroscopies have been developed, largely by physicists, so that it is now possible for physical chemists to study spectroscopically the binding of molecules on atomically clean single crystal surfaces.

In this thesis these modern surface science technologies are applied to study the surface bonding of unsaturated hydrocarbons after both stoichiometric and catalytic reactions with platinum and rhodium single crystal surfaces. In particular, the first two thirds of this thesis detail experiments in which stoichiometric C-H and C-C bond

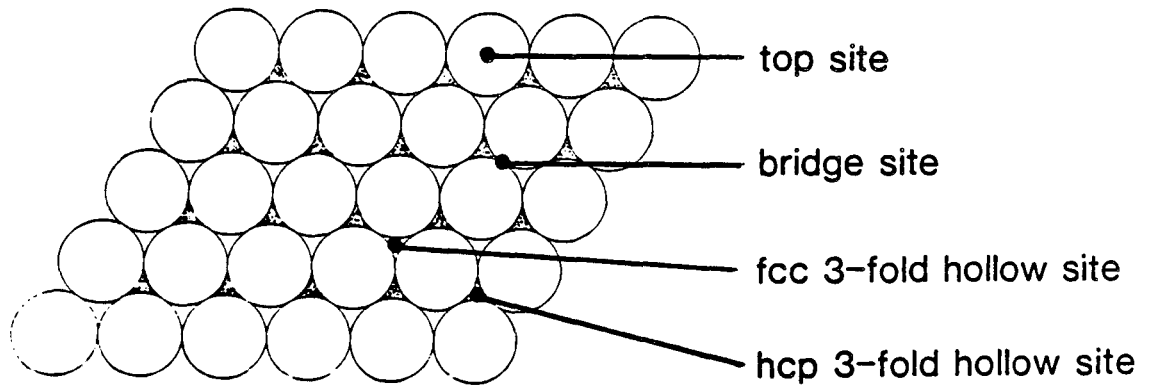
breaking were studied in UHV. Unsaturated hydrocarbons were molecularly adsorbed at low temperature on different Pt and Rh single crystal surfaces, and the surface bonding was studied as the temperature was increased to induce C-H and C-C bond breaking. In the last third of the thesis, studies of the catalytic hydrogenation of ethylene to ethane using Pt and Rh single crystal surfaces as catalysts are reported. In these studies a high pressure cell was used to shuttle the single crystals between UHV (for cleaning and surface analysis) and a catalytic reactor (for kinetic studies at 1 atm pressure). Catalytic bond making and breaking were studied indirectly by isotope labelling and by determining the effects of adsorbed monolayer structure on the catalytic reaction kinetics. The particular experimental systems, approaches and results in this thesis are outlined below.

Chemical Systems. There are many parameters that influence the bonding and reactivity of hydrocarbons with transition metal surfaces. Temperature, the elemental nature of the metal, metal surface structure, adsorbate coverage on the surface, and the structure of the adsorbing hydrocarbon are all important factors. The particular systems investigated in this thesis were chosen so that each of these parameters was varied at least once while the others were held constant: temperature (80-800 K), metal (Pt(111) vs. Rh(111)), surface geometry (Rh(111) vs. Rh(100)), surface coverage (0.1 monolayer - saturation), and adsorbed hydrocarbon (C_2 vs. C_3).

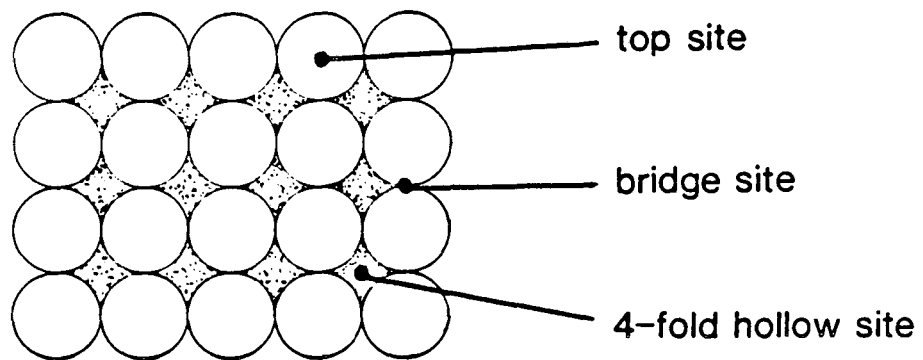
Platinum and rhodium were chosen in order to compare two metals which are, in their pure metallic state, among the best catalysts of

hydrocarbon reactions and which, despite being neighbors in the periodic table, do substantially different hydrocarbon catalysis. Rhodium surfaces are much better catalysts for the synthesis of hydrocarbons from carbon monoxide and hydrogen, while platinum surfaces are among the most active catalysts for the conversion of straight-chain hydrocarbons like n-hexane into aromatics, saturated rings and branched isomers [1].

The Rh(111) and (100) surfaces were chosen to study the effects of surface geometry on ethylene adsorption. Rh, like Pt, is a face-centered cubic (fcc) metal, so the geometries of the (111) and (100) planes are as shown in Fig. 1.1 [2]. The atoms on these two surfaces have different coordination numbers [9 on (111) and 8 on (100)]. There are also different types of high symmetry sites as shown in Fig. 1.1. On the (111) surface, the high symmetry binding sites are: (1) on top of a single atom (atop site), (2) between two metal atoms (bridge site) and (3) between three metal atoms (3-fold hollow site). Two types of 3-fold hollow sites (hexagonal close packed (hcp) and face centered cubic (fcc)) can be differentiated by whether or not there is an atom in the second layer beneath the site. On the (100) surface, atop and bridge sites are also present, but there are 4-fold instead of 3-fold hollow sites. The stable structure of both the Rh(111) and Rh(100) surfaces is as would be expected from termination of the bulk fcc lattice along these planes (except for small changes in the spacing between the outermost atomic layers [1]). This fact is significant, since clean Ir(100), Pt(100) and Au(100) surfaces are known to



fcc (111)



fcc (100)

XBL 8610-4098

Fig. 1.1 Top views of the atomic arrangement in the (111) and (100) planes of face-centered cubic (fcc) metals. Surface atoms are unshaded while second layer atoms are shaded. High symmetry binding sites on the surfaces are indicated.

reconstruct to give a pseudo close-packed structure having 3-fold hollow sites in the outermost atomic layer [3,4]. The fact that Rh(111) and (100) do not reconstruct means that the effects of 4-fold and 3-fold hollow sites on hydrocarbon bonding to Rh surfaces can be compared.

Unsaturated hydrocarbons were studied as opposed to saturated hydrocarbons primarily because unsaturated carbon-carbon bonds readily stick to flat, clean metal surfaces. Saturated hydrocarbons generally stick to flat transition metal surfaces only at either very low (<100 K) or very high (>800 K) temperatures. For example, normal alkanes adsorb on surfaces at low temperature by van der Waals interactions, but they desorb molecularly at about their sublimation temperature (50 to 150 K in UHV). At very high temperatures, n-alkanes will again stick to the surface because of their immediate decomposition to form surface carbon and gas phase hydrogen. Neither situation is conducive to studying C-H and C-C bond breaking. By contrast, alkenes and alkynes adsorb molecularly on Pt and Rh surfaces below 200 K, and rather than desorb at higher temperatures, they decompose through a series of hydrocarbon fragments which are stable in discrete temperature ranges [5]. Studying the bonding of these decomposition fragments can provide insights into C-H and C-C bond breaking.

Identification of Adsorbed Species. At present there is no single technique or even group of techniques capable of routine surface structure determinations. In this thesis, the complimentary techniques of Auger electron spectroscopy (AES), thermal desorption spectroscopy

(TDS), low-energy electron diffraction (LEED) and high-resolution electron energy loss spectroscopy (HREELS) were used to probe various aspects of hydrocarbon bonding to surfaces. AES and TDS were used primarily to determine the elemental composition and stoichiometry of the surface, while LEED and HREELS were used to probe surface structure.

The combination of LEED and HREELS for surface structure determinations has proven quite fruitful [6,7]. LEED, the surface equivalent of x-ray diffraction, is one of the few techniques by which bond lengths and bond angles in adsorbates can be determined. Unfortunately, the electron diffraction calculations that are necessary for a complete structure determination are too involved for routine structure determinations by LEED. However, with the use of faster computers and some reasonable approximations [8-11], surface structures with more and more atoms per unit cell are being solved. (The current record for commensurate overlayers is 20 atoms/overlayer unit cell for a benzene + CO coadsorption structure on Pt(111) [12].)

Fortunately, much surface chemistry can also be learned from less than complete surface structure determinations. In particular, valuable chemical information is obtained simply by learning which atoms are bonded to which -- for example, whether an adsorbate is HCCH or CCH₂. Surface vibrational spectroscopy is currently one of the most valuable tools for this purpose, and it was the primary means of determining the identity of hydrocarbon adsorbates in this thesis research.

There are several ways that surface vibrational frequencies, which are readily obtained by HREEL spectroscopy, can be used to determine which atoms are bonded to which. First, since vibrational frequencies vary with $1/\sqrt{\mu}$, where μ is the reduced mass, isotopic substitution of deuterium for hydrogen in hydrocarbons gives large frequency shifts for carbon-hydrogen vibrations and small frequency shifts for carbon-carbon vibrations. This means carbon-hydrogen and carbon-carbon bonds can be both detected and distinguished. Second, the normal modes of vibration for an adsorbate frequently involve primarily the motion of only a few atoms in one part of the adsorbate. These particular normal modes are called functional group modes [13,14], and they have vibrational frequencies which are characteristic of the specific groups of atoms. This allows one to distinguish, for example, between CH, CH₂, and CH₃ groups.

Vibrational frequencies also provide information about the nature of the chemical bonds. Vibrational force constants, which depend on the curvature at the bottom of the vibrational potential well, $(\partial^2 V / \partial X^2)_{X_0}$, can be determined from vibrational frequencies. Force constants can in turn be empirically correlated (at least for molecules and probably also for adsorbates) to bond orders, bond lengths and bond energies [15,16]. Bond dissociation energies can be determined from overtone vibrational frequencies with a few assumptions about the anharmonicity in the potential well [14].

Vibrational spectra can also be used in some cases to determine adsorbate symmetry, binding site and orientation on the surface. This information comes from the intensities of the vibrational peaks, and will be discussed along with the HREEL spectroscopy technique in Section 2.4.4. Intrinsic vibrational line widths contain information about vibrational lifetimes and mode couplings [17,18], but these cannot be determined with the $30\text{--}50\text{ cm}^{-1}$ resolution of HREELS and are not discussed here.

In this thesis most of the surface structural information is based on HREEL vibrational spectra; LEED surface crystallography studies are still pending to determine bond lengths and bond angles and confirm the vibrational spectral assignments. However, several hydrocarbon surface structures that have been solved by M.A. Van Hove using dynamical LEED calculations are cited, and they add much to the interpretation of this research.

Overview. The contents of this thesis are organized as four chapters. Chapter 2 presents the experimental apparatus, procedures and techniques. In Chapter 3 most of the HREEL spectra are assigned and used to identify adsorbed hydrocarbon species. Among the surface fragments identified are ethylidyne (CCH_3) on Rh(111) and Rh(100), propylidyne (CCH_2CH_3) on Rh(111) and Pt(111), vinylidene (CCH_2) on Rh(100), acetylide (CCH) on Rh(111) and Rh(100). All these species are compared with similar fragments on other transition metal surfaces and with hydrocarbon ligands in metal clusters. Also discussed are the HREEL

spectra for molecularly adsorbed ethylene; these spectra are used to predict carbon-carbon bond lengths in adsorbed ethylene.

Chapter 4 details studies of the stoichiometric thermal chemistry of unsaturated hydrocarbons on Pt and Rh single crystal surfaces. In many respects this chapter is an HREELS sequel to previous LEED studies by Roland Koestner [19]. The thermal fragmentation pathways of ethylene on Rh(111) and Rh(100) and of propylene on Pt(111) and Rh(111) are compared. Ethylene is found to decompose to similar fragments on Rh(111) and Rh(100), but the fragmentation sequence is coverage-dependent on Rh(100) and coverage-independent on Rh(111). Different decomposition pathways are found for propylene on Pt(111) and Rh(111); C-C bonds break on Rh(111) at over 150 K lower temperature than on Pt(111). Mechanisms involving elementary hydrogenation and dehydrogenation reactions on the surface are proposed to explain the surface chemistry, including the conversion of ethylene to ethylidyne, ethylidyne H,D-exchange, and ethylidyne decomposition.

Chapter 5 is devoted to identification of the hydrocarbon species remaining on Pt(111) and Rh(111) surfaces in UHV after catalytic ethylene hydrogenation at 1 atm pressure. These studies are complimentary to AES, LEED, TDS and kinetics studies of ethylene hydrogenation over Pt(111) surfaces by Francisco Zaera [20]. It is shown that (1) ethylidyne is the stable species remaining on Pt(111) and Rh(111) surfaces in UHV after ethylene hydrogenations between 300 and 400 K, (2) preadsorption of these ethylidyne species does not alter the hydrogenation

kinetics, and (3) the rate of catalytic ethylene hydrogenation is orders of magnitude faster than the rate of ethylidyne reaction with H_2 or D_2 . Isotope labelling and controlled catalyst poisoning implicate these ethylidyne species as a protective monolayer that inhibits adsorption of poisons but permits adsorption and dissociation of hydrogen.

REFERENCES

1. G.A. Somorjai, Chemistry in Two Dimensions: Surfaces, Cornell University Press, Ithaca (1981).
2. J.F. Nicholas, An Atlas of Models of Crystal Surfaces, Gordon and Breach, New York.
3. M.A. Van Hove, R.J. Koestner, P.C. Stair, J.P. Biberian, L.L. Kesmodel and G.A. Somorjai, Surf. Sci. 103 (1981) 189; Surf. Sci. 103 (1981).
4. E. Long, K. Muller, K. Heinz, M.A. Van Hove, R.J. Koestner and G.A. Somorjai, Surf. Sci. 127 (1983) 347, and references therein.
5. G.A. Somorjai and B.E. Bent, Progr. in Coll. and Polymer Sci. 70 (1985) 38.
6. J.E. Crowell, R.J. Koestner, L.H. Dubois, M.A. Van Hove and G.A. Somorjai, Recent Advances in Analytical Spectroscopy, K. Fuwa, ed., Pergamon Press (1982) 211.
7. B.E. Koel and G.A. Somorjai, "Surface Structural Chemistry", Chapter 3 in Catalysis: Science and Technology, 38, J.R. Anderson and M. Boudart, eds., Springer Verlag, New York (1983).
8. M.A. Van Hove, R.-F. Lin and G.A. Somorjai, Phys. Rev. Letters 51 (1983) 778; M.A. Van Hove and G.A. Somorjai, Surf. Sci. 114 (1982) 171.
9. D.K. Saldin, J.B. Pendry, M.A. Van Hove and G.A. Somorjai, Phys. Rev. Letters 31 (1985) 1216.

10. Z.-P. Hu, D.F. Ogletree, M.A. Van Hove and G.A. Somorjai, submitted to Surf. Sci. (1986).
11. M.A. Van Hove and S.Y. Tong, Surface Crystallography by LEED, Springer Verlag, New York (1979).
12. D.F. Ogletree, M.A. Van Hove and G.A. Somorjai, to be published.
13. G. Herzberg, Molecular Spectra and Molecular Structure II: Infrared and Raman Spectra of Polyatomic Molecules, Van Nostrand Reinhold, New York (1945).
14. D.C. Harris and M.D. Bertolucci, Symmetry and Spectroscopy: An Introduction to Vibrational and Electronic Spectroscopy, Oxford University Press, New York (1978).
15. L. Pauling, The Nature of the Chemical Bond and the Structure of Molecules and Crystals: An Introduction to Modern Structural Chemistry, 3rd edition, Cornell University Press, Ithaca (1960).
16. H. Ibach and D.L. Mills, Electron Energy Loss Spectroscopy and Surface Vibrations, Academic Press, New York (1982).
17. S. Chiang, R.G. Tobin, P.L. Richards, and P.A. Thiel, Phys. Rev. Letters 52 (1984) 648.
18. B.N.J. Persson and R. Ryberg, Phys. Rev. Letters, 54 (1985) 2119, and references therein.
19. R.J. Koestner, Ph. D. Thesis, University of California, Berkeley, 1982, unpublished.
20. F. Zaera, Ph. D. Thesis, University of California, Berkeley, 1984, unpublished.

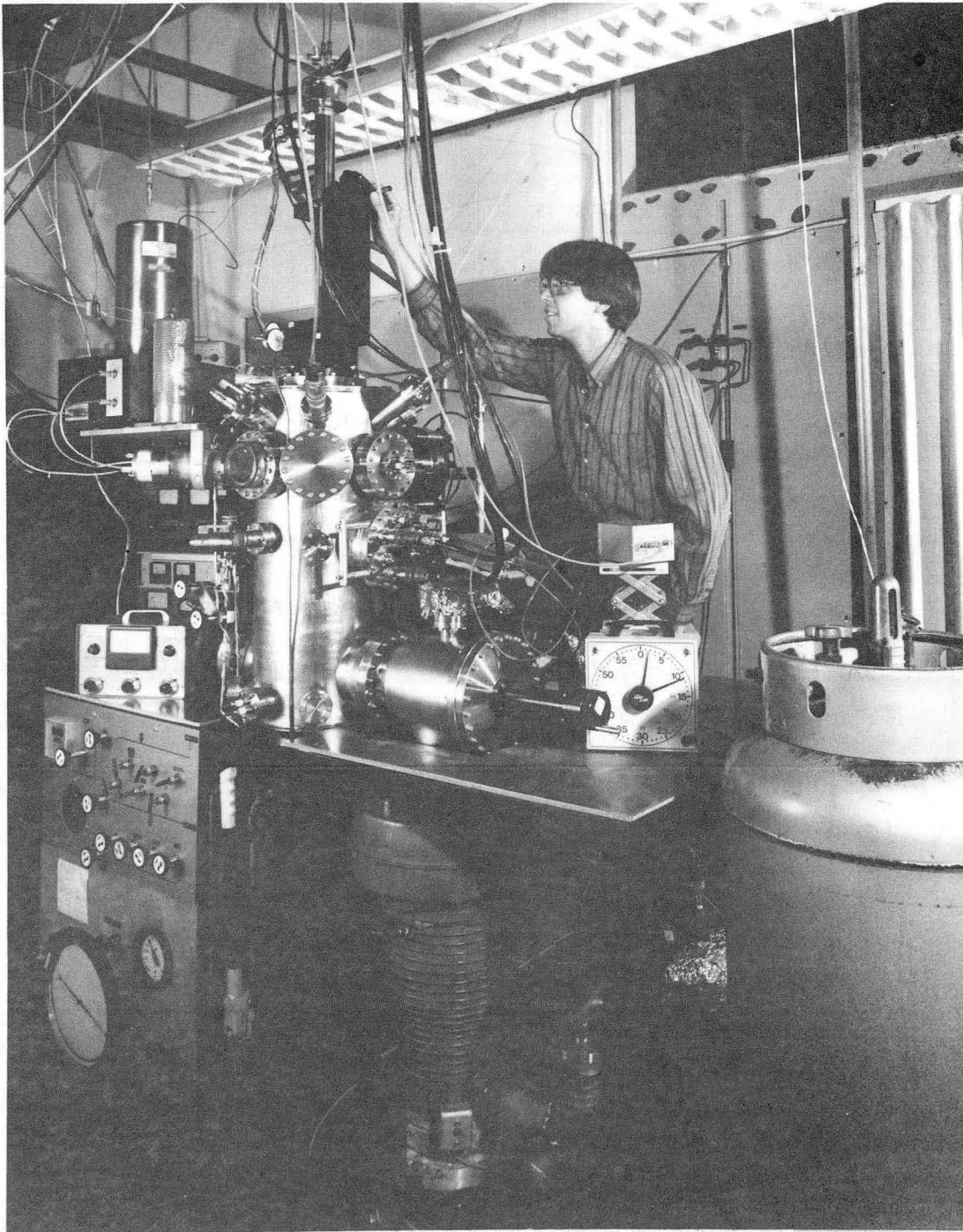
CHAPTER 2
EXPERIMENTAL METHODS

2.1 Apparatus

Most of the experiments in this thesis were performed using the ultra-high vacuum (UHV) system shown pictorially in Fig. 2.1 and schematically in Fig. 2.2. The basic features of this system are:

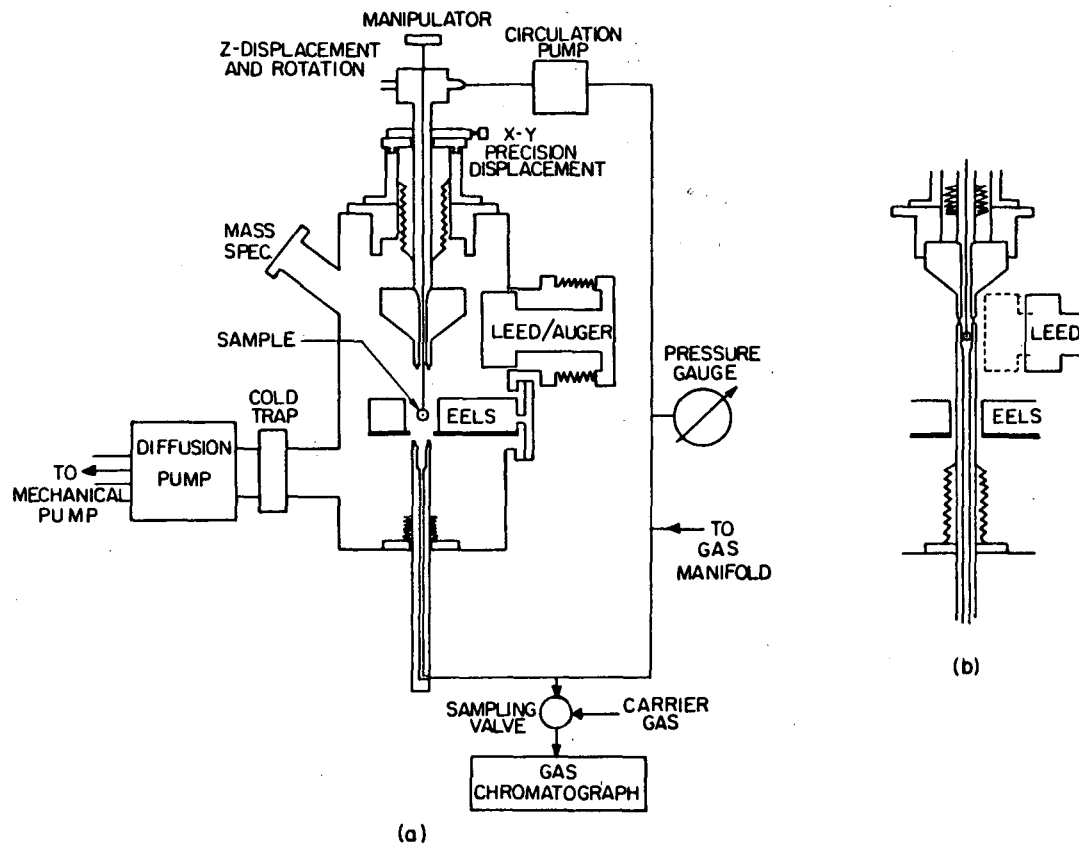
- (1) UHV chamber with a base pressure of $< 1 \times 10^{-10}$ torr
- (2) manipulator which holds and manipulates the single crystal samples under UHV
- (3) crystal temperature control from 77 to 1300 K
- (4) surface analysis by Auger electron spectroscopy (AES), thermal desorption spectroscopy (TDS), low-energy electron diffraction (LEED), and high-resolution electron energy loss spectroscopy (HREELS)
- (5) capability of shuttling the single crystals, in minutes, between UHV conditions and controlled atmospheres at over 1 atm pressure without exposure to ambient gases
- (6) reaction loop with gas chromatograph and circulation pump for running catalytic reactions at pressures > 1 atm over the single crystal surfaces

A few of the UHV experiments (HREEL spectra of ethylene and the C_3 hydrocarbons below room temperature and TDS of the alkenes and alkynes from 100 K) were performed in similar system described elsewhere [1].



CBB 869-7277

Fig. 2.1 Photograph of the author with the ultra-high vacuum (UHV) apparatus used in this thesis work. Beneath the table supporting the stainless steel vacuum chamber are the gas manifold (lower left), diffusion pump (lower right) and ion pump (behind the diffusion pump). The liquid nitrogen dewar (right foreground) fills the diffusion pump trap.



XBL 8111-6950

Fig. 2.2 Schematic diagram of the UHV apparatus photographed in Fig. 2.1. Figure 2.2A shows the entire system including the external reactor loop for catalytic reaction studies. The LEED/AES optics are shown retracted while the manipulator bellows are extended to position the sample in the HREEL spectrometer. Figure 2.2B shows a close-up of the manipulator retracted and the high pressure cell tube extended and sealed around the sample.

The design considerations for the UHV system shown in Fig. 2.2 and for similar systems having combined high pressure/low pressure surface science capabilities have been discussed [2,3]. The particular system used here has also been described in detail in the thesis of J.E. Crowell [4]; although, a new manipulator and bake-out lamps have been added since that time. For completeness, the components of this UHV system are described below.

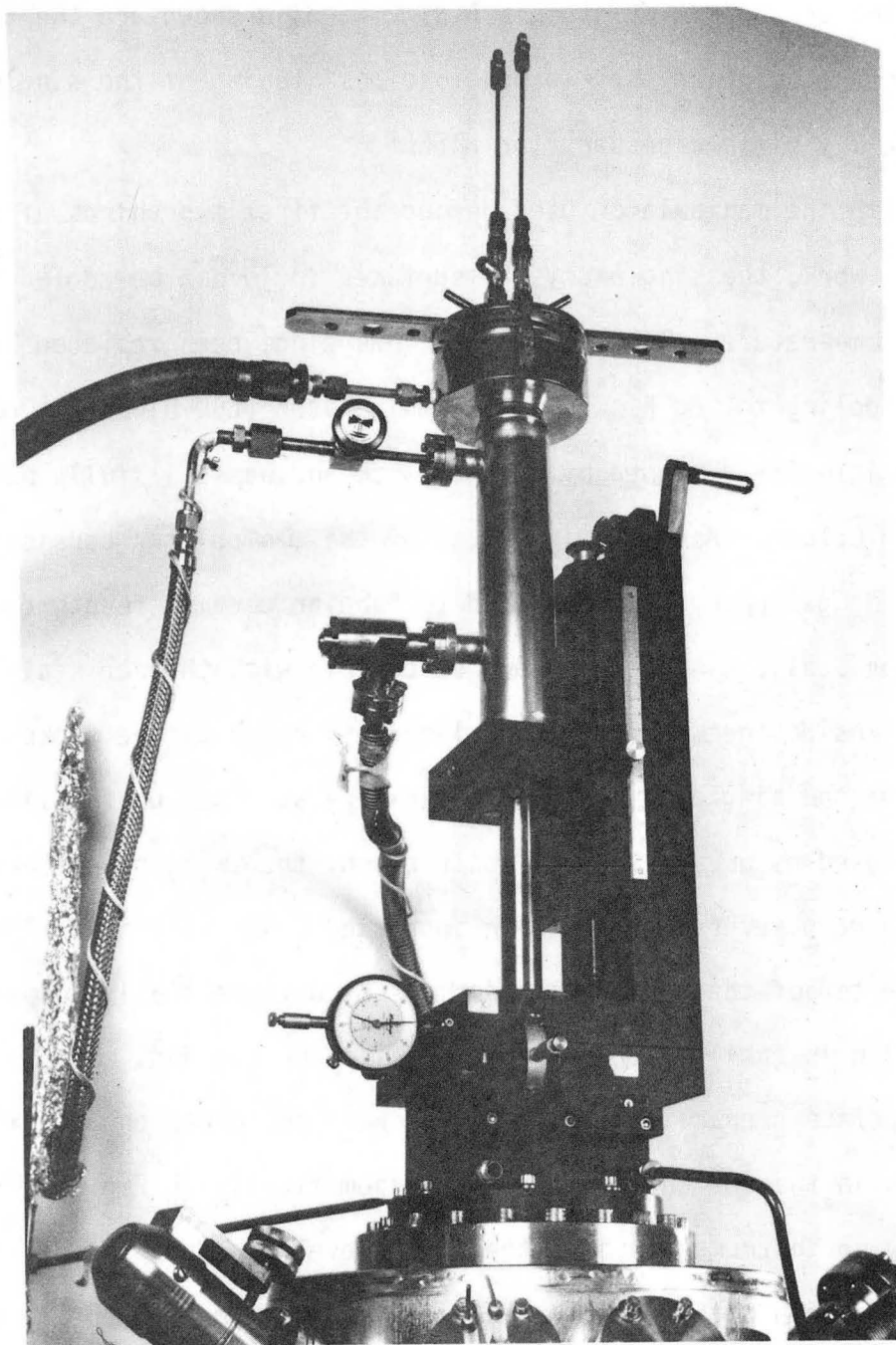
The UHV chamber is pumped by a 400 l/sec ion pump (Varian), a high speed oil diffusion pump (Varian VHS-6) with liquid nitrogen cooled cryotrap and extended cold cap (Varian), and a water cooled titanium sublimation pump (Varian Ti-ball). All pumps are separated from the chamber by viton O-ring seal gate valves. Routine operating pressures of 1×10^{-10} torr were obtained by baking the chamber at 400 K for 48 hours. The current bake-out system consists of two 1 ft long quartz halogen lamps which are mounted on the interior of the chamber near the top and bottom; heating tapes covered with aluminum foil are used to bake-out the manipulator, titanium sublimation pump, and diffusion pump appendages. The bakeout lamps insure that the high pressure cell tube on the interior of the chamber is well-baked.

Two different manipulators were used with this chamber. Both manipulators were capable of translating the single crystal samples 20 cm along the central (z) axis of the chamber between the upper and lower levels by means of welded bellows seals (Fig. 2.2); 1 cm of x and y translation and 360° of rotation about the z axis were also possible. The extremely stable translation stage for these manipulators is shown

with the second manipulator in Fig. 2.3; also shown are the travel gauges that allowed the reproducible positioning of the single crystal in the x,y plane necessary for HREELS.

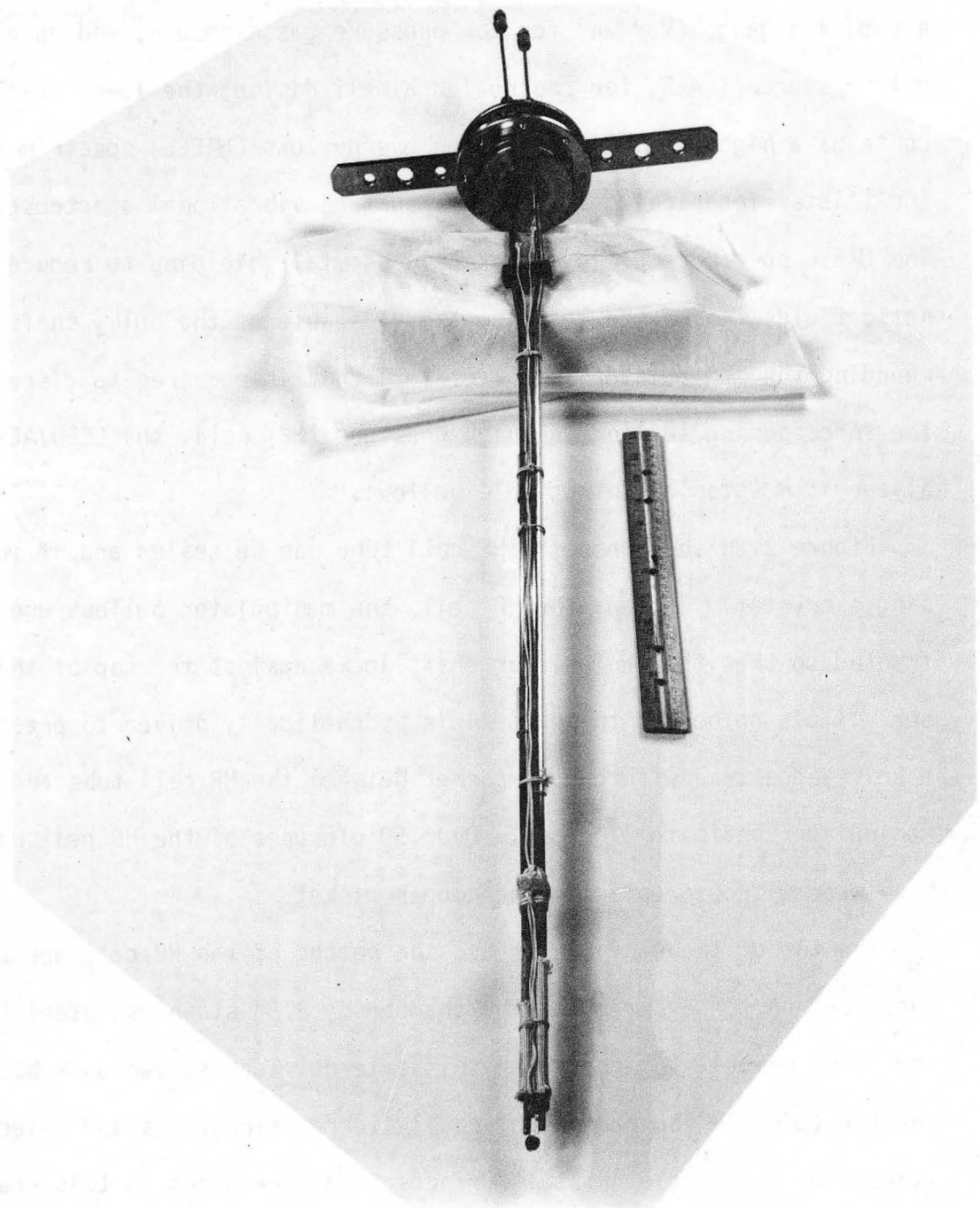
With the manipulator used during the first two thirds of this thesis work, the single crystal surfaces could not be cooled below room temperature. This manipulator has since been replaced by one with cooling to ~80 K. This new manipulator (LBL blueprint No. 21A963) was originally designed by Keith Franck and was skillfully built here by Dan Columb. As shown in Fig. 2.4, the manipulator consists of two, meter-long copper tubes attached to tubular ceramic feedthroughs (Insulator Seal). These tubes are concentric with thinner stainless steel tubes inside them through which liquid nitrogen can be sucked to within 3 cm of the single crystals. To minimize stresses on the single crystal caused by uneven thermal contraction, the two copper tubes are tied together in several places with insulated Cu-Be fittings. The UHV seal at the top of the manipulator is made by differentially-pumped O-rings. Rotation is facilitated by a Kaydon slimline bearing.

Surface preparation and analysis were performed on two different levels in the UHV chamber as shown schematically in Fig. 2.2 using the following instrumentation: the upper level is equipped with a four-grid electron optics energy analyzer (Varian) for low-energy electron diffraction (LEED) and Auger electron spectroscopy (AES), a glancing incidence electron gun (Varian) for Auger excitation, a quadrupole mass spectrometer (UTI 100C) for thermal desorption spectroscopy (TDS) and residual gas analysis, an ion sputter gun (PHI) for sample cleaning,



CBB 869-7279

Fig. 2.3 Photograph of the high-stability manipulator assembly used on the chamber shown in Figs. 2.1 and 2.2. The three exterior lines protruding from the left side are for (from top to bottom) differential pumping of the O-ring seal, circulation of gases during catalytic reactions, and rapid pump-out of the catalytic reaction mixtures.



CBB 869-7281

Fig. 2.4 Photograph of the meter-long manipulator and mounted single crystal sample before insertion into the UHV chamber.

a nude ion gauge (Varian) for low pressure gas exposure, and an alkali getter source (SAES) for controlled alkali dosing; the lower level contains a high-resolution electron energy loss (HREEL) spectrometer (McAllister Technical Services) for surface vibrational spectroscopy. The HREEL spectrometer is enclosed in μ -metal shielding to reduce magnetic fields inside the spectrometer. Because of the bulky shaft surrounding the manipulator (see Fig. 2.2) that is required to disperse the force during sealing the high pressure (HP) cell, the LEED/AES analyzer is mounted on retractable bellows.

Figure 2.2B shows how the HP cell tube can be sealed around the single crystal. To seal the HP cell, the manipulator bellows are contracted so that the manipulator shaft locks against the top of the chamber. A piston behind the HP cell is hydraulically driven to pressurize a knife-edge seal with copper gasket between the HP cell tube and the manipulator shaft to 2100 psi. Over 50 closures of the HP cell have been made without replacing the copper gasket.

The top of the manipulator and the bottom of the HP cell are also connected on the exterior of the chamber by 3/8" stainless steel tubing. The HP cell together with this external loop serves as a batch reactor (500 ml) for studies of catalytic reaction rates and selectivities over the single crystal surfaces. Gas pressures in this reactor are measured with a 0-25 psi Heise gauge (C-58992); the gases are circulated by a bellows pump, and 0.5 ml gas samples can be periodically taken and fed through an HP 5720A gas chromatograph equipped with an HP 3390-A integrator for product analysis. A typical reaction procedure is given in Section 2.3.

2.2 Materials and Sample Preparation

2.2.1 Single Crystals. In this work, 1 Rh(100), 2 Pt(111) and 3 Rh(111) single crystals were used. All six had already been cut and polished by Winnie Hepler of the LBL support staff before by arrival. The crystals were cut by spark erosion from single crystal rods (Materials Research Corporation) of at least 99.996 percent purity to give single crystal wafers about 1-2 mm thick with two parallel surfaces of about 0.5 cm^2 area each. The surfaces were within 1° of the (111) or (100) planes as determined by Laue back diffraction. The crystal faces were polished to a mirror finish by standard procedures [5]; in all TDS and reaction studies, both crystal faces were polished, but in a few HREELS studies only one face was polished.

The crystals were mounted on the manipulator by spot-welding 0.020 tantalum or platinum wire between the edges of the crystal and 1/8" Ta rods which were in turn fastened to the manipulator by set screws. In all catalytic reaction studies, Ta supports were used. The crystal temperature was measured by 0.005" chromel-alumel thermocouple wires spot-welded together and then to the edge of the crystal. Thermocouple voltages were referenced to an ice/water reference junction outside the vacuum chamber. The single crystals were resistively heated, the points of high resistance being the crystal/support-wire spot welds. Temperatures up to 1250 K were readily achieved with 10-20 amps of current at several volts. With the new manipulator, samples could be cooled to 80 K by liquid nitrogen flow through the manipulator (Section 2.1).

2.2.2 Crystal Cleaning. Despite the high purity of the single crystals used in this work, extensive cleaning was necessary to prepare atomically clean surfaces. This is because the low-level contaminants (S, B, Ca, Si, etc.) in the bulk single crystals have a lower surface free energy than the metal and segregate to the surface.

The strategy for preparing a clean single crystal surface is to remove these contaminants from the near surface region. For Pt and Rh, most contaminants could be brought to the surface by heating at 800–1200 K in UHV or in 1×10^{-8} – 1×10^{-6} torr of O_2 . (The O_2 helped segregate contaminants to the surface by forming oxides with them.) Carbon, and in some cases boron and sulfur, could also be removed from the surface by the oxygen treatments. Other contaminants were sputtered from the surface using 1 keV Ar^+ beams with 4–6 μA of current through the crystal to ground (5×10^{-5} – 1×10^{-4} torr Ar). Sometimes sputtering at elevated temperature (500–900 K) or sputtering with some oxygen mixed with the Ar was used to speed up the surface segregation and cleaning of contaminants. When cleaning both faces of a crystal, all sputtering was done at room temperature to avoid carbon build-up (from impurities in the chamber and in the Ar) on the face not being sputtered. All cleaning cycles were completed with 1–5 minutes of annealing in UHV at about 1/2 the metal melting temperature to produce smooth, well-ordered planes of the particular metal surface cut. A compilation of some single crystal surface cleaning procedures is given in Ref. 6.

Specific cleaning procedures routinely used on the Pt(111), Rh(111) and Rh(100) surfaces after much of the contamination in the near surface region was removed are given below. Cleaning of these surfaces has also been discussed in a number of other theses: Pt(111) [5,7,8], Rh(111) [4], Rh(100) [9].

For Pt(111), carbon, oxygen, sulfur, phosphorus and silicon were the contaminants detected by AES. They were removed by Ar⁺ sputtering at 900 K, heating in 5×10^{-7} torr O₂ at 900 K, and annealing in UHV at 1250 K for 2 min. Small amounts of carbon could sometimes be dissolved into the bulk by heating the crystal to 1250 K.

For Rh(111), carbon, oxygen, sulfur, boron and phosphorus were the contaminants detected by AES. They were removed by heating at 900 K in 5×10^{-7} torr O₂ followed by Ar⁺ sputtering at 900 K or room temperature and then annealing in UHV at 1250 K for 2 min. Carbon could be dissolved into the bulk by heating above 1100 K. The most persistent contaminant was boron which frequently segregated to the surface during oxygen treatments. As a result, most O₂ cleaning was followed by Ar⁺ sputtering. Boron contamination on Rh(111) has been discussed by Semancik et al. [10]. It has also been reported that treatment of Rh single crystals with 1 atm of H₂ at 1000 C for 90 hours helps to remove boron [11].

Rh(100) [12,13] was the most difficult surface to clean. Carbon, oxygen, sulfur, boron and phosphorus were detected by AES, but the main problem was removing surface oxygen and keeping water from the chamber background gases off the surface. The most successful

cleaning procedure was: Ar^+ sputtering at 1100 K, O_2 treatment (8×10^{-7} torr, 1000 K) and flash to 1100 K, followed by reacting residual oxygen off the surface by treatment with 10 L of carbon monoxide.

In initial cleaning cycles, surface contaminants were detected by AES. However, once the near surface region was free of most contamination, surface cleanliness was monitored by LEED and HREELS to avoid low levels of surface contamination produced by the 1.5 keV electron excitation beam in AES. HREELS proved to be especially sensitive to contaminants. Vibrational frequencies and LEED patterns for a few of the contaminants found on Rh(111), Pt(111) and Rh(100) are given in Table 2.1. As can be seen from this table, the observable HREELS vibrational peaks for most atomic adsorbates occur between 0 and 600 cm^{-1} . Other surface contaminants frequently gave poorly defined, but easily detectable, HREELS peaks. Adsorbed hydrocarbon fragments give peaks around $700\text{--}900 \text{ cm}^{-1}$, a broad hump at $1300\text{--}1400 \text{ cm}^{-1}$, and weak CH stretch peaks at $2850\text{--}3050 \text{ cm}^{-1}$. A high background between 400 and 1400 cm^{-1} with no CH stretching vibrational frequencies is generally due either to polymeric carbon on the surface or to poor spectrometer tuning. Well-defined peaks between 600 and 1400 cm^{-1} with no CH stretching frequency are suggestive of oxygenated species like PO_x , SiO_x and B_xO .

HREEL spectra were generally taken before each adsorption experiment until the cleaning procedure showed good reproducibility. At this point, HREEL spectra were used only periodically to spot-check

Table 2.1: Vibrational Frequencies and LEED Patterns
of Some Surface Contaminants

Surface	Adsorbate	LEED Patterns(s)	Vibrational Frequency(ies) (cm ⁻¹)
Pt(111)	O ₂ → 2O	(2x2)	490
Pt(111)	CO	low e - ($\sqrt{3} \times \sqrt{3}$)R30 high e - c(4x2)	480, 2080 360, 480, 1870, 2110
Rh(111)	O ₂ → 2O	(2x2) or (2x1)	520-550
Rh(111)	CO	low e - (2x2) split (2x2) high e - ($\sqrt{3} \times \sqrt{3}$)R30	470, 2015 385, 450, 1855, 2065
Rh(111)	S		255
Rh(111)	B _x O	complex	- 700, - 1400
Rh(100)	S S ₂	(2x2), c(2x2)	315 585
Rh(100)	O ₂ → 2O	low e - (2x2) high e - complex	450 450, 510
Rh(100)	C	c(2x2) graphite rings	535 535
Rh(100)	CO	low e - c(2x2) high e - complex	450, 2025 390, 450, 1930, 2020
Rh(100)	B _x O		760, 1015, 1405

surface cleanliness. Before each LEED experiment and before most HREELS experiments, a full cleaning cycle was performed. However, on Rh(111) and Pt(111), some hydrocarbon TDS experiments were performed with only flashing to 1200 K in between experiments to dissolve surface carbon into the bulk. In these cases, the first TDS experiment in each series was repeated at the end to check reproducibility.

2.2.3 Reagents. The reagents used in this thesis are given in Table 2.2. (Some common names, rather than IUPAC, have been used in cases where they are still commonly used.) All gases, except the deuterated isotopes, were obtained from lecture bottles. The deuterated gases were purchased from MSD isotopes in break-seal flasks which were fitted with O-ring-sealed, teflon stopcocks. A detachable, glass to metal seal between these stopcocks and the stainless steel gas manifold was made with Cajon ultra-torr fittings. The liquid reagents (iodoethane and benzene) were stored in vials also fitted with teflon stopcocks. Benzene was stored either over CaH_2 or over 3 Å molecular sieves, and iodoethane, which is light sensitive, was stabilized by copper wire and shielded from light. The liquids were also taken through several freeze-pump-thaw cycles before use. All gases except acetylene, O_2 and Ar were used as received. Acetylene was passed through a dry ice/acetone molecular sieve trap to remove acetone, while O_2 and Ar were passed through a liquid nitrogen cooled U-tube to remove water vapor.

Table 2.2: Reagents

Reagent	Source	Purity (wt %)	Contaminants
ethylene (C ₂ H ₄)	LBL-Matheson	CP, ~ 99.5	—
ethylene (C ₂ H ₄)	LBL-Matheson	Research, 99.98	—
ethylene-d ₄ (C ₂ D ₄)	MSD Isotopes	≥ 99 atom% D	C ₂ D ₃ H
propylene (C ₃ H ₆)	LBL-Matheson	CP, ~ 99	—
propylene-d ₆ (C ₃ D ₆)	MSD Isotopes	≥ 99 atom% D	—
propylene-3,3,3-d ₃ (C ₃ H ₃ D ₃)	MSD Isotopes	≥ 98 atom% D	—
propadiene (C ₃ H ₂)	LBL-Matheson	~ 97	—
1-butene (C ₄ H ₈)	Linde	CP, ~ 99	—
cis-2-butene (C ₄ H ₈)	Linde	CP, ~ 99	—
trans-2-butene (C ₄ H ₈)	Linde	CP, ~ 99	—
isobutene (C ₄ H ₈)	Phillips 66	Reagent grade	—
1,3 butadiene (C ₄ H ₆)	LBL-Matheson	CP, ~ 99	—
acetylene (C ₂ H ₂)	LBL-Matheson	~ 99.5	acetone
acetylene-d ₂ (C ₂ D ₂)	MSD Isotopes	≥ 98 atom% D	—
methylacetylene (C ₃ H ₄)	LBL-Matheson	~ 92	C ₂ H ₂
methylacetylene-1-d ₁ (C ₃ H ₃ D)	MSD Isotopes	≥ 98 atom% D	—
1-butyne (C ₄ H ₆)	LBL-Liquid carbonic	—	—
2-butyne (C ₄ H ₆)	Chemsampco/ Muetterties Group	> 90	—
benzene (C ₆ H ₆)	Fischer	~ 99.9	—
benzene-d ₆ (C ₆ D ₆)	Norell Chemical	≥ 99 atom% D	C ₆ D ₅ H
iodoethane (C ₂ H ₅ I)	Aldrich	~ 99	—
hydrogen (H ₂)	LBL-Matheson	~ 99.9	CO
deuterium (D ₂)	LBL-Matheson	~ 99.5 atom% D	HD, H ₂
carbon monoxide (CO)	LBL-Matheson	≥ 99.5	—
oxygen (O ₂)	LBL-Matheson	≥ 99.9	H ₂ O
argon (Ar)	LBL-Matheson	≥ 99.998	H ₂ O

Two grades of ethylene were used—CP and Research. The lower purity CP grade was adequate for the UHV chemistry, but the higher purity Research grade gave faster catalytic reaction rates and was therefore used in the ethylene hydrogenation studies. Apparently small amounts of contaminants in the unsaturated hydrocarbons do not affect the UHV surface chemistry and are not detected in the surface spectroscopy of these sticky hydrocarbons, but they readily poison catalytic reactions where many product molecules are produced per surface metal atom.

The two 3-carbon isomers, methyl acetylene and propadiene, were checked for purity and/or isomerization in the stainless steel gas handling lines by gas chromatography and by a chemical test to distinguish alkenes and alkynes [14]. The most definitive evidence that these molecules are pure and do not isomerize before adsorbing on the single crystal surface is that the low-temperature LEED, HREELS and TDS of these molecules on Rh(111) are quite different (Section 4.3).

2.2.4 Gas Dosing. The gas manifold was pumped with mechanical and sorption pumps to less than one $\mu\text{m Hg}$, and the gas lines were flushed with the gases to be used before filling. Gases were admitted to the chamber through two variable leak valves. One leak valve produced a diffuse spray of the gas which back-filled the chamber with a relatively uniform distribution of molecules. The other leak valve was attached to a microchannel array nozzle doser. Single crystal surfaces could be positioned about 4 cm from the nozzle doser to achieve (for CO) a factor of 5 enhancement over the measured chamber pressure in the molecular flux at the surface.

All gas exposures are reported in Langmuirs (L). One Langmuir is an exposure of 10^{-6} torr of gas for 1 second. For small molecules and single crystal surfaces which have about 10^{15} surface atoms per cm^2 , a 1 L exposure means that, on average, each surface atom will be struck by one molecule every couple of seconds. The reported exposures in this thesis account for the x5 enhancement of the nozzle doser, but are not corrected for different ion gauge sensitivities of the gases.

All surface coverages of adsorbates (θ_{ads}) in this thesis are reported in monolayers (ML), where 1 ML = a surface coverage of 1 adsorbate molecule for every surface atom. Thus a carbon monoxide surface coverage (θ_{CO}) of 0.5 means there is 1 CO molecule for every two surface metal atoms. Surface atomic densities of 1.5×10^{15} , 1.6×10^{15} and 1.4×10^{15} atoms/ cm^2 were used for the Pt(111), Rh(111) and Rh(100) surfaces respectively. The term saturation coverage is used to mean the maximum surface coverage attainable at the adsorption temperature. Typical saturation coverages of the hydrocarbons studied in this thesis are $\theta_{\text{HC}} = 0.25$, or 1 hydrocarbon molecule per four surface metal atoms.

2.3 Catalytic Reaction Procedure

The high pressure (HP) cell and reaction loop used to run catalytic reactions over single crystal surfaces were described in Section 2.1. This apparatus was used in a batch reactor mode, since for the ethylene hydrogenation studies reported in this thesis, it was necessary to accumulate products to obtain a detectable level. Use of similar systems under flow reaction conditions has been discussed by S.M. Davis [7] and R.C. Yeates [5].

In the ethylene hydrogenation studies in this thesis, the reactant ethylene and product ethane were separated and detected by gas chromatography using a 6' 80/100 Poropak N column and flame ionization detector at room temperature with a carrier gas flow of 100 cm³/min. The Ta support wires and the chromel-alumel thermocouple were tested for catalytic activity by replacing the single crystal with Ta foil, following the same cleaning procedure, and running an ethylene hydrogenation. There was almost no detectable ethane produced at any temperature from 300 to 640 K. The catalytic effects of the different crystal faces on the edges of the single crystal wafers were minimized by the Ta support wires which covered about 50 percent of the edges. Also, the crystal edges probably have catalytic activity in ethylene hydrogenation comparable to the (111) faces, since it was found (Section 5.2) that sputtering the Rh(111) surface did not affect the catalytic hydrogenation rate.

A typical reaction procedure follows. The clean or pretreated single crystal surface is enclosed in the high pressure cell. The reactant gases are added sequentially (the order was varied) from the gas manifold to the reactor loop and mixed by circulating for 15–20 minutes at room temperature after valving off the pressure gauge and gas manifold from the reactor loop. For typical reactant pressures of 20 torr ethylene and 100 torr hydrogen, only a fraction of 1 percent of the ethylene reacted during this mixing at room temperature. The crystal is then heated to the reaction temperature and the gases are sampled and analyzed every 5–10 minutes. The catalytic hydrogenation reactions were generally run to about 10 percent conversion and then the reaction mixture was pumped out either at the reaction temperature or after cooling to room temperature. Gases are pumped out from the HP cell through a rapid pump valve at the top of the manipulator using a combination of pumping by a mechanical pump, a liquid nitrogen cooled sorption pump, and a liquid nitrogen trapped 2" diffusion pump. It takes typically 5–10 minutes for ion gauge pressures above the diffusion pump trap to reach 1×10^{-6} torr. Opening the HP cell at this pressure, raises the chamber pressure to $\sim 5 \times 10^{-8}$ torr, water being the major contaminant. The time it takes for the chamber to return to its base pressure varies with the gases used in the HP cell. With 120 torr of H_2 and C_2H_4 as was used frequently in this thesis, a pressure of about 5×10^{-9} torr is reached after 15 min, but it is several hours before the chamber returns to base pressure. Surface analysis by

HREELS, LEED, AES and TDS was generally performed immediately after opening the HP cell.

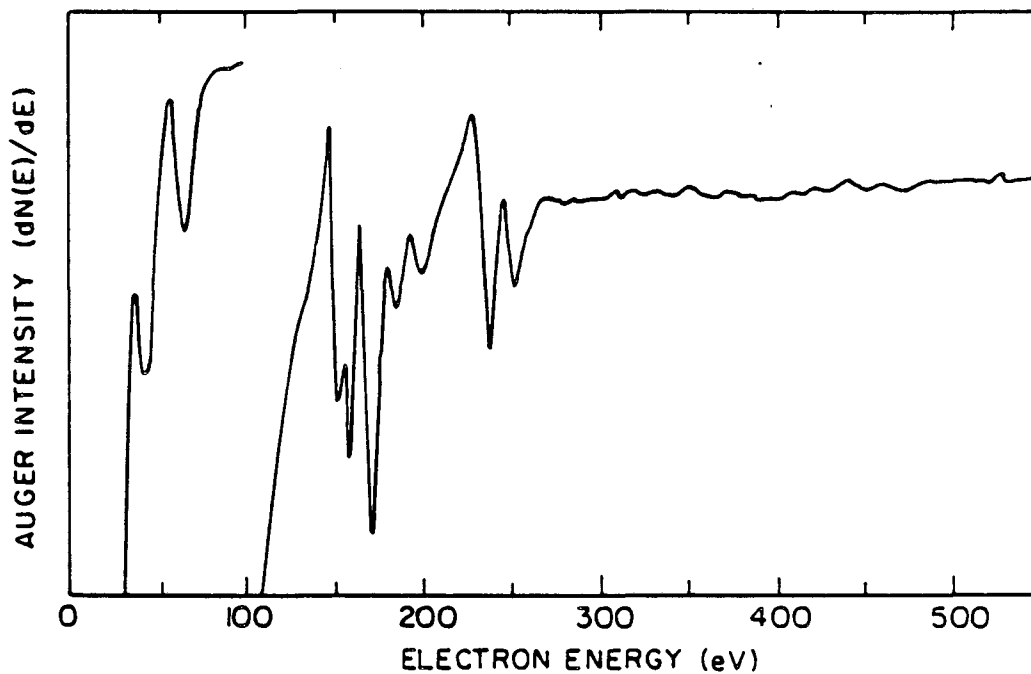
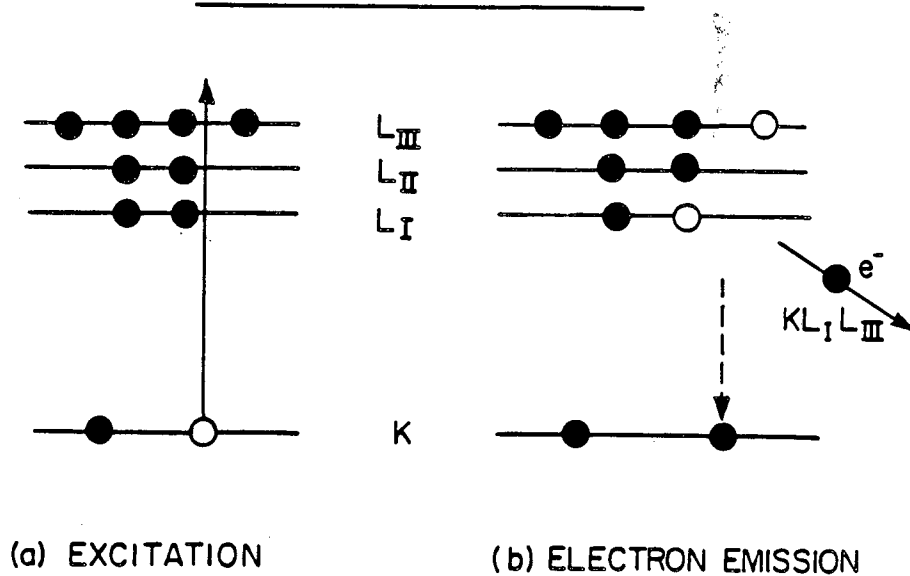
Reaction rates are reported as turnover frequencies, which are the number of ethylene molecules reacting per surface metal atom every second. The term turnover number refers to the number of product molecules that have been produced per surface metal atom. A turnover number greater than one is necessary to insure that the reaction is catalytic and not stoichiometric. In the ethylene hydrogenation reactions studied here, turnover numbers were usually about 10,000; turnover frequencies were typically 1-10 molecules of ethane per surface metal atom per second.

2.4 Surface Analysis Techniques: Principles, Applications and Procedures

Many techniques have been developed over the last 20 years to study, under UHV conditions, the adsorption, desorption and bonding of submonolayer quantities of molecules adsorbed on metal single crystal surfaces. In many of these, including HREELS, LEED and AES used in this thesis, the surface and adsorbates are probed by measuring the energy of slow electrons (3–1000 eV) that are diffracted, scattered and/or emitted from the surface. Electrons in this energy range are surface sensitive; they interact strongly with metal atoms and are able to penetrate through or escape from only the first few atomic layers near the surface [15]. A review of these techniques is neither feasible, nor appropriate here; there are extensive publications on the principles and applications of these surface analysis techniques [16–21] and UHV technology in general [22]. What follows are brief discussions of the principles of AES, TDS, LEED and HREELS and of the way these techniques were applied in this thesis work. References to published reviews of these techniques are also given.

2.4.1 Auger Electron Spectroscopy (AES). Auger electrons, like x-rays, are produced in the decay of electronically excited states of atoms as shown in Figs. 2.5A,B. Auger electron spectroscopy [reviewed in ref. 23–26] involves their detection as a function of kinetic energy. The kinetic energy of the emitted Auger electron depends mainly on the energy levels of the atom and its ionized states [23]. As a result, production of core holes in any element except hydrogen and

AUGER ELECTRON EMISSION



XBL 8312-6679

Fig. 2.5 Illustration of the Auger process along with a sample Auger electron spectrum. (A) Excitation to produce a singly ionized atom with a core hole. (B) De-excitation of the ionized atom by emission of an Auger electron to give a doubly ionized atom. (C) A typical Auger electron spectrum for clean Pt(111).

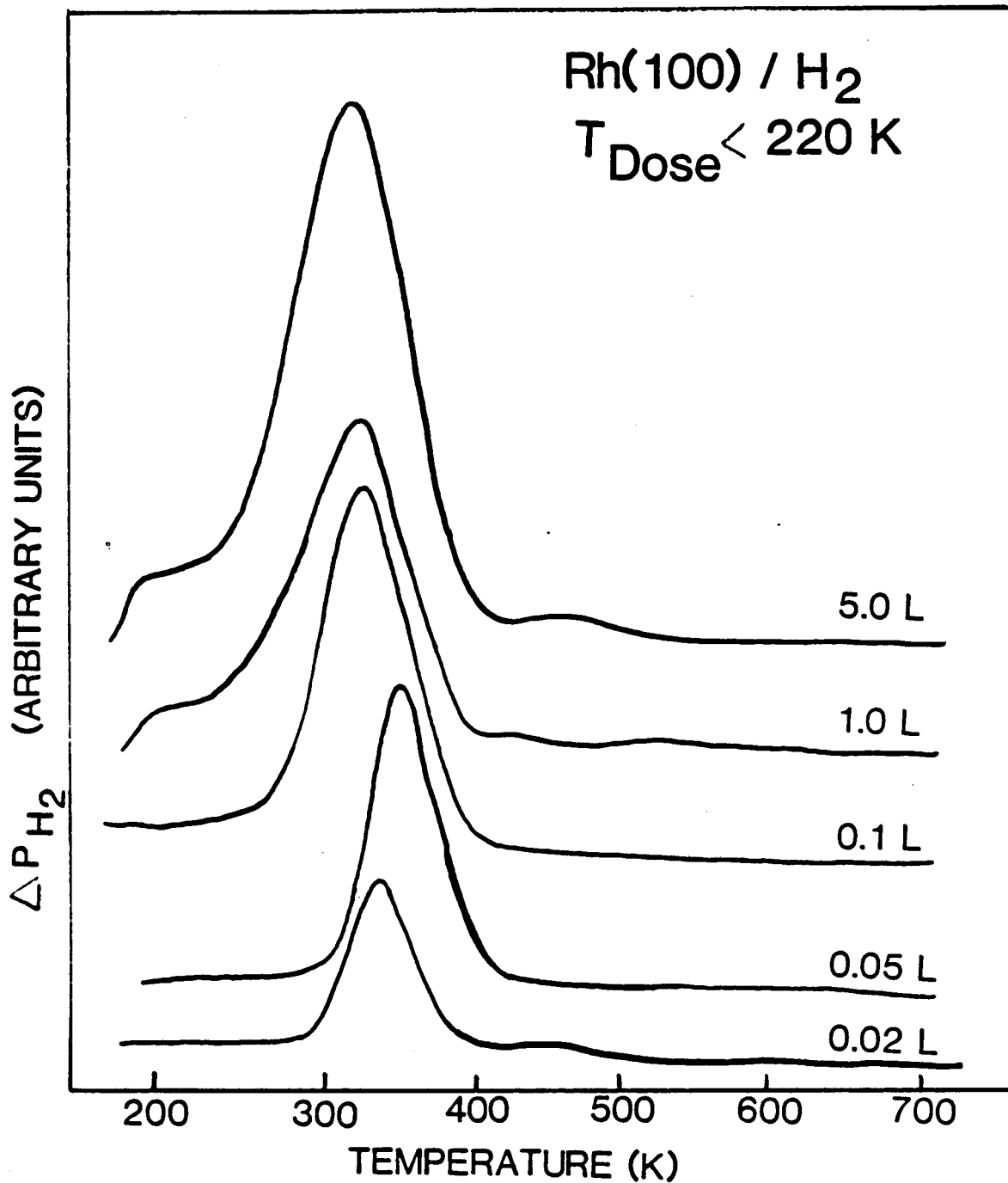
helium results in the emission of Auger electrons which have kinetic energies characteristic of that element and its chemical environment. Tabulations of Auger electron energies [27] and spectra [28] are published. In this thesis AES was used only to identify and quantify the atomic composition of the surface.

An AES spectrum for a clean Pt(111) surface is shown in Fig. 2.5C. The AES spectrum is recorded in derivative mode to achieve the necessary sensitivity. Therefore, the peak heights and peak areas are not directly related to surface coverage. However, if the non-differentiated Auger peaks are Gaussian [29] then the peak-to-peak height is proportional to coverage. AES was successfully used in this thesis to quantify submonolayer carbon coverages on Pt(111) using the rule: $\theta_c = I(C_{273})/I(Pt_{237}) \times 0.65$, where I is the peak-to-peak height of the indicated Auger peaks.

To obtain the AES spectra in this thesis work, the surface atoms were ionized using a 1500 eV electron beam incident on the surface at about 70° from the surface normal. The energies of the emitted Auger electrons were determined using the 4-grid LEED optics as a retarding field analyzer [ref. 17 and Fig. 2.7B]. The Auger electron spectra were recorded in derivative mode on an XY chart recorder (HP 7044B) by modulating the retarding field voltage on the LEED grids 2 and 3 at 10 V and ~2000 Hz and detecting the second harmonic of the modulated signal with an Ortec Brookdeal 9503 phase-sensitive lock-in amplifier.

2.4.2 Thermal Desorption Spectroscopy (TDS). TDS, also referred to as temperature programmed desorption (TPD), probes the kinetics of desorption from surfaces. In a typical TDS experiment, an adsorbate-covered surface is heated (usually linearly with time) in UHV, and the desorption products are detected as a function of temperature with a mass spectrometer. It can be shown that for TD spectra taken in UHV chambers under conditions of rapid pumping speeds the mass spectrometer signal is proportional to the desorption rate [31]. A typical TD spectrum is thus a measure of the desorption rate as a function of temperature. (Note, however, that the surface coverage also changes with temperature during a thermal desorption experiment.)

TD spectra for H_2 desorption from a Rh(100) surface after various exposures of hydrogen at 200 K are shown in Fig. 2.6. TD spectra like these contain information about the different types of adsorption sites on the surface, the energetics of the surface chemical bond, the kinetics of surface chemical reactions, adsorbate-adsorbate interactions and the surface chemical composition [30-35]. So much potential information makes TD spectra difficult to interpret. However, a few basic conclusions can be reached with some assumptions [31,36,37]. For example, assuming that the activation energy for desorption does not change with coverage, it can be shown that the temperature of the maximum desorption rate, T_p , is related to the activation energy for desorption, E_d , the preexponential factor, A , the heating rate, β , and the initial surface coverage, θ_0 , by:



XBL 868-3190

Fig. 2.6 Thermal desorption spectra monitoring mass 2 desorption from a Rh(100) surface exposed to increasing amounts of hydrogen at 100 K. The heating rates are 20 K/sec. The shift of the desorption peak maximum to lower temperatures with increasing surface coverage is consistent with second order desorption of hydrogen from the surface.

$$E_d/(RT_p^2) = (A_1/\beta)\exp[-E_d/RT_p] \quad \text{for first order, and}$$

$$E_d/(RT_p^2) = (A_2/\beta)\theta_0\exp[-E_d/RT_p] \quad \text{for second order desorptions}$$

Therefore, for first order desorptions the TDS peak temperature, T_p , is independent of surface coverage, while for second order desorptions the peak maximum shifts to lower temperature with increasing coverage. This latter effect is seen in the H_2 TDS spectra of Fig. 2.6 where the desorption rate for H_2 is second order in the surface coverage of hydrogen atoms.

Besides determining the order of the desorption process, the TD spectra in this thesis were used primarily to determine the desorption products, to determine approximate binding energies and reaction activation energies, and to determine the surface stoichiometry by integrating the TDS peak areas. Activation energies were determined using the equations above by assuming values for the preexponential factors A_1 and A_2 . TDS peak areas were integrated by cutting out the peaks and weighing them on an analytical balance. Overlapping peaks were integrated by drawing perpendiculars from the base line to the minimum in the overlap region.

TD spectra in this thesis were recorded either by plotting the desired mass signal from the mass spectrometer on chart recorders vs. time and vs. temperature or by using a commodore PET computer to multiplex the mass spectrometer and record up to 5 masses vs. time during a single thermal desorption [30]. (During the desorption experiment,

one face of the crystal was pointed towards the mass spectrometer ionizer, which was ~5 cm from the crystal surface.) The heating ramp was achieved by running a constant current through the crystal heating leads to achieve an approximately linear ramp of 15–30 K/sec from 80–800 K. Nonlinearity in the temperature scales between 80 and 300 K in this thesis is a result of the nonlinear response of the thermocouple voltage to temperature in this range; peak temperatures are reproducible to ±20 degrees.

Most of the TD spectra in this thesis are presented and discussed in Sections 3.5 and 4.3.

2.4.3 Low-Energy Electron Diffraction (LEED). The diffraction of low-energy electrons is a consequence of an electron's De Broglie wavelength. For 40–150 eV electrons, the De Broglie wavelength:

$$\lambda(\text{\AA}) = h/p = [150/E(\text{eV})]^{1/2}$$

is 1–2 Å. Interatomic distances for bonded atoms are also of this magnitude, so low-energy electrons can diffract from periodic atomic lattices. Like x-ray diffraction, the diffraction condition for LEED with a normal-incidence electron beam is given by the Bragg law [38]:

$$n = \text{integer } (1, 2, 3, \dots)$$

$$n\lambda = d(\sin\theta) = n [150/E(\text{eV})]^{1/2} \quad d = \text{separation between rows of surface atoms}$$

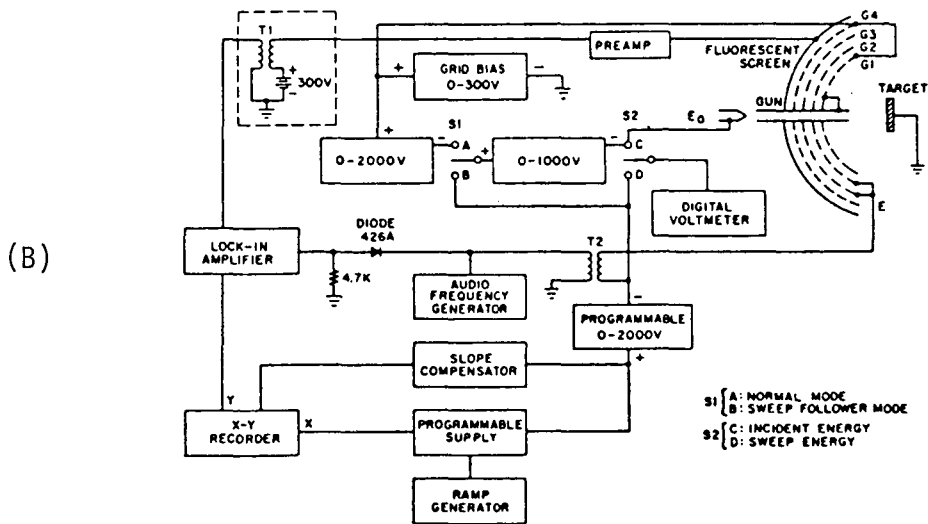
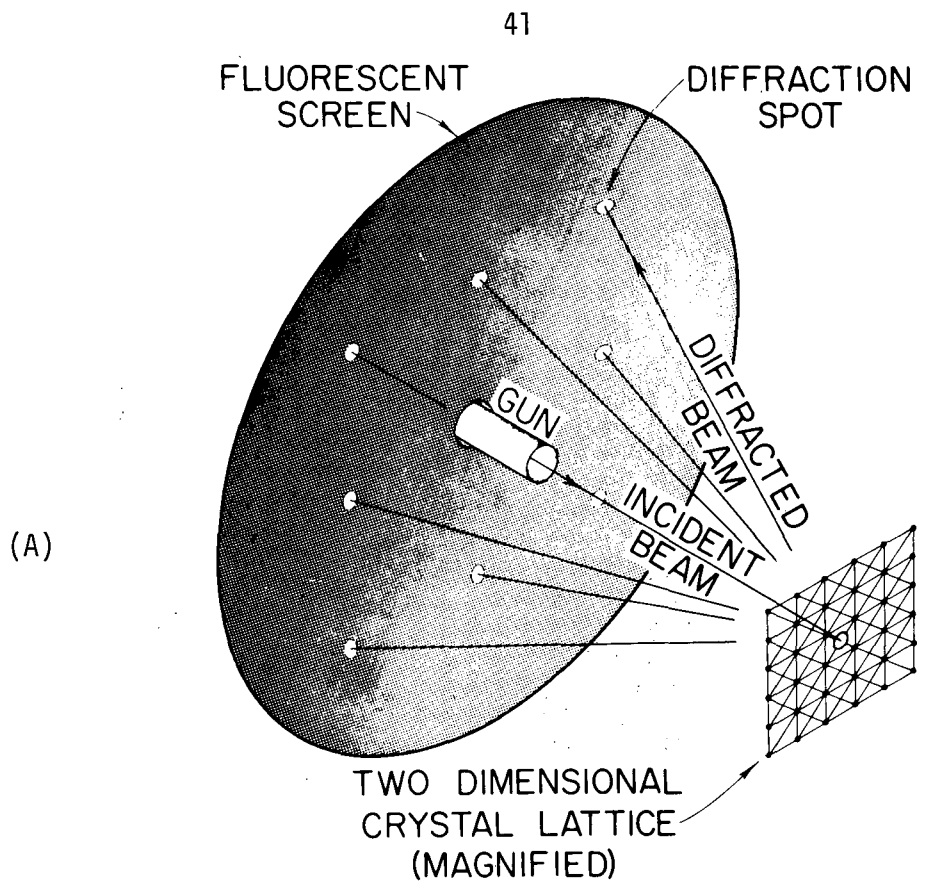
$$\theta = \text{angle from surface normal for constructive interference}$$

However, unlike x-rays which interact weakly with atoms, low-energy electrons interact strongly and can penetrate only several atomic

layers. LEED is therefore sensitive to surface atoms and contains information about surface periodicity, and surface bonding geometries [38-42].

A schematic diagram of the LEED experiment is shown in Fig. 2.7A. A monoenergetic electron beam of 10-500 eV energy is emitted through a hole in the center of a phosphor screen and impinges on the single crystal surface located at the center of curvature of the phosphor screen. The elastically back-scattered electrons are filtered from the inelastically scattered electrons by a retarding field analyzer (Fig. 2.7B) and post accelerated into the phosphor screen (5-8 kV) where their fluorescence can be viewed or photographed. If the atoms are periodically arranged, the diffracted electrons produce sharp spots at angles where the Bragg condition is satisfied for the particular electron wavelength (energy) used.

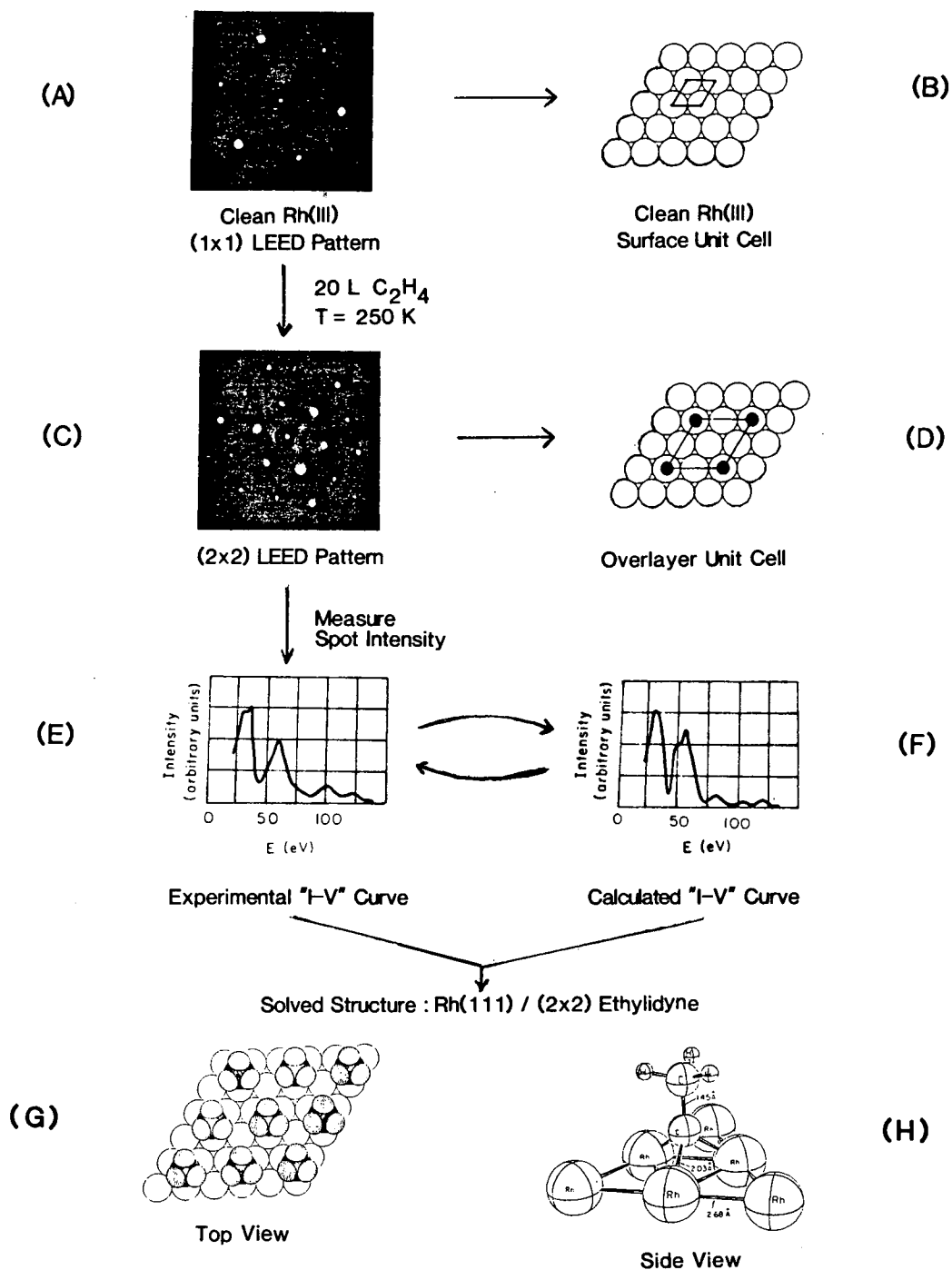
As mentioned in Chapter 1, surface structure determination from LEED patterns and intensities is not routine [41]. An outline of the steps to a solved structure is given in Fig. 2.8 for ethylene adsorption at 250 K on Rh(111). Figures 2.8A,C are photographs of the diffraction patterns of a 50 eV electron beam from a Rh(111) surface before and after exposure to ethylene. These patterns can be used to determine the size and shape of the surface unit cell as shown in 2.8B,D, but the patterns themselves do not provide any information about the adsorption site on the surface or the bonding within the adsorbate. To determine the bonding on the surface, the diffracted intensities (I) are measured as a function of the electron voltage



XBL 8312-6874

Fig. 2.7 (A) Schematic diagram of the low energy electron diffraction (LEED) experiment from an idealized two-dimensional crystal lattice. (B) Schematic diagram of the LEED/AES analyzer. In LEED the analyzing grids G2 and G3 are biased to eliminate inelastically scattered electrons. In AES these grids are biased to serve as a high-pass filter.

Steps to a Solved Surface Structure by LEED : Ethylidyne on Rh(III)



XBL 8610-4097

Fig. 2.8 Outline of the steps involved in solving an adsorbate surface structure by low-energy electron diffraction (LEED) using the (2x2) structure of ethylidyne on Rh(111) as an example.

(V). The resulting I-V curve for one diffracted beam of the ethylene/Rh(111) monolayer is shown in Fig. 2.8E. Surface structure is determined from this data by methods similar to those used in x-ray crystallography: a trial structure is assumed, and the theoretical I-V curves are then computed (Fig. 2.8F) by electron scattering calculations and compared to the experimental curve. The trial structure is then modified until theory matches experiment. Top and side views of the structure determined for ethylene adsorption at 250 K on Rh(111) are shown in Figs. 2.8G,H. The solved LEED structure shows that ethylene has dissociated at this temperature on Rh(111) to form CCH_3 species, whose metal-carbon and carbon-carbon bond lengths have been determined to $\approx 0.1 \text{ \AA}$ [43]. The adsorption site was also determined to be the 3-fold hollow site having an atom in the second layer below the surface.

In this thesis, LEED was used only to (1) determine long range order on the surface, (2) estimate surface coverages, and (3) find the size and shape of the surface unit cell. However, reference will be made to several structures that have been solved by a complete LEED analysis, especially in Chapter 3. The Wood notation [38] will be used in this thesis to describe the ordered adsorbate overlayers. In this notation, the overlayer is described by the size and orientation of the overlayer unit cell with respect to the substrate unit cell which is defined to be (1x1). Thus a $(\sqrt{3} \times \sqrt{3})R30$ adsorbate overlayer has a unit cell which is $\sqrt{3}$ times the substrate unit cell distances, but is rotated 30° . The prefix "c" in front of a Wood notation means

that the unit cell has an adsorbate in the center as well as at the corners of the unit cell.

2.4.4 High-Resolution Electron Energy Loss Spectroscopy (HREELS).

The usefulness of surface vibrational spectroscopy for determining how hydrocarbons bond to metal surfaces was discussed in Chapter 1. The techniques presently available for obtaining a surface vibrational spectrum are listed along with some of their characteristics in Table 2.3. For determining the chemistry of hydrocarbons on metal surfaces where very little is known about the surface structures and bonding, the most powerful technique at present and the one used in this thesis is HREELS. The major advantages of HREELS are its sensitivity, ease of acquisition, and wide spectral range. A number of excellent books [55,56] and reviews [57-61] on HREELS have been written in the last 10 years. In this section the principles used to interpret the HREEL spectra in this thesis are discussed and the HREEL spectrometer is described.

A schematic diagram of an HREELS experiment on a (2x2) monolayer of ethylidyne on Rh(111) is given in Fig. 2.9A. A monoenergetic electron beam with 1-100 eV energy is incident on the ethylidyne-covered surface. Most of the electrons are elastically scattered, but 0.1-1 percent lose discrete amounts of energy, $\hbar\omega$, as a result of exciting surface vibrations. The electrons scattered from the surface (usually those in a small solid angle about the specular direction) are energy analyzed, and the number of electrons are plotted versus energy loss to give a HREEL spectrum like that in Fig. 2.9B. The prefix "high-resolution" is used, even though the energy resolution ($30-50 \text{ cm}^{-1}$) is poor by comparison to

Table 2.3: Vibrational spectroscopies used to measure vibrational frequencies of atoms and molecules adsorbed on surfaces

Vibrational Spectroscopy	Principle	Samples	Resolution (cm ⁻¹)	Spectral Range (cm ⁻¹)	References
High-Resolution Electron Energy Loss Spectroscopy (HREELS)	Inelastic scattering of low energy (1-150 eV) electrons	single crystals, thin films, and foils in UHV	30-90	100-5000	55
Incoherent Inelastic Neutron Scattering (IINS)	Incoherent inelastic scattering of thermal neutrons	50-100 g of power	5-50	4-4000	44
Raman Spectroscopy and Surface-Enhanced Raman Spectroscopy (SERS)	Inelastic scattering of photons of visible light	100 mg powder, single crystals, electrodes	1-10	200-5000	45,46,47
Reflection Absorption Infrared Spectroscopy (RAIRS)	Absorption of infrared radiation detected in the reflected beam	foils, single crystals	1-10	700-5000	48
Transmission Absorption Infrared Spectroscopy (TAIRS)	Absorption of infrared radiation detected in the transmitted beam	10-100 mg pressed powder, solution	1-10	400-4000	47,49-51
Infrared Emission Spectroscopy (IES)	Detection of the emitted black body radiation from vibrating molecules	foils, single crystals, zeolite on a Au wire	1-10	400-4000	52,47
Inelastic Electron Tunneling Spectroscopy (IETS)	Inelastic tunneling of electrons between metals through an oxide layer containing the sample	1-10 mg Al or other metal oxide (20 Å thick supported on metal film)	10-50	10-5000	53
Photoacoustic Spectroscopy (PAS)	Vibrational excitation with pulsed light source and detection of the sound waves generated	100 mg powder or metal film	1-10	400-5000	54

High Resolution Electron Energy Loss Spectroscopy (HREELS): Ethylidyne on Rh(III)

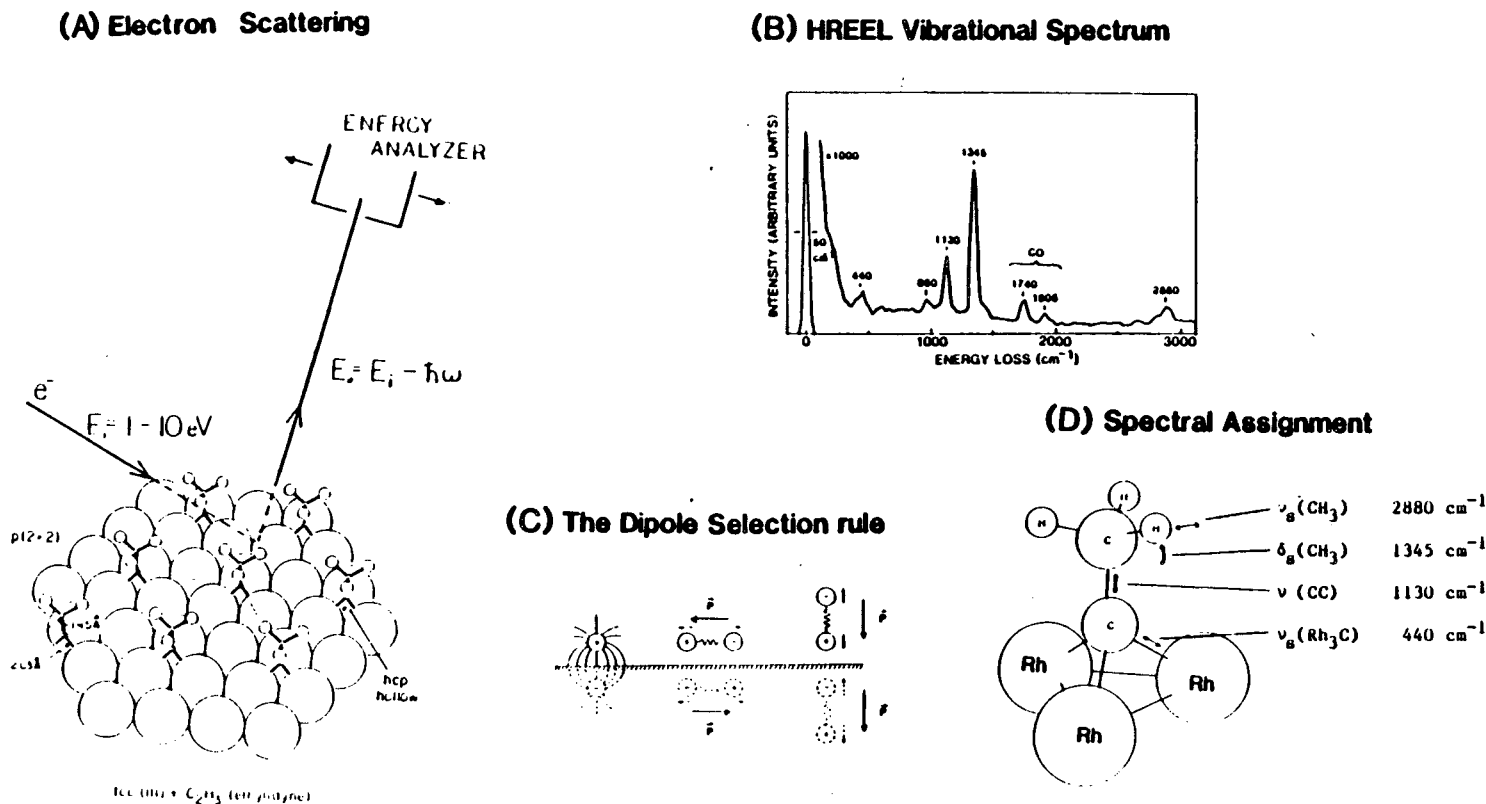


Fig. 2.9 Principles of high-resolution electron energy loss spectroscopy (HREELS) as applied to a (2x2) monolayer of ethylidyne on Rh(111): (A) the experiment, (B) the spectrum, (C) the phenomena responsible for the dipole selection rule, and (D) the spectral assignment for ethylidyne.

XBL 8610-4095

infrared spectroscopy [48], in order to distinguish vibrational energy loss spectra from electronic energy loss spectra (EELS) where the resolution is typically too low to resolve vibrational energy losses.

The HREEL spectrum taken in the specular direction ($\theta_{in} = \theta_{out}$) for ethynidyne species on Rh(111) is shown in Fig. 2.9B. The energy loss peaks are multiplied a factor of 1000 relative to the elastic peak. Most of the loss peaks correspond to vibrational modes in ethynidyne, however the two peaks at 1740 and 1905 cm^{-1} are due to a small amount of carbon monoxide coadsorbed in two types of sites on the surface. CO is an ever present contaminant from the background gases in the UHV chamber and is observed in most of the HREEL spectra in this thesis. The amount of coadsorbed CO in Fig. 2.9B is actually quite small (less than five percent of a monolayer) but is readily detected because adsorbed CO has a high cross section for vibrational excitation [55].

In order to fully interpret HREEL spectra like that in Fig. 2.9 B, the electron scattering processes responsible for vibrational excitation must be understood. The scattering process can be viewed from the point of view of either the electron or the adsorbed molecule. In this section the electron is considered, and the basic scattering principles that determine the HREEL selection rules and excitation cross sections are described; more detailed discussions have been published [55].

An electron incident on a surface can interact with and excite surface vibrations at distances up to 100 Å away from the surface. Which vibrational modes are excited and their probability of excitation depends strongly on the distance of the electron from the surface during

the excitation. HREEL spectral intensities can be qualitatively understood by considering the interactions between the incident electron and surface vibration that dominate in the two excitation extremes (near and far from the surface). Separating electron scattering probabilities into these two regimes is of course an arbitrary division of a complex phenomenon that changes continuously with distance; there is no distinct separation between long- and short-range scattering.

Long-range electron scattering at $\sim 10\text{--}100 \text{ \AA}$ distances from the surface is called dipole scattering. The dominant interaction is between an oscillating dipolar field component from a fourier decomposition of the incident electron's electric field and the oscillating dipolar field produced by a surface vibration. This long-range interaction is analogous to the interaction of infrared radiation with surface vibrations [48], and the selection rules are the same. For conducting materials, only surface vibrations with an oscillating dipole moment (dynamic dipole moment) normal to the surface can be excited by dipole scattering. This selection rule exists for two reasons as result of the image charge induced in conductors as shown in Fig. 2.9C. First, the dipolar field lines of the incident electron are normal to the surface at the surface by Gauss's law for conductors. Second, the image charge in the metal will cancel or screen vibrating dipole moments parallel to the surface, while enhancing those normal to the surface.

Determining which surface vibrations have a component of their oscillating dipole normal to the surface is facilitated by using group theory. The dipole scattering probability is given by $\langle \phi_i | V | \phi_f \rangle$ where ϕ_i and ϕ_f are the initial and final vibrational states respectively and V is the interaction potential between the electron and the vibrating dipole. Only ϕ_f for which this integral is nonzero will be excited. These ϕ_f can be determined on the basis of symmetry. Since (using the language of group theory) both ϕ_i and V for surface dipole scattering always transform as the totally symmetric irreducible representation of the adsorbate point group, ϕ_f must also transform as the totally symmetric irreducible representation to be excited. Stated simply, this means that only vibrations which maintain all the symmetry elements of the adsorbed species can be excited by dipole scattering.

Dipole scattering, is characterized by a scattered electron distribution peaked in the specular direction ($\theta_{in} = \theta_{out}$) [55]. As a result, specular HREEL spectra are generally dominated by the vibrational peaks excited by dipole scattering. The relative intensity of these dipole-allowed vibrations in the specular HREEL spectrum is proportional to the dynamic dipole normal to the surface.

Application of the dipole selection rule to the specular HREEL spectrum of ethynidyne on Rh(111) is summarized in Fig. 2.9D and will be discussed in detail in Section 3.1. Briefly, the only vibrations in adsorbed ethynidyne that maintain the 3-fold axis of rotation and all other symmetry elements are the symmetric CH_3 , Rh_3C , and CC

stretches and the symmetric CH_3 bend. These are indeed the most intense modes in the specular HREEL spectrum.

Vibrations like the $\delta_{\text{as}}\text{CH}_3$ mode ($\sim 1420\text{ cm}^{-1}$) are dipole-forbidden but are weakly detectable in the specular HREEL spectrum as a result of short-range electron scattering called "impact" or "resonance" scattering. In these short-range scatterings the incident electrons interact directly with atomic potentials and may even be temporarily captured to form a negative ion. As a result, vibrations with dynamic dipole moments parallel to the surface as well as those perpendicular to the surface can be excited. While the total scattering cross section for these short-range scatterings is often approximately the same as for long-range dipole scattering, the scattering distribution is more nearly isotropic [55]. Thus, the fraction of impact scattered electrons in the specular direction is generally small compared to dipole scattering. Impact scattering can be exploited to observe the vibrational frequencies of dipole-forbidden modes by taking HREEL spectra in off-specular directions outside the dipole scattering lobe. Off-specular HREEL spectra for ethylidyne on Rh(111) are presented and discussed in Section 3.1. There are selection rules for these short-range scatterings under certain conditions [55], but they did not aid the interpretation of the HREEL spectra in this thesis.

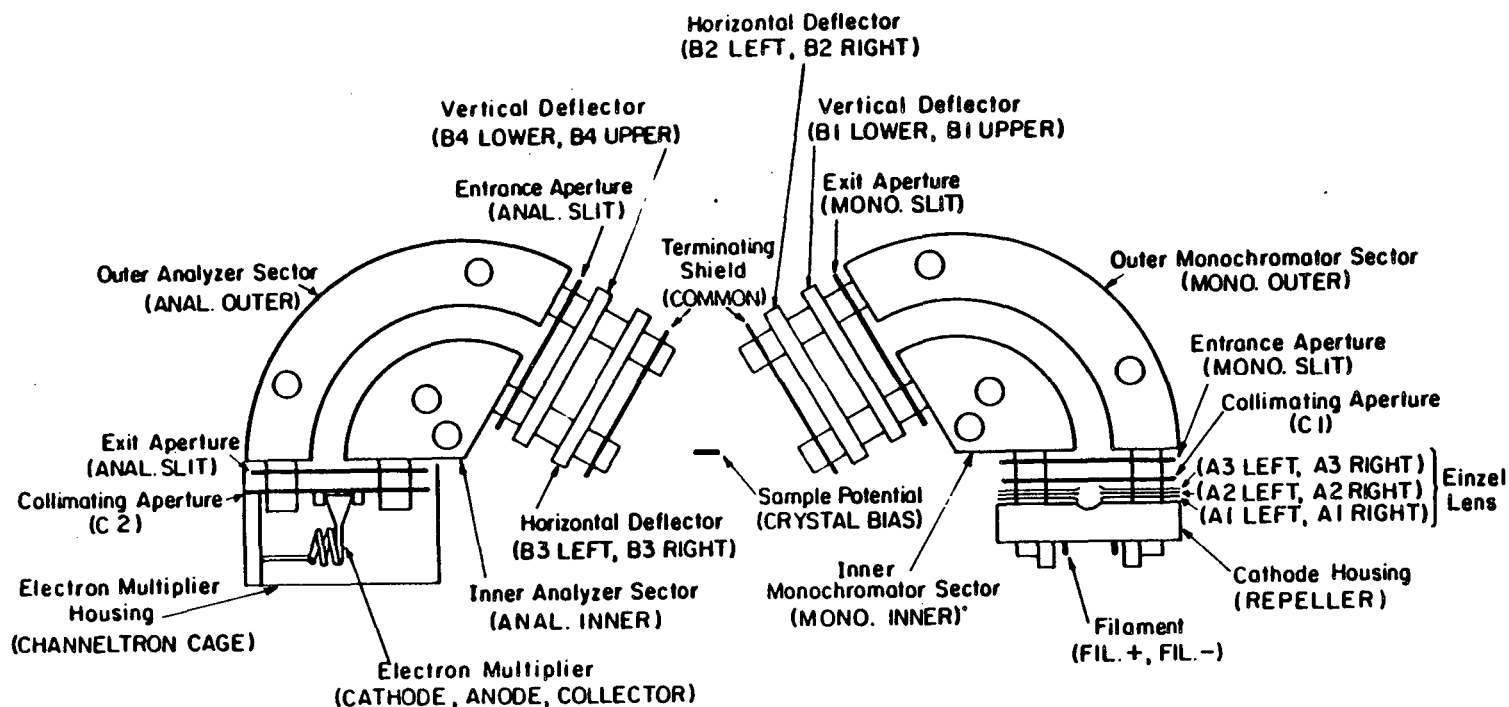
The HREEL spectra in this thesis were obtained with the HREEL spectrometer shown schematically in Fig. 2.10. This spectrometer (McCallister Technical) is similar to published designs [62,63] and has been described elsewhere [4]. The crystal sits between two 127°

electrostatic cylindrical deflectors and reflects the electron beam from the monochromator to the analyzer. The total scattering angle is fixed at 120° , so the angles of incidence and detection were varied by rotation of the crystal. Most spectra were recorded with specular reflection, $\theta_{in} = \theta_{out} = 60^\circ$ from the surface normal.

Control of the electrostatic lens voltages in the spectrometer was achieved using an ultra-stable power supply designed and built at LBL [64]. This power supply also controls the output of a power supply (Lambda LP-520-FM) to the electron filament. A ramp generator (LBL 7S1113) was used to sweep the analyzer assembly voltages; a high voltage power supply (Fluke 2565018) provides the high voltage (distributed by a resistor/zener diode assembly) for the electron multiplier (Galileo 4028). The electron pulses detected by the electron multiplier are decoupled from the high voltage bias, amplified and shaped (Ortec 142PC preamplifier and Ortec 570 amplifier), discriminated (Ortec 550 SCA) and then counted with a rate meter (Ortec 449). The output of the ratemeter is plotted versus analyzer voltage on an X-Y chart recorder to give the HREEL spectrum.

Tuning of the spectrometer has been described [4]. The two major and somewhat independent variables are the sample position and the voltage settings of the spectrometer. Generally the spectrometer could be tuned in 5 minutes or less by setting the crystal at the position used in the previous spectrum and adjusting the spectrometer voltages and crystal bias while ramping back and forth in energy and observing the elastic peak on an oscilloscope. When it was difficult

HREELS SPECTROMETER



XBL 639-639

Fig. 2.10 Schematic diagram of the HREEL spectrometer used to obtain the vibrational spectra in this thesis. Electrostatic potentials are applied to the labelled elements to focus, monochromatize and energy analyze the 1-10 eV electron beam.

to get many counts in the elastic peak by this method, it was frequently found that the surface reflectivity was truly low, the surface was dirty, or the surface was not properly annealed. In other cases a weak elastic peak was improved by one of the following: (1) changing the beam energy, (2) retuning the spectrometer voltages with the crystal bias at 0 V, (3) changing the crystal position, or (4) setting the spectrometer voltages back to previously recorded ones that worked. Throughout this thesis work the HREEL spectrometer was not once removed from the vacuum chamber and voltage settings from almost four years ago still give a good elastic peak in most cases. No adverse effects were observed from the pressure increases that occurred after catalytic reactions using the high pressure cell.

HREEL spectra in this thesis were typically taken at monochromator and analyzer pass energies of about 0.6 eV and with electron beam energies of 3 to 8 eV. The energy resolution (FWHM) in the elastic peak was generally $40\text{--}60\text{ cm}^{-1}$ ($5\text{--}7\text{ meV}$, $1\text{ meV} = 8.0655\text{ cm}^{-1}$) with $10^{-9}\text{--}10^{-11}$ amps beam current at the crystal and $10^5\text{--}10^6$ counts per second in the elastic scattering peak.

REFERENCES

1. C.M. Mate, Ph.D. thesis, University of California, Berkeley, 1986, unpublished.
2. D.W. Blakely, E.I. Kozak, B.A. Sexton and G.A. Somorjai, J. Vacuum Sci. Technol. 13 (1976) 1091.
3. A.L. Cabrera, N.D. Spencer, E. Kozak, P.W. Davies and G.A. Somorjai, Rev. Sci. Instr. 53 (1982) 1888.
4. J.E. Crowell, Ph.D. thesis, University of California, Berkeley, 1984, unpublished.
5. R.C. Yeates, Ph.D. thesis, University of California, Berkeley, 1985, unpublished; write-up by Winnie Hepler, unpublished.
6. R.G. Musket, W. McLean, C.A. Colmenares, D.M. Makowiecki and W.J. Siekhaus, Appl. Surf. Sci. 10 (1982) 143.
7. S.M. Davis, Ph.D. thesis, University of California, Berkeley, 1981, unpublished.
8. F. Zaera, Ph.D. thesis, University of California, Berkeley, 1984, unpublished.
9. D.G. Castner, Ph.D. thesis, University of California, Berkeley, 1979, unpublished.
10. S. Semancik, G.L. Haller and J.T. Yates, Jr., Appl. Surf. Sci. 10 (1982), 133.
11. R.J. Baird, R.C. Ku and P. Wynblatt, Surf. Sci. 97 (1980) 346.
12. D.G. Castner, B.A. Sexton and G.A. Somorjai, Surf. Sci. 71 (1978) 519.

13. L. Dubois, J. Chem. Phys. 77 (1982) 5228.
14. F.O. Rice and W.S. Haynes, J. Amer. Chem. Soc. 70 (1948) 964.
15. G.A. Somorjai, Chemistry in Two Dimensions: Surfaces, Cornell University Press, Ithaca (1981).
16. G.A. Somorjai, Principles of Surface Chemistry, Prentice-Hall, Englewood Cliffs (1972).
17. G. Ertl and J. Kupperts, Low Energy Electrons and Surface Chemistry, Verlag Chemie, Weinheim (1974).
18. H. Ibach, ed. Electron Spectroscopy for Surface Analysis, Topics in Current Physics Vol. 4, Springer-Verlag, New York (1977).
19. M.W. Roberts and C.S. McKee, Chemistry of the Metal-Gas Interface, Oxford Univ., Oxford (1978).
20. M. Prutton, Surface Physics, Clarendon Press, Oxford (1975).
21. G.A. Somorjai and M.A. Van Hove, Structure and Bonding 38: Monolayers, Springer-Verlag, New York (1979).
22. J.F. O'Hanlon, A User's Guide to Vacuum Technology, John Wiley, New York (1980); R. W. Roberts and T. A. Vanderslice, Ultra-High Vacuum and It's Applications, Prentice Hall (1963).
23. Chuan C. Chang, "Analytical Auger Electron Spectroscopy," Chapter 20 in Characterization of Solid Surfaces, P.F. Kane and G.B. Larabee, eds., Plenum, New York (1974).
24. R.R. Rye, J.E. Houston, D.R. Jennison, T.E. Madey and P.H. Holloway, "Chemical Information in Auger Electron Spectroscopy," Ind. Eng. Chem. Prod. Res. Dev. 18 (1979) 2.

25. N.A. Alford, A. Barrie, I.W. Drummond and Q.C. Herd, "Auger Electron Spectroscopy (AES): An Appraisal," *Surface and Interface Analysis*, 1 (1979) 36.
26. G.A. Somorjai, "Auger Electron Spectroscopy", write-up from a course presented at Exxon Corp., Linden, N.J., LBL-11720 (1980).
27. W.A. Coghlan and R.E. Clausing, A Catalogue of Auger Transitions for the Elements, Oak Ridge National Laboratory, ORNL-TM-3576, Nov. 1971.
28. F.N. Palmberg, G.E. Riach, R.E. Weber and N.C. MacDonald, Handbook of Auger Electron Spectroscopy, Physical Electronics Ind., Minnesota (1972).
29. P.B. Needham, T.J. Driscoll and N.G. Rao, *Appl. Phys. Lett.* 21 (1972) 502.
30. E.L. Garfunkel, Ph.D. thesis, University of California, Berkeley, 1983, unpublished.
31. P.A. Redhead, *Vacuum* 12 (1962) 203.
32. D.A. King, *Chem. and Phys. of Solid Surf. II*, CRC Press (1979).
33. L.A. Petermann, *Prog. Surf. Sci.* 3 (1972) 1.
34. R. Gorte and L. Schmidt, *Surf. Sci.* 76 (1978) 559.
35. F.C. Tompkins, Chemisorption of Gaseous Metals, Academic Press, London (1978).
36. C.M. Chan, R. Aris and W.H. Weinberg, *Appl. Surf. Sci.* 1 (1978) 360.
37. D. Edwards, Jr., *Surf. Sci.* 54 (1976) 1.

38. L.J. Clarke, Surface Crystallography: An Introduction to Low Energy Electron Diffraction, John Wiley, New York (1985).
39. J.B. Pendry, Low Electron Diffraction: The Theory and its Application to Determination of Surface Structure, Techniques in Physics Series No. 2, C.K.T. Conn and K.R. Coleman, eds., Academic Press, New York (1974).
40. P.M. Marcus and F. Jona, eds., Determination of Surface Structure by LEED, Plenum Press, New York (1980).
41. M.A. Van Horne and S.Y. Tong, Surface Crystallography by LEED: Theory, Computation and Structural Results, Springer Series in Chemical Physics 2, Springer-Verlag, New York (1979).
42. K. Heinz and K. Muller, "LEED Intensities - Experimental Progress and New Possibilities of Structure Determination" in Springer Tracts in Modern Physics, Vol. 91: Structural Studies of Surfaces, G. Hohler, ed., Springer-Verlag, New York (1982).
43. R.J. Koestner, M.A. Van Hove and G.A. Somorjai, Surf. Sci. 121 (1982) 321.
44. P.G. Hall and C.J. Wright, "Neutron Scattering from Adsorbed Molecules, Surfaces, and Intercalates, published in Chemical Physics of Solids and their Surfaces, Vol. 17.
45. R.P. Cooney, G. Lurthoys, and N.T. Tam, Advan. Catal. 24 (1975) 293.
46. R.K. Chang and T.E. Furtak, eds., Surface Enhanced Raman Scattering, Plenum, New York, 1982.
47. G.T. Haller, Catal. Rev. - Sci. Eng. 23 (1981) 477.

48. F.M. Hoffmann, Surf. Sci. Reports 3 (1983) 107.
49. R.P. Eischens and W.A. Pliskin, Adv. Catal. 10 (1958) 1.
50. W.N. Delgass, C.L. Haller, R. Kellerman, and J.H. Lunsford, Spectroscopy in Heterogenous Catalysis, Academic, New York, 1979.
51. M.L. Hair, Infrared Spectroscopy in Surface Chemistry, Marcel Dekker, New York, 1967.
52. S. Chiang, R.G. Tobin, and P.L. Richards, Phys. Rev. Lett. 49 (1984) 648.
53. R.M. Kroeker and P.K. Hansma, Catal. Rev. - Sci. Eng. 23 (1981) 553.
54. F. Trager, H. Coufal, and T.J. Chuang, Phys. Rev. Lett. 49 (1982) 1720.
55. H. Ibach and D.L. Mills, Electron Energy Loss Spectroscopy and Surface Vibrations, Academic, New York, 1982, and references therein.
56. R.F. Willis Ed., Vibrational Spectroscopy of Adsorbates, Springer-Verlag, Berlin-Heidelberg-New York, (1980).
57. H. Froitzheim, Electron Energy Loss Spectroscopy, published in Electron Spectroscopy for Surface Analysis, Topics in Current Physics 4, H. Ibach ed., Springer-Verlag, Berlin-Heidelberg-New York (1977) 205-250.
58. H. Ibach, H. Hopstser, and B. Sexton, Appl. Surface Sci. 1 (1977) 1.
59. B.A. Sexton, Appl. Phys. A26 (1981) 1.
60. Ph. Avouris and J.E. Demuth, Ann. Rev. Phys. Chem. 35 (1984) 49.

61. N. Sheppard and J. Erkelens, *Applied Spectroscopy* 38 (1984) 471.
62. H. Froitzheim, H. Ibach and S. Lehwald, *Rev. Sci. Instrum.* **46** (1975) 1325.
63. D. Roy and J.D. Carette, *Design of Electron Spectrometers for Surface Analysis*, Published in Electron Spectroscopy for Surface Analysis, Topics in Current Physics 4, H. Ibach, ed., Springer-Verlag Berlin-Heidelberg-New York, 1977, 13-58.
64. J.E. Katz, P. W. Davies, J.E. Crowell and G.A. Somorjai, *Rev. Sci. Instrum.* 53 (1982) 785.

CHAPTER 3

IDENTIFICATION OF SURFACE HYDROCARBON SPECIES: HREELS, LEED AND TDS STUDIES ON Rh(111), Rh(100) AND Pt(111)

3.1 Interpretation of HREEL Spectra: Ethylidyne (CCH_3) on Rh(111)

3.1.1 Background. Ethylidyne (CCH_3) is the adsorbed hydrocarbon species which has been most extensively studied and whose surface bonding is best understood. This interesting species readily forms by the dissociative adsorption of ethylene at room temperature on the close-packed (111) surfaces of Pt, Pd, and Rh and on the close-packed Ru(001) surface.

Ethylidyne species were first isolated (unknowingly) on Pt(111) in 1976 by the reaction of acetylene with contaminant surface hydrogen atoms [1]. The first identification of ethylidyne species came in 1979 [2] and was based on an analysis of the (2x2) ethylidyne LEED structure on Pt(111) and a comparison of the HREEL vibrational spectra for this monolayer to model compounds. Since then, ethylidyne has been thoroughly characterized on Pt(111) by UPS [3], XPS [4], TDS [5-9], LEED [2,10], HREELS [5,11], SIMS [12], NEXAFS [13] and molecular orbital calculations [14-17] and on Pt particles by NMR [18] and transmission IR [19].

The initial confusion about the identity of surface ethylidyne [CHCH_3 (ethylidene) and CHCH_2 (vinyl) were also proposed] arose from (1) not knowing the surface stoichiometry and (2) misinterpretations of the HREEL spectra. Extensive accounts of this controversy have been given [20,21]. The issue was resolved by using TDS to determine the

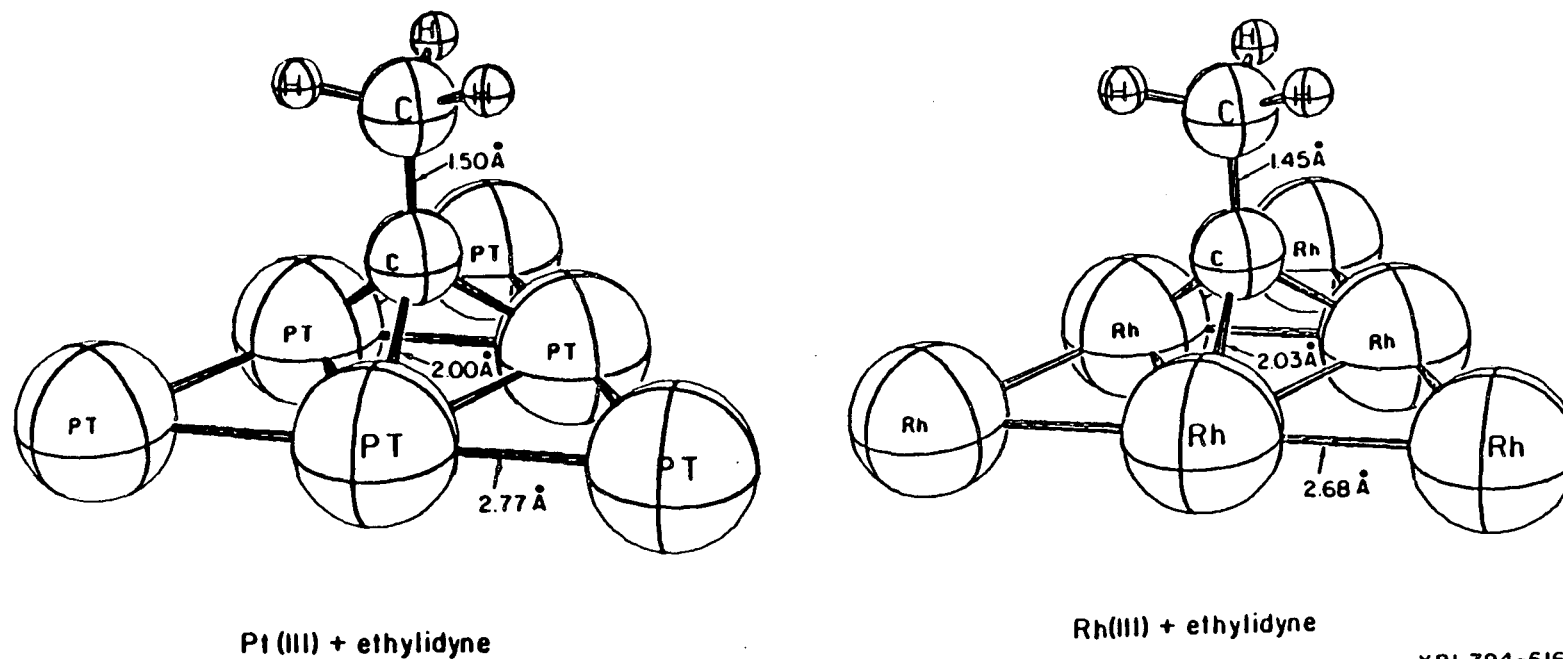
H:C ratio, comparing the HREEL spectra to model compounds, and performing a LEED analysis using the model suggested by HREELS.

The bonding geometries determined by LEED for ethynidyne on Pt(111) [2] and Rh(111) [22] are shown in Fig. 3.1. The bond lengths are accurate to $\pm 0.1 \text{ \AA}$. These geometries are compared in Fig. 3.2 to the geometries determined by x-ray crystallography for ethynidyne ligands in trimetallic clusters. The similarities are quite remarkable. On both Pt(111) and Rh(111) and in these clusters the ethynidyne ligand binds symmetrically between three metal atoms with its C-C bond perpendicular to the plane of metal atoms. The C-C bond lengths are approximately the same as the single bond in ethane and the metal-carbon bond lengths are nearly equal to the sum of the carbon and metal covalent radii. The major difference in ethynidyne bonding to Pt(111) and Rh(111) is that ethynidyne binds to an fcc hollow site on Pt(111) and to a hcp hollow site on Rh(111) (Fig. 1.1).

In the following section the HREEL spectra for this ethynidyne species on Rh(111) are used to illustrate the techniques for interpreting HREEL spectra that are employed throughout this thesis. The HREEL spectra presented offer improved resolution over previously published spectra [23] as well as new data at off-specular collection angles.

3.1.2 Interpretation of the HREEL Spectra. There is no set recipe for assigning a new surface vibrational spectrum. Usually the spectra are interpreted by a combination of deductive reasoning and process of elimination: vibrational frequencies and intensities are used along

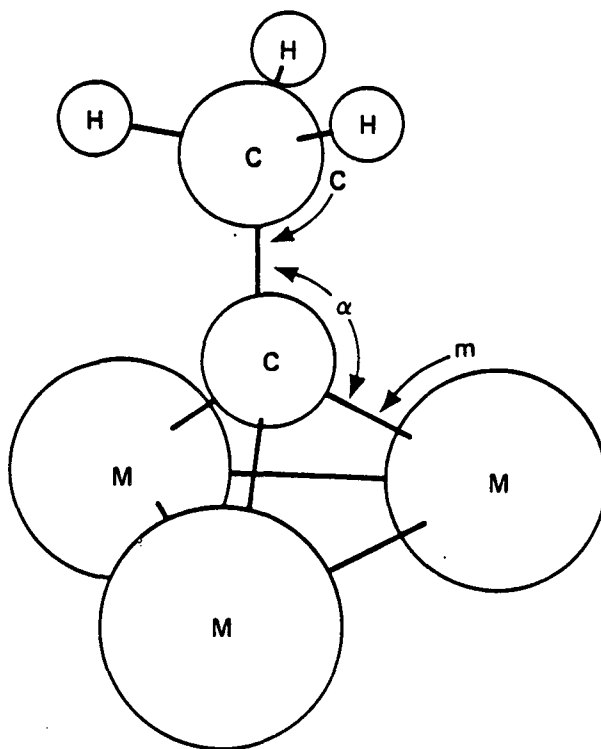
Bonding of Ethylidyne on Pt(III) and Rh(III)



XBL794-6167A

Fig. 3.1 Bonding geometries determined by LEED surface crystallography for ethylidyne (CCH_3) on Pt(111) and Rh(111). Ethylidyne is the stable surface species that is produced by dissociative adsorption of ethylene on these surfaces at room temperature.

Different ethylidyne species: bond distances and angles
 (r_C = carbon covalent radius; r_M = bulk metal atomic radius)



	C [Å]	m	r_M	r_C	α [°]
$\text{Co}_3(\text{CO})_9\text{CCH}_3$	1.53 (3)	1.90 (2)	1.25	0.65	131.3
$\text{H}_3\text{Ru}_3(\text{CO})_9\text{CCH}_3$	1.51 (2)	2.08 (1)	1.34	0.74	128.1
$\text{H}_3\text{Os}_3(\text{CO})_9\text{CCH}_3$	1.51 (2)	2.08 (1)	1.35	0.73	128.1
$\text{Pt}^\dagger(111) + (2 \times 2)\text{CCH}_3$	1.50	2.00	1.39	0.61	127.0
$\text{Rh}(111) + (2 \times 2)\text{CCH}_3$	1.45 (10)	2.03 (7)	1.34	0.69	130.2
$\text{H}_3\text{C} - \text{CH}_3$	1.54			0.77	109.5
$\text{H}_2\text{C} = \text{CH}_2$	1.33			0.68	122.3
$\text{HC} \equiv \text{CH}$	1.20			0.60	180.0

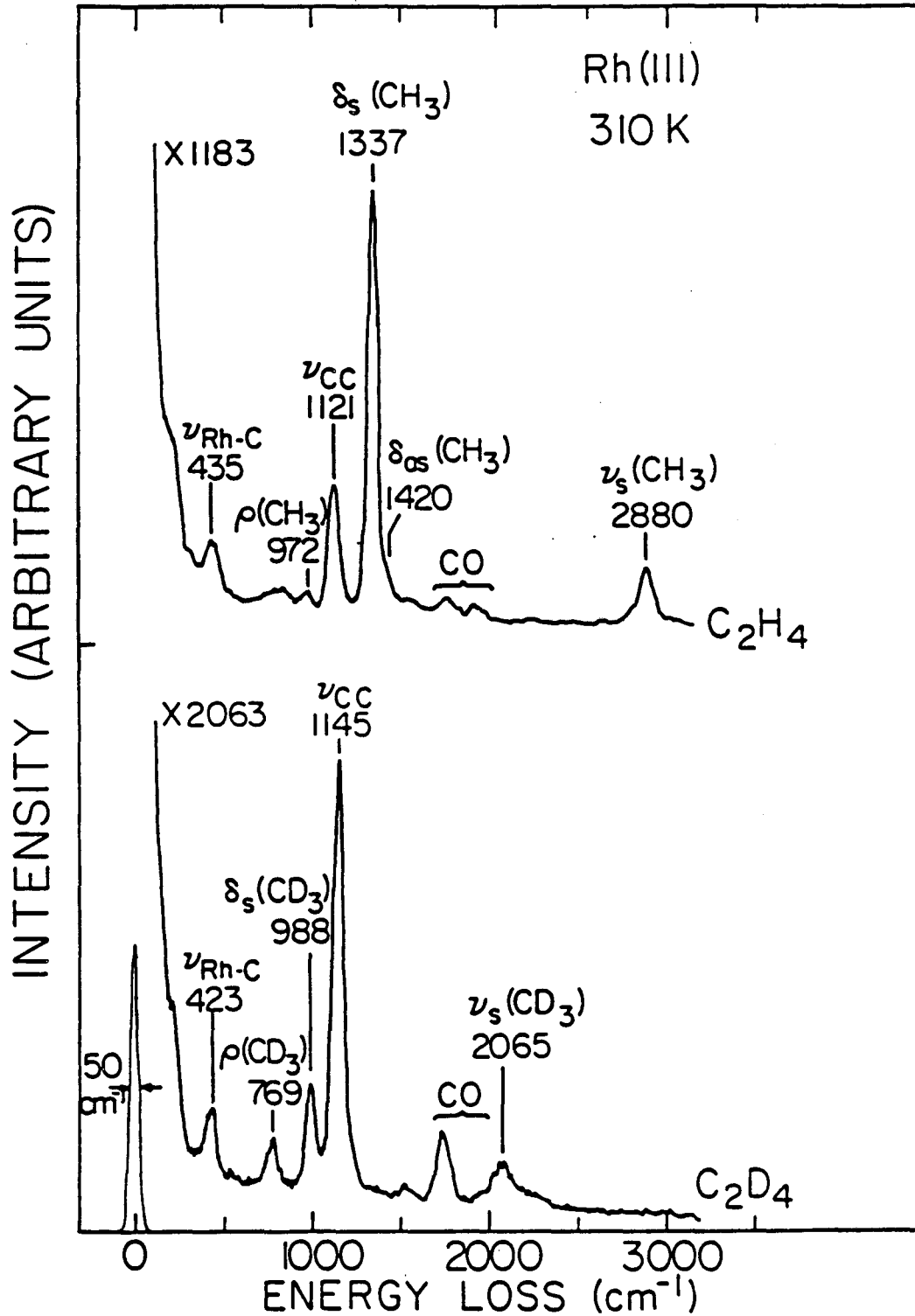
XBL 818-11196

Fig. 3.2 Comparison of bond lengths and bond angles in surface- and cluster-bound ethylidyne species. Corresponding parameters for acetylene, ethylene and ethane are also given for comparison.

with information from other techniques to deduce the presence of certain functional groups and rule out the presence of others. For the sake of illustration the ethylidyne HREEL spectra will be interpreted without assuming that the surface species is ethylidyne. However, this discussion is predicated on the previous discussions of vibrational spectroscopy in Chapter 1 and of HREELS in Section 2.4.4.

a) Information From Other Techniques. HREEL spectral assignments are greatly simplified by using other surface science techniques to limit the possible surface species. For example, AES and TDS are particularly useful for determining surface composition and stoichiometry, while ordered LEED patterns can be strong evidence for the presence of only one surface species. In the case of ethylidyne on Rh(111), AES and TDS show that the surface stoichiometry is about $\text{CH}_{1.5}$ [5-9]. Also, a number of ordered LEED structures (which will be discussed in Section 3.2) are found for ethylidyne [22,24]. If we assume, based on the formation of ordered structures, that only one species exists on the surface, then its stoichiometry must be C_2H_3 if no polymerization occurs.

b) Functional Group Frequencies. As discussed in Chapter 1, certain bonding arrangements of a group of atoms, called functional groups, can have characteristic vibrational frequencies that are largely independent of the surrounding molecular environment. For adsorbed hydrocarbons the functional group modes and frequencies are generally quite similar to those for gas phase hydrocarbons. The functional group modes for CH_2 and CH_3 groups are illustrated in



XBL 838-6209

Fig. 3.3 Specular HREEL spectra of a Rh(111) surface following saturation doses of C_2H_4 and C_2D_4 at 310 K to form surface ethylidyne species.

refs. 25 and 26. The vibrational frequencies for such groups depend mainly on the hybridization of the carbon atom and on the number of hydrogens attached. Expected frequency ranges for these different CH_x groups have been given by Ibach and Mills [26].

Different regions of the vibrational spectrum can be distinguished based on the type of functional group vibration. For example, each CH_x group has vibrational frequencies in two distinct frequency regions; the CH_x stretching region ($2600\text{--}3300\text{ cm}^{-1}$) and the CH_x bending region ($700\text{--}1500\text{ cm}^{-1}$) [27]. Generally the CH_x stretching frequencies lie above 2800 cm^{-1} unless there is a direct interaction between the C-H bonds and the metal surface [28]. Carbon-carbon stretching frequencies ($900\text{--}1900\text{ cm}^{-1}$) overlap the C-H bending region, while vibrations below 700 cm^{-1} for hydrocarbon adsorbates are generally vibrations of the entire molecule against the surface.

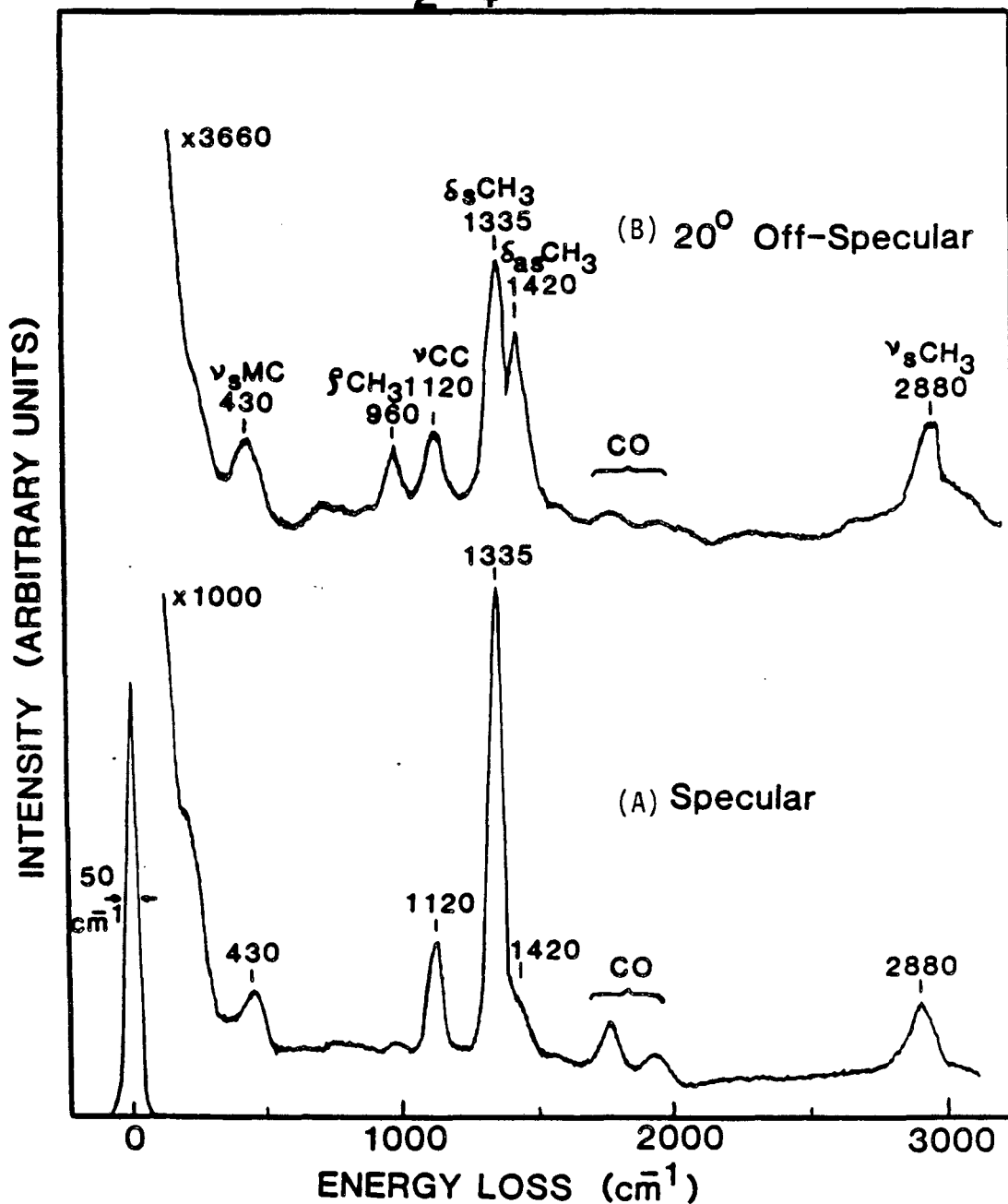
These different types of vibrations are evident in the HREEL spectrum of ethylidyne on Rh(111) shown in the top of Fig. 3.3. The frequency at 2880 cm^{-1} in the CH_x stretching region is characteristic of an sp^3 hybridized carbon with two or three attached hydrogens. The 435 cm^{-1} peak falls in the metal-molecule vibration region. Of the three peaks (972 , 1121 , and 1337 cm^{-1}) in the CH_x bend/C-C stretch region, the intense 1337 cm^{-1} peak can be narrowed down to a CH_2 bending, a CH_3 bending, or a C-C stretching vibration, since a CH group has no mode near this frequency.

c) Isotope Shifts. Deuteration of ethylidyne (Fig. 3.3 bottom) shows that the 1337 cm^{-1} peak in the hydrogenated spectrum cannot be a C-C stretching vibration. This is because no peak is observed near 1337 cm^{-1} in the deuterated spectrum, and C-C stretching frequencies are not substantially shifted by deuteration.

Two species are possible which have C_2H_3 stoichiometry as well as either a CH_2 or a CH_3 group: HCCH_2 and CCH_3 . An HCCH_2 species can be ruled out by HREEL spectra taken at off-specular collection angles as detailed below.

d) Off-Specular HREEL Spectra. The simplest use of off-specular HREEL spectra is for observing modes obscured by intense, dipole-active modes in the specular HREEL spectrum. Figure 3.4 shows HREEL spectra of ethylidyne on Rh(111) taken at (A) specular and (B) 20° off-specular collection angles. From the off-specular spectrum in Fig. 3.4B it is obvious that there are two vibrational frequencies near 1400 cm^{-1} : one at 1335 cm^{-1} and one at 1420 cm^{-1} . This rules out a CH_2 group, since a CH_2 group has only one vibrational mode in this frequency range (a CH_2 scissors vibration [26]) while a methyl group has three (1 symmetric and 2 antisymmetric bends [26]). In this case, the methyl group symmetric bend occurs at 1335 cm^{-1} and the two antisymmetric bends occur unresolved and possibly doubly degenerate at 1420 cm^{-1} . The surface species is therefore CCH_3 .

e) Dipole Selection rule. As mentioned in Section 2.4.4, the dipole selection rule can be used to determine the symmetry, binding site and orientation of adsorbed ethylidyne. First, the on- and

HREELS $C_2H_4 / Rh(111)$ T = 310 K

XBL 8512-4942

Fig. 3.4 HREEL spectra of a saturation coverage of ethylidyne on Rh(111) at 310 K taken at (A) specular and (B) 20° off-specular collection angles. Also shown is the spectral assignment which is tabulated in Table 3.1 and discussed in the text.

off-specular HREEL spectra must be compared to determine which modes are dipole-active. Comparison of Figs. 3.4A and 3.4B shows that the 1335 cm^{-1} symmetric CH_3 bend is dipole-active while the 1420 cm^{-2} antisymmetric CH_3 bend is dipole-inactive based on the large increase in the relative intensity of the 1420 cm^{-1} peak in the off-specular spectrum. In other words, the symmetric CH_3 bend maintains all the symmetry elements in adsorbed ethylidyne while the antisymmetric bend does not.

The highest possible symmetry for adsorbed ethylidyne is C_{3v} . To achieve this symmetry the ethylidyne species must stand vertically on the surface. Tilting of the C-C bond away from the surface normal along a symmetry plane on the surface lowers the point group symmetry to C_s , while tilting along some nonsymmetric plane lowers the symmetry to C_1 [29,30].

Only for C_{3v} symmetry will the ethylidyne molecular symmetry be maintained by the symmetric CH_3 bend and broken by the antisymmetric CH_3 bend. This means the ethylidyne species stand vertically on the surface with C_{3v} symmetry. C_{3v} symmetry also requires that ethylidyne bind either on a top site to a single atom or in a 3-fold hollow site between three metal atoms.

f) Model Compounds. A complete HREEL spectral assignment can generally be made once the identity of the surface species is known by comparing the surface vibrational frequencies to those of model compounds. For ethylidyne, an organic molecule like Br_3CCH_3 [3] or organometallic complexes like $(\text{CO})_4(\text{I})\text{W}(\text{CCH}_3)$ [32] and $(\text{CO})_9\text{Co}_3(\text{CCH}_3)$

[33] are appropriate model compounds. The vibrational frequencies measured for the tribromide and the tricobalt ethylidyne cluster are compared to the Rh(111)/ethylidyne vibrational frequencies in Table 3.1. The tricobalt cluster, gives excellent agreement with the surface vibrational frequencies.

g) Normal Coordinate Analysis. The complete assignment of the observed frequencies to the functional group modes in Column 1 of Table 3.1 is possible, because a normal coordinate analysis was performed on the tricobalt cluster [11]. In such a normal coordinate analysis the vibrational frequencies and amplitudes are calculated by treating the molecule as collection of hard spheres held together by springs. The atomic masses, bond distances, and appropriate spring constants are input into the calculation, and the classical equations of motion are solved in the harmonic oscillator approximation to determine the vibrational normal modes and their frequencies. Such normal coordinate analyses are not yet readily attainable for surface species, because bond distances and appropriate metal-carbon spring constants for surface species are generally not known.

Several points about the assignment of the ethylidyne vibrational frequencies in Table 3.1 deserve comment. First, the modes with A_1 symmetry ($\nu_s CH_3$, $\delta_s CH_3$, ν_{CC} , and $\nu_s MC$) are those that (1) maintain all the C_{3v} symmetry elements in ethylidyne, (2) are most intense in the specular HREEL spectrum, and (3) are dipole-active judging by their decrease in relative intensity in the off-specular spectrum. Second, the isotope shifts upon deuteration are as

Table 3.1: Comparison of the vibrational frequencies (cm^{-1}) for ethylidyne on the Rh(111) surface with those for CCH_3 ligands in model compounds

Mode Description	Symmetry	$\text{CH}_3\text{C} - \text{Rh}(111)$ [a]	$\text{CH}_3\text{C} - \text{Co}_3(\text{CO})_9$ [b]	$\text{CH}_3\text{C} - \text{CBr}_3$ [c]
$\nu_{\text{as}}(\text{CH}_3)/\nu_{\text{as}}(\text{CD}_3)$	E	2920(vw)/2178(vw)	2930(m)/2192(w)	2993(m)/2241
$\nu_{\text{s}}(\text{CH}_3)/\nu_{\text{s}}(\text{CD}_3)$	A_1	2880(w)/2065(vw)	2888(m)/-----	2938(m)/2116
$\delta_{\text{as}}(\text{CH}_3)/\delta_{\text{as}}(\text{CD}_3)$	E	1420(sh)/-----	1420(m)/1031(w)	1432(m)/1038(w)
$\delta_{\text{s}}(\text{CH}_3)/\delta_{\text{s}}(\text{CD}_3)$	A_1	1337(s)/ 988(w)	1356(m)/1002(vw)	1373(m)/1100(w)
$\nu(\text{CC})$	A_1	1121(m)/1145(m)	1163(m)/1182(ms)	1045(m)/ 953(w)
$\rho(\text{CH}_3)/\rho(\text{CD}_3)$	E	972(vw)/ 769(vw)	1004(s)/ 828(s)	1064(s)/ 883(m)
$\nu_{\text{s}}(\text{MC})$	A_1	435(w)/ 419(w)	401(m)/ 393(m)	408(m)/ 388(s)

a) this work

b) Skinner et al., ref. 11

c) Stengle and Taylor, ref. 31

s - strong, m - medium, w - weak,

v - very, sh - shoulder

expected, except for the ν_{CC} mode which actually shifts the wrong way with deuteration. This effect is the result of coupling of this mode with the $\delta_s CH_3$ and $\delta_s CD_3$ modes which have the same symmetry. Since the ν_{CC} frequency is greater than the $\delta_s(CD_3)$ frequency but less than the $\delta_s(CH_3)$ frequency, its frequency is pushed up in the former case and pushed down in the latter case by coupling. This produces the anomalous isotope shift.

It should also be noted that the relative intensities of the dipole active vibrations in ethylidyne on Rh(111) parallel the observed infrared (IR) intensities for ethylidyne in the tricobalt cluster. This is expected, since in both cases the vibrational excitation probability depends on the magnitude of the dynamic dipole moment.

h) Surface Chemistry. The use of surface chemistry to help confirm adsorbate structure has been largely overlooked. This is no doubt mainly a result of our present lack of understanding of surface chemistry. However, two examples of the use of surface chemistry in relation to ethylidyne deserve mention. First, TDS studies of propylene and 1-butene on Pt(111) give the expected results for "ethylidyne-type" chemistry [7]. These methyl- and ethyl-substituted ethylenes each lose one hydrogen at about 270K the way ethylene does to form ethylidyne. It was asserted based on these studies that propylidyne and butylidyne form in analogous fashion to ethylidyne, and this assertion is supported by recent HREEL spectra. Second, studies of H,D exchange in the ethylidyne methyl group on Rh(111) [34,35] and on Pt(111) [34] give the expected HREEL vibrational spectra for partially deuterated methyl

groups. More studies like these are needed to both support spectroscopic determinations and further our understanding of basic surface chemical reactions.

3.2 Ethylidyne Adsorbed on Rh(111) and Rh(100) in the Temperature Range of 200–400K

3.2.1 Background. All of the HREEL spectra for ethylidyne on Rh(111) in the previous section were obtained for saturation coverages [36] of ethylidyne at room temperature. However, it is known [21] that ethylidyne is also formed at low surface coverages, and at temperatures down to 200 K and up to 400 K. Further, a number of LEED patterns have been observed under these varied conditions [22,24,37]. For example, adsorption of a saturation coverage of ethylene between 200 and 270 K on Rh(111) produces the (2x2) LEED structure that was solved as shown in Fig. 3.1 [22]. However, it has also been reported that this (2x2) structure disorders when warmed rapidly to room temperature, and orders into a c(4x2) structure when warmed slowly [23,24]. HREELS does not show any changes in the ethylidyne vibrational frequencies in this (2x2) to c(4x2) transformation, and yet the c(4x2) structure has not been solved by LEED [37].

One obvious difference between the (2x2) and c(4x2) structures is that surface hydrogen atoms (produced in the formation of ethylidyne at 200 K) desorb during the conversion of the (2x2) structure to the c(4x2) structure at 270 K. This can explain why the long-range surface order changes, but it does not explain the difficulties in the LEED calculation which is insensitive to hydrogen atoms.

The recent observation that coadsorption of carbon monoxide (an ever present UHV contaminant) with organic adsorbates can lead to ordered coadsorption structures [38,39] led to an investigation of the

effects of CO on the (2x2) to c(4x2) ethylidyne transformation. The effects of surface coverage and temperature on the local bonding and long-range order of ethylidyne on Rh(111) were also investigated. The results of these studies are detailed in Section 3.2.2.

These results in turn inspired coadsorption studies of ethylene with CO on Rh(100) in which it was found that ethylidyne species can be produced by ethylene adsorption, if half a monolayer of CO is preadsorbed. The results of these studies are presented in Section 3.2.3. Finally, in Section 3.2.4 ethylidyne bonding to different metal surfaces and in various metal clusters is compared.

3.2.2 Ethylidyne + Carbon Monoxide on Rh(111). Low-Energy Electron Diffraction (LEED). The (2x2) LEED structure previously reported [12] for saturation coverages of ethylidyne on Rh(111) between 200 and 270 K was reproducible. However, upon warming to room temperature, only disordering of the (2x2) LEED pattern was observed; the c(4x2) structure could only be produced by coadsorption of CO. The LEED pattern that results from either warming the (2x2) ethylidyne structure to room temperature or adsorbing a saturation coverage of ethylidyne at room temperature is shown in Fig. 3.5B. The reproducible diffuse blotches that form around the $\sqrt{3}R30$ LEED spot positions indicate some short-range ordering of the ethylidyne species. This diffuse pattern is similar to the diffuse x-ray and electron scattering intensity calculated by Moret et al. [40] for microdomains of order in $Ti_{1-x}S_x$ compounds. In particular, the diffuse scattering intensity that they calculate (Fig. 3.5A) for small $(\sqrt{3} \times \sqrt{3})R30$ domains (Fig. 3.5C) compares

quite well to the ethylidyne/Rh(111) LEED pattern in Fig. 3.5B. Thus it appears that ethylidyne, which is stable in a (2x2) structure on Rh(111) in the presence of surface hydrogen, bunches up into small $(\sqrt{3}\times\sqrt{3})R30$ domains when the surface hydrogen desorbs.

It was observed that the (2x2) to c(4x2) transformation previously reported could be induced by warming the (2x2) ethylidyne structure to room temperature in the presence of CO(g). Up to 0.25 monolayers of CO can be coadsorbed with a (2x2) coverage of ethylidyne to produce a sharp c(4x2) LEED pattern. The best ordering is achieved by preadsorbing the quarter monolayer of CO followed by exposure to 10 L of ethylene. Although preadsorption of CO does not change the temperature at which ethylidyne forms, the c(4x2) structure can be produced preferentially over the (2x2) structure even at 220 K by CO preadsorption. Coadsorption of ethylidyne and CO did not substantially change either the CO desorption temperature (500 K) or the ethylidyne decomposition temperature (400 K).

High Resolution Electron Energy Loss Spectroscopy (HREELS). HREELS was used to detect any changes in the bonding of ethylidyne that may occur in the various ethylidyne and ethylidyne + CO monolayers on Rh(111). First, the HREEL spectra and surface structures of ethylidyne in the absence of coadsorbed CO are discussed. The (2x2) ethylidyne monolayer below 270 K and the disordered ethylidyne monolayer from 270-400 K have virtually identical HREEL spectra. It is concluded that the ethylidyne bonding in the disordered monolayer is the same as previously determined and shown in Fig. 3.1 for the (2x2) monolayer [22].

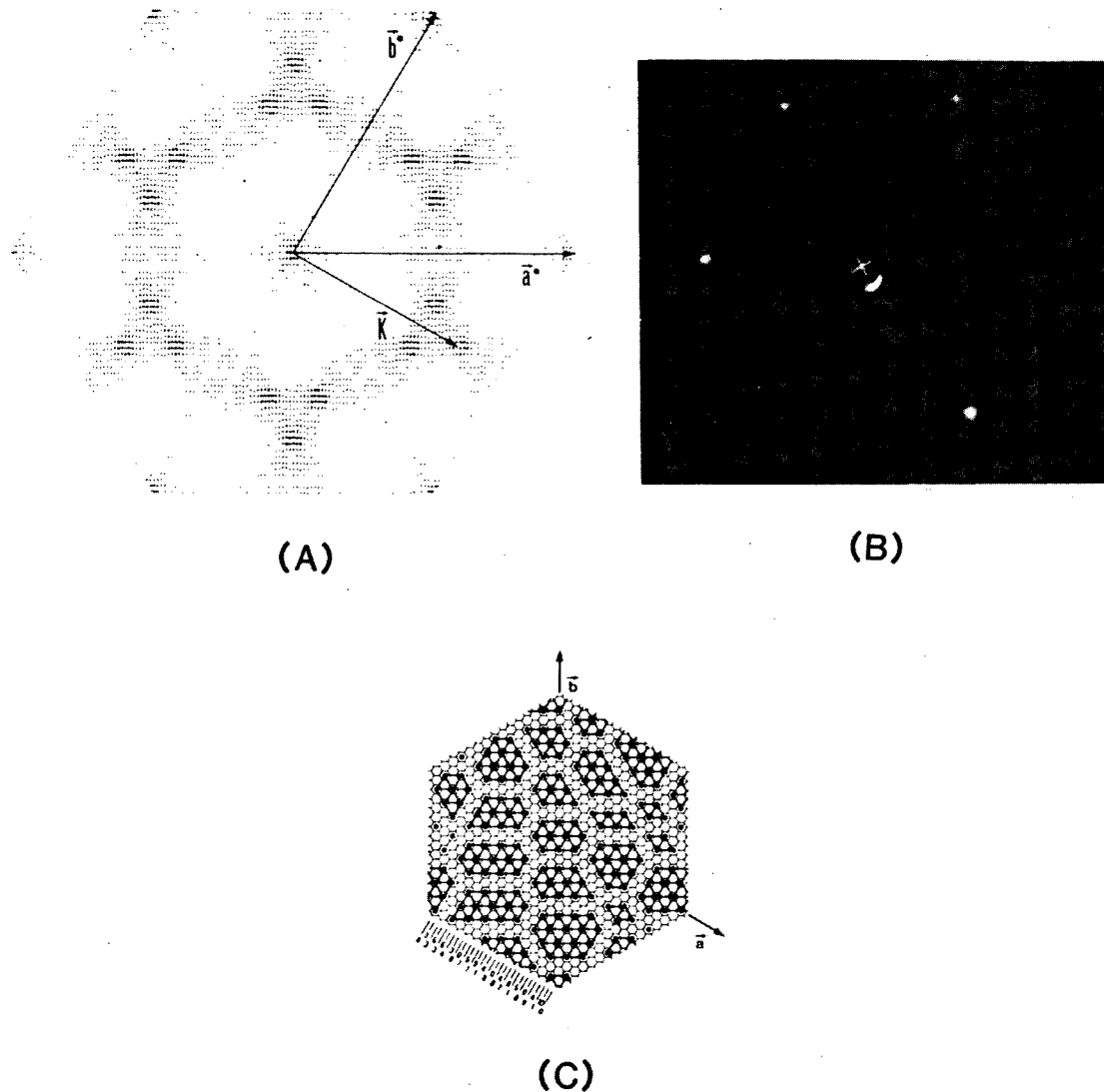


Fig. 3.5 Comparison of (B) the LEED pattern for a partially disordered ethylidyne overlayer at 310 K on Rh(111) with (A) the diffuse scattering intensity calculated by Moret et al. [40] for (C) a real space model containing adsorbates at a coverage of 0.3 in $(\sqrt{3}\times\sqrt{3})R30$ microdomains.

XBB 866-4939

The effects of coadsorbed CO on ethylidyne bonding are illustrated by the three representative HREEL spectra and LEED photos in Fig. 3.6. The LEED photo for ethylidyne plus 0.03 monolayers of CO is characteristic of ethylidyne adsorption at 310 K. Adding CO causes the blotches in the $\sqrt{3}R30^\circ$ positions of the LEED pattern to spread apart until the c(4x2) pattern shown in Fig. 3.6 is reached for 0.25 monolayers of added CO. While preadsorption of CO was necessary to form a sharp c(4x2) pattern, it was found that adsorption of NO, a ligand similar to CO, readily produced a sharp c(4x2) pattern even when adsorbed after formation of a disordered ethylidyne monolayer.

Several features of the ethylidyne + CO vibrational spectra in Fig. 3.6 are noteworthy. First, the ethylidyne frequencies are unchanged when CO is added, suggesting that ethylidyne bonding at 3-fold hollow sites is unchanged. Second, the predominant C-O stretching frequency at 1790 cm^{-1} is substantially lower than that observed for CO bonded at bridge ($\sim 1835\text{ cm}^{-1}$) or top ($\sim 2050\text{ cm}^{-1}$) sites on the clean Rh(111) surface [41,42]. This low frequency is characteristic of CO bonded at 3-fold hollow sites on Rh(111) [38,39]. These observations and use of van der Waals radii to determine the most probable packing of adsorbates lead to an obvious structural model for the c(4x2) CCH₃ + CO monolayer as shown in Fig. 3.7. Also shown are the (2x2) and disordered ethylidyne monolayer structures, and the temperature ranges for which each structure is stable.

Coadsorption of CO and Saturation Coverage of Ethylidyne

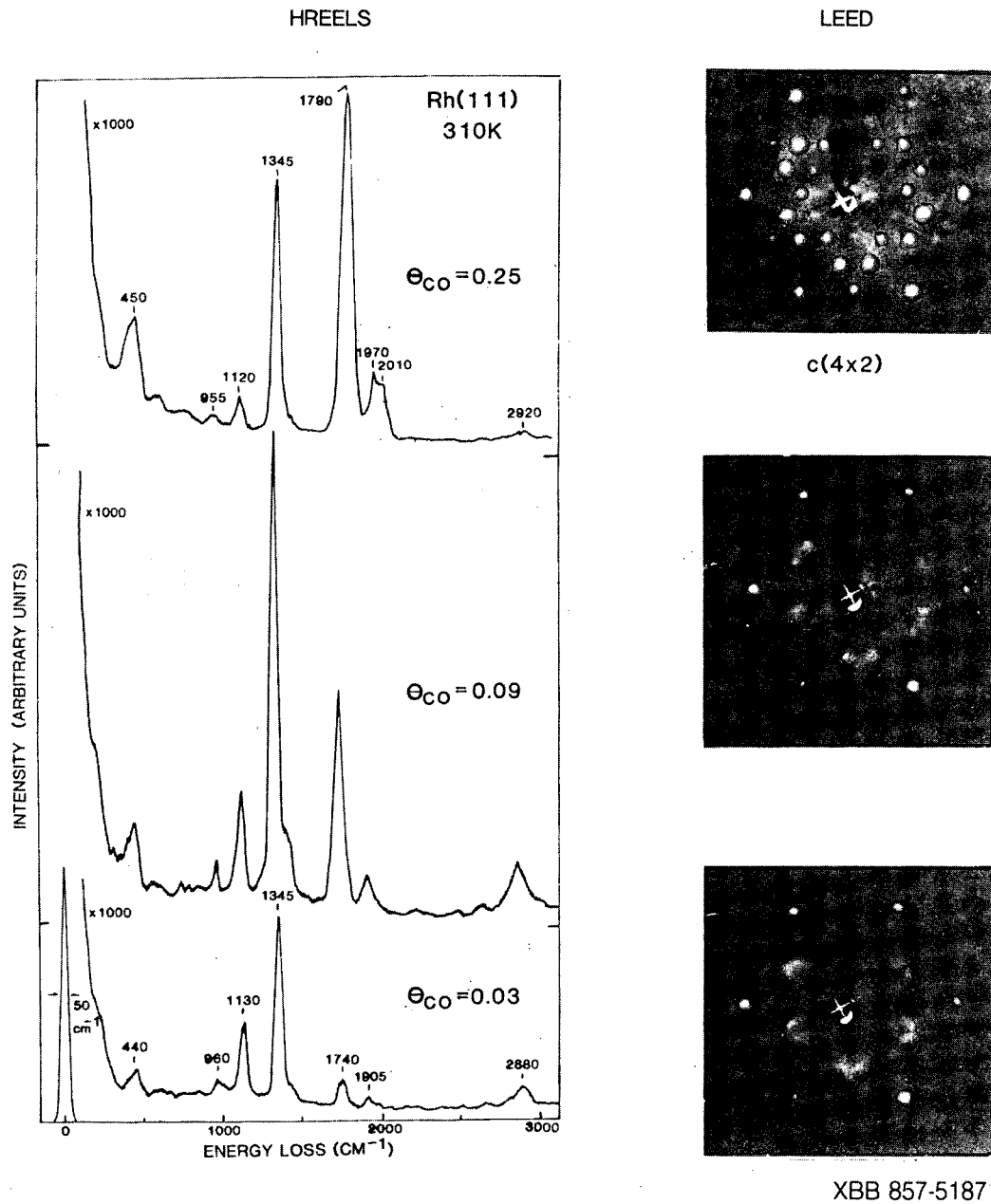


Fig. 3.6 HREEL spectra and LEED patterns obtained for ethylidyne and ethylidyne plus CO adsorbed on Rh(111) at 310 K. The coadsorbed monolayers were produced by preadsorption of the indicated CO coverages followed by 10 L exposures of C_2H_4 . The CO coverage, θ_{CO} , is defined as the number of CO molecules per surface Rh atom.

Recently, the $c(4 \times 2)$ structure has been solved by a dynamical LEED analysis [43]. This analysis, consistent with the proposed structure above, has determined that ethylidyne bonds in hcp 3-fold hollow sites with the same bond lengths as in the CO-free (2×2) structure. The co-adsorbed CO bonds in fcc 3-fold hollow sites.

It is interesting that CO and ethylidyne individually adsorb at quarter monolayer coverage in (2×2) lattices, and they coadsorb to give a $c(4 \times 2)$ lattice which is comprised of interpenetrating rectangular lattices of CO and CCH_3 . For a 0.25 monolayer coverage, the (2×2) structure leads to closer packing of the ethylidyne, but the $c(4 \times 2)$ arrangement leaves more room for another adsorbate like CO or NO. There is no obvious explanation for the previously published HREEL spectrum of a $c(4 \times 2)$ ethylidyne monolayer without CO [23], but it is possible that coadsorbed hydrogen or a hydrocarbon fragment (880 cm^{-1}) may be functioning like the CO.

One interesting feature of the HREEL spectra in Fig. 3.6 is that, with the addition of coadsorbed CO, the intensities of the ethylidyne ν_{CC} (1130 cm^{-1}) and $\nu_s CH_3$ (2880 cm^{-1}) peaks decrease dramatically relative to the intensity of the $\delta_s CH_3$ (1350 cm^{-1}) peak. Since a similar decrease is observed for deuterated ethylidyne, it is unlikely that coupling between the C-O stretching mode and the ethylidyne modes is responsible for the decreases in relative intensity. Also, a change in orientation of the ethylidyne can be ruled out as the cause, since this would result in all the modes of A_1 symmetry decreasing in intensity by approximately the same amount, while a change in the

Rh(111) / Ethylidyne Ordering

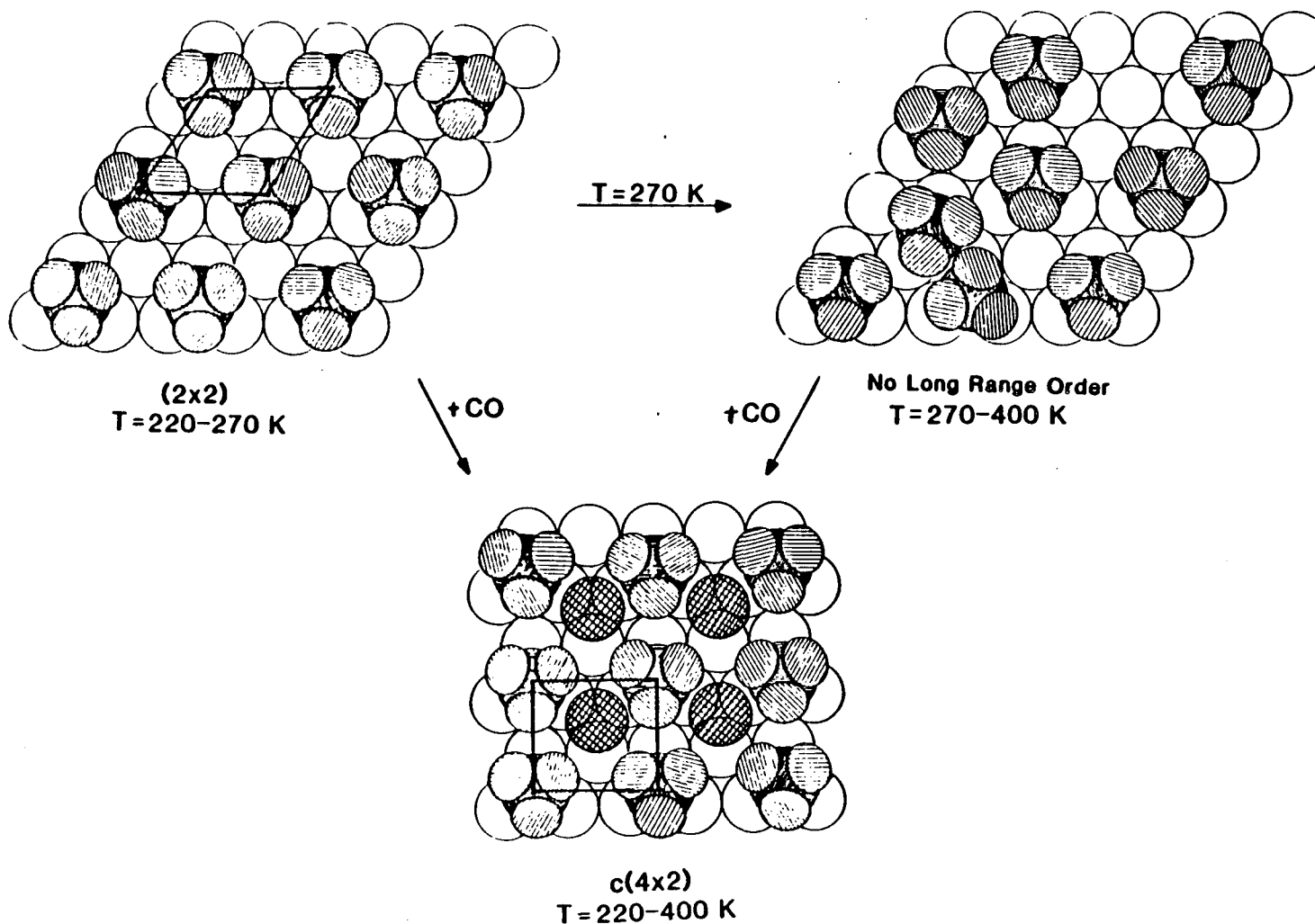


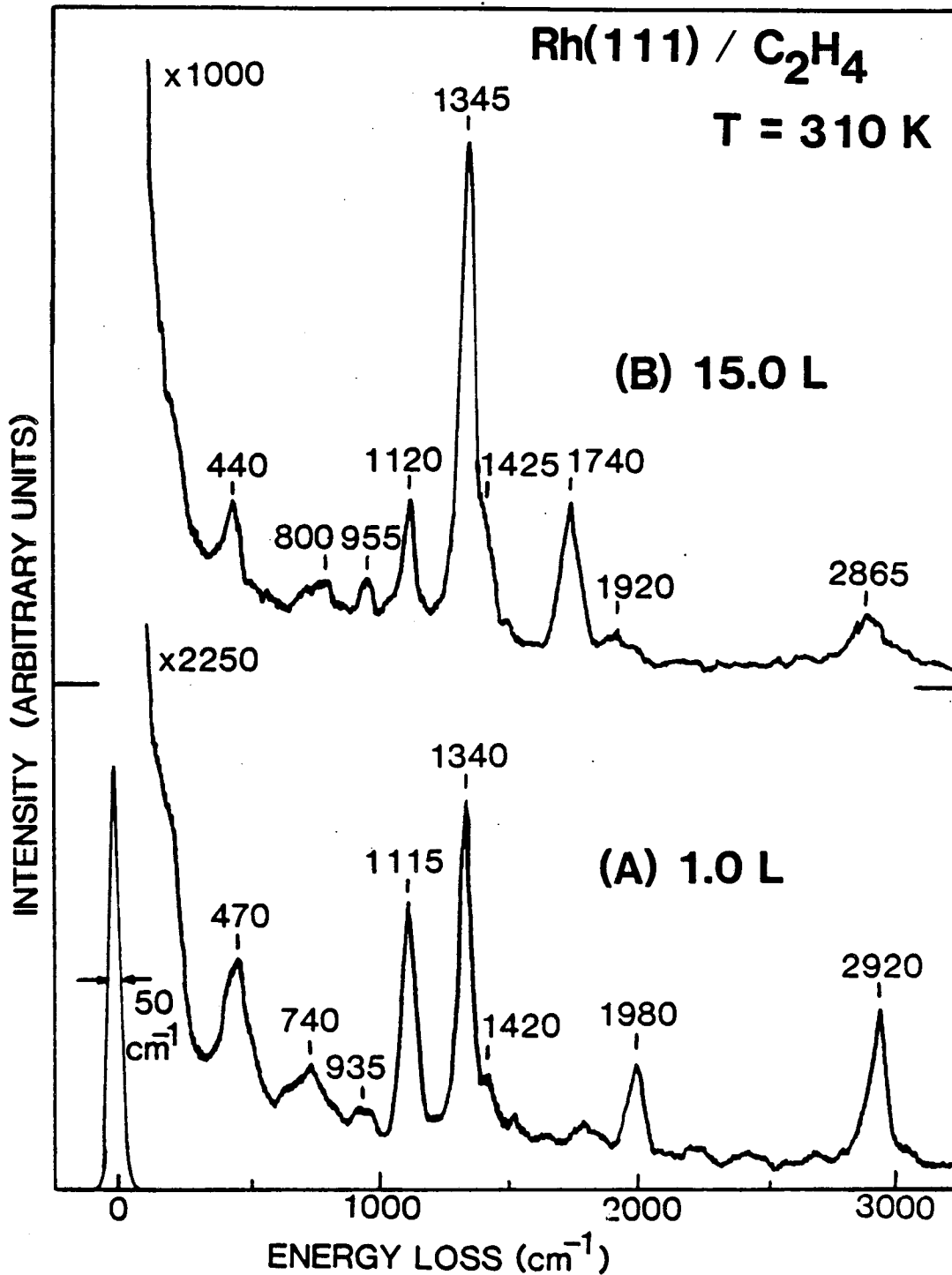
Fig. 3.7 Top views of Rh(111) surfaces showing the effects of temperature and CO on the ordering of a quarter monolayer of ethylidyne (CCH_3) species. The bonding sites and geometries for both of the ordered structures have been determined by LEED surface crystallography.

XBL 866-2421

ethylidyne adsorption site or internal bonding geometry would produce frequency shifts which are not observed.

The effects of CO coadsorption on the ethylidyne HREELS peak intensities are in fact a continuation of the changes observed in the relative ethylidyne peak intensities as the ethylidyne surface coverage is increased in the absence of CO. Figure 3.8 shows the specular HREEL spectra for low and high coverages of ethylidyne on Rh(111). At low ethylidyne coverages the relative intensity of the $\delta_s(\text{CH}_3)$ peak (1350 cm^{-1}) is less than at saturation coverage and much less than in the CO + ethylidyne $c(4 \times 2)$ HREEL spectrum (Fig. 3.6, top). Thus, the change in the relative peak intensities appears to depend more on surface coverage (and the distance between adsorbates) than on the chemical nature of the neighboring adsorbate.

This effect is reminiscent of the nonlinear intensity changes observed as a function of coverage for adsorbed carbon monoxide. In that case, saturation of the HREELS peak intensities was observed at high CO surface coverages, and has been attributed to the polarizability of the carbon monoxide [44]. In particular, an HREELS electron, besides exciting the CO stretching vibration, can also induce charge fluctuations in neighboring adsorbed CO's that oscillate with frequency components (including the ν_{CO} frequency) up to the HREELS cut-off [45] frequency. These oscillating dipolar fields can substantially decrease the effective electric field strength felt by an adsorbate at high surface coverages. Such induced dipole effects can explain why increasing the surface coverage of ethylidyne and coadsorbing CO with ethylidyne



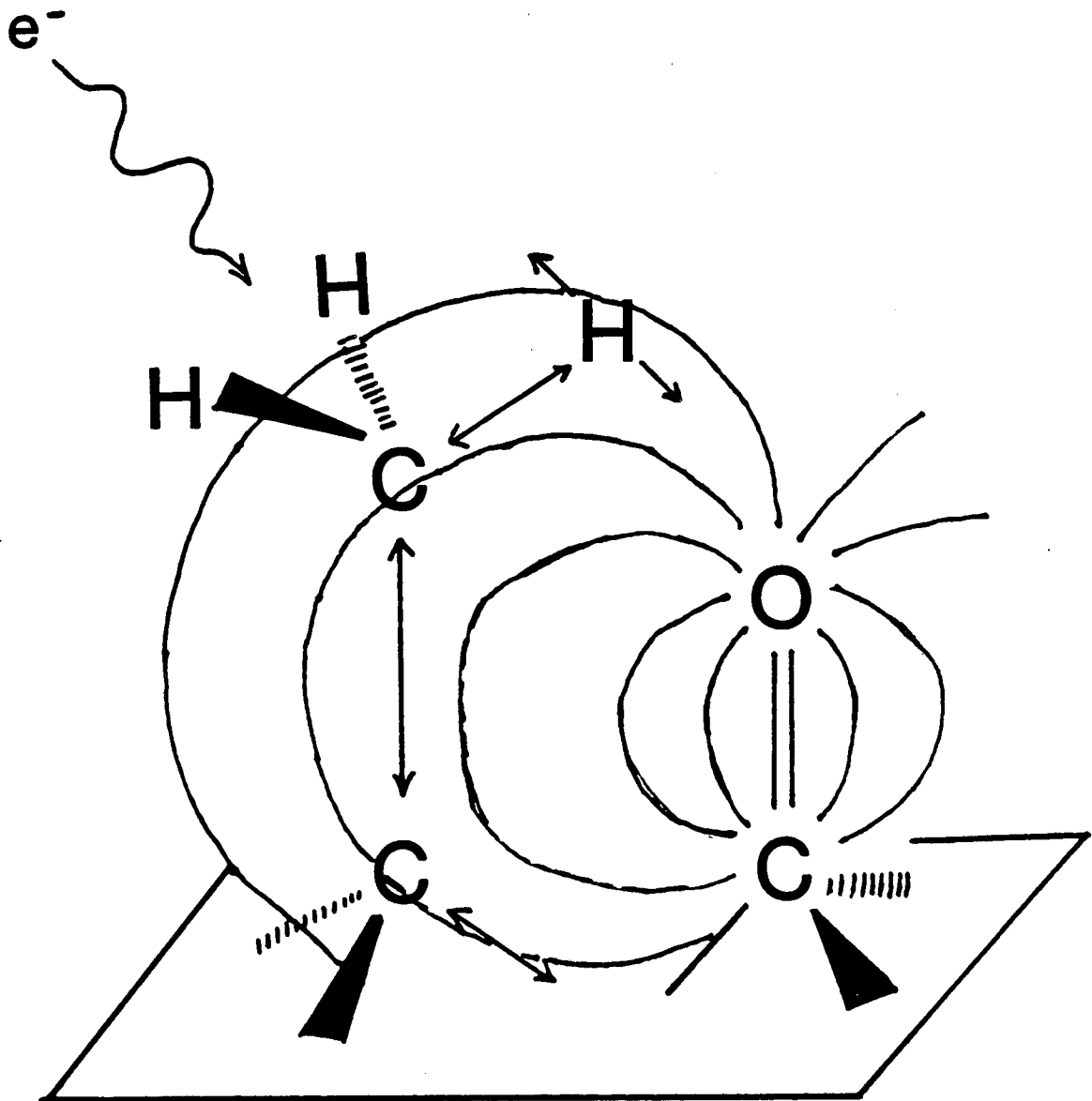
XBL 8610-3639

Fig. 3.8 Specular HREEL spectra for (A) 1.0 and (B) 15.0 L exposures of ethylene on Rh(111) at 310 K. The surface species in each case is ethynidyne.

have similar effects on the relative intensities. Further, the effect is expected to be more pronounced for coadsorbed CO, because the adsorbate coverage in the $c(4 \times 2)$ CO + ethylidyne structure is 0.5 ML while a saturation coverage of ethylidyne is only 0.25 ML.

If this induced dipole explanation is correct, then some HREELS peaks must be effected differently than others by the neighboring dipoles in order for the relative intensities to change. This could occur as shown Fig. 3.9. Here, the orientation of the dipolar field lines induced at a CO next to an ethylidyne are shown relative to the atomic motion for several ethylidyne normal modes. Those normal modes with atomic motion along the oscillating dipolar field lines from CO will show more intensity reduction than those modes whose atomic motion is more nearly perpendicular to the field lines. As seen in the schematic of Fig. 3.9, the C-H and C-C stretch motions occur much more along the field lines than the C-H bending motion, consistent with the observed intensity decreases in Fig. 3.6.

While induced oscillating dipoles are a likely explanation for the observed relative intensity changes with coverage in the ethylidyne HREEL spectra, the picture in Fig. 3.9 is quite simplistic. In particular, calculations are needed to include the effects of the induced dipoles in CCH_3 on CO, as well as the effects of CO on CO, and CH_3 on CCH_3 . Further, the effects of image charges induced in the metal (which have not been included in Fig. 3.9) must be explicitly considered.



XBL 8610-4112

Fig. 3.9 Schematic drawing of how the oscillating dipolar field induced in adsorbed carbon monoxide by an HREELS electron might be aligned with respect to the ethylidyne vibrational modes. The effects of image charges are not explicitly considered. As discussed in the text, it is proposed that this induced field is the major reason that the relative intensities of the ethylidyne HREELS peaks change in the presence of coadsorbed CO.

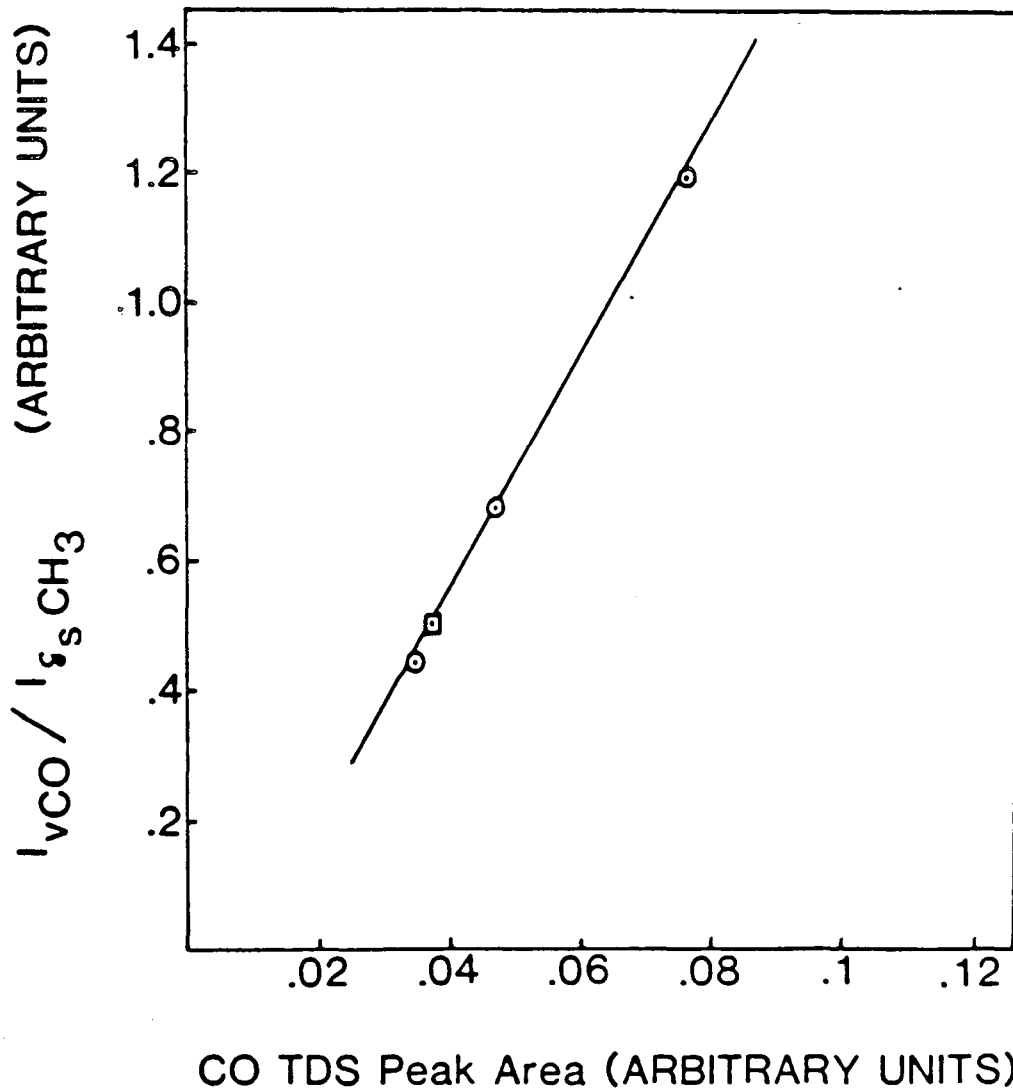
It is interesting to note that while the relative intensities of the ethylidyne peaks change with added CO, the intensity of the CO stretching frequency with respect to the $\delta_s(\text{CH}_3)$ mode intensity for ethylidyne remains proportional to CO coverage. This is shown in Fig. 3.10 which plots the $I(\nu\text{CO})/I(\delta_s\text{CH}_3)$ intensity ratio versus CO coverage measured by TDS.

It appears, then, that the local bonding of ethylidyne to Rh(111) is not substantially affected by changing the surface coverage, the surface temperature, or by coadsorbing CO or hydrogen. However, all of these parameters effect the long-range order on the surface.

3.2.3 Ethylene + Carbon Monoxide on Rh(100). The thermal chemistry of ethylene on Rh(100) is more complex than on Rh(111). More than one decomposition pathway is observed as a function of surface coverage and the branching ratio is affected by coadsorbed species. If ethylene is adsorbed on clean Rh(100) at room temperature, it decomposes to C_2H species up to surface coverages of $\theta_{\text{C}_2\text{H}} = 0.5$ (Section 3.5). Above this coverage, ethylene decomposes to ethylidyne. It has been found that preadsorption of CO has the same effect as C_2H on ethylene decomposition. That is, when 0.7 L of CO are dosed to make $\theta_{\text{CO}} = 0.5$, subsequent ethylene adsorption produces only ethylidyne.

In this section the HREEL spectra and LEED patterns for ethylene coadsorbed with CO on Rh(100) at room temperature are discussed. It is shown by assignment of the HREEL spectra that ethylidyne species can form on the Rh(100) surface.

Correlation of HREELS Peak Heights and
CO Coverage in Ethylidyne+CO Monolayers
on Rh(111)



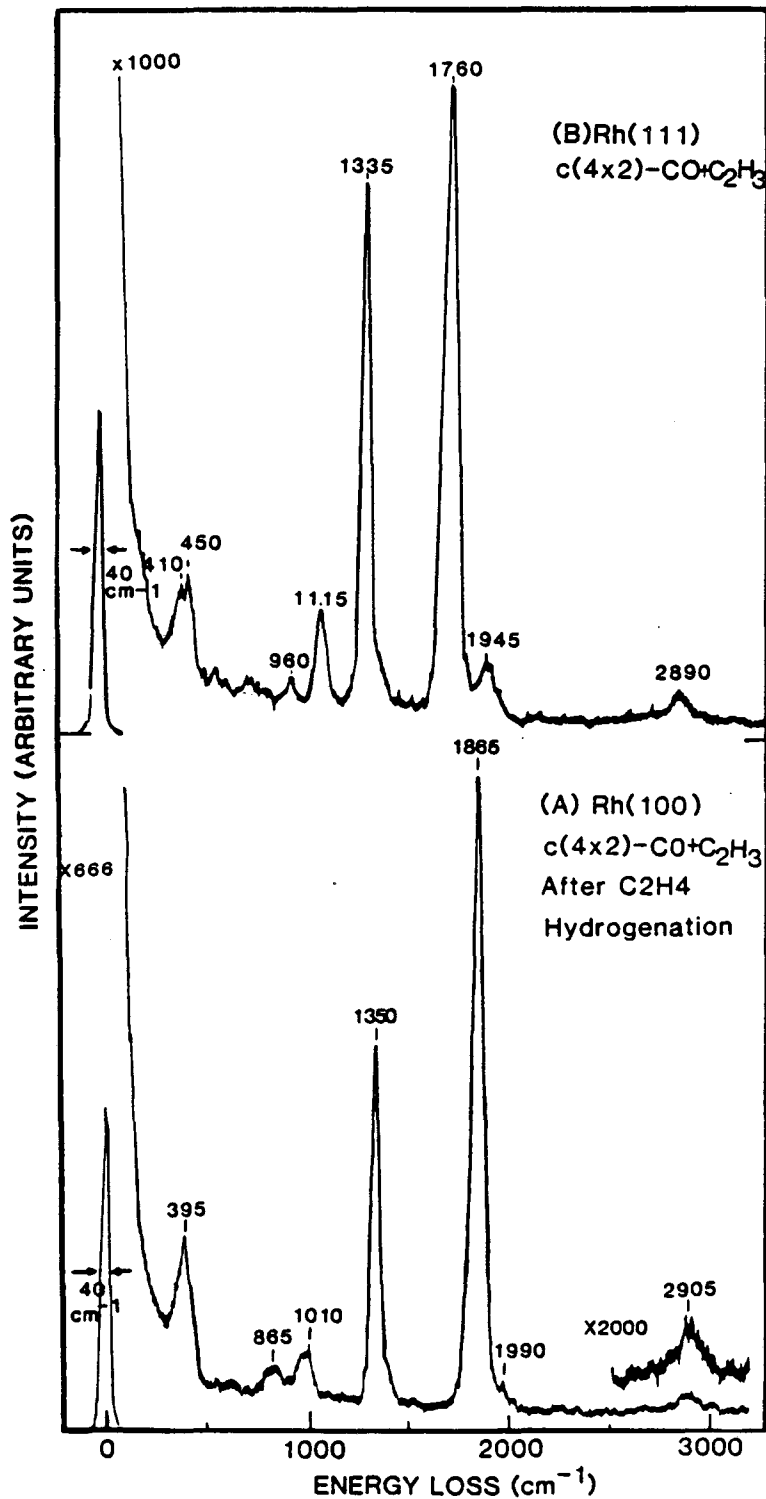
XBL 8610-4099

Fig. 3.10 Plot of the HREELS peak intensity ratio $I(\delta_s CH_3)/I(\nu CO)$ versus CO coverage (determined by TDS) in an ethylidyne monolayer on Rh(111).

Results. The HREEL spectra and LEED patterns that are attributed to ethylidyne + CO on Rh(100) in the following discussion are shown in Figs. 3.11-3.14. Figure 3.11 compares the HREEL spectrum of the monolayer remaining on Rh(100) after a catalytic ethylene hydrogenation reaction (Section 2.3) to a spectrum for ethylidyne + CO on Rh(111). This Rh(100) monolayer was produced accidentally by having contaminant CO in the high pressure cell. The similar numbers of peaks, relative intensities and peak frequencies in the Rh(111) and Rh(100) spectra is strong evidence for ethylidyne species on Rh(100).

Studies of ethylene coadsorption with CO in UHV were subsequently undertaken to try to reproduce this spectrum. Figure 3.12 shows the effects of CO preadsorption on ethylene decomposition at 320 K on Rh(100). Without any preadsorbed CO, the HREEL spectrum (Fig. 3.12A) is complex and is due to a mixture of surface fragments as discussed in Section 4.1. Preadsorption of 0.4 L of CO (Fig. 3.12B) reduces the relative intensity of the peaks at ~ 855 and $\sim 3035 \text{ cm}^{-1}$, and the CO stretching frequency for coadsorbed CO appears at 1870 cm^{-1} . By preadsorbing 0.7 L of CO, the 855 and 3035 cm^{-1} peaks are almost completely eliminated and the spectrum (Fig. 3.12C) is dominated by the 1355 cm^{-1} and 1880 cm^{-1} peaks. (The peak at $\sim 1000 \text{ cm}^{-1}$ is shown as two unresolved peaks because the peak width is greater than the spectral resolution.) Preadsorbing more than 0.7 L of CO does not change the peaks observed, but the intensity of the ethylene-derived peaks is reduced.

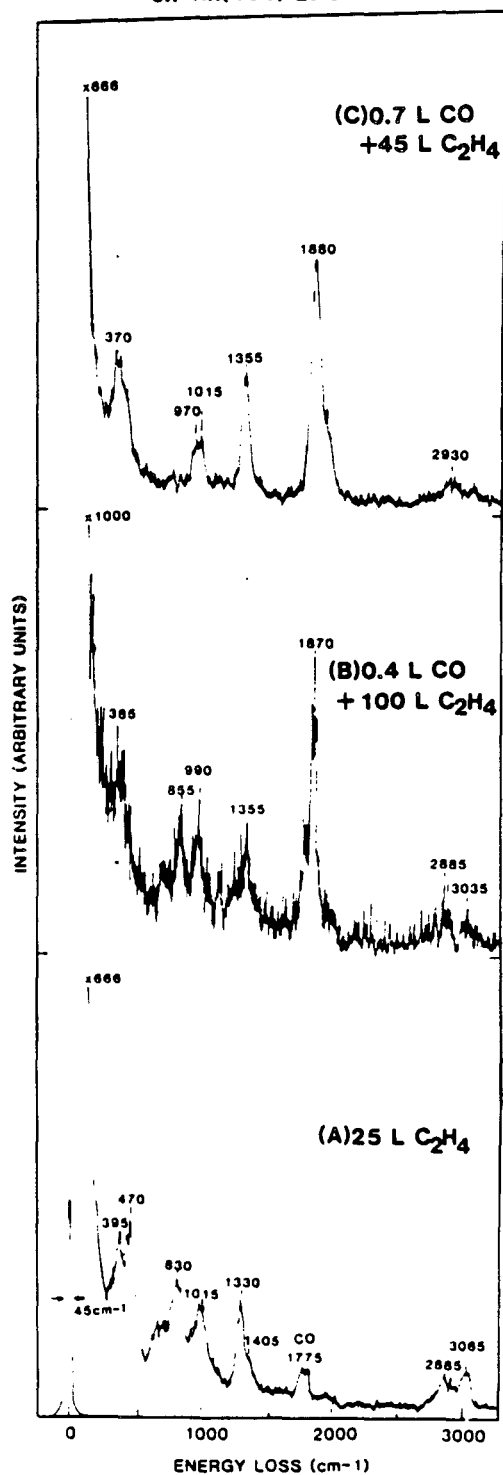
Coadsorption of CO with Ethylidyne



XBL 8610-3641

Fig. 3.11 Specular HREEL spectra of ethylidyne + CO monolayers on (A) Rh(100) and (B) Rh(111) surfaces. Both monolayers have c(4x2) LEED patterns. The Rh(100) structure was produced accidentally during a catalytic ethylene hydrogenation reaction at atmospheric pressure in which contaminant CO was present. The Rh(111) structure was produced by preadsorbing $\theta_{\text{CO}} = 0.25$ followed by 15 L of C₂H₄.

Coadsorption of CO with Ethylene
on Rh(100) at 320 K



XBL 86 10-3640

Fig. 3.12 Specular HREEL spectra showing the effects of CO preadsorption on ethylene decomposition on Rh(100) at 320 K. There are substantial differences between the spectra where (A) no CO, (B) 0.4 L of CO and (C) 0.7 L of CO are preadsorbed. For preadsorption of 0.7 L of CO, all the subsequently adsorbed ethylene decomposes to ethylidyne at 320 K.

The HREEL spectrum for preadsorption of 0.7 L of CO (Fig. 3.12C) is compared in Fig. 3.13 to the HREEL spectrum for the monolayer left after the high pressure ethylene hydrogenation. Also shown are the LEED patterns for these monolayers as well as the HREEL spectrum for the deuterated analogue of the UHV CO/ethylene monolayer. The HREEL spectra for the UHV- and high pressure-derived monolayers are quite similar, but the LEED patterns, as shown in Fig. 3.13, are different. The notation "split c(2x2)" indicates that the initially adsorbed 0.7 L of CO produces a c(2x2) LEED pattern ($\theta_{\text{CO}} = 0.5$), while the resulting pattern after ethylene adsorption (Fig. 3.13B) has four spots split around each of these c(2x2) positions. The splitting is, however, less than in the c(4x2) pattern shown in Fig. 3.13A.

Figure 3.14 shows HREEL spectra for the split c(2x2) structure taken in the specular and 10° off-specular directions. The most significant difference in these spectra is the appearance of the 1420 cm^{-1} peak in the off-specular spectrum.

Interpretation. As mentioned previously, the HREEL spectra in Figs. 3.13A and 3.13B, which are quite similar, can be assigned to a mixture of CO and ethylidyne species. The 370 and 1880 cm^{-1} peaks are typical values for the ν_{MC} and ν_{CO} frequencies of bridge-bonded CO on Rh(100) [46]. The remaining peaks at 2930 , 1355 and $\sim 1000 \text{ cm}^{-1}$ are attributable to ethylidyne. The 865 cm^{-1} peak in Fig. 3.13A was absent in spectra taken on the opposite face of the Rh(100) crystal and is presumably a contaminant.

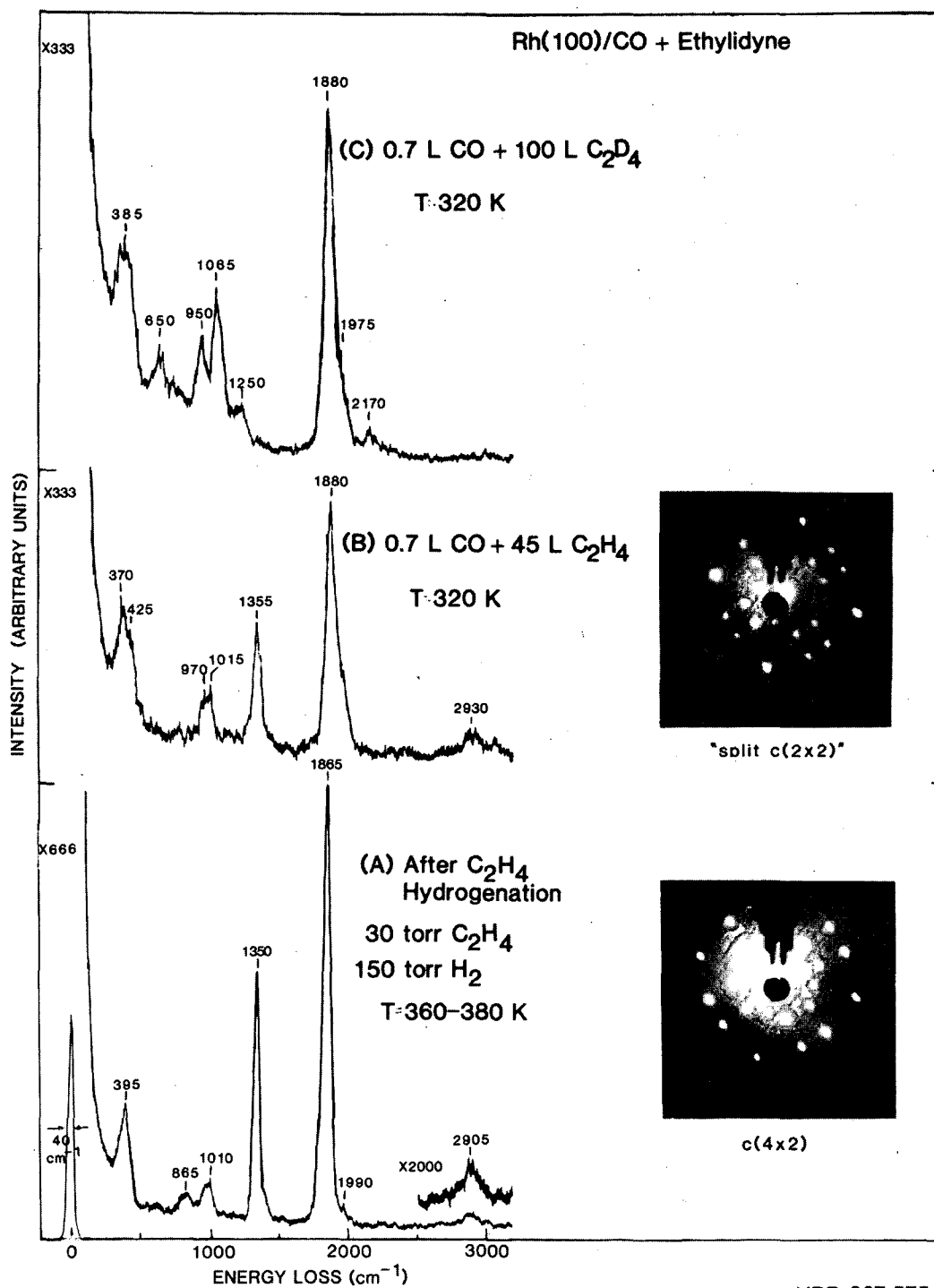
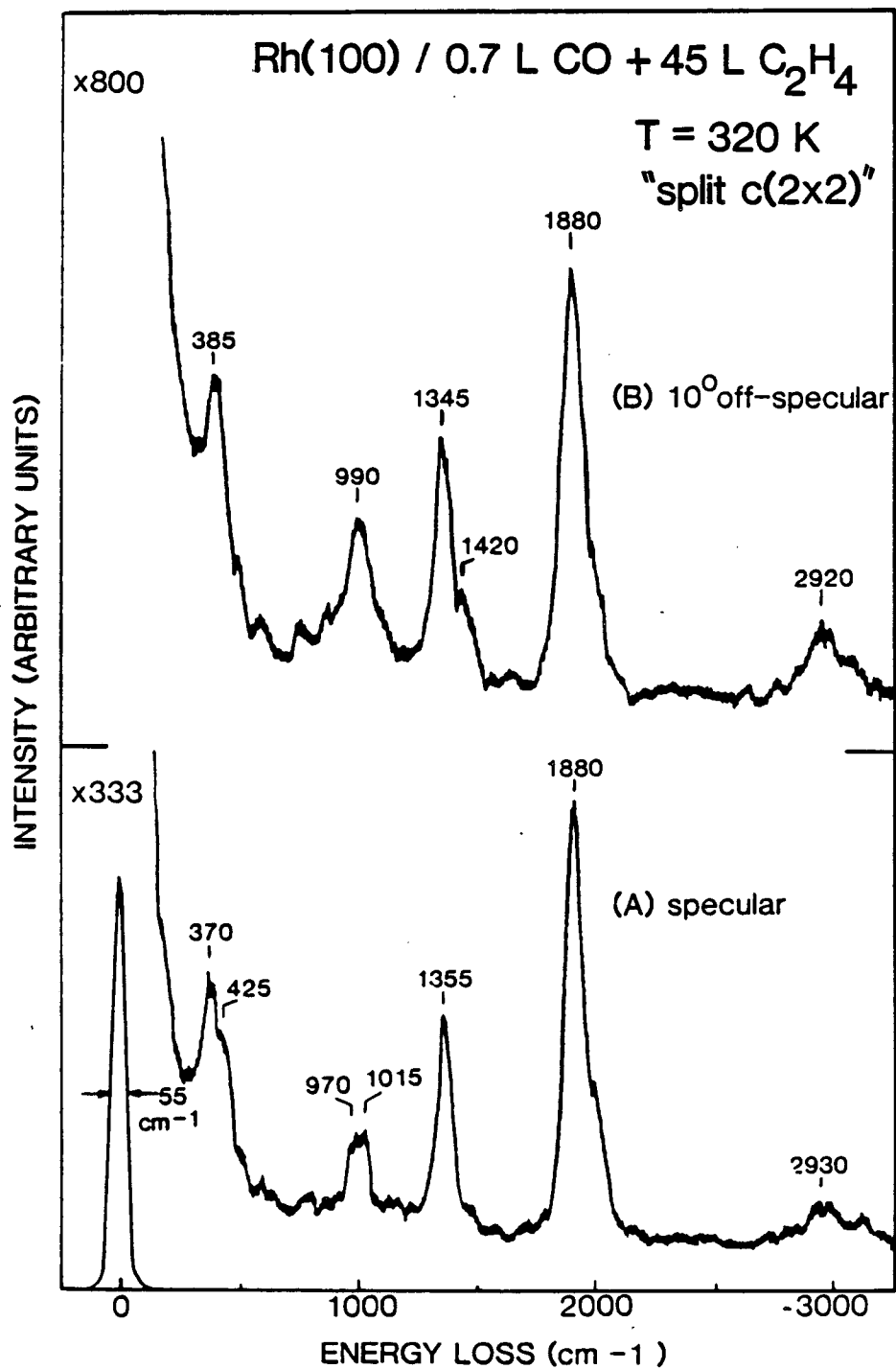


Fig. 3.13 Specular HREEL spectra of Rh(100) after (A) a catalytic ethylene hydrogenation at 360 - 380 K that was contaminated with CO, (B) preadsorption of 0.7 L CO followed by a saturation exposure of C₂H₄, and (C) preadsorption of 0.7 L CO followed by a saturation exposure of C₂D₄. Also shown are the LEED patterns for the hydrogenated monolayers. All three monolayers are comprised of CO and ethylidyne species.



XBL 868-3197

Fig. 3.14 (A) Specular and (B) 10° off-specular HREEL spectra of Rh(100) after adsorption of 0.7 L CO followed by 45 L of ethylene at 320 K to form the split c(2x2) ethylidyne + CO structure.

The intense 1350 cm^{-1} peak is typical for a methyl group symmetric CH_3 bending mode. This umbrella mode occurs at $1335\text{--}1340\text{ cm}^{-1}$ for ethylidyne on Rh(111) and at 1387 cm^{-1} for gas phase CD_3CH_3 . The fact that this peak shifts down with deuteration (Fig. 3.13C) rules out a C-C stretching vibration, while the presence of the 1420 cm^{-1} peak in the off-specular spectrum (Fig. 3.14B) rules out a CH_2 group which has only one peak (CH_2 scissors) in this $1300\text{--}1500\text{ cm}^{-1}$ frequency range. The 1420 cm^{-1} peak is assigned to the $\delta_{\text{as}}\text{CH}_3$ vibration which has the same frequency and a similar relative intensity for ethylidyne on Rh(111) (Table 3.1). The fact that the relative intensity of the $\delta_{\text{as}}\text{CH}_3$ mode increases substantially in the off-specular spectrum means that the methyl group must stand with its 3-fold axis along the surface normal. Further, it is highly unlikely that the ethylene C-C bond has broken so that the methyl group is bound directly to the metal surface; methyl groups bound directly to Pt(111) have a strongly perturbed $\delta_{\text{s}}\text{CH}_3$ frequency of 1220 cm^{-1} [47].

Thus, simply by analyzing the intense 1350 cm^{-1} and weak 1420 cm^{-1} peaks in the specular and off-specular spectra, one can conclude that ethylidyne species are formed and stand vertically on the surface. The other HREELS peaks support this identification. The $2900\text{--}2930\text{ cm}^{-1}$ peak is typical for a $\nu_{\text{s}}\text{CH}_3$ vibration, while the 1000 cm^{-1} peak is the expected value for a single bond C-C stretching vibration ($\nu_{\text{CC}} = 995\text{ cm}^{-1}$ in ethane). The other vibration expected to be dipole active and to have substantial intensity in the specular HREEL spectrum

is the $\nu_{\text{S}}\text{MC}$ mode. This vibration may be obscured by the $\nu_{\text{S}}\text{MC}$ vibration for coadsorbed CO at 370 cm^{-1} .

The deuterated spectrum in Fig. 3.13C also supports the ethylidyne identity. Only the weak 1250 cm^{-1} peak cannot be reasonably correlated with any peak in the hydrogenated spectrum. However, this frequency is characteristic of a CH bending vibration in a partially deuterated methyl group [48]. Further, H,D-exchange has been observed in the ethylidyne methyl groups on Rh(111) (Section 4.2), so it is reasonable that a small fraction of the ethylidyne- d_3 species undergo H,D-exchange with residual surface hydrogen atoms on Rh(100).

The rest of the peaks in the deuterated spectrum are assigned along with the hydrogenated ethylidyne peaks on Rh(100) in Table 3.2. The peak frequencies are quite similar to those for ethylidyne on Rh(111) except for the ν_{CC} frequency which occurs at 100 cm^{-1} lower frequency on Rh(100). This difference will be discussed in the following section. Species like vinyl and ethylidene, which were previously proposed to explain the ethylidyne on Rh(111) spectra, can be ruled out by looking at the published vibrational frequencies for $(\text{HCCH}_2)\text{Os}_3(\text{H})(\text{CO})_{10}$ [49], ClHCCH_2 [50], and Cl_2HCCH_3 [51]. In particular, both vinyl and ethylidene would be expected to have a dipole-allowed C-H bending vibration at $1200\text{--}1300\text{ cm}^{-1}$ for the lone C-H bond on the carbon bonded to the metal. No peak is detectable in this range on Rh(100). Also, both species would probably bond with their carbon-carbon bonds tipped from the surface normal; this binding symmetry, which is C_s or lower, would have

Table 3.2: Assignment of the HREEL spectra for ethynidyne + CO on Rh(100) and comparison to ethynidyne on Rh(111)

Mode Description	Symmetry		Rh(100)/CCH ₃ + CO		Rh(111)/CCH ₃	
	C _{3v}	C _s	Frequencies ^b (cm ⁻¹)	$\nu_{\text{CH}}/\nu_{\text{CD}}$	Frequencies (cm ⁻¹)	$\nu_{\text{CH}}/\nu_{\text{CD}}$
$\nu_{\text{as}}(\text{CH}_3)/\nu_{\text{as}}(\text{CD}_3)$	E	A', A''	3050 / ----	----	2920 / 2178	1.34
$\nu_{\text{s}}(\text{CH}_3)/\nu_{\text{s}}(\text{CD}_3)$	A ₁	A'	2915 / 2170	1.34	2880 / 2065	1.30
$\delta_{\text{as}}(\text{CH}_3)/\delta_{\text{as}}(\text{CD}_3)$	E	A', A''	1420 / ----	----	1420 / ----	----
$\delta_{\text{s}}(\text{CH}_3)/\delta_{\text{s}}(\text{CD}_3)$	A ₁	A'	1350 / 950	1.42	1337 / 988	1.35
ν_{CC}	A ₁	A'	1015 / 1065	.95	1121 / 1145	.98
$\rho(\text{CH}_3)/\rho(\text{CD}_3)$	E	A', A'	970 / ----	----	972 / 769	1.26
$\nu_{\text{s}}(\text{MC})$	A ₁	A'	---- / ----	----	435 / 419	1.04
ν_{CO}	A ₁		1870	----	----	----
$\nu_{\text{s}}\text{MC} [\text{CO}]$	A ₁		380	----	----	----

b) Average of several spectra

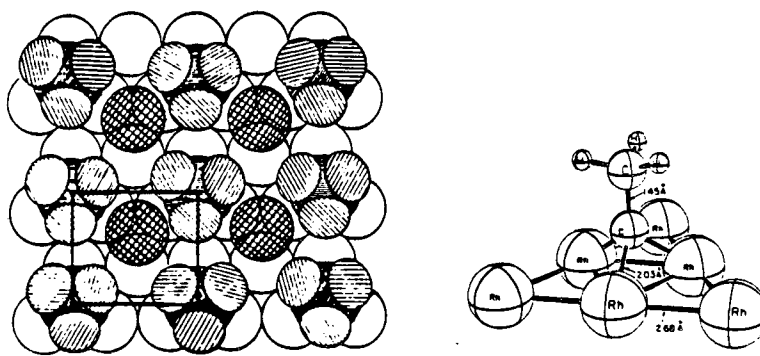
substantially more dipole-allowed vibrational modes than observed in the Rh(100) spectra.

Based on the HREEL spectra and LEED patterns for ethylidyne + CO on Rh(100), a model for the surface packing of these species can be proposed. However, as shown in Fig. 3.13, CO and ethylidyne formed a sharp $c(4 \times 2)$ LEED pattern on Rh(100) only after the high pressure catalysis. It appears, though, from calculations [52] and similar phenomena on other surfaces [53] that the split $c(2 \times 2)$ structure formed in UHV (Fig. 3.13B) is due to small $c(4 \times 2)$ domains of ethylidyne + CO that have antiphase boundaries. Possibly ethylidyne does not diffuse readily enough on Rh(100) under UHV conditions to form large, ordered domains, while under catalytic reaction conditions enhanced diffusion along with desorption/readsorption processes can produce the large, ordered domains.

Figure 3.15 shows a top view of the proposed $c(4 \times 2)$ CO/ethylidyne on Rh(100) as well as the packing in the solved CO + ethylidyne structure on Rh(111). In the Rh(100) structure the CO molecules were placed near bridge sites as suggested by the CO stretching frequency of 1870 cm^{-1} . The CO stretching frequency for the 3-fold hollow in the Rh(111) structure is 1760 cm^{-1} . The ethylidynes on Rh(100) are drawn in 4-fold hollow sites, for reasons discussed later, although top or bridge-site bonding of ethylidyne also allows CO to bond near bridge sites.

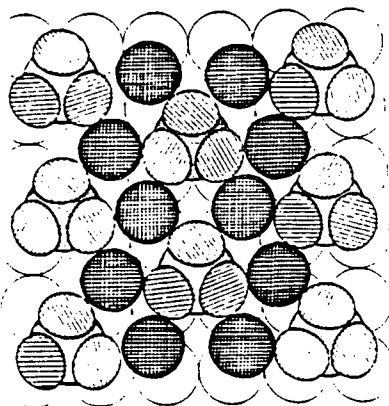
Surface Structure of CO + Ethylidyne

(A) Solved Structure on Rh(111) Surface



$c(4 \times 2)$
 $T = 220-400 \text{ K}$

(B) Proposed Structure on Rh(100) Surface



$c(4 \times 2)$
 $T = 300-380 \text{ K}$

XBL 8610-3638

Fig. 3.15 Models for the CO + ethylidyne ordered structures on Rh(111) and Rh(100). (A) Top view of the solved $c(4 \times 2)$ structure on Rh(111). (B) Top view of the proposed $c(4 \times 2)$ structure on Rh(100).

The CO coverage in Rh(100) structure was taken to be $\theta_{\text{CO}} = 0.5$ (2 CO/primitive cell) as compared to $\theta_{\text{CO}} = 0.25$ (1 CO/primitive cell) on Rh(111) for three reasons. First, the $c(2 \times 2)$ CO LEED pattern requires θ_{CO} to be 0.5 if CO is uniformly distributed on the surface. Second, the diamond shape of the $c(4 \times 2)$ primitive cell leaves two equally spacious vacancies in the cell. Finally, the HREELS peak intensity ratio of the CO stretch to the $\delta_s \text{CH}_3$ peak is larger than that on Rh(111). If the same correlation of this ratio to CO coverage (Fig. 3.10) holds on Rh(100), then $\theta_{\text{CO}} > 0.25$ on Rh(100). It is interesting that this Rh(100) structure has ethyldynes arranged in a pseudo close-packed array on the square lattice substrate while the CO/ethyldyne structure on the close-packed Rh(111) surface is comprised of interpenetrating square lattices of CO and ethyldyne.

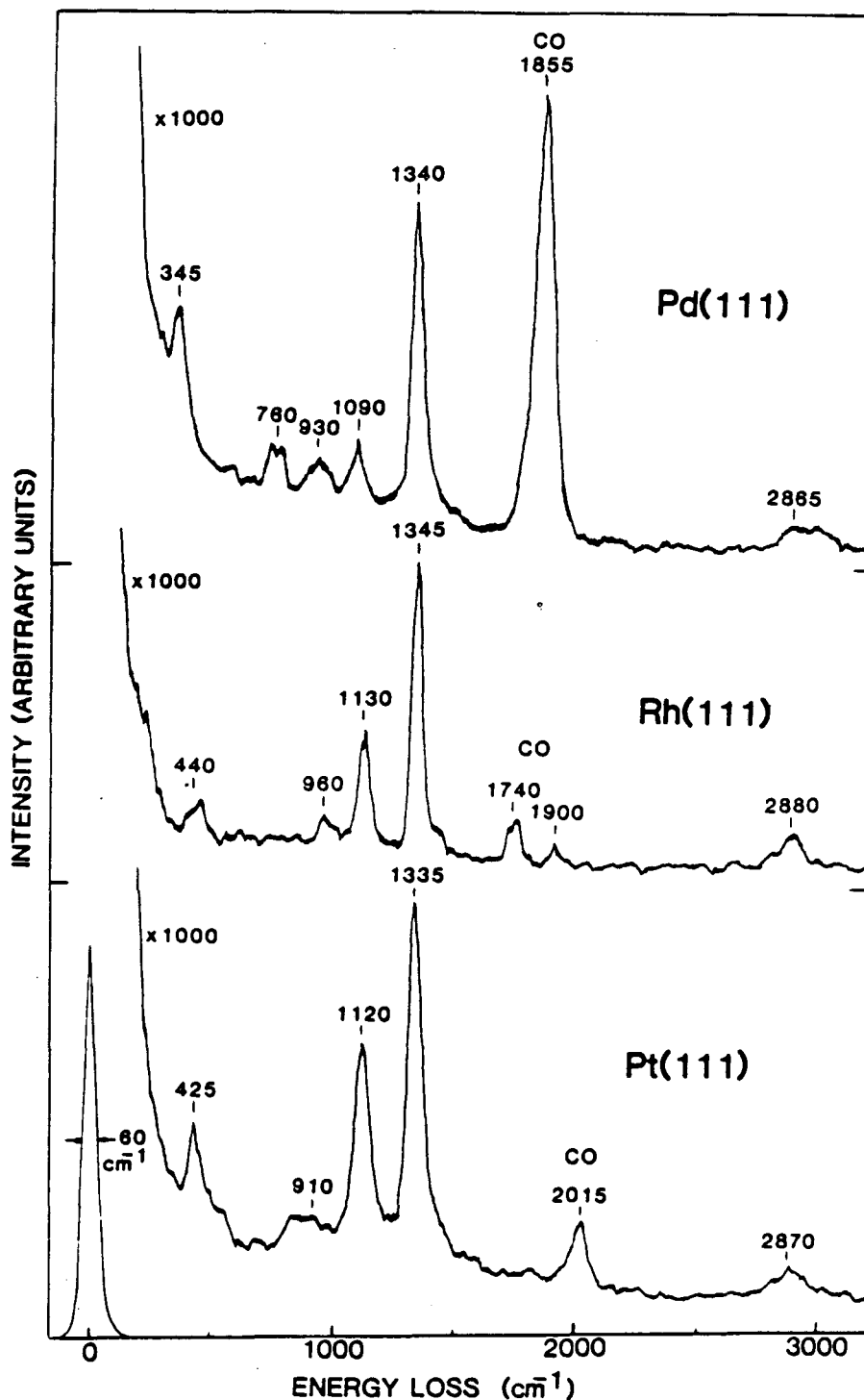
3.2.4 Comparison of Ethyldyne Bonding on Metal Surfaces and in Metal Clusters. Ethyldyne has been shown to be the stable, room temperature ethylene decomposition product on a number of groups 8-10 metal surfaces: Pt(111) [2-13], Rh(111) [22,23], Pd(111) [54], Ru(001) [55], Pt(100) 5×20 [56], and now Rh(100) surfaces precovered with CO. On Pt(111), as discussed in Section 3.1.1, many techniques support the identity of ethyldyne. On the other surfaces ethyldyne has been identified primarily by HREELS, LEED, TDS and comparison to the Pt(111) spectra. Rh(100) is the only surface without 3-fold hollow sites [(5×20) reconstructed Pt(100) has pseudo 3-fold hollow sites] on which ethyldyne species have been identified; this is significant, since LEED analyses [2,24] show that ethyldyne bonds to 3-fold hollow sites

on Pt(111) and Rh(111), and similar bonding is presumed on Ru(001) and Pd(111). It is also significant that (1) clean Pd(100) [57] and unreconstructed Pt(100) [58] show no ethylidyne formation during ethylene decomposition, and (2) Ni(111) [59], despite 3-fold hollow sites, forms acetylene rather than ethylidyne. Explanations for these chemical differences and for why ethylene decomposes to ethylidyne will be given in Section 4.1. Here, the ethylidyne vibrational frequencies on these different metal surfaces and in clusters are compared.

Figure 3.16 compares the HREEL spectra for saturation coverages of ethylidyne on Pt(111), Pd(111) and Rh(111). These ethylidyne vibrational frequencies are summarized in Table 3.3 along with those for ethylidyne on other metal surfaces and in trimetallic clusters. On all the surfaces with 3-fold hollow sites the peak frequencies are quite similar. The most significant differences are the ν_{CC} and ν_{MC} frequencies on Pd(111) which are $40\text{--}60\text{ cm}^{-1}$ below the other close-packed surfaces. These differences could be the result of subsurface hydrogen which is almost certainly present in Pd [60]. Based on this Pd (111) spectrum, it therefore appears that the ν_{MC} and ν_{CC} vibrations may be the most sensitive indicators of changes in the metal-ethylidyne bonding.

On Rh(100) there are no 3-fold hollow sites. Not surprisingly, the ν_{CC} frequency is 110 cm^{-1} lower than on Rh(111), indicating different bonding to the surface. Unfortunately, the ν_sMC frequency is either weak or obscured by the ν_{MC} frequency for CO. Surface crystallography is needed to determine where ethylidyne binds on the Rh(100)

Saturation Coverage of Ethylidyne / 310 K



XBL 861-76

Fig. 3.16 Comparison of the specular HREEL spectra for saturation coverages of ethylidyne on Pt(111), Rh(111) and Pd(111) at 310 K. These monolayers were prepared by adsorbing greater than 10 L of ethylene on the clean surfaces at 310 K. Note that the contaminant CO stretching frequency is quite different on all three surfaces.

Table 3.3: Vibrational Frequencies (cm^{-1}) for A_1 Modes of Ethynidyne (CCH_3)
Bound on Metal Surfaces and in Trimetallic Clusters

Mode	Rh(100) ^a	Rh(111) ^a	Pd(111) ^b	Pt(111) ^c	Ru(001) ^d	Pt(100)5x20 ^e	Co ₃ cluster ^f	H ₃ Os ₃ cluster ^g	H ₃ Ru ₃ cluster ^g
$\nu_s(\text{MC})$	---	435	409	435	480	440	401	---	---
ν_{CC}	1015	1120	1080	1130	1140	1130	1163	1147	1125
$\delta_s(\text{CH}_3)$	1350	1335	1335	1350	1370	1350	1355	1361	1356
$\nu_s(\text{CH}_3)$	2915	2880	2920	2920	2945	2950	2888	2889	2881

a) this work

b) Gates and Kesmodel, ref. 54

c) Steininger and Ibach, ref. 5

d) Hills et al., ref. 55

e) Ibach, ref. 56; Hatzikos and Masel, ref. 58

f) Skinner et al., ref. 11

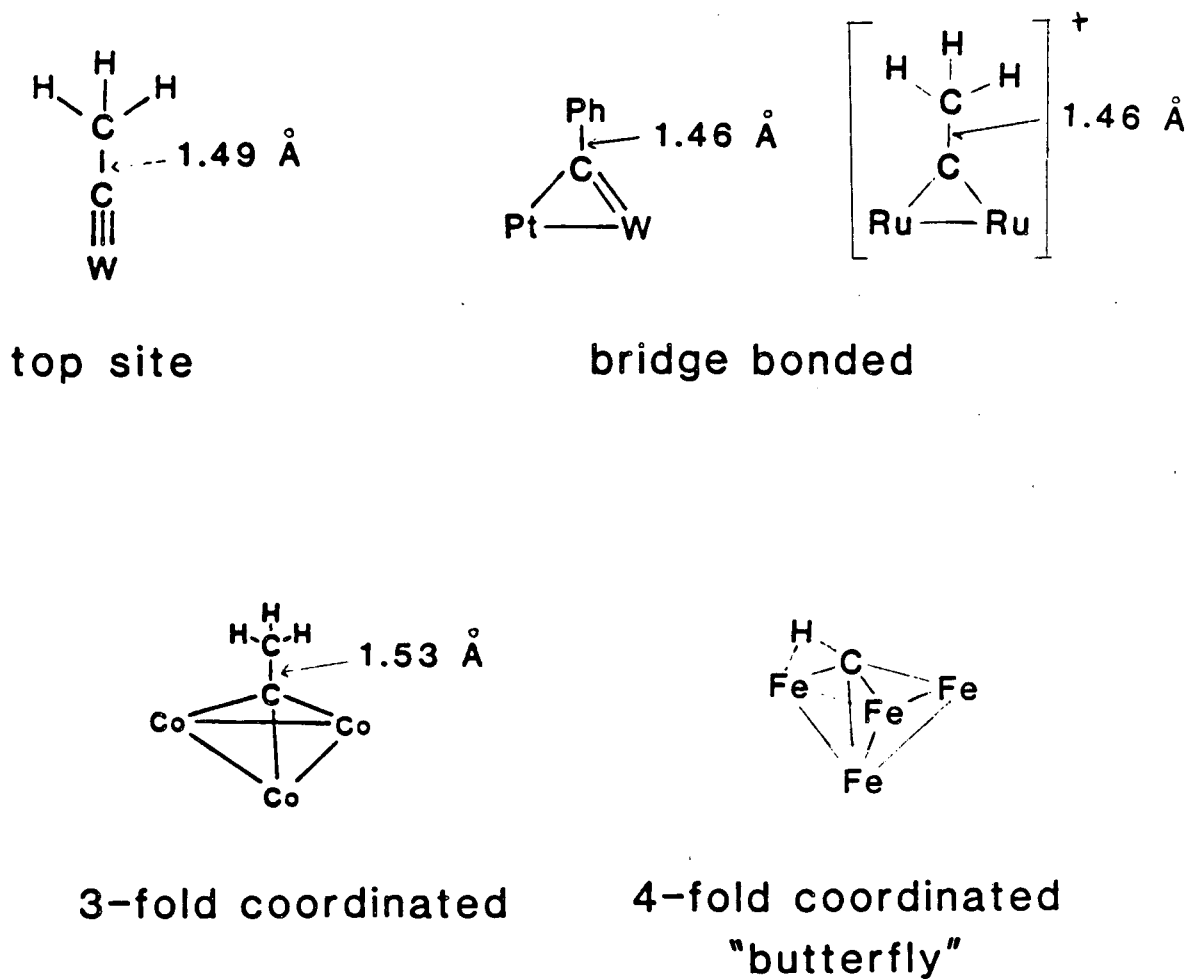
g) Evans and McNulty, ref. 63b

surface. However, in the absence of such a determination, organometallic clusters can be used to compare ethylidyne coordination to different numbers of metal atoms. The various types of metal-alkylidyne clusters known are shown in Fig. 3.17 and are considered individually below as models for ethylidyne coordination to Rh(100).

Top Site Ethylidyne. Monometallic ethylidyne complexes of Cr, Mo and W have been reported [32]. These complexes have extremely short metal-carbon bonds and are therefore drawn with metal-carbon triple bonds as shown in Fig. 3.17. The C-C bond in the Cr-ethylidyne complex $[\text{I}(\text{CO})_4\text{Cr}(\text{CCH}_3)]$ is found to be colinear with the Cr-C bond and has been determined to be $1.49 \pm 0.02\text{\AA}$ long. While no vibrational frequencies of the ethylidyne ligand in these monometallic complexes have been reported, the MC force constant for the Cr-methylidyne analogue $[(\text{CO})_5\text{Cr}(\text{CH})]$ has been calculated to be 8.6 mdynes/\AA [61]. If a similar force constant is applicable to ethylidyne bound to top sites on Rh(100), then the ν_{MC} frequency is expected to be $\sim 700 \text{ cm}^{-1}$. Since no peak is observed in this frequency range (Fig. 3.11A), top site bonding seems unlikely. The rather short C-C bond length in the ethylidyne complex is also inconsistent with the low C-C stretching frequency on Rh(100).

Further, it appears from the chemistry of monometallic alkylidynes in solution that top site bonding of ethylidyne on clean transition metal surfaces is, in general, unlikely. For example, it is known that tungsten-alkylidyne triple bonds are attacked by Pt complexes (in

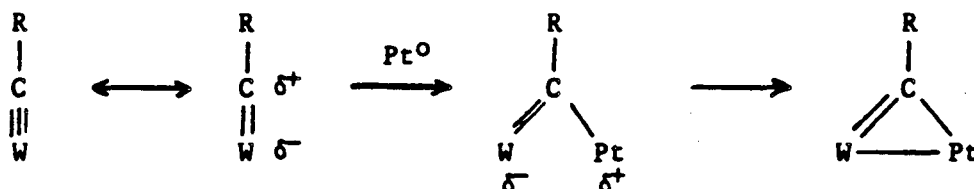
Alkylidyne Coordination in Organometallic Complexes



XBL 8610-4113

Fig. 3.17 Comparison of the different types of alkylidyne coordination that are known for organometallic complexes.

which Pt is formally in a zero oxidation state) to form bridge-bonded alkylidyne complexes [62]:



One might therefore expect that if a top site surface alkylidyne were to form, it would immediately react with an uncoordinated adjacent metal atom to form a bridge-bonded alkylidyne. In the presence of 3-fold hollow sites this process can be repeated once more with the M=C double bond to form 3-fold coordinated alkylidyne.

Bridge Site Ethylidyne. Two types of bridge site cluster alkylidynes have been reported. One is the neutral mixed metal type shown above and in Fig. 3.17 [62]. The other is the diruthenium ethylidyne cation also shown in Fig. 3.17 [63]. The C-C bond lengths in both clusters are 1.46 Å, substantially shorter than C-C single bonds (1.54 Å). However, because of the hyperconjugation that occurs in carbon-phenyl bonds [64], the C-C bond in the Pt-W cluster probably underestimates by 0.02 Å the C-C bond in an analogous ethylidyne complex. Still, the vibrational frequency for the C-C bond should be similar to that in the diruthenium-ethylidyne complex which is reported to be 1287 cm⁻¹, over 250 cm⁻¹ higher than on Rh(100). Thus, bridge-bonded ethylidyne on Rh(100) seems unlikely.

Three-Fold Hollow Site Ethylidyne. This is clearly the favored bonding geometry for the ethylidyne ligand. Trinuclear cobalt [33], nickel [66], ruthenium [65] and osmium [63b] alkylidynes have been readily synthesized. Also, to date, the surfaces that most readily form ethylidyne have 3-fold hollow sites. The Rh(100) surface which lacks these sites requires some preadsorbed species (either for thermodynamic or kinetic reasons) in order to form ethylidyne. It is also significant that ethylidyne stabilizes the 5x20 reconstructed Pt(100) surface with its 3-fold hollow sites while other adsorbates remove this reconstruction and restore the 4-fold hollow sites [37,67]. This apparent thermodynamic stability of alkylidynes in 3-fold hollow sites seems intuitively reasonable since sp^3 hybridization and tetrahedral coordination of the carbon atom can be maintained. Further, molecular orbital calculations find that ethylidyne bonding in 3-fold hollow sites is favored over top and bridge sites [14-17].

The bonding of ethylidyne on close-packed surfaces is indeed quite similar to ethylidyne in trimetallic clusters (Fig. 3.2). However, there is still some question about how well localized valence bonds can describe the bonding in trinuclear alkylidynes. In particular, the C-C bond length in cluster ethylidynes is ~ 0.03 Å shorter than in gas phase ethane. This has been attributed, in valence bond terms, to hyperconjugation [22]. It has also been suggested, based on NMR studies of alkylidyne clusters [68], that the metal-alkylidyne bond is not properly represented by localized bonds. This latter point may be

significant for ethynidyne bonding on Rh(100) where there are no 3-fold hollow sites.

Four-Fold Hollow Site Ethynidyne. No surface or cluster species with ethynidyne bonding in this site have, to my knowledge, been reported. Tetrametal clusters generally buckle to form "butterfly" complexes [69] and are inappropriate analogues for 4-fold hollow sites. However, a square-pyramidal pentaruthenium cluster with a C_2H species bonding in the 4-fold hollow site has been synthesized [70, Section 3.5]. A similar ethynidyne complex is needed to compare with ethynidyne on Rh(100).

By process of elimination, bonding of ethynidyne in the 4-fold hollows on Rh(100) seems most likely. It is also intuitively plausible that the high electron density in the 4-fold sites would overlap effectively with the C-C antibonding orbitals in CCH_3 , weaken the C-C bond, and produce the low C-C stretching frequency observed.

Two distinct geometries for ethynidyne bonding vertically in a 4-fold hollow are possible: in the center or displaced along the diagonal. (There is no obvious driving force for other displacements from the center.) In both of these geometries, as well as in top and bridge sites, the point group symmetry for ethynidyne is C_s . According to the dipole selection rule for this symmetry, many of the weak peaks (all the A' modes in Table 3.2) in the Rh(100)/ethynidyne spectrum must be dipole-allowed. The fact that ethynidyne appears C_{3v} symmetric based on the HREEL spectral intensities means either that the dynamic dipole moment for some of the dipole-allowed modes is quite small or

that both the ethylidyne bonding and the electron scattering are relatively unaffected by the surface symmetry.

In summary, the bonding of ethylidyne on surfaces with 3-fold hollow sites [Pt(111), Pd(111), Rh(111), Ru(001), Pt(100) 5x20] is quite similar to the bonding of ethylidyne in trimetallic clusters. Studies here on Rh(111) show that the binding site and local bonding geometry of ethylidyne are not detectably effected by changing the surface temperature (200-400 K), the surface coverage of ethylidyne, or the coverage of coadsorbed H or CO. These parameters do, however, effect the long range ordering of ethylidyne, which in turn effects the relative intensity of the HREELS peaks. Studies on Rh(100) show that ethylidyne can be formed on a surface without 3-fold hollow sites, but in this case another adsorbate like CO must be preadsorbed up to $\theta_{\text{ads}} = 0.5$ in order to form ethylidyne. It appears that the C-C stretching frequency is a readily discernable vibrational feature that is sensitive to both the bonding site and bonding strength of ethylidyne to the metal. Based on a comparison with organometallic clusters, the low ν_{CC} frequency for ethylidyne on Rh(100) is suggestive of bonding in a 4-fold hollow site.

3.3 Propylidyne Adsorbed on Pt(111) (T = 270-430 K) and on Rh(111)

(T = 200-270 K)

3.3.1 Background. Studies of propylene adsorption on Pt(111) and Rh(111) were initiated in our group in order to compare the surface chemistry of this methyl-substituted ethylene to ethylene. By introducing the methyl group, the relative rates of alkene and alkane C-H bond breaking can be compared. The expectation was that if alkene C-H bond breaking is favored, then propylidyne (CCH_2CH_3) will be formed analogous to ethylidyne. If instead the methyl group alkane C-H bonds break first then surface allyl (CH_2CHCH_2) or trimethylene ($\text{CH}_2\text{CH}_2\text{CH}_2$) species are likely to form. Allyl cations, anions and radicals and trimethylene are familiar gas phase and solution intermediates. Such species are also relevant to the 1,3-hydrogen shift mechanisms that have been proposed to explain isotope labelling results in catalysis [71,72]. On the other hand, propylidyne species, which have been proposed to form on Pt(111) and Rh(111) in UHV [7,24,73-75], are not common gas phase or solution intermediates, and they have only recently been considered as possible intermediates in surface reactions [76,77].

Previous studies of propylene adsorption on Pt(111) [7,73] and Rh(111) [24,78] utilized AES, TDS and LEED to investigate the surface chemistry. The LEED results were quite similar to those for ethylene and were used to propose propylidyne species. Specifically, it was found that propylene adsorption on Pt(111) above 270 K (the ethylidyne formation temperature) produces a (2x2) LEED pattern as ethylidyne does. This structure is stable up to 400 K, just 60 K below the

temperature at which ethylidyne thermally decomposes. TDS on Pt(111) shows that molecular propylene decomposes by losing 1 hydrogen atom at 270 K, consistent with propylidyne stoichiometry, but subsequent molecular orbital calculations have suggested that this stable C_2H_5 species on Pt(111) is allyl [119].

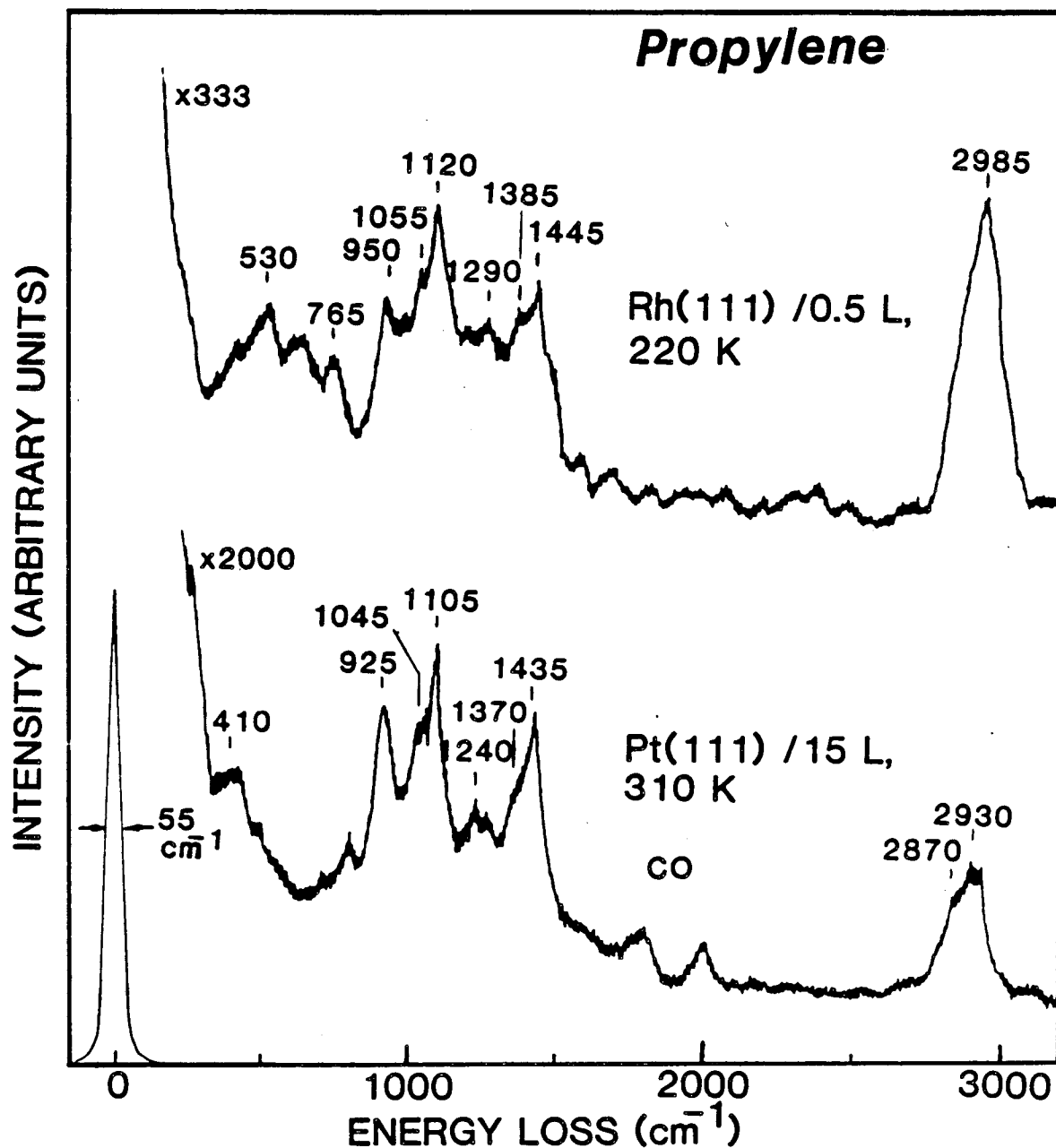
On Rh(111), LEED studies showed that propylene adsorption produces a (2x2) pattern as low as 220 K, the same temperature as ethylidyne formation on this surface. Propylidyne species with randomly oriented methyl groups were proposed for this surface structure based on the similarity of the LEED I-V curves to the (2x2) ethylidyne structure [73]. Further, this (2x2) structure was found to convert to a c(4x2) structure when warmed slowly to room temperature. The surface species in this structure was also proposed to be propylidyne based on the similarities to the ethylidyne c(4x2) I-V curves [37].

It was also observed in these LEED studies that very large doses (~ 1000 L) of propylene on Rh(111) between 220 and 270 K produced a $(2\sqrt{3} \times 2\sqrt{3})R30$ rather than (2x2) LEED structure. It was proposed that propylidyne species were responsible for both of these structures, the difference being that the propylidyne methyl groups become "locked in" to a $(2\sqrt{3} \times 2\sqrt{3})R30$ super lattice at high surface coverages. Curiously, large exposures of propylene on Pt(111) did not "lock in" the methyl groups, even though the Pt lattice constant is only 4% larger than that for Rh(111).

3.3.2 Results and Discussion. HREEL studies were undertaken to establish the identity of the propylene-derived species in these

ordered LEED structures on Pt(111) and Rh(111). The LEED patterns for propylene on Pt(111) and Rh(111) were reproduced as prescribed except for the $(2\sqrt{3} \times 2\sqrt{3})R30$ and $c(4 \times 2)$ structures on Rh(111). The $(2\sqrt{3} \times 2\sqrt{3})R30$ structure, previously formed from the (2×2) structure by large exposures of propylene, could be produced here only by co-adsorption of CO in the (2×2) structure. The $c(4 \times 2)$ structure, previously formed by slowly warming the (2×2) structure to room temperature, could not be reproduced. It was found instead that diffuse blotches were formed in the $\sqrt{3}R30$ LEED positions by warming the (2×2) structure above 270 K. HREELS also showed that further decomposition occurs at 270 K. This chemistry is described in Section 4.3. Here, only the HREEL spectra for the (2×2) propylene-derived structure on Pt(111) (270 - 400 K), the (2×2) propylene-derived structure on Rh(111) (200 - 270 K), and the $(2\sqrt{3} \times 2\sqrt{3})R30$ CO/propylene coadsorption structure on Rh(111) (200 - 270 K) are discussed.

Figure 3.18 shows the HREEL vibrational spectra for the propylene-derived (2×2) monolayers on Pt(111) and Rh(111). The spectra are indeed quite similar. (The extra modes between 500 and 700 cm^{-1} on Rh(111) are probably the result of a coadsorbed condensed contaminate, since this spectrum was recorded at 77 K). The complexity in these HREEL spectra is quite consistent with propylidyne for two reasons: (1) there are almost twice as many normal modes for propylidyne as there were for ethylidyne and (2) since the adsorption symmetry is low (a maximum of C_s), a much larger fraction of these modes are dipole active. The situation is further complicated by the fact that many of



XBL 866-2416

Fig. 3.18 Specular HREEL spectra of propylene adsorbed on Pt(111) at 310 K and on Rh(111) at 220 K to produce (2x2) LEED patterns. The Pt(111) spectrum was taken at room temperature while the Rh(111) spectrum was taken at 77 K. Both of these vibrational spectra are attributable to propylidyne (CCH_2CH_3) species, and they are assigned in Table 3.4

the vibrational modes are coupled so that the normal modes in propylidyne are combinations of the traditional functional group modes. Fortunately, the vibrational spectra of model gas phase compounds have been assigned using a normal coordinate analysis. Thus, while the HREEL spectra have too many unresolved peaks to be definitively assigned, they are consistent with propylidyne as shown by comparison to the model compound $\text{Cl}_3\text{CCH}_2\text{CH}_3$ in Table 3.4.

In Table 3.4, the first two columns list the measured IR frequencies and approximate normal mode descriptions determined by a normal mode analysis for 1,1,1-trichloropropane [79], a propylidyne species bonded to three chlorine atoms. Only frequencies for modes of A' symmetry are listed, since only these modes will show dipole activity for a surface propylidyne species having C_s symmetry. The vibrational frequencies of 1,1,1-trichloropropane were chosen to predict the surface vibrational frequencies of propylidyne, since an analogous comparison between the vibrational spectra of gas phase 1,1,1-tribromoethane and surface ethylidyne showed good agreement [2]. Columns 3 and 4 of Table 3.4 list the frequencies observed here by HREELS for the (2x2) propylene-derived monolayers on Pt(111) and Rh(111). Column 5 tabulates the frequencies observed by Avery and Sheppard [75] for propylene adsorbed on Pt(111) at 300 K. Column 6 lists the IR frequencies attributed to a propylidyne ligand in an organometallic tricobalt cluster: $\text{Co}_3(\text{CO})_9(\text{C}_2\text{H}_5)$ [80].

Qualitatively, the Rh(111) frequencies are consistent with propylidyne. Also, the relative intensities are similar to those for

Table 3.4: Vibrational Frequencies of A' Normal Modes in CCH₂CH₃ Species

Approximate Normal Mode Description ^a	C ₁₃ CCH ₂ CH ₃ ^a	Rh(111)/C ₃ H ₆ , 240 K ^b	Pt(111)/C ₃ H ₆ , 310 K ^b	Pt(111)/C ₃ H ₆ , 300 K ^c	Co ₃ (CO) ₉ (C ₃ H ₅) ^d
ν_s' CH ₃	2989		2930	2980	
ν_s CH ₂	2944		2870	2920	
ν_s CH ₃	2933				
δ_s' CH ₃ + δ_s CH ₂	1455	1445	1435	1465	1450
δ_s CH ₂	1430				1420
δ_s CH ₃	1382	1385	1370		1370
δ_w CH ₂ + ν CC	1323	1290	1240	1295	
ρ CH ₃	1107	1120	1105	1115	1155
	1066	1055	1045	1055	1050
ν CC+ ρ CH ₃ + δ_w CH ₂	929	950	925	940	1040

^aA. Goursot-Leray, M. Carles-Lorjou, G. Pouzard, and H. Bodot, ref. 31.

^bThis work

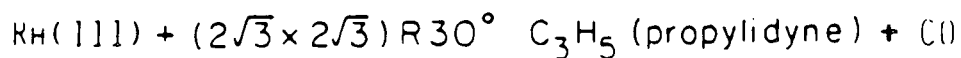
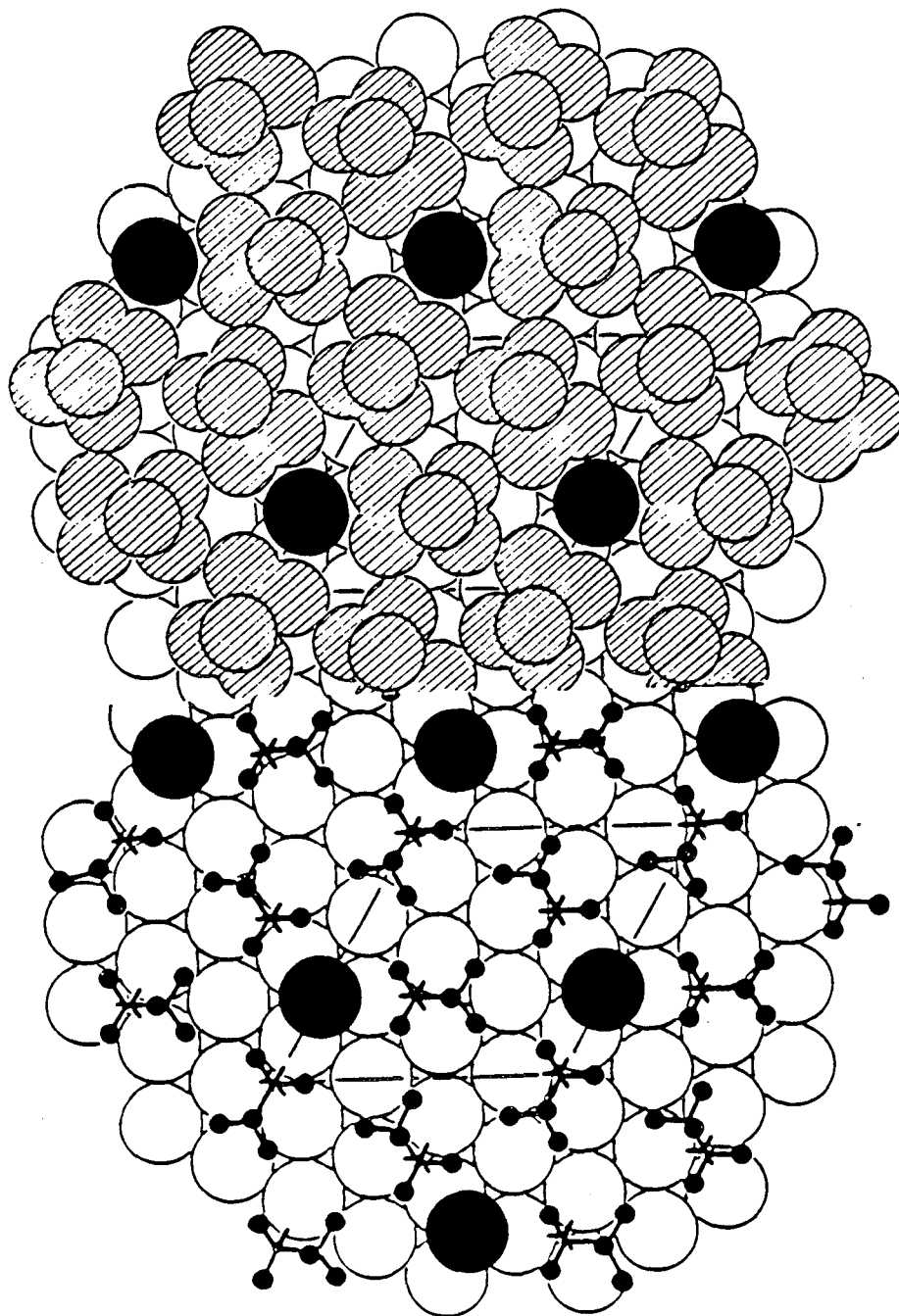
^cD. Seyferth, C. N. Rudie, and J. S. Merola, ref. 32.

^dN. Avery and N. Sheppard, ref. 29.

propylidyne on Pt(111) and to those for analogous modes in 1,1,1-trichloropropane. There are also two aspects of these HREEL spectra that argue against the presence of surface allyl or trimethylene species. First, the large number of peaks with substantial intensity in the specular HREEL spectra is not expected for flat-lying surface allyl or trimethylene species. Second, neither of these species has a methyl group, so they are not expected to have the large intensity observed in the 1350 cm^{-1} region. Therefore, based on the vibrational spectra and on the chemical similarities between the ethylene and propylene on Pt(111) and Rh(111), it is concluded that propylidyne is the stable species formed by propylene decomposition on Pt(111) in the temperature range of 270 - 400 K and on Rh(111) in the temperature range of 200 - 270 K. Presumably these propylidyne species bond in 3-fold hollow sites as previously proposed [24].

The HREEL vibrational spectra for the $(2\sqrt{3} \times 2\sqrt{3})R30$ propylidyne + CO structure on Rh(111) are the same as that in Fig. 3.18 except for an added CO stretching frequency at 1750 cm^{-1} . This CO stretching frequency is the same as that found for CO bound in a hollow site when co-adsorbed with ethylidyne on Rh(111) (Section 3.2.2). Thus, it appears that CO bonds in the vacant hollow sites present in the $(2\sqrt{3} \times 2\sqrt{3})R30$ propylidyne structure previously proposed by Koestner et al. [24]. Top views of the resulting propylidyne + CO structure is shown in Fig. 3.19.

In summary, the HREEL spectra presented here support the formation of propylidyne from propylene adsorption between 200 and 270 K on



XBL 813-5410 A

Fig. 3.19 An atop view of the proposed $(2\sqrt{3} \times 2\sqrt{3})R30$ propylidyne + CO structure on Rh(111). In the upper portion of the figure, the slashed circles represent hydrogen atoms and the solid circles represent CO molecules; van der Waals dimensions are shown. In the lower portion of the figure, the hydrogen atoms are represented by small solid circles in order to make more visible the Rh surface atoms and the carbon skeleton of propylidyne.

Rh(111) and between 270 and 400 K on Pt(111). Thus, despite the added methyl group, propylene follows ethylene-type chemistry and stands up on these surfaces. An obvious question is: "How long can the 1-alkene be and still stand up on the surface to form ordered, paraffinic chains dangling away from the surface?" Monolayers of such long-chain hydrocarbons which are strongly bound to the surface through the alkylidyne linkage might make excellent lubricating films or corrosion resistant coatings. Indeed, even the short-chain ethylidyne monolayers on Pt(111) and Rh(111) can be exposed to air without appreciable degradation [81]. Alkenes up to 1-pentene have been studied on Pt(111) in UHV. TDS [7,76] and HREELS [75] studies show that at room temperature these longer-chain alkenes do bind as alkylidynes. However, the thermal stability of these monolayers decreases with increasing chain length so that pentylidyne decomposes only slightly above room temperature. A less reactive substrate is probably needed for such monolayers to be of practical utility. The factors that control alkylidyne formation and decomposition will be discussed in Chapter 4.

3.4 Molecular Ethylene Adsorbed on Rh(111) and Rh(100) in the Temperature Range of 80–200 K

3.4.1 Background. The low temperature bonding and chemistry of hydrocarbons on single crystal transition metal surfaces in ultra-high vacuum (UHV) may be particularly relevant for heterogeneous catalysis. By going to low temperature there is the possibility of isolating adsorbed reactants and catalytic intermediates that are unstable on clean surfaces in UHV at the actual catalytic reaction temperature. Weakly bound adsorbates, which are likely to be catalytically active, can be stabilized at low temperatures and studied spectroscopically. Further, it may be possible to mimic, in UHV, catalytic hydrocarbon chemistry that is performed with high hydrogen pressures by studying the surface chemistry of hydrocarbons below the temperature at which surface hydrogen desorbs (usually about 300 K).

Surprisingly, the molecular adsorption of only a few hydrocarbons has been studied. The lack of study is mainly due to the subambient temperatures that are required to isolate molecularly adsorbed species on the highly-reactive, clean surfaces of transition metals. For example, on groups 8–10 transition metal surfaces, alkenes and alkynes decompose between 150 and 300 K. However, since temperatures down to 77 K can now be routinely achieved, molecular adsorption can be readily studied. Further, the interpretation of the surface spectra should be especially tractable, since the adsorbate identity is already known.

In this section the results of LEED, TDS and HREELS studies for molecular ethylene adsorption on Rh(111) and Rh(100) are presented and

compared to the results from other transition metal surfaces on which molecular ethylene adsorption has been studied. In these previously published studies it was found (primarily by HREELS) that the bonding of molecularly adsorbed ethylene is highly sensitive to the metal, the surface geometry, and the presence of coadsorbates [82,83]. In all cases, the main interaction with the metal is through the electrons in the C-C bond, causing the carbon atoms to rehybridize from sp^2 towards sp^3 .

Sheppard has recently noted that the vibrational spectra for chemisorbed ethylene can be divided into three basic categories - type I, type I', and type II [82]. Type I spectra are typified by ethylene on Pt(111), where the spectra indicate strong distortion from gas phase bonding towards di- σ bonding [5,86]. Type II spectra are typified by ethylene on Cu(100) where little distortion and π -bonding are indicated. The third type of spectra, type I', generally have vibrational frequencies between those for type I and type II and relative intensities different from both types I and II; no satisfactory structural model has been proposed for type I'. Surface crystallography is needed to substantiate and extend this correlation.

In the absence of surface crystallography, the surface vibrational spectra can potentially provide some information about the C-C bond length in adsorbed ethylene. It is shown here, based on a detailed interpretation of the HREEL spectra, that a general correlation may exist between the vibrational frequencies in the C_2D_4 spectra and the C-C stretching force constant in adsorbed ethylene. From this

correlation, along with Badger's rule relating force constants to bond lengths, bond lengths in adsorbed ethylene are predicted.

The results are discussed below in three parts: LEED, TDS, and HREELS. In each section the Rh(111) data is presented first, followed by the Rh(100) data and a comparison to other surfaces. An appendix is included which discusses in more detail the assignment of the HREEL spectra for molecularly adsorbed ethylene.

3.4.2 Low-Energy Electron Diffraction (LEED). Two LEED patterns can be formed by adsorption of ethylene at 90 K on a clean Rh(111) surface. A 1.5 L exposure of ethylene produces a (2x2) LEED pattern, and a 2 L exposure produces a superposition of a (2x2) and a $(\sqrt{3} \times \sqrt{3})R30^\circ$ pattern. Finally, after a 4 L exposure, a pure $(\sqrt{3} \times \sqrt{3})R30^\circ$ pattern develops. Both of these ordered overlayers are sensitive to electron bombardment, and they rapidly disorder under the microamp crystal currents above 100 eV used in the LEED experiments.

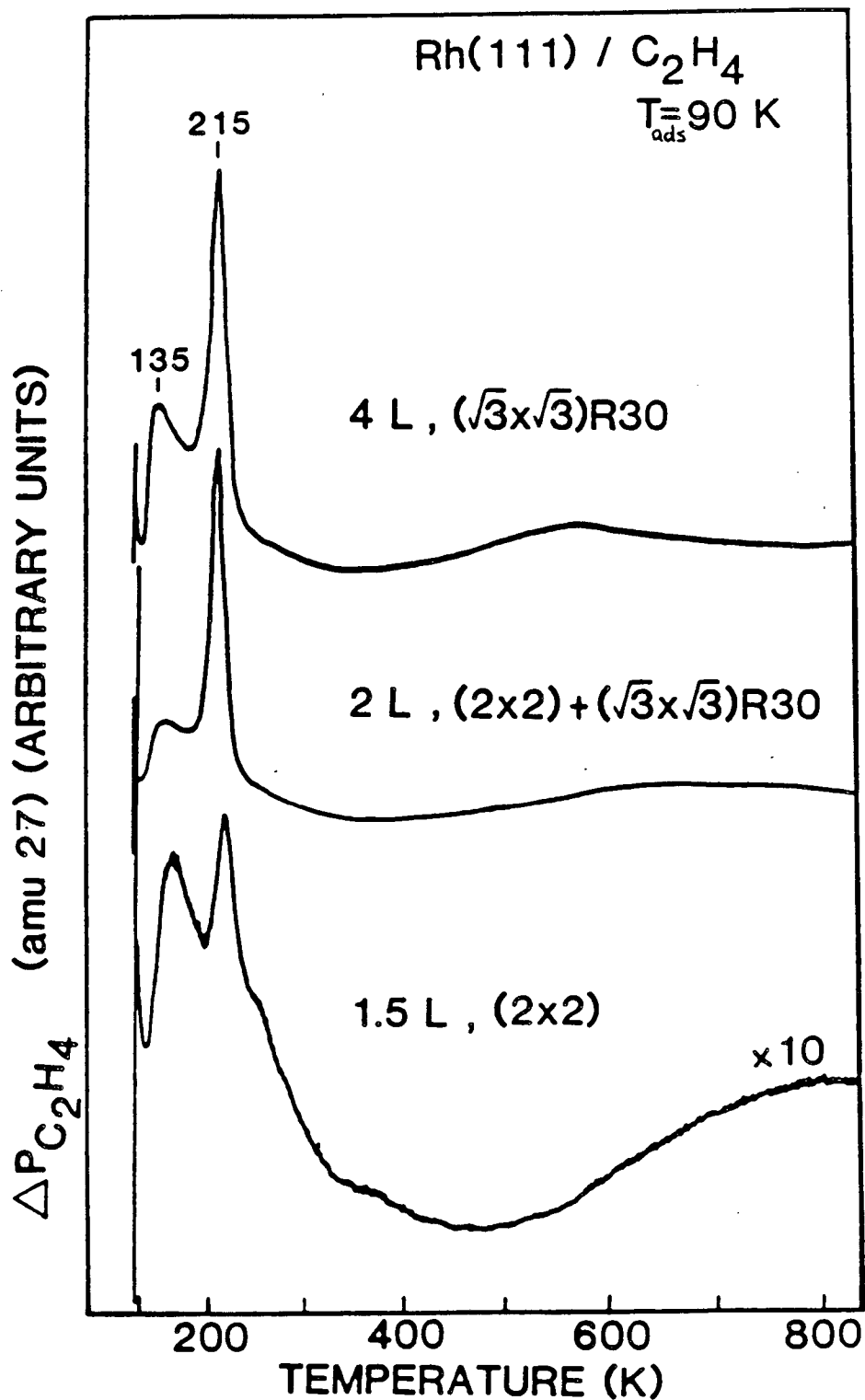
These ordered LEED structures are thermally stable from 90 to 200 K. TDS and HREELS indicate that this is also the temperature range in which the adsorbed ethylene is molecularly intact on Rh(111). From packing arguments using Van der Waals radii, it appears that the $(\sqrt{3} \times \sqrt{3})R30^\circ$ structure has 1 ethylene molecule per unit cell, corresponding to a surface coverage of 1 ethylene molecule for every 3 surface Rh atoms ($\theta_{C_2H_4} = 0.33$). Since the (2x2) LEED structure forms for lower ethylene exposures, this structure must also have one C_2H_4 per unit cell or a coverage, $\theta_{C_2H_4}$, of 0.25.

On Rh(100) no sharp LEED patterns were observed for ethylene adsorption between 90 and 200 K. A diffuse (2x2) LEED pattern was

obtained near saturation coverage, but small islands of some contaminant like water could not be ruled out as the cause of this pattern. Adsorption of residual water on clean Rh(100) at 90 K was particularly a problem. Since adsorption was much slower on top of an ethylene monolayer, high surface coverages of ethylene were used to avoid contamination.

The only other transition metal surfaces on which ethylene has been reported to form ordered monolayers below 150 K are Pt(111), where a (2x2) pattern has been reported [5], and Ni(110), where a complex pattern was reported [85]. No surface crystallography by LEED has been reported for these ordered overlayers, but an analysis of the LEED spot intensities for the (2x2) structure on Rh(111) below 100 eV is in progress. The C-C bond length for adsorbed molecular ethylene on Pt(111) has been determined by near edge x-ray absorption fine structure (NEXAFS) to be 1.49 Å [84].

3.4.3 Thermal Desorption Spectroscopy (TDS). On Rh(111) the strongest evidence that ethylene molecularly adsorbs at 90 K is that some ethylene molecularly desorbs above 100 K. Molecular ethylene desorption spectra for several exposures of ethylene at 90 K on Rh(111) are shown in Fig. 3.20. Two peaks are evident below 220 K (the adsorption temperature in previous studies), but the previously reported small peak at 375 K [23] is not observed. (The broad, high temperature feature is due to desorption from the manipulator as it slowly warms up during the desorption experiment.) For a 1.5 L exposure, which produces a sharp (2x2) pattern, the peak at 215 K is quite small,



XBL 866-2425

Fig. 3.20 Thermal desorption spectra for molecular ethylene C₂H₄ desorption from Rh(111) after the indicated C₂H₄ exposures at 90 K. The heating rate was 25 K/sec. Molecular desorption at 215 K is correlated to the formation of the ($\sqrt{3} \times \sqrt{3}$)R30° LEED pattern. Note that the 1.5 L spectrum is multiplied by a factor of 10.

as indicated by the $\times 10$ expansion on this spectrum. This peak grows relative to that at 135 K as the ethylene exposure is increased to form the saturation $(\sqrt{3} \times \sqrt{3})R30^\circ$ LEED structure. The 135 K peak can be attributed to ethylene desorption from the thin support wires and the 215 K peak to desorption of the ethylene in excess of the (2×2) LEED structure from Rh(111). This means that 25% of the ethylene adsorbed at saturation coverage desorbs molecularly, while the remaining 75% decomposes.

On Rh(100), like Rh(111), most of the ethylene is irreversibly adsorbed and decomposes rather than desorbing molecularly. A small amount of molecular desorption is observed in a broad peak centered at 155 K for high (10 L) exposures of ethylene. However, the broadness of this peak (see Fig. 4.5) suggests that it may be due to desorption from the manipulator or the Ta support wires rather than from the crystal.

Besides Rh(111), some molecular ethylene desorption has definitely been observed from Pt(111) [7-9], Pd(111) [54], Ru(001) [55], Ni(110) [85], Pd(100) [54] and Cu(111) [87] surfaces below room temperature. In general, the percentage of adsorbed ethylene that desorbs molecularly from transition metal surfaces increases as one moves to the right in the periodic table. Only 20% molecularly desorbs from Ru(001) [55], while 60% desorbs molecularly from Pt(111) [5-9], and 100% desorbs from Cu(111) [87]. On Pt(111) some ethane also desorbs from adsorbed ethylene monolayers at about 290 K, slightly above the temperature at which molecular ethylene desorbs and the remaining

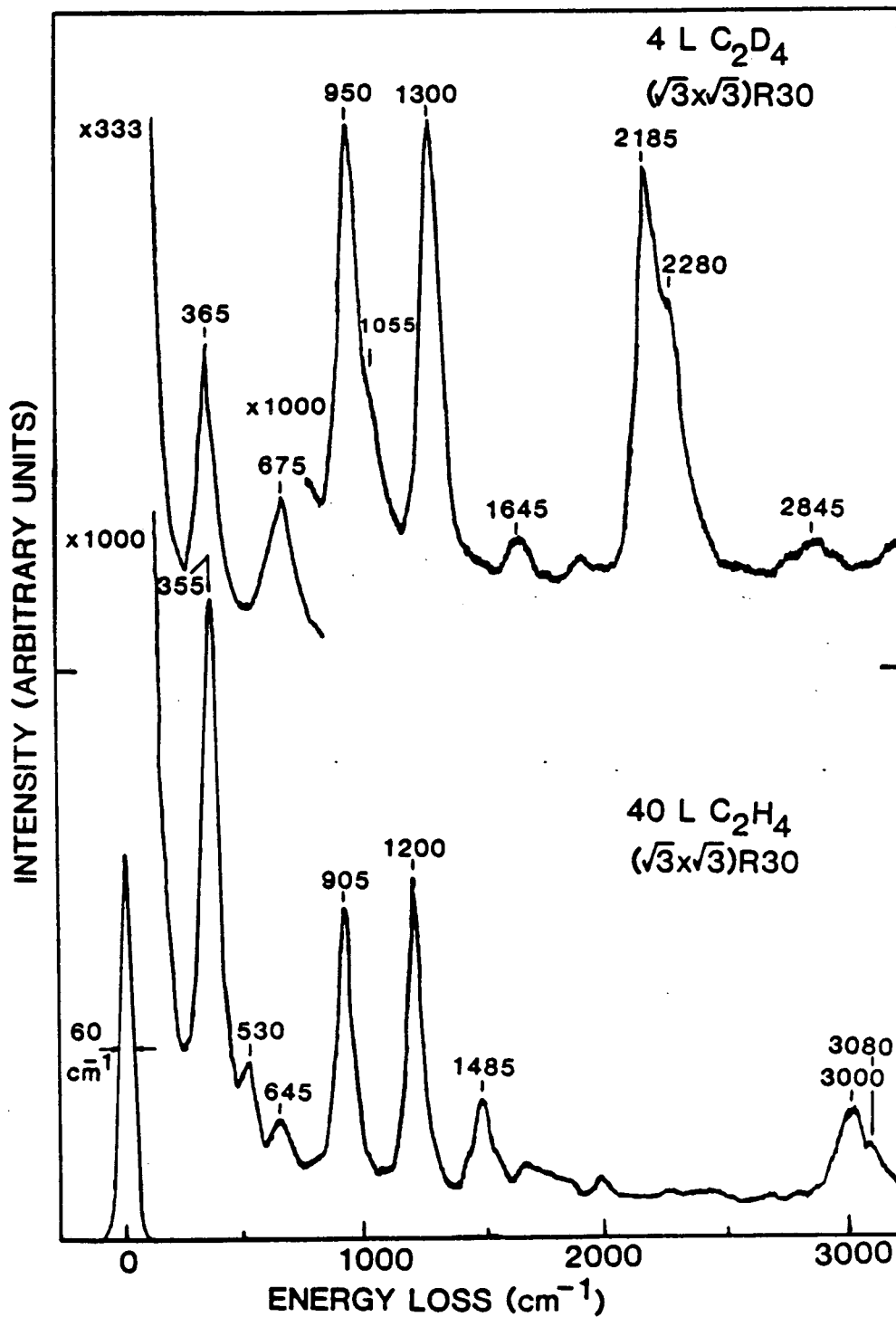
adsorbed ethylene begins to decompose [5,8,9]. Coadsorption of H_2 with ethylene on Pt(111) increases the amount of ethane produced and lowers the desorption temperature to 250 K [9]. While no ethane desorption is observed for ethylene adsorption alone on Rh(111), when 10 L of H_2 are coadsorbed with 0.2 L of C_2H_4 , about 10% of the adsorbed ethylene can be hydrogenated and desorbed as ethane at 230 K.

3.4.4 High-Resolution Electron Energy Loss Spectroscopy (HREELS).

In Fig. 3.21 the HREEL spectra of C_2H_4 and C_2D_4 ordered on Rh(111) at 90 K in $(\sqrt{3} \times \sqrt{3})R30^\circ$ LEED patterns are compared. These spectra are nearly identical to the spectra for the lower coverage (2x2) monolayers and are unchanged by annealing to just below the C_2H_4 molecular desorption peak. This indicates that the 25% of the ethylene that desorbs molecularly has the same bonding as the 75% that decomposes. Based on the strong intensity of all modes observed in the C_2H_4 and C_2D_4 spectra in Fig. 3.21, ethylene on Rh(111) appears to fit into Sheppard's type I' category. The most similar published spectra for molecularly adsorbed ethylene are for Pd(100) [57], Ru(001) [55] and Fe(111) [88].

HREEL spectra of ethylene at low temperature on Rh(100) were taken only at saturation coverage to avoid contamination. At less than saturation coverage contaminant HREELS peaks were observed at 275, 455, 665, 940, and 1630 cm^{-1} . While this contaminant(s) was (were) not definitively identified, these peaks correspond closely to the vibrational frequencies for water adsorbed on Pt(111) [89]. The contaminant-free HREEL spectra for 4 L exposures of C_2H_4 and C_2D_4 on Rh(100) below

Rh(111) T=90 K



XBL 866-2422

Fig. 3.21 Specular HREEL vibrational spectra for saturation coverages of C₂H₄ and C₂D₄ on Rh(111) at 90 K. Both overlayers were ordered in $(\sqrt{3} \times \sqrt{3})R30^\circ$ LEED patterns

200 K are shown in Fig. 3.22. Presumably ethylene is molecularly adsorbed at this temperature.

The HREEL peaks in Fig. 3.22 for ethylene on Rh(100) are not nearly as sharp as those in Fig. 3.21 for molecular ethylene on Rh(111). Those features that are reproducible are labelled in Fig. 3.22. The peak positions at 1420, 1475, 2905 and 3015 cm^{-1} are approximate because of peak overlap, but the peak widths (3 times the instrumental resolution) justify the assignment as two peaks. In the C_2D_4 spectrum of Fig. 3.22B, the feature at 1275 cm^{-1} is quite weak, but reproducible. Its relative intensity is larger in some spectra and appears to scale with the intensity of the 2275 cm^{-1} peak. It is possible that this weak feature may be the result of some H,D-exchange by residual hydrogen atoms or of a small fraction of adsorbed C_2D_4 bound near surface defects or contaminants.

Interpretation of the HREEL spectra for ethylene on Rh(111) and Rh(100) in Fig. 3.21 and 3.22 is difficult. The vibrational frequencies are very different than those of gas phase ethylene, indicating at least that the chemical bonding has changed substantially within the chemisorbed molecules. In the absence of ethylene complexes having similar vibrational frequencies, interpretation of the vibrational frequencies is facilitated by considering the general characteristics of ethylene bonding that have been determined by vibrational spectroscopy. The vibrational frequencies observed by HREELS for molecularly adsorbed C_2H_4 and C_2D_4 are given in Tables 3.5 and 3.6. In all cases the "carbon-carbon stretching" frequency (1623(1515) cm^{-1} for gas phase C_2H_4 (C_2D_4)) is either not observed or is shifted to lower frequency

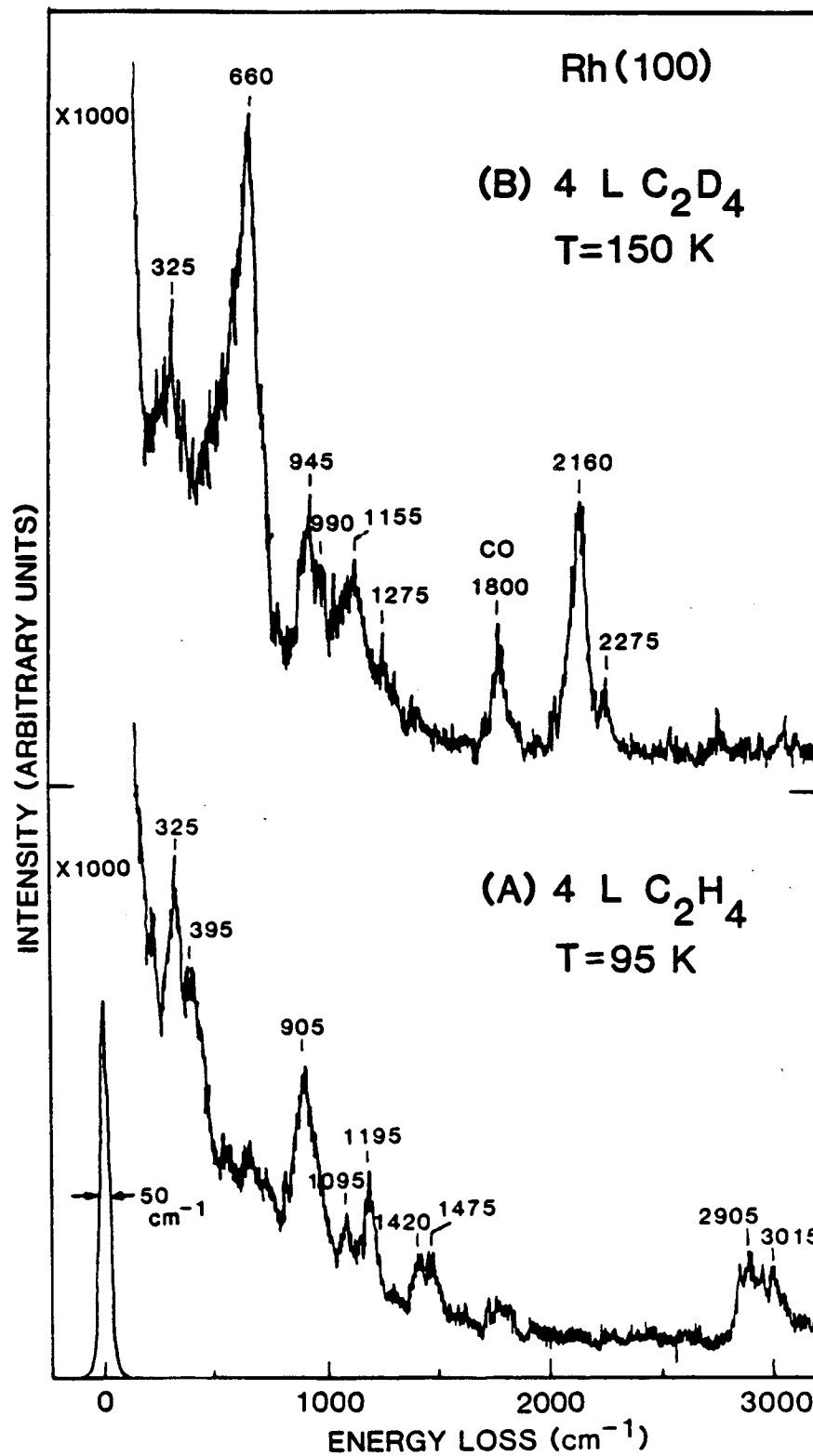


Fig. 3.22 Specular HREEL spectra for saturation coverages of (A) C₂H₄ adsorbed at 95 K and (B) C₂D₄ adsorbed at 150 K on Rh(100). Both overlayers showed diffuse (2x2) LEED patterns; both spectra were recorded at 90 K.

Table 3.5: Vibrational Frequencies for C₂H₄ Molecularly Adsorbed on Transition Metal Surfaces

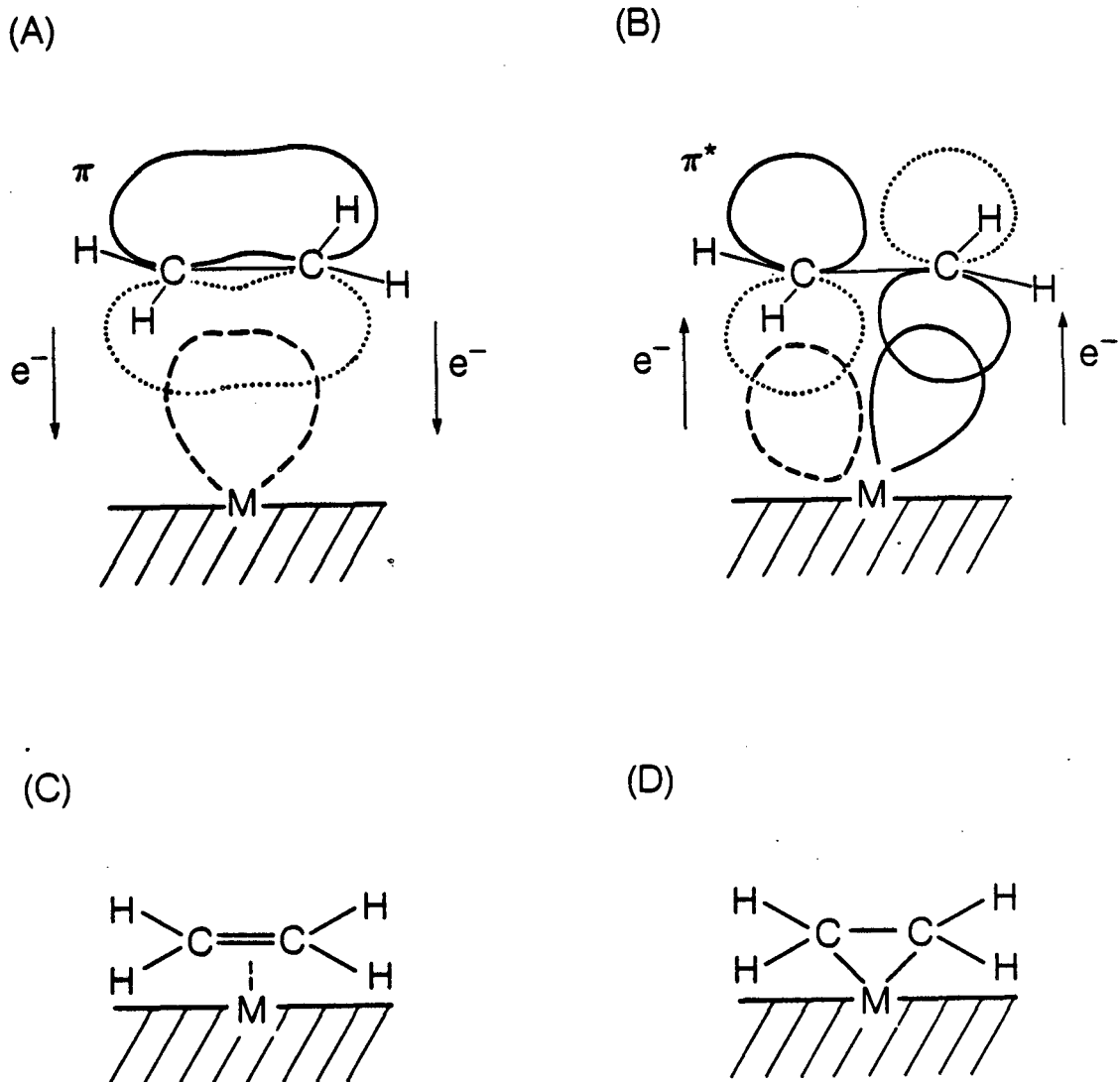
Surface	Observed Vibrational Frequencies (cm ⁻¹)											Ref.		
Cu(100)					903			1290		1557		2992	94	
Pd(110)	270	350	530		906		1151	1243	1413	1520		3003	3074	95
Pd(111)	256	341	533		911	1078	1145	1229	1418	1502	2780	2996		54
Zeise' Salt	219	405	493		975			1234		1515		3031	3094	93
Rh(111)	355	415	530	645	905			1185		1485		3000	3080	this work
Ni(110)	420				850			1145		1435		2970		85
Pd(100)	390				920			1135		1455		2980		57
Ru(001)	460			775	900	1040		1145		1450		2985		55
Fe(111)	385		580		886			1130		1410	2740	2950		88
Ni(111)	440		610	740	880		1100	1200		1440		2970		59
Ni(100)	420		620		900		1150			1420	2780	2990		96
Fe(110)	410	480		720	915		1105	1250		1410		2960		97
Rh(100)	325	395			905	1095		1195	1430	1475		2905	3015	this work
Pt(111)	470			660	790	980		1060		1430		2930	3000	5

Table 3.6: Vibrational Frequencies for C₂O₄ Molecularly Adsorbed on Transition Metal Surfaces

Surface	Observed Vibration Frequencies (cm ⁻¹)										Ref.		
Cu(100)				672		952		1347	1420		2234	94	
Pd(110)	272	322	536	665		937	1035	1246	1371		2233	2319	95
Pd(111)	270	365		673	840	953	1058		1355		2246		54
Zeise's Salt	200	385	451	757		962	1059		1353		2224	2349	93
Rh(111)	365		590	675		950	1055		1300		2185	2280	this work
Ni(110)	390			615		925			1235		2170	2290	85
Pd(100)	385			660		920			1220		2215		57
Ru(001)	420			700		900	1040		1210		2210	2295	55
Ni(111)	420		590	650		810			1200		2170	2280	59
Fe(110)	440		540	635	700	850			1160		2175		97
Rh(100)	325			660		945	990		1155	1275	2160	2275	this work
Pt(111)	450			600	740	900			1150		2150	2250	5

after adsorption, suggesting that ethylene bonds to the metal surface with the electrons originally involved in the carbon-carbon double bond. This type of bonding can be described by the Dewar-Chatt-Duncanson (DCD) [90] model originally proposed to explain ethylene coordination in inorganic complexes. In this model, as shown in Figs. 3.23A and 3.23B, the filled, ethylene π orbital donates electron density to an empty metal orbital, and the empty, ethylene π^* orbital accepts electron density from filled metal orbitals. Both interactions increase the heat of adsorption of ethylene on the surface, but weaken the carbon-carbon bond in ethylene. In valence bond terms, these donor and acceptor interactions between electrons in the surface and in ethylene rehybridize the ethylene carbon atoms to somewhere between sp^2 (Fig. 3.23C) and sp^3 (Fig. 3.23D).

This DCD coordination model for ethylene adsorption on transition metal surfaces has been implicitly assumed in previous interpretations of adsorbed molecular ethylene vibrational spectra. Based on this model, molecularly adsorbed ethylene vibrational spectra have been assigned using gas phase C_2H_4 [100] and $C_2H_4Br_2$ [101] as models for the sp^2 and sp^3 hybridization extremes in DCD coordination and interpolating between the vibrational frequencies of these model compounds. The interpolated vibrational peaks have then been attributed to traditional CH_2 functional group modes (CH_2 scissor, CH_2 wag, etc.). However for rehybridizations midway between sp^2 and sp^3 , these functional group modes are inadequate descriptions of the actual normal modes of vibration which involve motion of several functional group modes at once. This point is explicitly made in the appendix.



XBL 866-11177

Fig. 3.23 The Dewar-Chatt-Duncanson model of ethylene coordination to transition metal surfaces. Diagrams A and B show the interaction of the ethylene highest occupied (π) and lowest unoccupied (π^*) molecular orbitals with filled and empty metal surface orbitals respectively. Diagrams C and D depict, using valence bond formalism, the resulting extremes in bonding to the surface.

Assigning the vibrational spectra in terms of these functional group modes does not substantially increase our understanding of how ethylene bonds to transition metal surfaces. Such assignments can in fact lead to confusion. For example, the molecular ethylene vibrational spectra on Pd(100), Ru(001), and Fe(111) are similar to the Rh(111) spectra. However, as shown in Table 3.7, the spectral assignments in terms of functional group modes are different, disguising the spectral similarities. The inconsistencies merely reflect the inadequacy of functional group modes to describe the actual normal modes.

However, useful information can be extracted from the surface vibrational spectra about the bonding of molecular ethylene by explicitly considering the couplings between functional group modes. Coupling between the C-C stretch and CH₂ scissors modes of ethylene has been previously discussed for organometallic complexes by Powell, et al. [119] and for surfaces by Stuve and Madix [83]; in the appendix their discussions are extended to include coupling with other CH₂ bending modes. The conclusion is that the C₂D₄ vibrational spectra, where coupling between the C-C stretch and CD₂ bending modes is minimal, can be used to determine the C-C stretching force constant, k_{CC} , for adsorbed ethylene. The resulting correlation (derived in the appendix) is shown in Fig. 3.24. The correlation predicts that the observed vibrational frequency between 1100 and 1550 cm⁻¹ in the C₂D₄ vibrational spectrum (there should be only one peak per type of adsorbed ethylene in this region) continuously decreases in frequency with rehybridization from sp² to sp³. This trend should be independent of

Table 3.7: Published peak assignments for the vibrational spectra of molecularly adsorbed ethylene on transition metal surfaces having similar, type I', vibrational spectra

Mode Description	Vibrational Frequencies (cm ⁻¹)			
	Pd(100) [a]	Ru(001) [b]	Ru(001) [c]	Fe(111) [d]
$\nu_{as}CH_2$	---	3050(2295)	3110	2725
ν_sCH_2	2980(2215)	2940(2210)	2910	2980
CH ₂ scissor	1455(920)	1450(1210)	1400	1385
CC stretch	1135(1220)	1040(---)	1330	1115
CH ₂ wag	920(660)	1145(900)	1110	870
CH ₂ twist	---	900(700)	940	---
CH ₂ rock	---	775(---)	830	---
$\nu_{as}MC_2$	---	---	---	580
ν_sMC_2	390(348)	460(420)	450	450

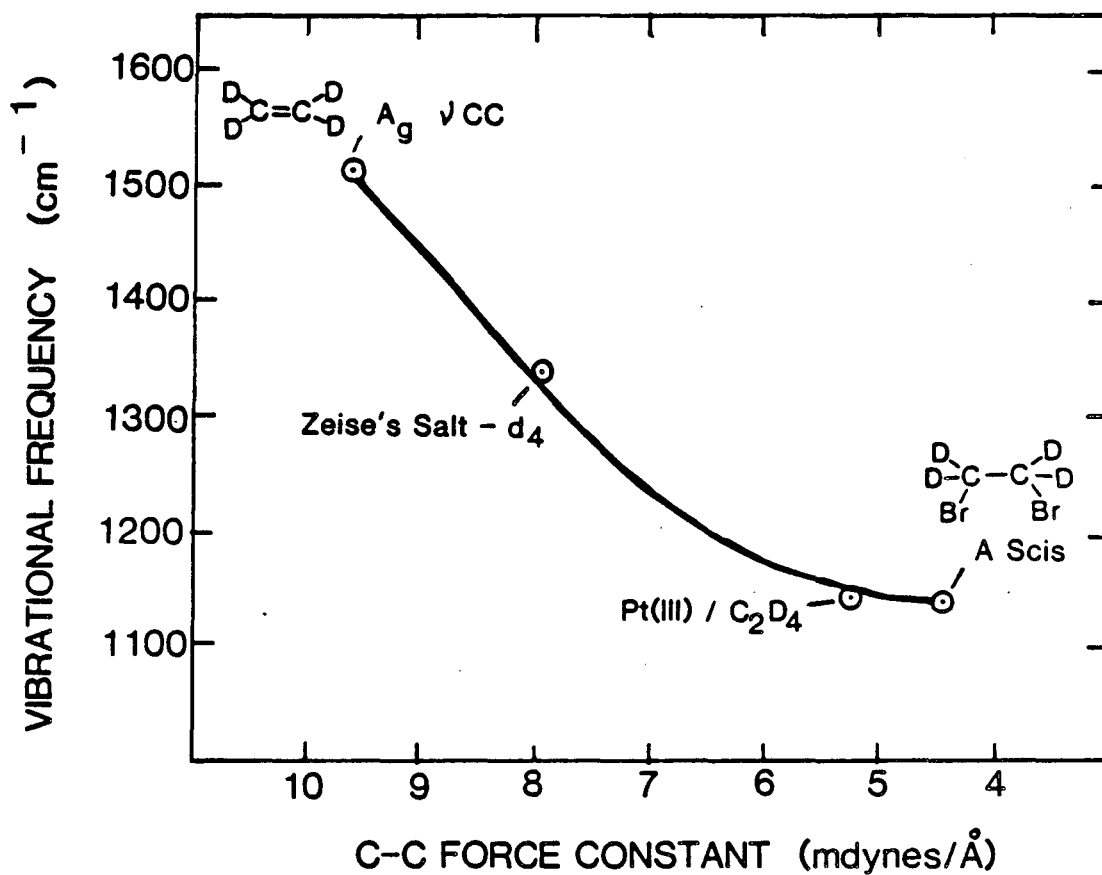
Frequencies in parenthesis are for C₂D₄

a) Stuve and Madix, ref. 47
b) Hills et al., ref. 55

c) Barteau et al., ref. 98
d) Seip et al., ref. 88

Correlation of Adsorbed Ethylene-d₄

Vibrational Frequencies with C-C Stretching Force Constant



XBL 868-3188

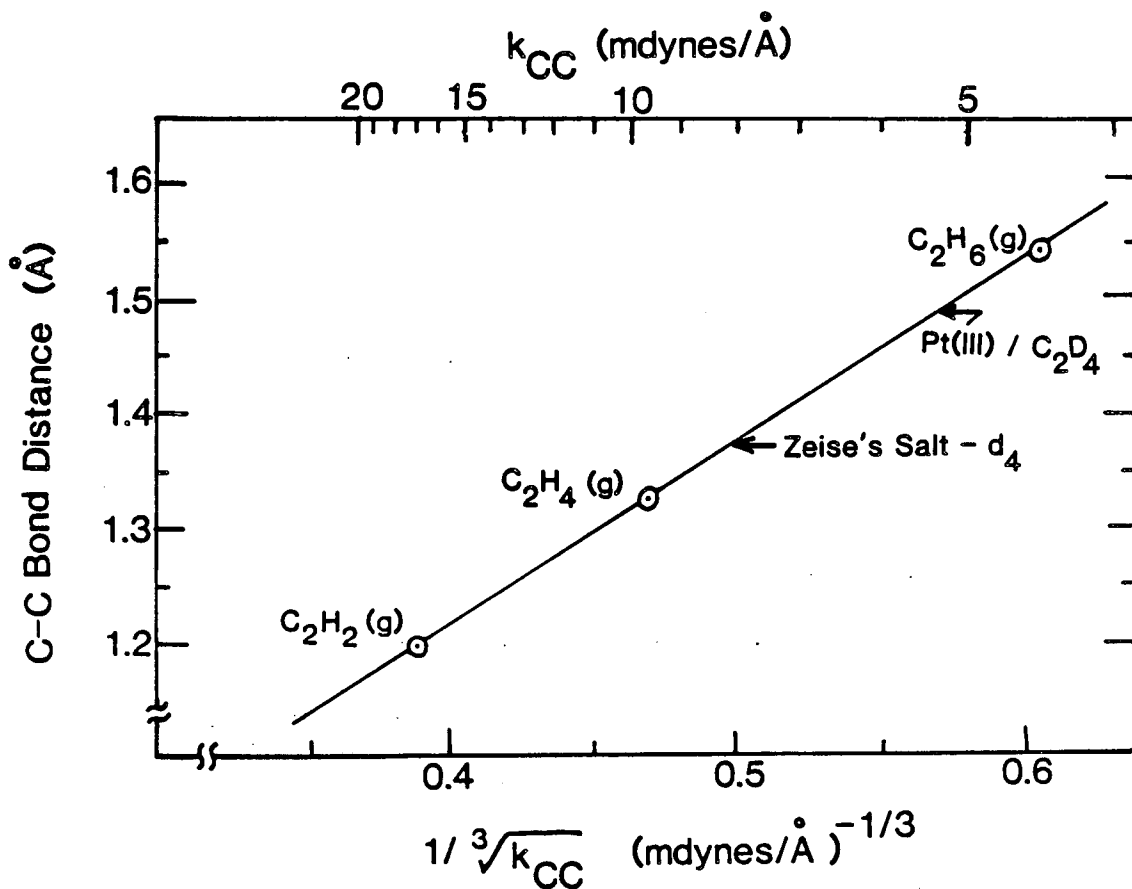
Fig. 3.24 Proposed correlation between the vibrational frequency observed in the 1100 to 1550 cm⁻¹ range for adsorbed C₂D₄ and the C-C stretching force constant. The points for Zeise's salt-d₄ and for C₂D₄/Pt(111) are discussed in the text. The correlation is predicted to hold for surfaces where the Dewar-Chat-Duncanson model for ethylene coordination is applicable.

adsorbed ethylene geometry as long as the C-C bond is approximately parallel to the surface, the C-H bonds point away from the surface, and both ends of the ethylene molecule are nearly equivalent. (Under these conditions, carbon atom hybridization will be the major factor in determining the vibrational frequencies.)

The points for Zeise's salt ($K[PtCl_3(C_2H_4)] \cdot H_2O$) and for C_2D_4 adsorbed on Pt(111) shown in Fig. 3.24 were determined using measured vibrational frequencies, measured C-C bond lengths, and an empirical correlation between C-C bond length and force constant. The correlation between bond length and force constant, known as Badger's Rule [91], is shown in Fig. 3.25 for the C-C bonds in gas phase C_2H_2 , C_2H_4 , and C_2H_6 . Such a relation has been assumed to hold for coordinated and surface-bound ethylene in order to use the measured C-C bond lengths in Zeise's salt (1.375 Å, x-ray crystallography [92]) and in C_2D_4 on Pt(111) (1.49 Å, NEXAFS [84]) to determine C-C force constants of 8.0 and 5.3 mdynes/Å respectively for these ethylene moieties. The vibrational frequencies from IR and HREELS are 1353 cm^{-1} for Zeise's salt- d_4 [93], and 1150 cm^{-1} for C_2D_4 on Pt(111) [5]. The fact that the resulting points in Fig. 3.24 fall close to the line that was drawn without knowledge of these experimental results supports both the correlation of vibrational frequencies with C-C force constant and the application of Badger's rule to surface-bound species.

For ethylene on Rh(111), the C_2D_4 vibrational frequency of 1300 cm^{-1} corresponds (Fig. 3.24) to a C-C force constant of 7.7 mdynes/Å. Using Badger's rule (Fig. 3.25), the predicted C-C bond length on the surface

Badger's Rule for C-C Bonds



XBL 868-3189

Fig. 3.25 The linear relation between C-C bond distance and $(1/k_{CC})^{-1/3}$ as suggested by Badger [91]. The arrows indicate the C-C bond distance determined for C₂H₄ in Zeise's salt and for C₂D₄ adsorbed on Pt(111).

is 1.4 Å, midway between C-C single (1.54 Å) and double (1.33 Å) bonds. From other empirical relations [99], this k_{CC} corresponds to a bond order of 1.5 and to a bond energy of 110 kcal/mol. The bonding geometry, while not known, is probably similar to that of ethylene on Ru(001) [55], Pd(100) [57], and Fe(111) [88]. Also, since only one peak is detected between 1100 and 1550 cm^{-1} in the C_2D_4 vibrational spectrum, it appears (see appendix) that there is only one type of bonding geometry for adsorbed ethylene on Rh(111). This seems generally to be the case for ethylene adsorption on transition metal surfaces, but two types of ethylene bonding have been observed on Pd(110) [95] and possibly Rh(100) as detailed below.

On Rh(100), as shown in Fig. 3.22, there are two peaks between 1100 and 1550 cm^{-1} . This indicates two different types of ethylene bonding to the surface, unless the weak 1275 cm^{-1} peak is due to contamination as previously discussed. The predominant peak at 1155 cm^{-1} corresponds (from Fig. 3.24) to a C-C force constant of 5.3 $\text{mdynes}/\text{Å}$ for adsorbed ethylene. The predicted C-C bond length from Badger's rule in Fig. 3.25 is 1.50 Å. The much weaker peak at 1275 cm^{-1} corresponds to a C-C force constant of 7.3 $\text{mdynes}/\text{Å}$ and a C-C bond length of 1.38 Å. Interestingly, these 1155 and 1275 cm^{-1} peaks can be correlated to the 1420 and 1475 cm^{-1} peaks in the C_2H_4 spectrum on Rh(100) shown in Fig. 3.22A. The separation between the peaks is much less in the C_2H_4 spectrum because of the different coupling between functional group modes. This is illustrated in Figs. 3.26 and 3.27 in the appendix which show that for force constants of 7.3 and 5.3 $\text{mdynes}/\text{Å}$, the

splitting between the "C-C stretching" frequencies should be much greater for C_2D_4 than for C_2H_4 . Like ethylene on Rh(111), the frequencies and intensities for molecular ethylene on Rh(100) appear to fit Sheppard's Type I' category of molecular ethylene HREEL spectra.

The correlation of C_2D_4 vibrational frequencies to C-C force constant (Fig. 3.24) can be used to compare the amount of rehybridization in adsorbed ethylene on Rh(111) to ethylene on other transition metal surfaces. Table 3.8 lists the transition metal surfaces on which molecular C_2D_4 vibrational spectra have been reported along with the CC force constants, bond lengths, and bond orders predicted by Figs. 3.24 and 3.25. Predictions of the C-C bond length in adsorbed ethylene on Cu(111), Ni(110), Pd(111) and Pt(111) have previously been made based on ultraviolet photoelectron spectra [87]. These spectra were interpreted using an SCF-LCAO method with the known levels of gas phase ethylene as a basis. While the agreement for Pt(111) is quite good and the prediction for Cu(111) is quite similar to the C-C bond length predicted here for ethylene on Cu(100), the Ni(111) and Pt(111) predictions are in poor agreement with the predictions in Table 3.8. It should be noted, however, that similar UPS calculations for acetylene on Pt(111) [87] predict a C-C bond length substantially shorter than that determined by NEXAFS [84].

An intriguing aspect of the amount of rehybridization in adsorbed ethylene on transition metal surfaces as judged by the bond lengths and bond orders in Table 3.8 is the lack of an obvious reason for the observed rehybridization trend. The rehybridization does not correlate to the position of the metal in the periodic table, the lattice

Table 3.8: Predicted* C-C force constants, bond lengths, and bond orders for ethylene molecularly adsorbed on transition metal surfaces

Surface	C-C Force Constant (mdynes/Å)	C-C Bond Length (Å)	C-C Bond Order
Cu(100)	8.7	1.35	1.66
Pd(110)	8.3	1.36	1.61
Pd(111)	8.2	1.37	1.59
Rh(111)	7.7	1.39	1.52
Ni(110)	6.9	1.41	1.41
Pd(100)	6.7	1.42	1.38
Ru(001)	6.5	1.43	1.33
Ni(111)	6.3	1.44	1.33
Fe(110)	5.4	1.48	1.20
Rh(100)	5.3	1.50	1.17
Pt(111)	5.0	1.51 [#]	1.13

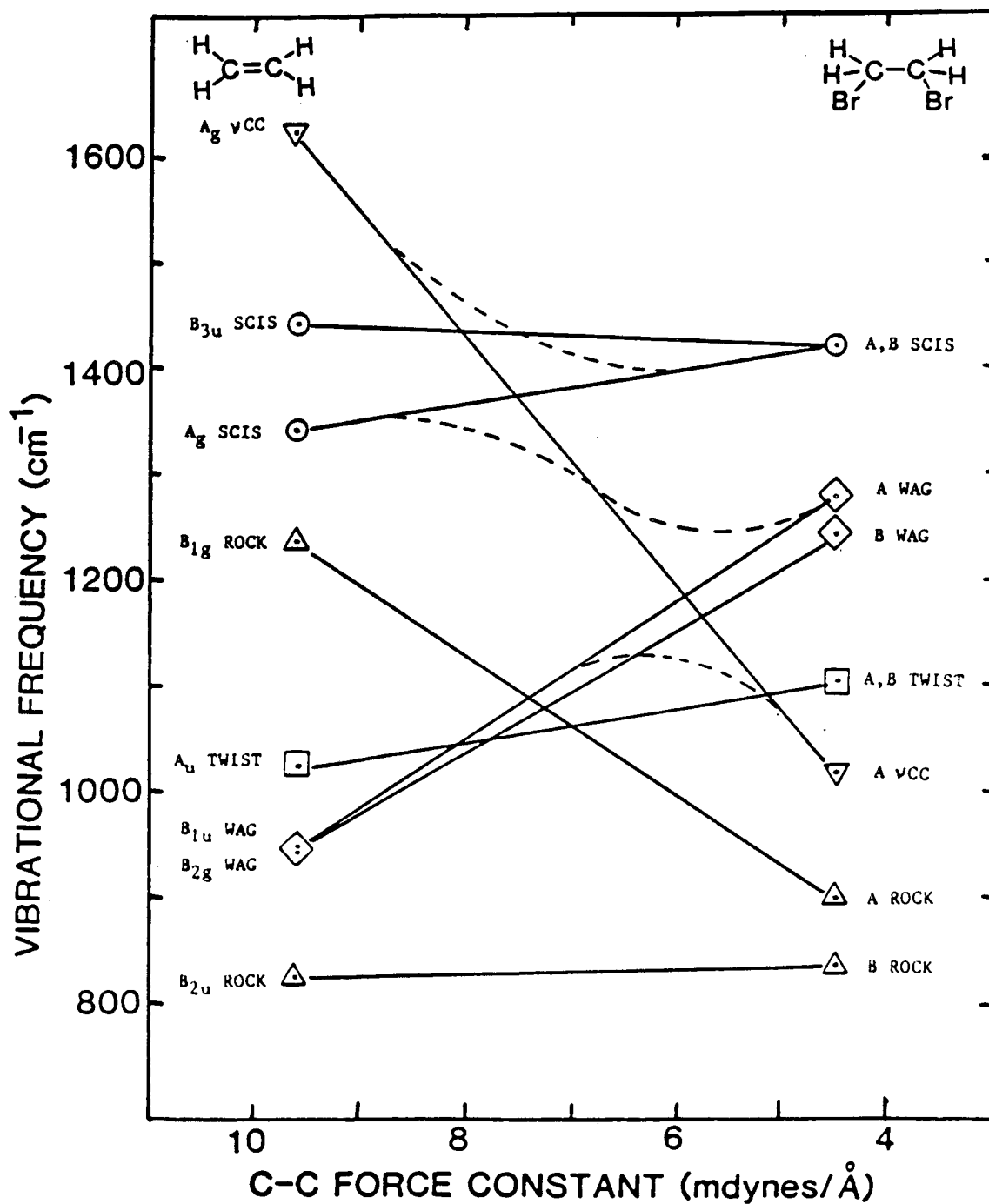
*) Force constant predicted based on vibrational frequencies from Table 3.6 and the correlation in Fig. 3.24.
 C-C bond length predicted from Fig. 3.25
 C-C bond order predicted using the relation: bond order
 $= (k_{CC}/4.2)^{.69}$ [20].

#) The C-C bond length for ethylene on Pt(111) has been determined by NEXAFS [84] to be 1.49 ± 0.03 Å.

constant, the types of high symmetry sites available, the work function of the surface, the metal-molecule stretching frequency, the heat of adsorption, the amount of molecular desorption, or the type of decomposition fragments. There may be a trend within a given row of the periodic table or as a function of crystal surface geometry for a given metal, but there is too little data to tell. It is highly recommended that the parameters mentioned above (along with the work function change after C_2H_4 adsorption) be measured whenever possible and reported. Clearly the molecular bonding of ethylene is a sensitive probe of the steric and electronic differences between these transition metal surfaces, and these surface-specific ethylene structures that are "frozen in" at low temperature may correlate with the weak, high coverage bonding that occurs in heterogeneous catalysis.

3.4.5 Appendix. Assignment of adsorbed ethylene vibrational frequencies by interpolating between the vibrational frequencies of C_2H_4 and $C_2H_4Br_2$ (models for sp^2 and sp^3 hybridized carbons) is not straightforward. While the vibrational frequencies should be determined almost completely by the carbon hybridization (if the DCD coordination model is valid), they cannot be determined by linearly interpolating between the functional group frequencies in C_2H_4 and $C_2H_4Br_2$ because of mode couplings.

This coupling of functional group vibrational modes is illustrated in Fig. 3.26. Here an interpolation is made between the vibrational frequencies in C_2H_4 [100] and gauche $C_2H_4Br_2$ [10] as a function of C-C stretching force constant, a measure of rehybridization. The solid

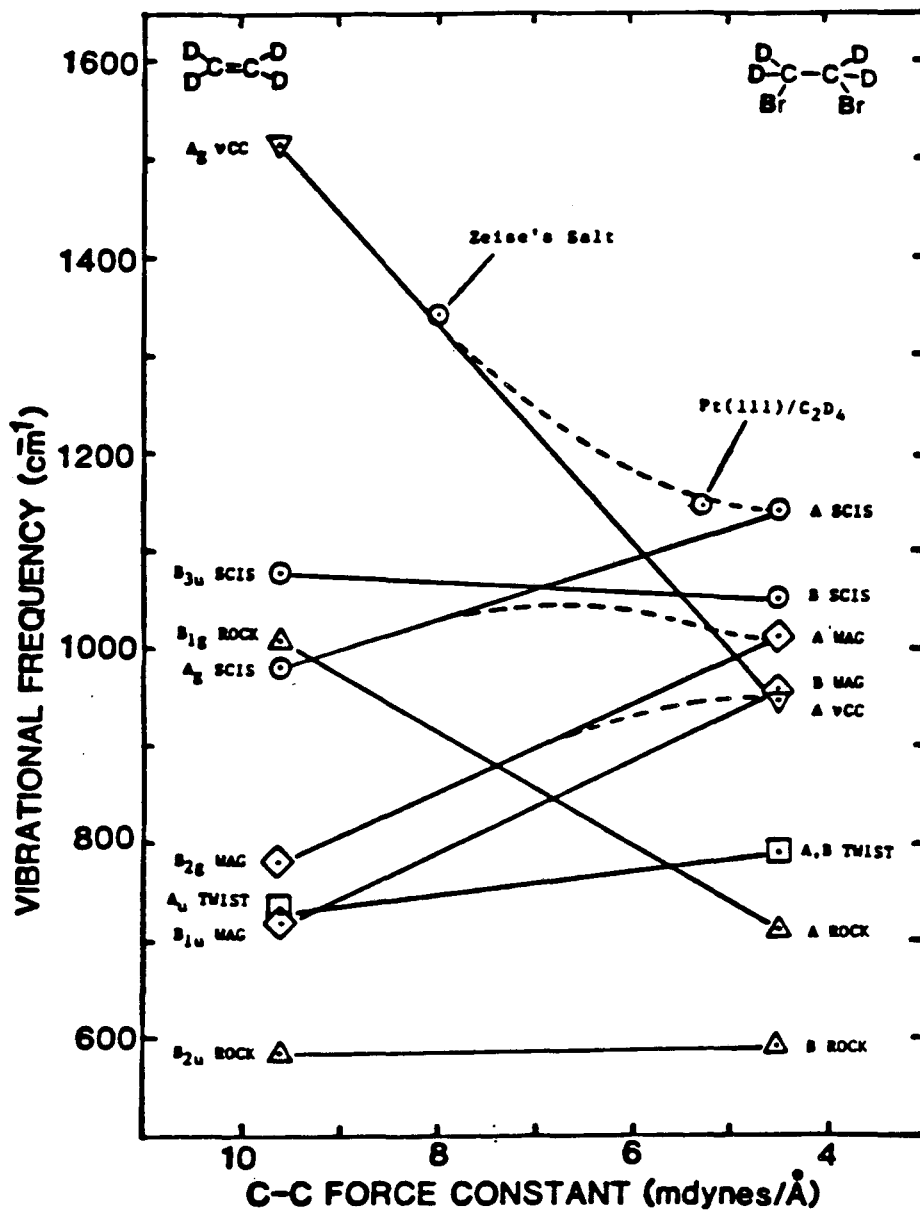


XBL 866-2420

Fig. 3.26 Correlation of the vibrational frequencies in C_2H_4 and $C_2H_4Br_2$ (gauche) as a function of the C-C stretching force constant. The solid lines connect similar functional group modes in the two compounds. The dashed lines indicate the couplings that can occur between the various group modes.

lines are approximations for the square root dependence of the vibrational frequencies on force constant. The dashed lines illustrate the kinds of couplings that can occur between modes having the same symmetry when ethylene is adsorbed on the surface. In this case, C-C stretch, CH₂ scissor and CH₂ wag modes were chosen, since these modes commonly have the same symmetry on the surface. These mode couplings mean that the observed vibrational frequencies do not continuously increase or decrease as the carbon atoms rehybridize from sp² to sp³. Further, different functional group modes will couple depending on the adsorption symmetry. Thus ethylene could bond with an identical C-C force constant but with different symmetry on two different surfaces, and the vibrational frequencies would be quite different. It is not surprising that the vibrational frequencies observed for ethylene adsorption on transition metal surfaces (Table 3.5) show no uniform trends. Furthermore, for rehybridizations midway between sp² and sp³, it is not appropriate to assign the observed vibrational frequencies to functional group modes. For example, an observed vibrational frequency of 1000 cm⁻¹ will probably, as shown in Fig. 3.26, involve substantial amounts CH₂ wag, twist and rock motion.

More information about ethylene bonding can be extracted from the C₂D₄ spectra. Here, because of the isotope shift, the CD₂ bending vibrations couple substantially less with the C-C stretching vibration. This is evident in the vibrational correlation between C₂D₄ and C₂D₄Br₂ given in Fig. 3.27. The only substantial coupling with the C-C stretch is due to the CD₂ scissors vibration. The approximated coupling between these modes given by the dashed line in Fig. 3.27 shows that,



XBL 866-2419

Fig. 3.27 Correlation (analogous to Fig. 3.26) of the vibrational frequencies in C_2D_4 and $\text{C}_2\text{D}_4\text{Br}_2$ (gauche). The dashed lines indicate coupling between the vCC , CD_2 scissors modes, and CD_2 wag modes, which is much less than in the hydrogenated case. The two circled points for Zeise's salt- d_4 and for C_2D_4 adsorbed on Pt(111) were plotted using measured vibrational frequencies along with C-C force constants determined from C-C bond lengths using Badger's rule as discussed in the text.

even with coupling, the observed vibrational frequency between 1100 and 1550 cm^{-1} in the C_2D_4 spectrum will probably decrease continuously with carbon rehybridization. Further, the degree of coupling will not be substantially affected by different adsorption geometries, since the symmetric CD_2 scissor and C-C stretch modes will always have the same symmetry. This means that the type of correlation shown in Fig. 3.24 should hold for ethylene on all surfaces where the DCD coordination model is applicable. The accuracy of the correlation in Fig. 3.24 for surface-bound ethylene depends on (1) how well the symmetric CD_2 scissor frequency in $\text{C}_2\text{D}_4\text{Br}_2$ approximates the surface frequency for sp^3 carbons and (2) how well the coupling between the scissors and stretch modes was chosen. Based on the points for Zeise's salt and for C_2D_4 on Pt(111) (shown in Fig. 3.24 and discussed in Section 3.4.3), the correlation appears reasonable.

Extracting the degree of rehybridization in adsorbed ethylene from the vibrational spectra has previously been discussed by Stuve and Madix [83]. By considering the coupling of the C-C stretch and the CH_2 (CD_2) scissor vibrations, they proposed a parameter called σ_π which combines the percentage shift to lower frequency upon adsorption of both the gas phase CC stretch and CH_2 (CD_2) scissor vibrations; the parameter is normalized to 0 for gas phase C_2H_4 and 1 for $\text{C}_2\text{H}_4\text{Br}_2$. However, the σ_π parameter has several drawbacks: (1) it does not include coupling to the CH_2 wag motion which can occur as shown in Fig. 3.26, (2) the number of modes coupled may vary with adsorption geometry, resulting in different σ_π parameters for similar rehybridizations, (3) it

is not always clear which peaks to use in calculating the parameter, and (4) the deuterated parameter does not give the same correlation as the hydrogenated parameter.

It appears that the observed vibrational frequency between 1100 and 1550 cm^{-1} in the C_2D_4 vibrational spectra can be used along with Fig. 3.24 as a simpler and more reliable indicator of C-C bond rehybridization. In the spirit of Stuve and Madix, a parameter (basically the C-C part of the C_2D_4 $\sigma\pi$ parameter) called DCD after the Dewar-Chart-Duncanson ethylene coordination model [90] is proposed. This parameter, defined as:

$$\text{DCD} (\text{C}_2\text{D}_4) = \frac{1515 - \text{Band I} (\text{C}_2\text{D}_4)}{374} \quad \text{Band I} = \text{highest frequency peak below } 1600 \text{ cm}^{-1}$$

has a value of 1 for $\text{C}_2\text{D}_4\text{Br}_2$ and 0 for C_2D_4 gas.

In Table 3.9, this DCD parameter is compared to the two $\sigma\pi$ parameters for all transition metal surfaces on which C_2D_4 vibrational spectra have been taken. Also included are the values of $\nu_s\text{CH}_2$ and $\nu_s\text{CD}_2$ which, although somewhat uncertain because of overlap with the anti-symmetric stretches, are uncoupled and may be good indicators of rehybridization if determined more accurately by infrared measurements. The $\sigma\pi(\text{C}_2\text{H}_4)$ parameter and the DCD parameter agree quite well except for the Fe(110) and Rh(100) surfaces. On the Fe(110) surface, the C-H (C-D) stretches and $\sigma\pi(\text{C}_2\text{D}_4)$ parameter suggest that the rehybridization is close to sp^3 as suggested by the DCD parameter of 0.94 rather than midway between sp^3 and sp^2 as suggested by the $\sigma\pi(\text{C}_2\text{H}_4)$ parameter of 0.55. However, the $\sigma\pi(\text{C}_2\text{H}_4)$ increases from 0.55 to 0.84 when the

Table 3.9: Comparison of Parameters Correlating Vibrational Frequencies to C-C Bond Hybridization in Ethylene Molecularly Adsorbed on Transition Metal Surfaces

Surface	Parameter					Reference
	DCD ^a	$\sigma\pi(\text{C}_2\text{H}_4)^b$	$\sigma\pi(\text{C}_2\text{D}_4)^b$	$\nu_s(\text{CH}_2)$	$\nu_s(\text{CD}_2)$	
$\text{C}_2\text{D}_4/\text{C}_2\text{H}_4(\text{g})$	0	0	0	xxxx	2251	100
Cu(100)	0.25	0.21	0.27	2992	2234	94
Pd(110)	0.38	0.38	0.38	3003	2233	95
Pd(111)	0.42	0.43	0.37	2996	2246	54
Zeise's salt	0.43	0.38	0.35	3031	2224	93
Rh(111)	0.57	0.50	0.47	3000	2185	this work
Ni(110)	0.74	0.72	0.66	2970	2170	85
Pd(100)	0.77	0.78	0.70	2980	2215	57
Ru(001)	0.80	0.85	0.78	2985	2210	55
Ni(111)	0.83	0.80	1.04	2970	2170	59
Fe(110)	0.94	0.55 ^c	1.00	2960	2175	97
Rh(100)	0.96	0.64	0.75	2905	2160	this work
Pt(111)	0.96	0.92	0.88	2930	2150	5
$\text{C}_2\text{D}_4\text{Br}_2/\text{C}_2\text{H}_4\text{Br}_2$	1.00	1.00	0.78	2953	2174	101

a) Parameter correlated to hybridization of the C-C bond in adsorbed ethylene — ranges from 0 for C_2D_4 gas to 1 for $\text{C}_2\text{D}_4\text{Br}_2$ gas. Defined in the appendix.

b) Parameters related to the C-C bond hybridization in adsorbed ethylene — $\sigma\pi(\text{C}_2\text{H}_4)$ has the same range as the DCD parameter while $\sigma\pi(\text{C}_2\text{D}_4)$ ranges from 0 to C_2D_4 gas to 0.78 in $\text{C}_2\text{D}_4\text{Br}_2$ gas. Parameters are defined and discussed in reference 83.

c) See appendix.

1105 rather than 1250 cm^{-1} peak is used for Band II in calculating that parameter. This type of ambiguity is avoided with the DCD parameter.

The 1100 - 1550 cm^{-1} region of the vibrational spectra of molecularly adsorbed C_2D_4 can also be used to determine if there is more than one bonding geometry for molecularly adsorbed ethylene. From the correlation in Fig. 3.27, it can be seen that any peaks observed in the molecularly adsorbed C_2D_4 vibrational spectra between 1100 and 1600 cm^{-1} must be due either to a C-C stretching motion or an overtone or combination band of lower frequency modes. Indeed, C_2D_4 adsorbed on most transition metal surfaces gives only one vibrational peak between 1100 and 1600 cm^{-1} as can be seen from Table 3.6. Cu(100), Pd(110) and Rh(100) are the three exceptions. For Cu(100), the 1347 cm^{-1} peak is almost certainly an overtone of the very intense 672 cm^{-1} peak, and the 1420 cm^{-1} peak is the C-C stretch. However, on Pd(110), the two peaks at 1246 and 1371 cm^{-1} have indeed been interpreted as C-C stretches for two different types of molecular ethylene on the surface. Of course while multiple peaks between 1100 and 1600 cm^{-1} are a good indicator for multiple ethylene bonding geometries on the surface, there can be cases where the C-C stretching vibration in adsorbed ethylene will be of weak intensity and be undetected.

3.5 C_xH Fragments on Rh(111) and Rh(100) Formed by Thermal
Decomposition of Alkenes, Alkynes, Dienes and Aromatics
Between 400 and 800 K

3.5.1 Background

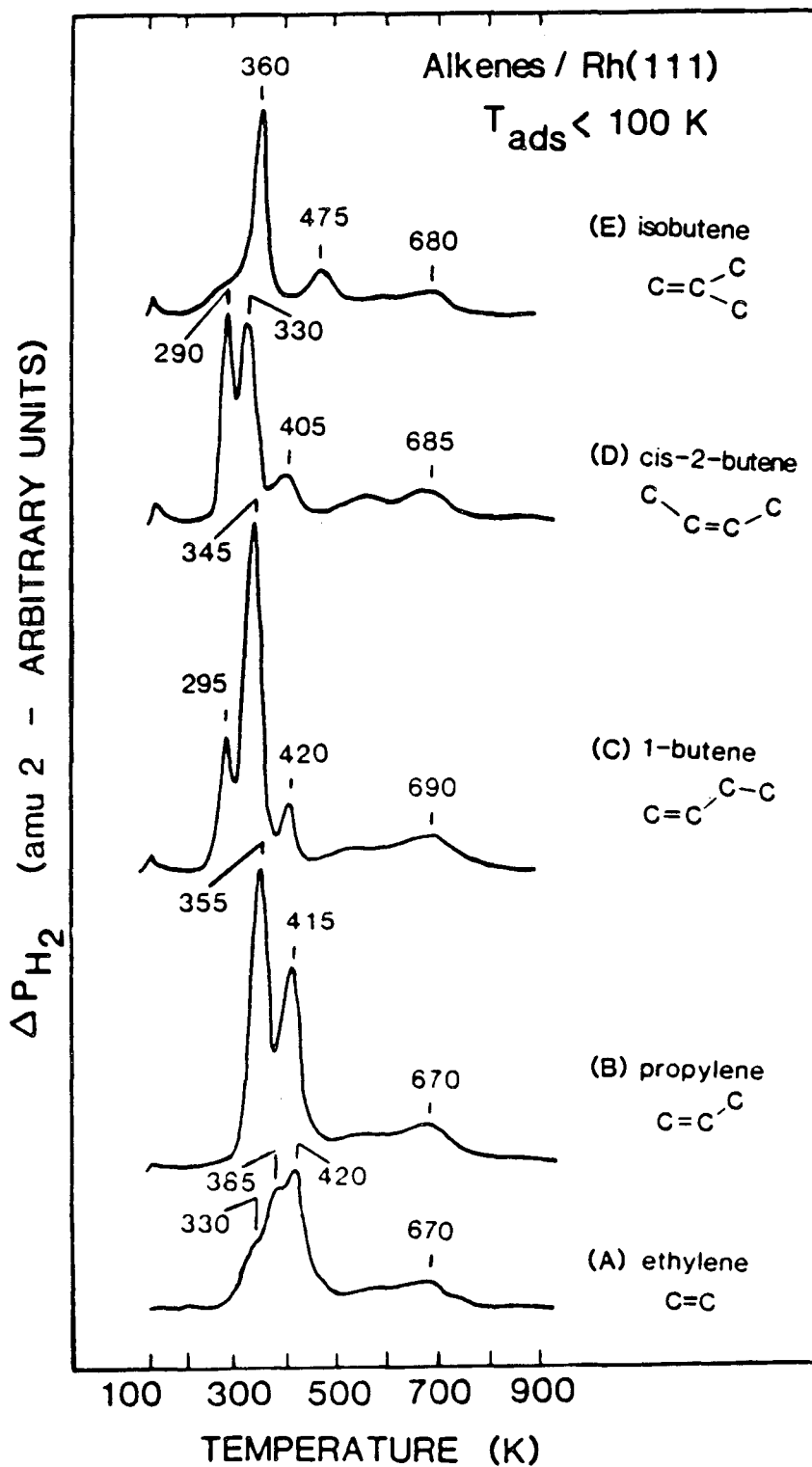
Surface science studies have revealed that during catalyzed hydrocarbon conversion reactions over metal surfaces, the active catalysts are partially covered with hydrocarbon fragments that have a characteristic H/C atomic ratio [102,103]. Catalyst deactivation occurs when this layer dehydrogenates completely to form a graphitic overlayer. Consequently, it is important to elucidate the nature of the stable hydrocarbon fragments that might be present on metal surfaces during catalytic reactions throughout the temperature range employed in catalytic reactions.

Catalytic hydrogenolysis and skeletal isomerization reactions over group 8-10 metal catalysts are performed industrially at 200-500°C. On the other hand, most surface studies of hydrocarbon adsorption and reaction with metal single crystal surfaces in UHV have been performed at room temperature. In this section, results of studies of the hydrocarbon fragments that form on Rh(111) and Rh(100) in UHV at these higher temperatures are reported. A wide variety of small alkenes, alkynes and dienes as well as benzene have been studied. TDS was used to monitor the sequential hydrogen evolution that accompanies the thermal decomposition of these irreversibly adsorbed hydrocarbons, while the identities of the disordered carbonaceous fragments produced on the surface were studied by HREELS.

It is found that the decomposition pathways below 400 K are molecule- or functional group-specific, while above 500 K all the hydrocarbons studied decompose to similar fragments on Rh(111) and Rh(100). Since mixtures of species coexist on the surface for all temperatures between 450 and 800 K, the vibrational spectra cannot be definitively assigned. However, the possible surface fragments can be narrowed down to CH, C₂H or partially hydrogenated polymeric carbon rings and chains. The HREEL spectra of C₂H species produced by low exposures of ethylene to Rh(100) at room temperature, are also presented; these HREEL spectra support the presence of C₂H species in the high temperature hydrocarbon monolayers.

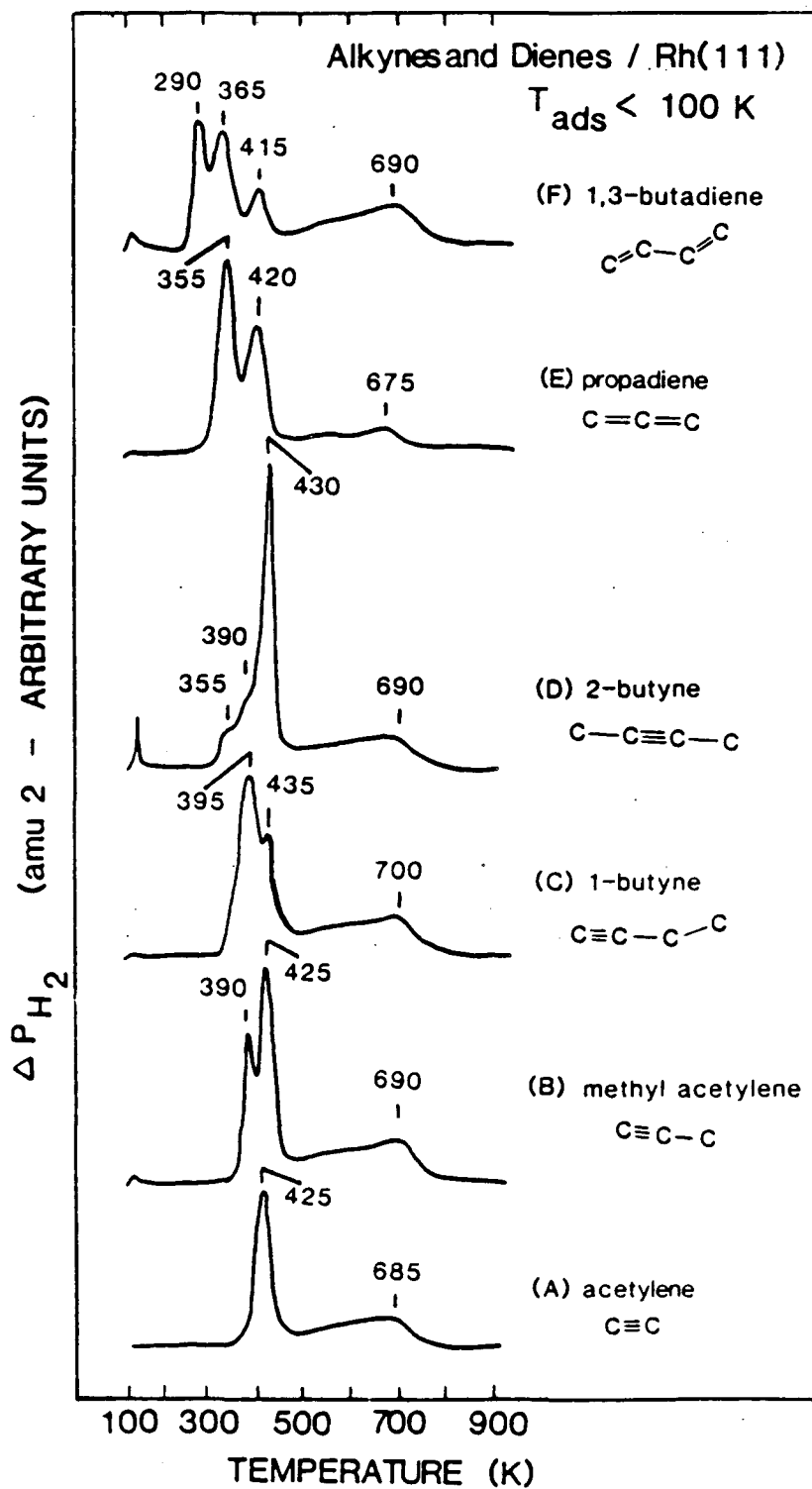
3.5.2 Results and Interpretation. The results are presented and interpreted in several subsections. First the hydrogen TDS and specular HREEL spectra on Rh(111) are presented and the general features and similarities of the high temperature fragments for different molecules are noted. Then, benzene and propylene decomposition are used to illustrate the effects of temperature, deuteration, and detection angle on the HREEL spectra. The possible surface species are identified by a combination of deductive reasoning, process of elimination, comparison to organometallic complexes, and comparison to the HREEL spectra for a C₂H species isolated at room temperature on Rh(100).

Alkene, Alkyne and Diene TDS on Rh(111). Figures 3.28 and 3.29 show the hydrogen thermal desorption spectra for all the hydrocarbons studied except benzene, whose spectrum is published [104,105]. The spectra were obtained by adsorbing 10 L (saturation coverage) of each



XBL 868-3195

Fig. 3.28 H_2 TDS for 10 L of the indicated alkenes on Rh(111). The alkenes were adsorbed below 100 K, and the heating rates were 15-20 K/sec.



XBL 868-3194

Fig. 3.29 H_2 TDS for 10 L of the indicated alkynes and dienes on Rh(111). Adsorption was performed below 100 K, and the heating rates were 15-20 K/sec.

molecule on Rh(111) at less than 100 K. In all cases, hydrogen is the predominant desorbing species. Only a small fraction, if any, of the adsorbed molecules desorbed molecularly.

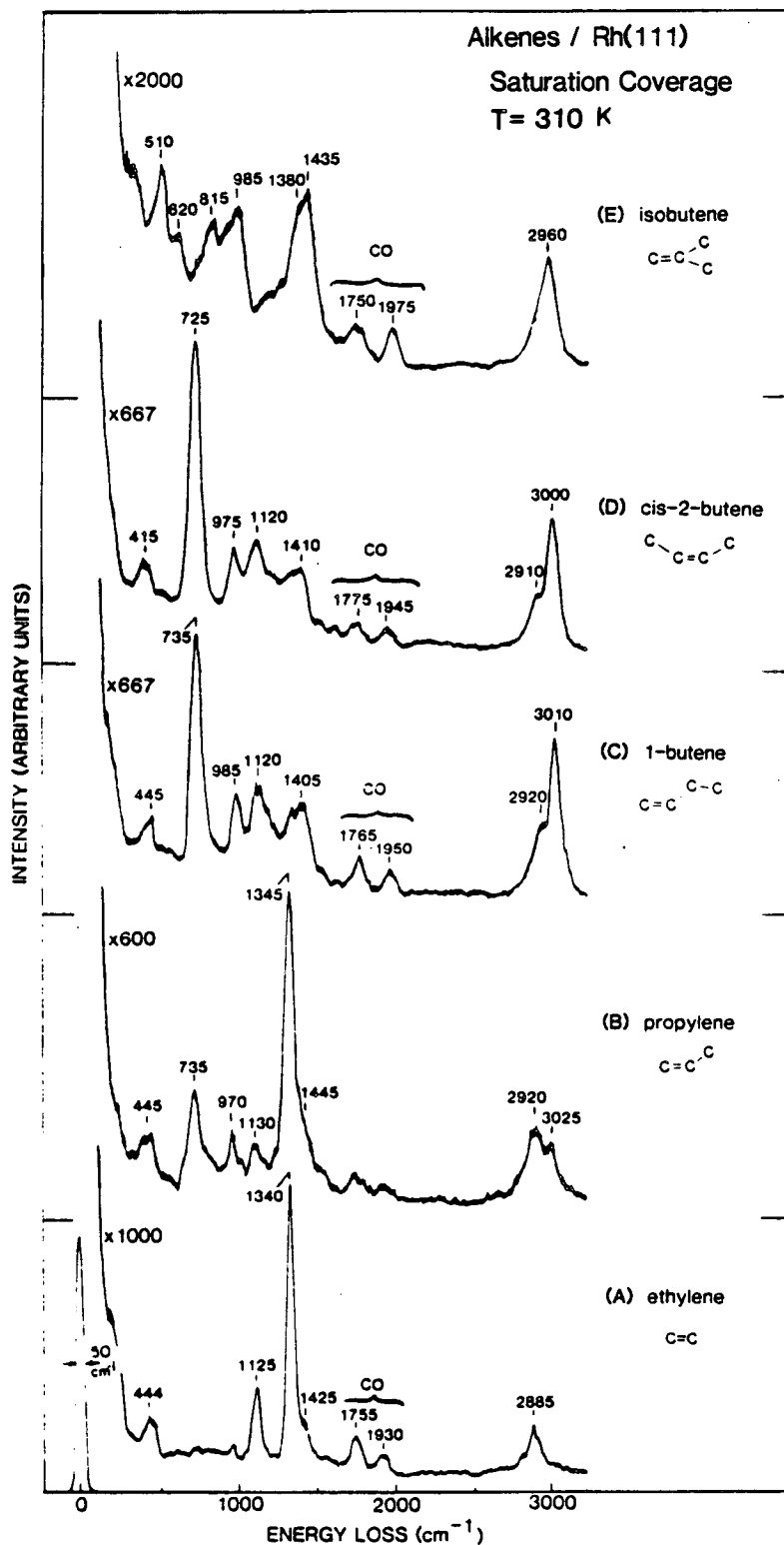
In comparing the thermal desorption spectra in Figs. 3.28 and 3.29, the two most striking features are their differences below 500 K and their similarities above 500 K. All molecules show a long tail from 500–800 K, while the sharp peaks below 500 K vary dramatically in position and intensity from one molecule to another. The emphasis here will be on the similarities above 500 K.

To quantify these similarities, the H_2 TDS curves were integrated to determine the H/C stoichiometries for each molecule at 500 K. These values are given in Table 3.10. In almost every case, the stoichiometry to within the ± 10 accuracy of TDS is C_2H , independent of the carbon chain length in the molecule adsorbed. With increasing temperature this H/C ratio continuously decreases until by 800 K only carbon is left on the surface.

Alkene HREEL spectra at 310 and 500 K on Rh(111). The HREEL spectra of ethylene, propylene, 1-butene, cis-2-butene, and isobutene adsorbed on Rh(111) at 310 and 500 K are shown in Figs. 3.30 and 3.31; these spectra support the TD spectra in Fig. 3.28. The 310 K HREEL spectra show that similar surface species are produced by ethylene and propylene and by 1-butene and cis-2-butene, but these species are quite different from each other and from the species formed by isobutene adsorption. However, by 500 K the HREEL spectra for all these molecules (as shown in Fig. 3.31) are quite similar to one another.

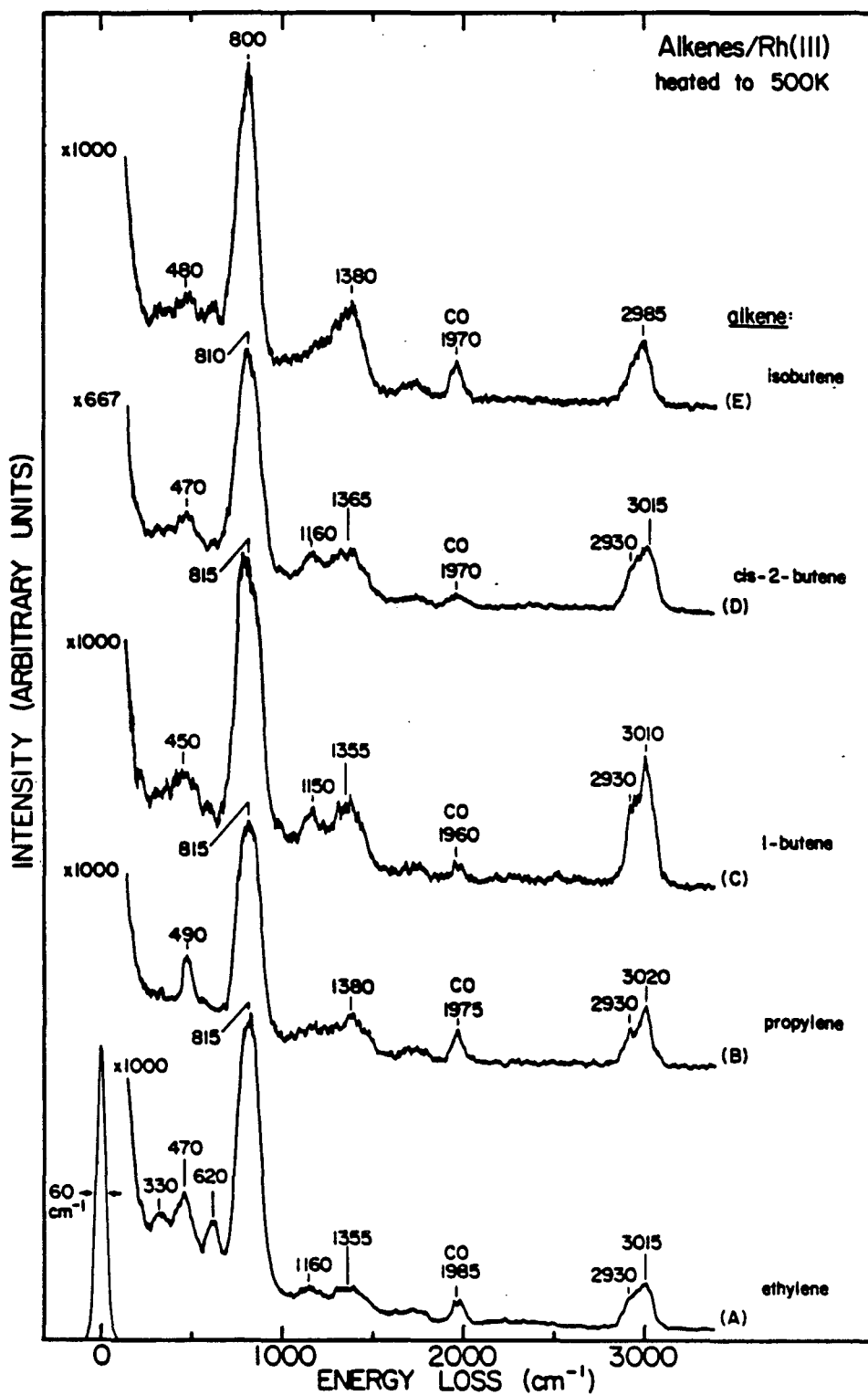
Table 3.10: Average stoichiometry and C/H composition at 500 K of the species produced upon thermal decomposition of adsorbed hydrocarbons. The composition is derived from the amount of hydrogen evolved in distinct desorption states below 500 K, as measured by TDS.

Absorbed Hydrocarbon	Average Stoichiometry	C/H Composition
ethylene (C ₂ H ₄)	C ₂ H _{0.9}	2.2
propylene (C ₃ H ₆)	C ₃ H _{1.5}	2.0
1-butene (C ₄ H ₈)	C ₄ H _{2.1}	1.9
trans-2-butene (C ₄ H ₈)	C ₄ H _{2.1}	1.9
cis-2-butene (C ₄ H ₈)	C ₄ H _{2.1}	1.9
isobutene (C ₄ H ₈)	C ₄ H _{2.2}	1.8
acetylene (C ₂ H ₂)	C ₂ H _{1.0}	2.0
methylacetylene (C ₃ H ₄)	C ₃ H _{1.3}	2.3
1-butyne (C ₄ H ₆)	C ₄ H _{2.6}	1.5
2-butyne (C ₄ H ₆)	C ₄ H _{2.2}	1.8
1,2-propadiene (C ₃ H ₄)	C ₃ H _{1.0}	3.0
1,3-butadiene (C ₄ H ₆)	C ₄ H _{2.6}	1.5



XBL 868-3202

Fig. 3.30 Specular HREEL spectra for saturation coverages of the indicated alkenes adsorbed on Rh(111) at 310 K. The spectra show that ethylene and propylene have decomposed to similar species, while 1-butene and cis-2-butene have formed a different surface species. These spectra are to be compared with the spectra after annealing to 500 K (Fig. 3.31) at which point all the surface species are the same.



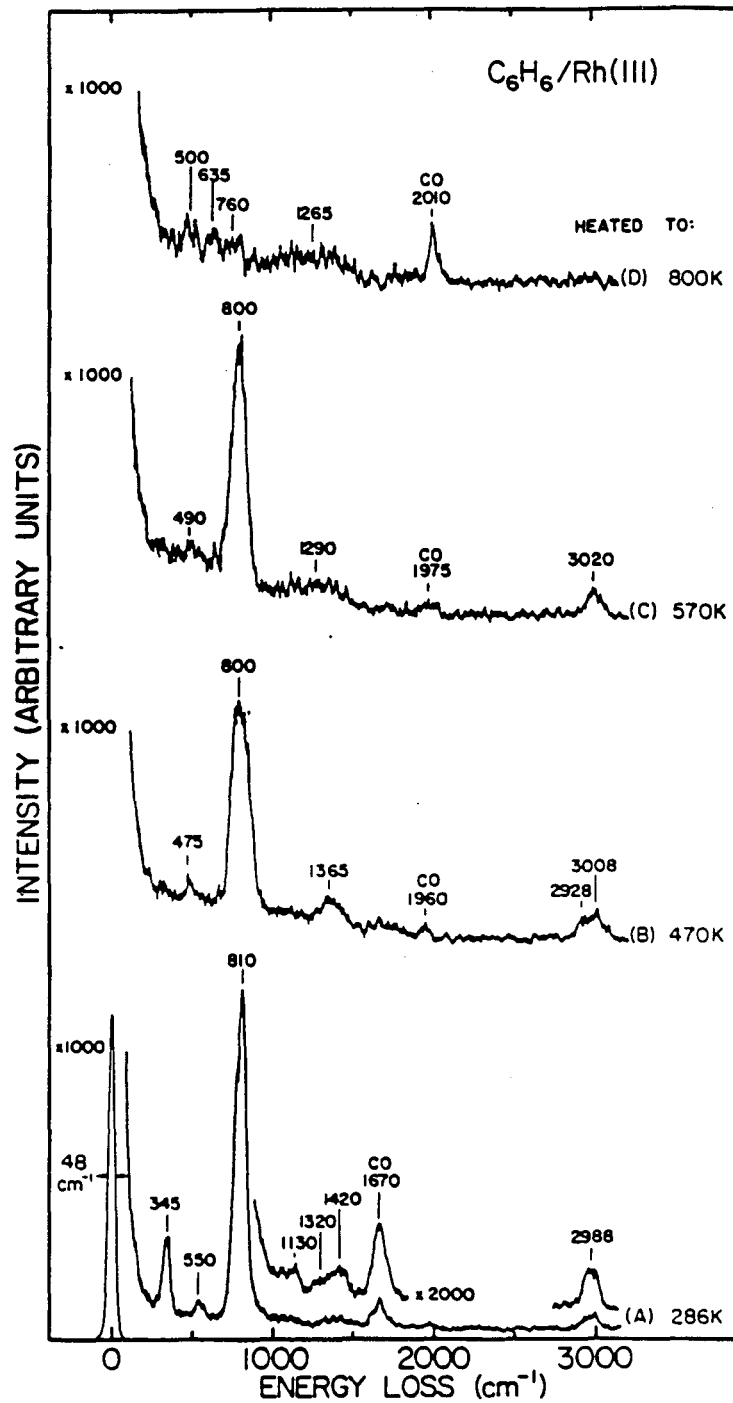
XBL 8610-3636

Fig. 3.31 Specular HREEL spectra for saturation coverages of the indicated alkenes after adsorption on Rh(III) at 310 K and brief annealing to 500 K. As discussed in the text, these HREEL spectra show that these different alkenes all decompose to the same types of C_xH_x species at 400 K.

The most distinguishing features of these 500 K HREEL spectra are the broad, intense peak at $\sim 800 \text{ cm}^{-1}$, the weak, but reproducible hump at $\sim 1380 \text{ cm}^{-1}$ and two C-H stretching frequencies at ~ 2930 and $\sim 3020 \text{ cm}^{-1}$. There are also weak metal-adsorbate vibrations in the $350\text{--}500 \text{ cm}^{-1}$ range and occasionally a weak peak at 1150 cm^{-1} . Both the broadness of the HREELS peaks and the absence of an ordered LEED pattern (LEED shows a (1x1) pattern with diffuse background scattering) for these 500 K monolayers suggest a mixture of surface species.

Benzene HREEL Spectra From 300-800 K on Rh(111). The HREEL spectral sequence shown in Fig. 3.32 for benzene decomposition on Rh(111) is comparable to those for the other unsaturated hydrocarbons and offers further evidence that a mixture of hydrocarbon species are present on the Rh(111) surface at 500 K. The spectrum in Fig. 3.32A is the HREEL spectrum for molecular benzene which bonds with its π -ring parallel to the Rh(111) surface. The assignment of this spectrum has been discussed [104,105]. Benzene begins to thermally decompose at 400 K as evidenced by the evolution of hydrogen from the surface. Thus, while the 470 and 570 K HREEL spectra in Fig. 3.32 appear at first glance similar to the molecular benzene spectrum, there is actually no molecular benzene remaining on the surface at these temperatures as evidenced by the complete disappearance of the benzene-metal vibrations at 345 and 550 cm^{-1} . These 470 and 570 K spectra are comparable to the 500 K spectra of the alkenes in Fig. 3.31.

The evidence for more than one surface species comes from an analysis of the C-H stretching frequency region. This spectral region



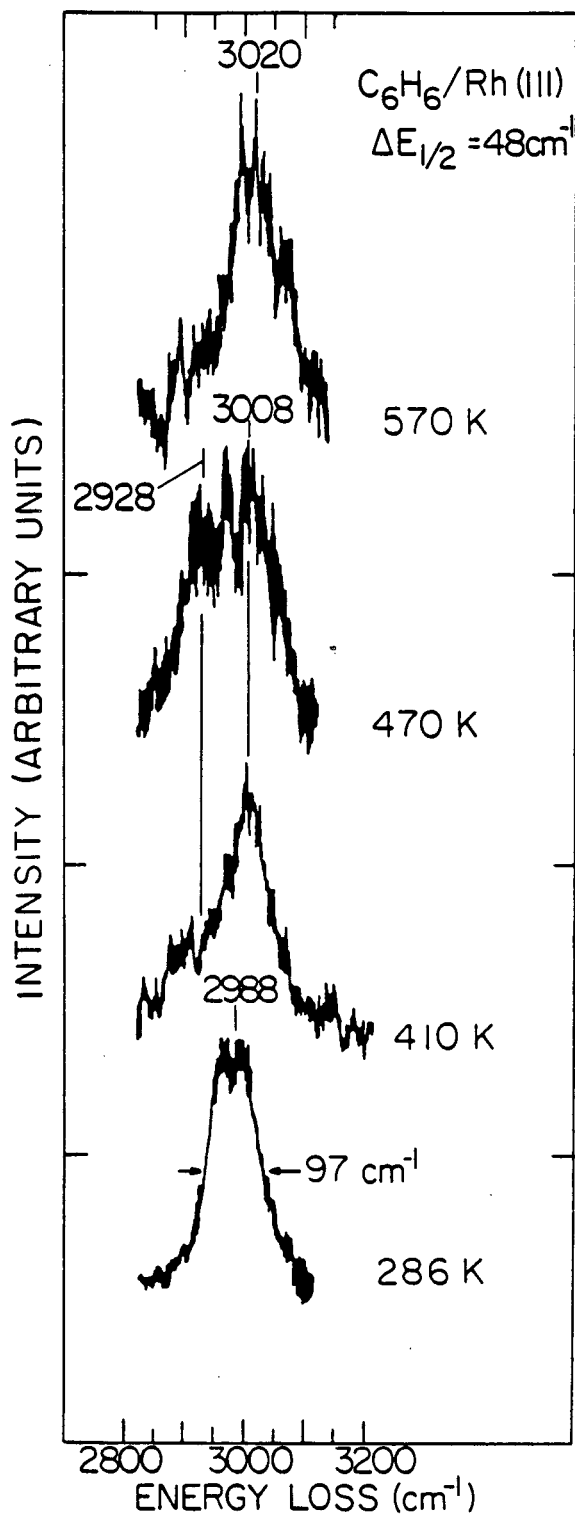
XBL 859-4048

Fig. 3.32 Specular HREEL spectra taken following step-wise warming of the Rh(111) surface after obtaining a saturation coverage of benzene at 290 K. The surface layer was momentarily warmed to the temperature indicated and then allowed to cool to 300 K before recording the spectrum.

for benzene decomposition is expanded in Fig. 3.33. As seen here, the molecular benzene C-H stretch at 2988 cm^{-1} clearly splits into at least two peaks (one at ~ 2928 and one at $\sim 3008\text{ cm}^{-1}$) as benzene begins to decompose at 410 K. The relative intensities of these modes change with temperature. They attain comparable intensities by 470 K and then collapse to a much narrower peak at 3020 cm^{-1} by 570 K. A plausible explanation for the change in relative intensities with increasing temperature is that the relative concentrations of two surface species are changing as dehydrogenation occurs in this temperature range. This is consistent with the hydrogen desorption tail in the TDS. However, it cannot be ruled out that both of the C-H stretching peaks are due to a single species whose orientation or stoichiometry changes with temperature, causing the relative intensity changes.

Haaland [107] has reported very similar spectra of the $\nu(\text{CH})$ region as a function of temperature in studies of benzene decomposition on $\text{Pt}/\text{Al}_2\text{O}_3$ catalysts using Fourier transform infrared spectroscopy. He concluded that two distinct species were formed: di- σ - and π -bonded benzene. The results here rule out the presence of molecular benzene at these temperatures on $\text{Rh}(111)$ in UHV, so the assignment of these peaks to decomposition products differs from the work by Haaland. While these two systems are certainly quite different, the similarity in the $\nu(\text{CH})$ frequencies and in the intensity changes that occur with temperature indicate that any benzene decomposition on $\text{Pt}/\text{Al}_2\text{O}_3$ would complicate the previous interpretation of the supported Pt spectra.

The benzene decomposition spectra in Fig. 3.32 also illustrate the insensitivity of HREELS to the structural changes on the surface



XBL 837-5994

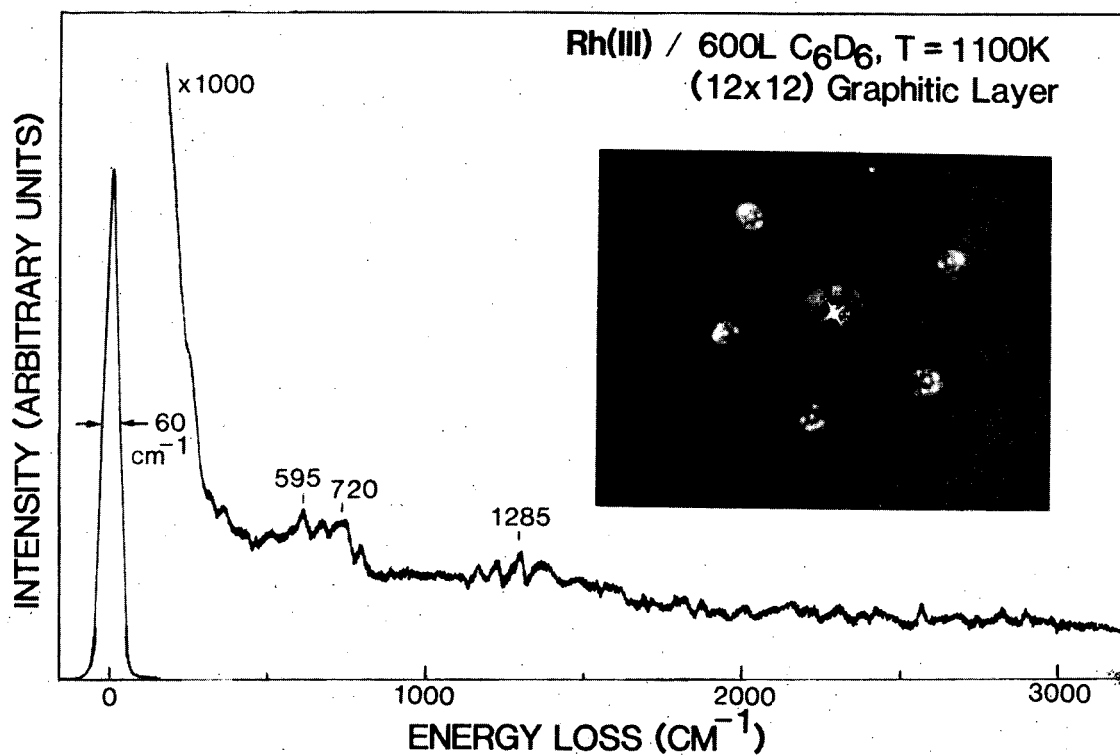
Fig. 3.33 The CH stretching region of the HREEL spectra (shown on an expanded scale) for a benzene monolayer on Rh(111) heated as in Fig. 3.32. The formation of two peaks at ~ 2930 and $\sim 3010 \text{ cm}^{-1}$ in this temperature range is also observed for all the other unsaturated hydrocarbons studied on Rh(111).

between 400 and 600 K. The HREEL spectra for benzene decomposition throughout this temperature range show the same general features despite the continuous dehydrogenation occurring in this temperature range. The same is true of the HREEL spectra of the other alkenes, alkynes and dienes. The intense 800 cm^{-1} peak is maintained up until the surface monolayer is completely dehydrogenated at 800 K. The spectrum of this dehydrogenated monolayer (Fig. 3.32D) is almost identical to that of an ordered (12x12) graphitic overlayer as shown in Fig. 3.34 (see also [108]). Formation of this ordered graphitic layer on Rh(111) actually required a 600 L dose of C_6D_6 at 1100 K in order to saturate the near surface region with carbon, since carbon dissolves into bulk Rh at this temperature.

Off-Specular HREEL Spectra For Benzene and Propylene Fragments.

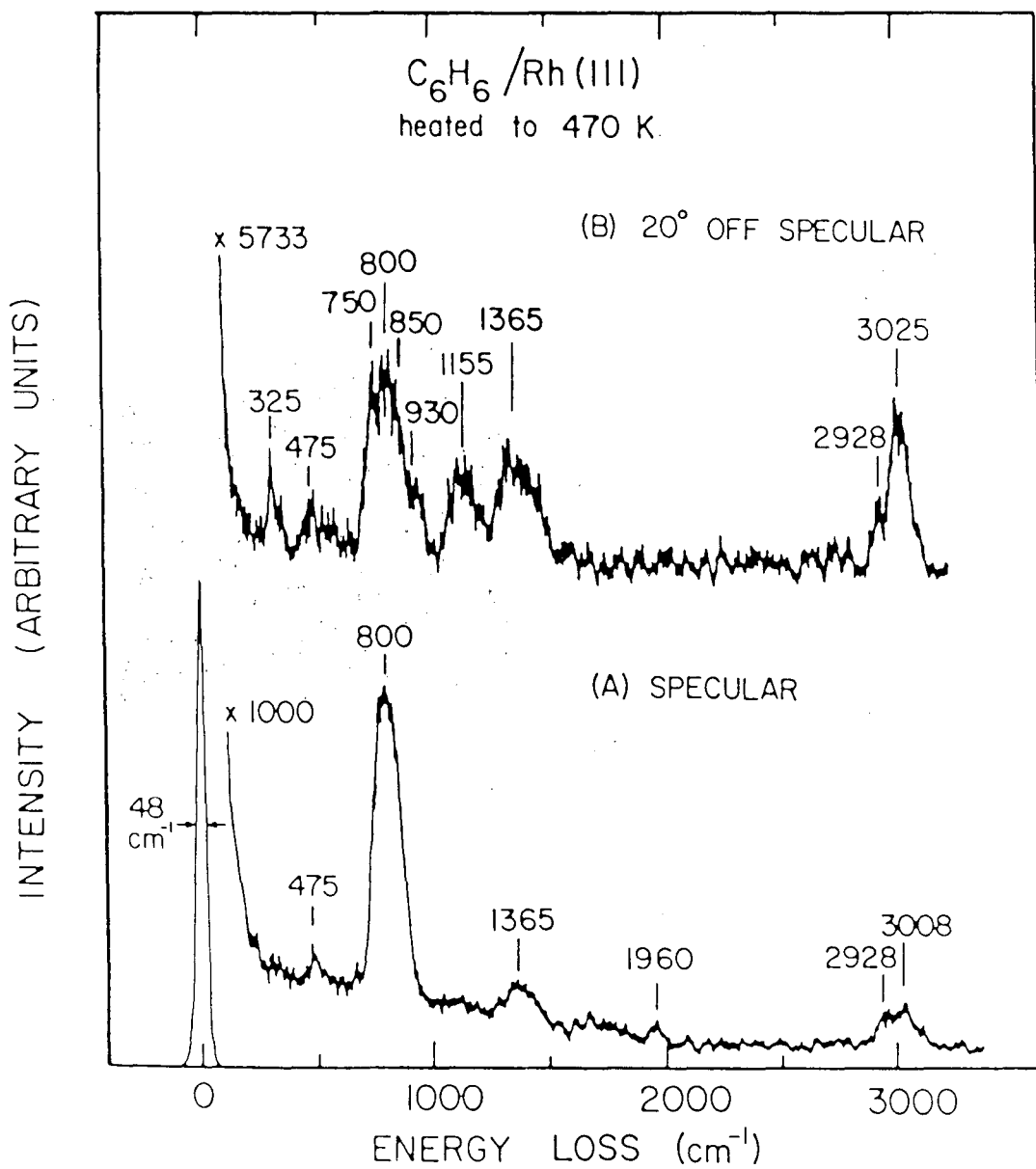
Off-specular spectra provided critical information about the dipole activity of several peaks. Specular and 20° off-specular HREEL spectra for benzene adsorbed at 470 K and propylene adsorbed at 500 K on Rh(111) are shown in Figs. 3.35 and 3.36 (bottom) respectively. The spectra are quite similar. The 20° off-specular spectra show clearly that at least two peaks contribute to the 800 cm^{-1} feature. Further, the large decrease in the relative intensity of the 800 cm^{-1} feature in the off-specular spectrum means that at least one of the modes involved is dipole active. By contrast, the increase in the relative intensity of the 1170 cm^{-1} peak suggests that this mode is dipole inactive.

HREEL Spectra of the Deuterated Propylene Fragments. The effects of deuteration on the 500 K fragment are shown in Fig. 3.36 (top) for



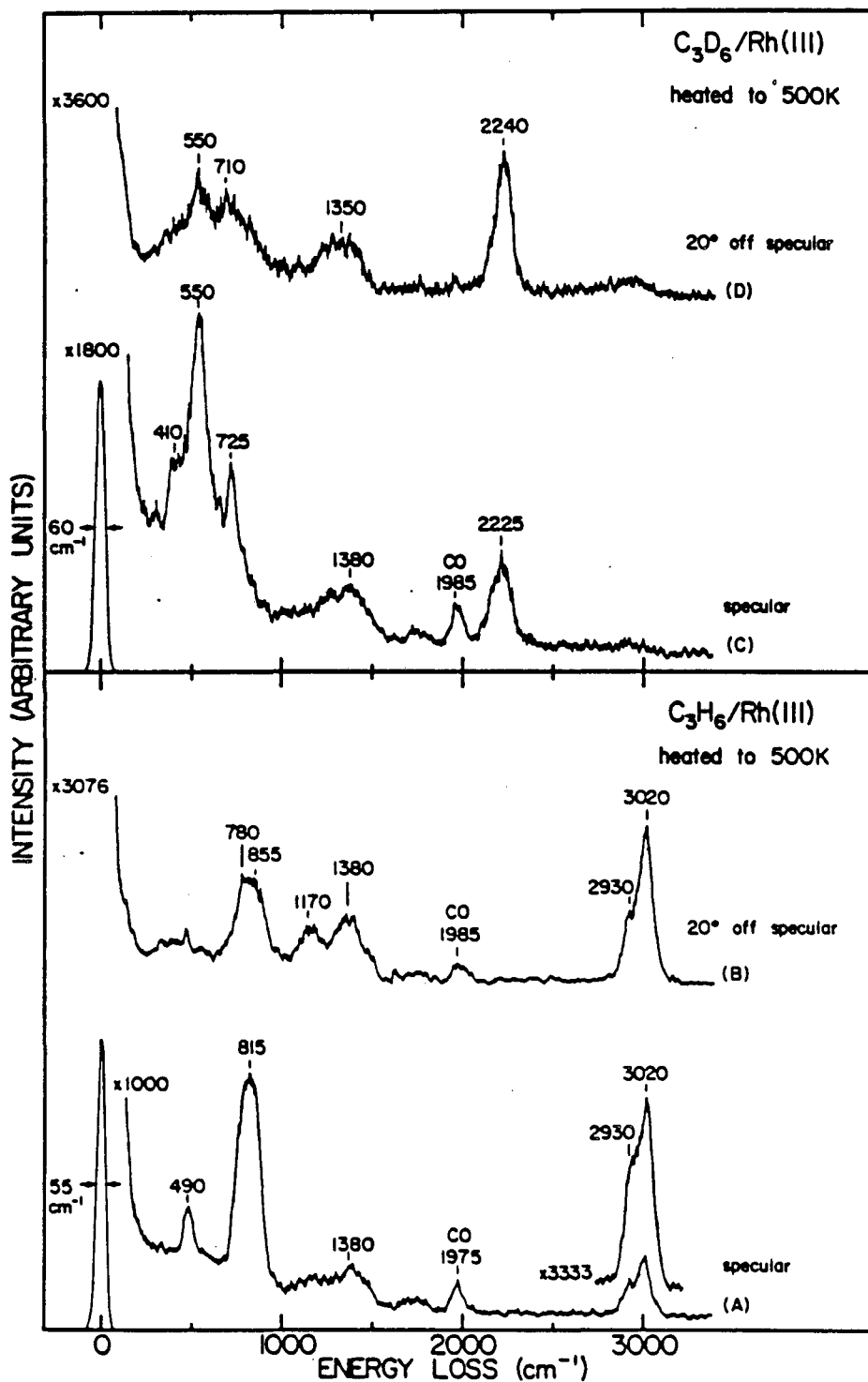
XBB 859-7809

Fig. 3.34 HREEL spectrum and LEED pattern for an ordered graphitic overlayer on Rh(111). This surface structure was produced by heating the Rh(111) crystal surface at 1100 K in 1×10^{-6} torr of C₆D₆ for 10 minutes. This large hydrocarbon exposure was needed to saturate the near-surface region with carbon, since carbon dissolves into bulk Rh at this temperature.



XBL 859-4000

Fig. 3.35 HREEL spectra taken with (A) specular and (B) 20° off-specular scattering angles for a Rh(111) surface which was saturated with benzene at 290 K and momentarily heated to 470 K as in Fig. 3.32.

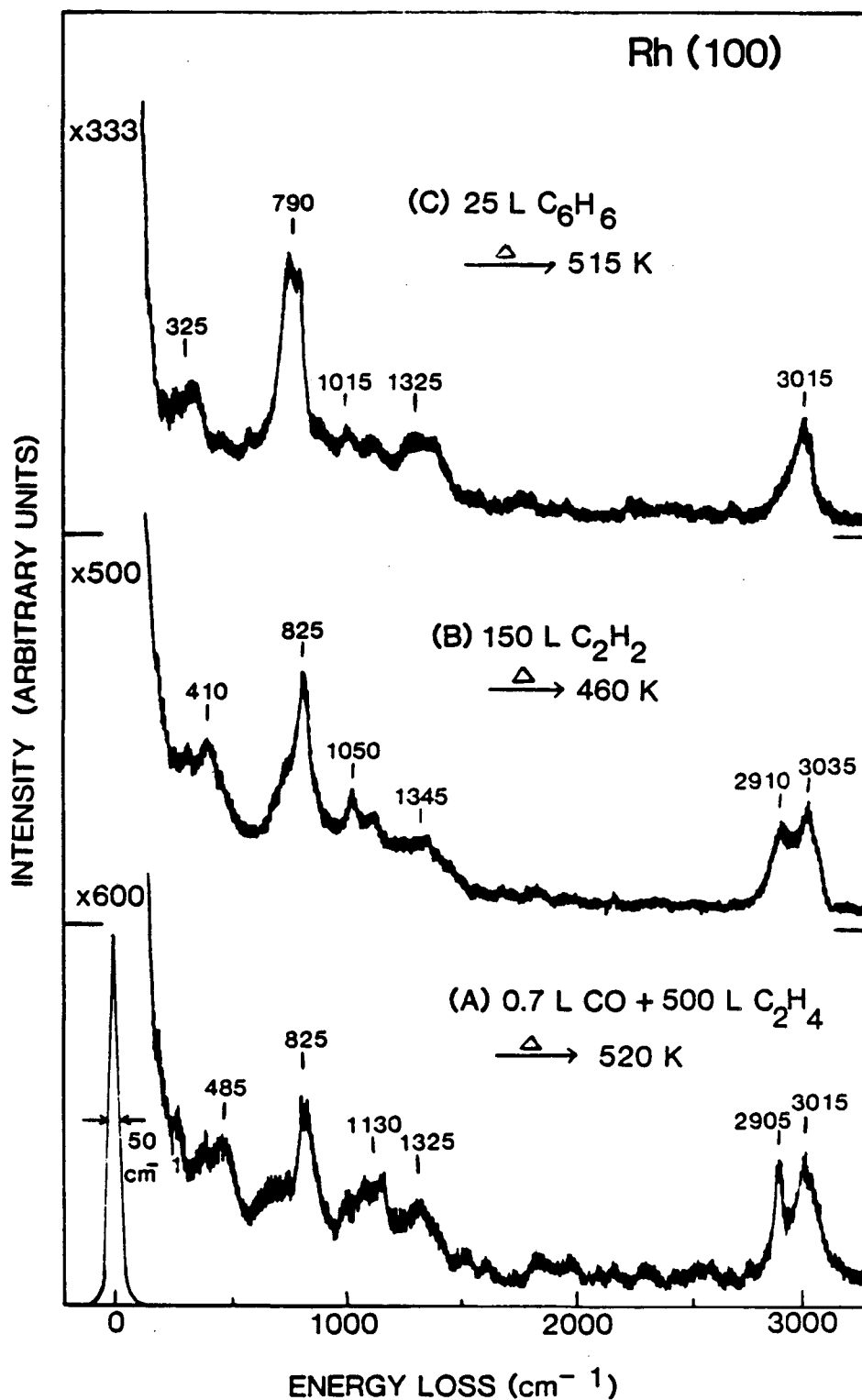


XBL 8610-3637

Fig. 3.36 HREEL spectra of a saturation coverage of propylene and propylene- d_6 adsorbed on Rh(111) at room temperature and annealed to 500 K. The lower panel shows the specular and 20° off-specular spectra for the hydrogenated fragments. These spectra are comparable to the benzene fragment spectra in Fig. 3.35. The upper panel shows the companion specular and 20° off-specular for the deuterated propylene fragments at 500 K.

propylene- d_6 . Both the specular and 20° off-specular spectra are shown. Looking first at the specular spectrum, it is clear that the 800 cm^{-1} peak has shifted down to 550 cm^{-1} upon deuteration. Also, the peak at 725 cm^{-1} must be a metal-adsorbate mode, since there is no counterpart at $\sim 1000\text{ cm}^{-1}$ in the hydrogenated spectrum, and this is too low a frequency for a carbon-carbon stretching vibration. Both the 725 and 550 cm^{-1} peaks decrease substantially in relative intensity in the off-specular spectrum, showing that these are both dipole active vibrations. The peak at $\sim 1380\text{ cm}^{-1}$ (which must be a carbon-carbon stretching vibration since it doesn't shift with deuteration) is either dipole inactive or has a weak dynamic dipole normal to the surface.

Hydrocarbon Fragment HREELS on Rh(100). Before discussing the possible surface fragments on Rh(111), it should be noted that similar hydrocarbon fragments are also formed on Rh(100). Figure 3.37 shows the HREEL spectra that result from thermal annealing of ethylene, acetylene, and benzene monolayers to between 450 and 550 K on Rh(100). The 0.7 L of preadsorbed CO in the ethylene case was used to selectively produce ethylidyne (see Section 3.2.3); the fragment spectrum at 520 K is unaffected by this CO. These fragment spectra on Rh(100) show many similarities to the 500 K alkene spectra on Rh(111). In particular, the features at ~ 800 , ~ 1325 , and $2900\text{--}3050\text{ cm}^{-1}$ have similar frequencies and relative intensities to peaks in the Rh(111) fragment spectra. Thus, presumably both the identity and the bonding of the high temperature hydrocarbon fragments on these surfaces are similar.



XBL 868-3198

Fig. 3.37 Specular HREEL spectra of a Rh(100) surface after adsorbing benzene, acetylene, and CO + ethylene at room temperature followed by annealing to the indicated temperatures. In the case of ethylene, the CO was added to selectively produce ethylidyne at room temperature and does not effect the decomposition.

Possible Surface Species. Since the surface stoichiometry and therefore also the surface fragments are continually changing in the 450–800 K temperature range, a temperature must be specified when discussing the surface species. The 500 K fragments will be discussed here first. At this temperature the surface stoichiometry (Table 3.10) is $\sim C_2H$. Also, if the interpretation of the benzene decomposition C–H stretch region in Fig. 3.33 is correct, there must be at least two surface species present.

The possible surface species can be substantially reduced by process of elimination based on the basic features of the 500 K fragment HREEL spectra. The presence of species containing a CH_2 group can be ruled out, since the scissor mode of a CH_2 group would cause loss peaks at ~ 1400 and $\sim 1000\text{ cm}^{-1}$ in the hydrogenated and deuterated spectra, respectively, which are not observed in the 500 K spectra. Species containing CH_3 groups are also absent, since these groups have characteristic vibrational modes at ~ 1030 , ~ 1350 , and $\sim 1450\text{ cm}^{-1}$ in hydrogenated spectra and at ~ 730 , ~ 950 , and $\sim 1025\text{ cm}^{-1}$ in deuterated spectra [100].

The remaining possibilities are C_xH species which have no more than one hydrogen bonded to any one carbon or C_x species. Since there appear to be at least two "CH-containing" species from the analysis of Fig. 3.33, the former species are considered first. Benzene and acetylene can be ruled out as the surface species since these molecules begin to decompose at 270 [23] and 400 K [105] respectively on Rh(111). This leaves CH, C_2H or polymeric species with three or

more carbons as the possibilities. Comparison below to model compounds suggests that at least CH and C₂H are likely fragments on Rh(111) at 500 K.

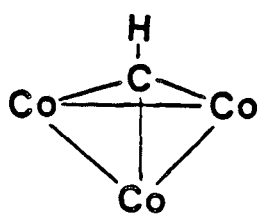
Model Compounds. There are a number of organometallic complexes in which the methylidyne (CH) or ethynyl (C₂H) ligand is coordinated to various numbers of metal atoms. In a few cases the vibrational frequencies of the CH or C₂H moiety in these complexes have been measured and can be compared to the 500 K fragment surface vibrational frequencies. For most of these clusters the vibrational frequencies have not been measured, but the positions of the carbon atoms with respect to the metal atoms have been determined by x-ray crystallography. While vibrational frequencies are really needed to determine how well these cluster species model the surface fragments whose vibrational spectra have been measured, the geometry alone can be useful because of the empirical correlation between bond lengths and force constants (vibrational frequencies) [91,99].

a) CH Species. The various types of known CH organometallic complexes are shown (minus other ligands) in Fig. 3.38. Also shown is the proposed surface coordination geometry on Rh(111) based on the discussion below.

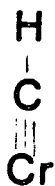
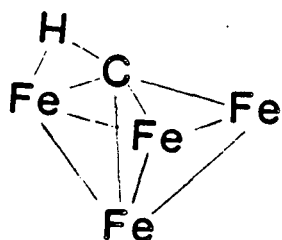
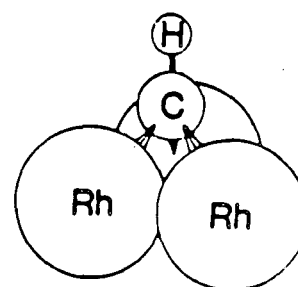
The vibrational frequencies for two trinuclear methylidyne clusters have been reported and are given in Table 3.11. Also tabulated are the frequencies determined by a normal coordinate analysis of the tricobalt cluster, the frequencies attributable to CH species in the 500 K propylene fragment spectrum, and the frequencies previously attributed to a CH species on W(110) and Ru(001). The strongest evidence

Surface and Cluster Bonding of Methylidyne

Known Cluster
Coordination



Proposed Surface Geometry
on Rh(111)



XBL 8610-4100

Fig. 3.38 Cluster bonding geometries known for the CH ligand in organometallic chemistry along with the proposed CH bonding geometry on Rh(111).

Table 3.11: Observed Vibrational Frequencies of CH Species

Mode Assignment	H ₃ Ru ₃ (μ ₃ CH)(CO) ₉ ^b	Co ₃ (ν ₃ CH)(CO) ₉ ^b	Normal Coordinate Analysis ^b	Rh(111)/C ₃ H ₆ ^c T = 500 K	W(110)/C ₂ H ₂ ^d T = 300 K	Ru(001)/C ₂ H ₃ ^e T = 500 K
ν(CH)	2988 [w]	3041(2258,1.35) [m]	3045(2263,1.34)	2930(2200,1.33) [m]	2930 [w]	3010(2250,1.34)[m]
δ(CH)	894 [vs]	850(680,1.25) [s]	852(679,1.25)	---	925 [vw]	810(615,1.32)[s]
ν _s (MC)	670 [m]	715(697,1.03) [m]	715(694,1.03)	--- (720) [m,sh]	581 [w,sh]	465(415,1.12)[m]
ν _{as} (MC)	427 [m]	417(410,1.01) [w,sh]	432(393,1.10)	---	---	

Frequencies are in cm⁻¹; numbers in parenthesis are (deuterated frequency, νCH/νCD)

s - strong, m - medium, w - weak, v - very, sh - shoulder, * - new assignment

a) Oxtan, ref. 110

d) Backx and Willis, ref. 111

b) Howard et. al., ref. 109

e) Hills et al., ref. 55; the surface species may actually be C_xH polymers

c) This work

for a CH species on Rh(111) from the 500 K fragment spectrum is the 720 cm^{-1} peak in the deuterated spectrum (Fig. 3.36 (top)). This peak, as discussed previously, must be due to a dipole-active metal-adsorbate vibration. Further, it occurs at too high a frequency to be anything other than a 1-carbon species [115]. This leaves CH and C as the only possibilities; the agreement between the surface and CD cluster ν_{MC} frequencies is reasonable.

The only other mode expected to dipole active for a CH species standing vertically in the 3-fold hollow is ν_{CH} . In the 500 K propylene fragment spectrum the lower frequency CH stretch at 2930 cm^{-1} is attributed to this mode. The cluster frequency is closer to the higher frequency CH stretch, but the higher frequency mode is better attributed to C_2H as shown below.

Other surface bonding geometries for CH, while not analogous to the bonding established for ethynidyne, should also be considered. The vibrational frequencies for top-site CH (Fig. 3.38) have not been measured, but the metal carbon force constant for a CrCH complex has been calculated to be 8.6 mdynes/\AA . This value corresponds to a ν_{MC} frequency of $\sim 1000\text{ cm}^{-1}$ for CD, much higher than the 720 cm^{-1} observed on Rh(111). Another bonding geometry previously proposed for surface CH on Ni(111) [113] and Pt(111) [112] has the CH species bound on one side of a three-fold hollow site with tilting of the CH bond towards one or two metal atoms. Such a species, which seems chemically unlikely and has no organometallic analogue, was proposed to explain the intense and presumably dipole-active CH bending frequency at $\sim 800\text{ cm}^{-1}$

in the Ni(111) and Pt(111) spectra. However, this peak, like the one in the 500 K fragment spectra on Rh(111), is more reasonably assigned to a dipole-active C-H bend in a tilted C_2H species. Indeed, the Pt(111) and Ni(111) spectra show weak modes at 1300-1400 cm^{-1} which can be attributed to the C-C stretching vibration in C_2H .

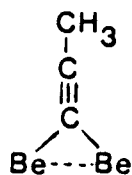
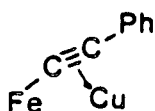
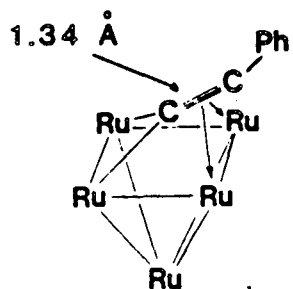
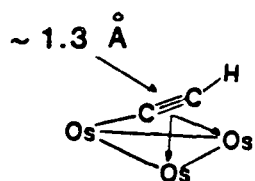
The presence of CH species on Rh(100) can not be determined from the present spectra. By comparison to the bonding of ethynidyne on Rh(100) (Section 3.2.4), a four-fold hollow site seems the most likely coordination site; no organometallic complexes with CH or alkynidyne species in four-fold hollow sites have yet been synthesized. The closest analogue is the Fe_4CH "butterfly" cluster shown in Fig. 3.38.

b) C_2H Species. The various coordination modes found for the C_2H ligand in organometallic clusters are shown in Fig. 3.39, along with the proposed bonding geometries on Rh(111) and Rh(100) which are based on the following discussion. The observed C-C stretching frequency of $\sim 1380\text{ cm}^{-1}$ on Rh(111) and Rh(100) is about 100 cm^{-1} lower than the C-C stretching frequency reported for any C_2H cluster and is most consistent with a highly coordinated, tilted C_2H species. In such a tilted C_2H species, occupied metal orbitals can overlap with the C-C antibonding orbitals in C_2H , weakening this bond and lowering the stretching frequency. The 500 K Rh(111) fragment spectra actually show quite good agreement with the vibrational frequencies reported for the Os_3C_2H species shown in Fig. 3.39.

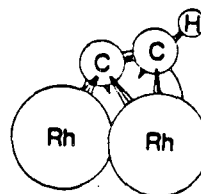
Table 3.12 compares the vibrational frequencies of this cluster to the those attributable to C_2H in the 500 K Rh(111) spectrum. Also

Surface and Cluster Bonding of Acetylide

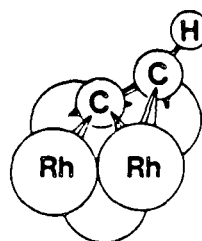
Known Cluster Coordination



Proposed Surface Geometry



Rh(111)



Rh(100)

XBL 8610-4101

Fig. 3.39 Cluster bonding geometries known for the C₂H ligand in organometallic chemistry along with the proposed C₂H bonding geometries on Rh(111) and Rh(100).

Table 3.12: Observed Vibrational Frequencies of C₂H Species

Mode Assignment	Os ₃ (CO) ₉ (μ-H)(μ ₃ -η ² -CCH) ^a	Rh(111)/C ₃ H ₆ ^b T = 500 K	Rh(100)/C ₂ H ₄ ^b T = 300 K	Pd(111), (100)/C ₂ H ₂ ^c T = 450 K
ν(CH)	3157(2377,1.33) [ms]	3020(2240,1.35) [m]	3025(2290,1.32) [m]	3000(2240,1.34) [m]
ν(CC)	1534(1496,1.03) [ms]	1380(1380,1.00)[w,br]	1305(1280,1.02) [w]	1340(1340,1.00) [w,br]
δ(CH)	861 (714,1.21) [#] [m] 854 (709,1.20) [#] [m]	-815(-550,1.48)[s,br]	805(660,1.22) [ms]	750 (545,1.38) [s]
δ(CH)	762 (----) [w] 759 (----) [w]	----	----	----
combination ν(MC)+δ(CH)	1259 (----) [m]	1170 (----) [w]	----	----
ν _s (MC)	----	490 (----) [m]	- 430	----
ν _{as} (MC)	----	----	- 370	----

Frequencies are in cm⁻¹; Numbers in parenthesis are (frequencies for deuterated analogues, νCH/νCD)
s - strong, m - medium, w - weak, br - broad # - doublets are reported by J.R. Shapley from spectra taken in a KBR pellet and are probably solid state splittings.

a) Evans and McNulty, ref. 63b; and J.K. Shapley, unpublished results

b) This work

c) Kesmodel et. al., ref. 114

Table 3.12: Continued

Mode Assignment	Ni(110)/C ₂ H ₄ ^d T = 300 K	Pt(111)/C ₂ H ₄ ^{e*} T = 500 K	Ni(111)/C ₂ H ₂ ^{f*} T = 450 K	Ru(001)/C ₂ H ₄ ^g T = 360 K
$\nu(\text{CH})$	2990(2275,1.31) [m]	3000 [m]	2980(2160,1.38) [w]	2960(2210,1.34) [m]
$\nu(\text{CC})$	1290(1275,1.01) [m,br]	1430 [w]	1300(----) [vw]	1290(1260,1.02) [m]
$\delta(\text{CH})$	890 (725,1.23) [s]	~ 800 [m]	790 (550,1.44) [s]	750 (550,1.36) [ms]
$\delta(\text{CH})$	----	----	----	----
combination $\nu(\text{MC}) + \delta(\text{CH})$	----	1170 [w]	----	----
$\nu_s(\text{MC})$	465 (445,1.04) [m]	420 [w]	----	435 (----) [-]
$\nu_{as}(\text{MC})$	380 (360,1.06) [m]	----	----	----

Frequencies are in cm^{-1} ; Numbers in parenthesis are (frequencies for deuterated analogues, $\nu\text{CH}/\nu\text{CD}$)

s - strong, m - medium, w - weak, br - broad

d) Strocio et.al., ref. 85

e) Baro and Ibach, ref. 112

f) Demuth and Ibach, ref. 113

*) Spectra reassigned to C₂H; previously attributed to CH

g) Hills et.al., ref. 55

included are the vibrational frequencies assigned to C_2H species on Pd(111), (100) [114], Ni(110) [85], Ru(001) [55], and Rh(100) [discussed below]. The vibrational frequencies shown for Pt(111) and Ni(111) were previously attributed to CH but have been reassigned here to C_2H as noted above.

For tilted C_2H , about half of all normal vibrational modes should be dipole active if the species is adsorbed as shown in Fig. 3.39 with C_s symmetry. Such a geometry can readily explain the assignment in Table 3.12 of the dipole active CH bend at $\sim 815\text{ cm}^{-1}$, the weak CC stretch at $\sim 1380\text{ cm}^{-1}$ and the higher frequency CH stretch at $\sim 3020\text{ cm}^{-1}$. The remaining dipole inactive 1170 cm^{-1} band can be assigned by analogy to the cluster as a combination band, and the dipole-active 490 cm^{-1} peak is consistent with the ν_{5MC} frequency of 465 cm^{-1} reported for C_2H on Ni(110). Presumably the dipole-inactive CH bend occurs unresolved with the dipole active bend at 815 cm^{-1} . It should be noted, however, that if the adsorption symmetry for C_2H is lower than C_s , then this mode will become dipole-active. This possibility cannot be ruled out based on these spectra and may account for the substantial width of the 800 cm^{-1} feature even in the specular spectra. Inhomogeneous broadening is another plausible explanation for the broadness of the 800 cm^{-1} peak. In particular, the broad C-C stretch peak at $\sim 1380\text{ cm}^{-1}$ may indicate differing degrees of C-C bond tilt and interaction with the surface. These different tilt configurations would be expected to have different CH bending frequencies.

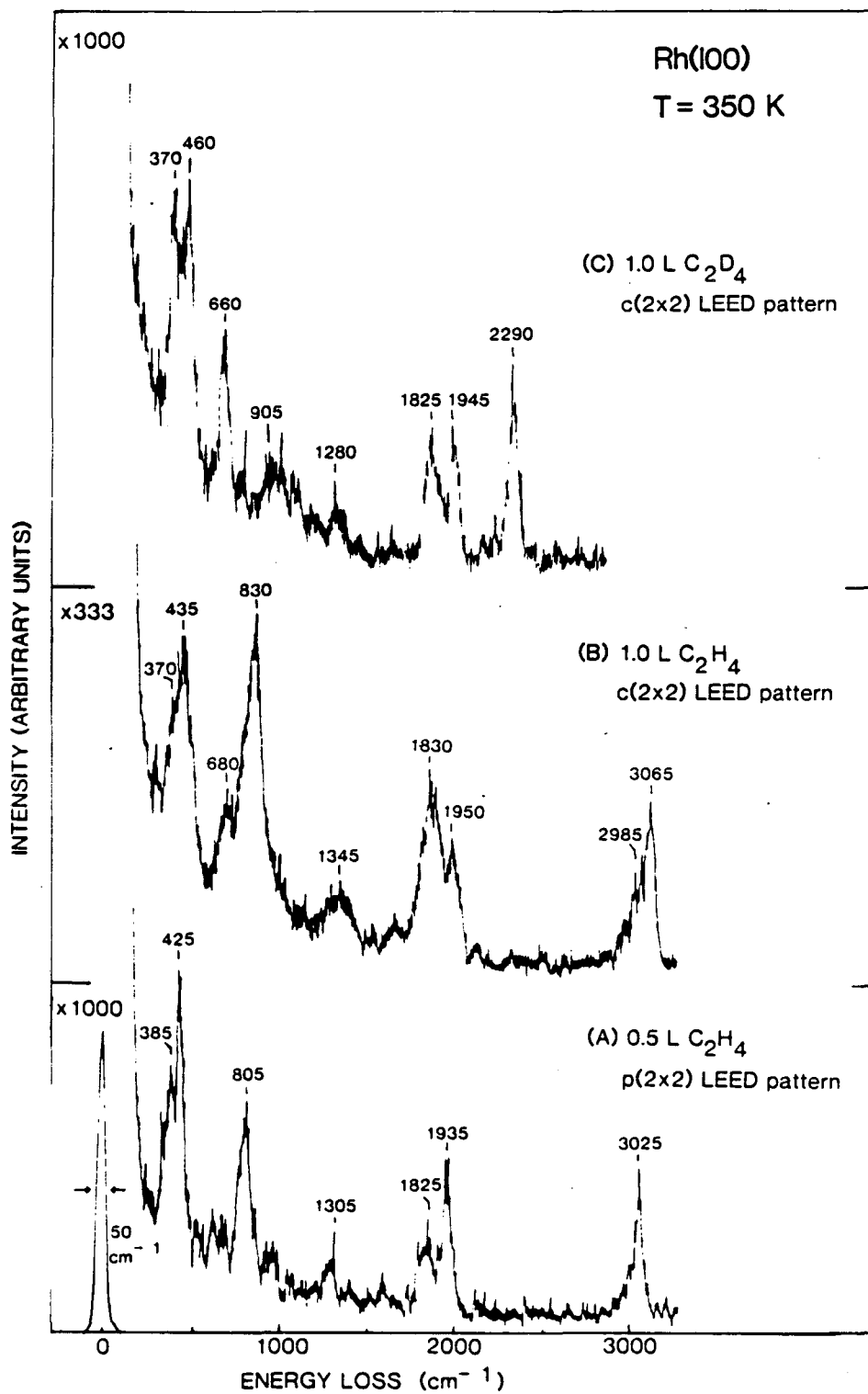
This C_2H spectral assignment on Rh(111) is supported by HREEL spectra of C_2H species formed in the absence of other hydrocarbon

fragments on Rh(100). It was found that low exposures of ethylene (≤ 1 L) on Rh(100) at 300–350 K produced HREEL spectra very similar to the 500 K alkene fragment spectra on Rh(111). These monolayers, whose HREEL spectra are shown in Fig. 3.40, not only have sharper HREELS peaks but also form a weak $p(2 \times 2)$ LEED pattern for 0.5 L exposures and a sharp $c(2 \times 2)$ pattern for 1.0 L exposures [117]. Both of these facts suggest a single surface species is formed, and this species can be assigned as C_2H .

Using the peak frequencies for the 0.5 L C_2H_4 dose in Fig. 3.40A and those for the 1.0 L C_2D_4 dose in Fig. 3.40C, the HREEL spectra can be assigned as given in Table 3.12 (deuterated frequencies are in parenthesis): $805(660) = \delta CH$, $1305(1280) = \nu CC$ and $3025(2290) = \nu CH$. The peaks at ~ 385 and $\sim 425 \text{ cm}^{-1}$ are attributable to metal–molecule vibrations, but they may also contain contributions from the νMC vibrations of the small amounts of contaminant CO. The broad blob around 905 cm^{-1} in the deuterated spectrum is also probably a contaminant.

The sharpness of the δCH (δCD) peaks in Figs. 3.40A and C suggests that C_2H on Rh(100) rigorously maintains a mirror plane of symmetry so that only one CH bending mode is dipole active and observed. Off-specular studies are planned to confirm the presence of the unobserved dipole-inactive CH bending frequency. The sharp νCC peaks at $1305 (1280) \text{ cm}^{-1}$ indicate a specific tilt angle for C_2H (at least at low coverages) on Rh(100).

A proposed bonding geometry for C_2H on Rh(100) is shown in Fig. 3.39. This structure is based on the known geometry of the pentaruthenium



XBL 868-3201

Fig. 3.40 Specular HREEL spectra for low coverages of ethylene and ethylene- d_4 on Rh(100) at 350 K. The surface species for these 0.5 and 1.0 L exposures is identified as C_2H .

$C_2(\text{phenyl})$ complex which is also shown. While the vibrational frequencies of this pentaruthenium cluster have not been reported the C-C bond length of 1.34 Å is close to C-C double bond length (1.33 Å). The surface vibrational frequency of 1305 cm^{-1} is midway between that for C-C single ($\sim 950\text{ cm}^{-1}$) and C-C double ($\sim 1620\text{ cm}^{-1}$) bonds, suggesting that the C_2H ligand interacts more strongly with the Rh(100) surface than with the pentaruthenium cluster. The same is true on Rh(111) where the C-C stretching frequency is $\sim 1380\text{ cm}^{-1}$ while the C-C bond length in a model triiron $C_2(\text{phenyl})$ complex is 1.3 Å.

Supported by this assignment of C_2H on Rh(100), the 500 K hydrocarbon fragment spectra on Rh(111) and Rh(100) can be assigned as predominately C_2H species. This also agrees with the surface stoichiometry of C/H ~ 2 . However, as the temperature is raised above 500 K, TDS shows that these species must dehydrogenate. Yet the surface vibrational spectrum shows few changes until all the hydrogen is removed. This can be explained by a polymerization process wherein C_2H species dehydrogenate and condense to form C_x polymers terminated with hydrogen atoms (C_xH species). These polymeric species should have C-H bending and stretching frequencies similar to C_2H and should gradually broaden the C-C stretching frequency as is observed in Fig. 3.32. The generally high background intensity from 0-1400 cm^{-1} in all decomposition spectra is characteristic of carbon polymerization [118]. Polymeric species are also consistent with the ultimate formation of graphitic carbon at high temperature.

One could argue based on the data here that substantial carbon polymerization occurs even at 500 K on these surfaces. Thus, instead

of concluding that benzene, the C_3 and C_4 hydrocarbons decompose into C_2 and C_1 species before polymerizing at higher temperature, one argues that the C_2 , C_3 and C_4 hydrocarbons polymerize as chains or benzene-like rings, and C-C bond breaking is not required. This interpretation cannot be completely ruled out. An interesting study that might distinguish these two cases would be to compare the high temperature decomposition of hydrocarbons on a highly-corrugated, early transition metal surface and on a smooth, late transition metal surface. Since carbide formation will be favored on the former and graphite in the latter case, this experiment would differentiate high temperature C-C bond breaking and polymerization.

In any case, the data and discussion in this section have shown that a wide variety of unsaturated hydrocarbons all decompose to the same species above 450 K on both Rh(111) and Rh(100). The HREEL spectra and continuous evolution of hydrogen in the TDS between 450 and 800 K are indicative of carbon polymerization on the surface to give C_xH species. At 500 K, the surface stoichiometry and HREEL spectra suggest that the majority surface species is C_2H . Bonding models for this surface species on Rh(111) and Rh(100) as well as for CH on Rh(111) were proposed by analogy to organometallic clusters. LEED surface crystallography is planned to solve the ordered C_2H structures on Rh(100).

Finally, it should be noted that the stable surface fragments observed here in UHV may be quite different from those present on active hydrocarbon conversion catalysts under reaction conditions.

Hydrocarbon fragment stability is effected by the surface H atom concentration which is determined by the ambient H_2 pressure. The studies here in UHV favor dehydrogenation accompanied by hydrogen desorption, while catalytic hydrocarbon conversion reactions are carried out in high pressures of hydrogen, increasing the stability of hydrogenated surface fragments. Indeed, the H/C ratio for the high-temperature fragments in UHV on Rh(111) and Rh(100) is ≤ 0.5 while the H/C stoichiometry of the monolayers that remain bound to active hydrocarbon conversion catalysts after reactions at 300–400°C is $\sim 1-1.5$ [103]. The polymeric C_xH species that form on Rh(111) and Rh(100) at 300–400°C in UHV may be appropriate models for the lower H/C carbonaceous residues that slowly build up and deactivate catalysts.

REFERENCES

1. L.L. Kesmodel, P.C. Stair, R.C. Baetzhold and G.A. Somorjai, Phys. Rev. Lett. 36 (1976) 1316.
2. L.L. Kesmodel, L.H. Dubois and G.A. Somorjai, J. Chem. Phys. 70 (1979) 2180.
3. M.R. Albert, L.G. Sheddon, W. Eberhardt, F. Greuter, T. Gustafsson and E.W. Plummer, Surf. Sci. 120 (1982) 19.
4. N. Freyer, C. Pirug and H.P. Bonzel, Surf. Sci. 126 (1983) 487.
5. H. Steininger, H. Ibach and S. Lehwald, Surf. Sci. 117 (1982) 685.
6. J.E. Demuth, Surf. Sci. 80 (1979) 367.
7. M. Salmeron and G.A. Somorjai, J. Phys. Chem. 86 (1982) 341.
8. P. Berlowitz, C. Megiris, J. Butt and H. Kung, Langmuir 1 (1985) 206.
9. D. Godbey, F. Zaera, R. Yeates and G.A. Somorjai, Surf. Sci. 167 (1986) 150.
10. L.L. Kesmodel, L.H. Dubois and G.A. Somorjai, Chem. Phys. Lett. 56 (1978) 267.
11. P. Skinner, M.W. Howard, I.A. Oxtan, S.F.A. Kettle, D.B. Powell and N. Sheppard, J. Chem. Soc., Faraday Trans. 2 77 (1981) 1203.
12. J.R. Creighton and J.M. White, Surf. Sci. 129 (1983) 327.
13. R.J. Koestner, J. Stohr, J.L. Gland and J.A. Horsley, Chem. Phys. Lett. 105 (1984) 332.
14. A. Gavezzoti and M. Simonetta, Surf. Sci. 99 (1980) 453.
15. C. Minot, M.A. Van Hove and G.A. Somorjai, Surf. Sci. 127 (1982) 441.

16. D.B. Kang and A.B. Anderson, Surf. Sci. 155 (1985) 639.
17. J. Silvestre and R. Hoffmann, Langmuir 1 (1985) 621.
18. P.-K. Wang, C.P. Slichter and J.H. Sinfelt, J. Phys. Chem. 89 (1985) 3606.
19. T.P. Beebe and J.T. Yates, Jr., private communication.
20. H. Ibach and D.L. Mills, Electron Energy Loss Spectroscopy and Surface Vibrations, Academic, New York (1982).
21. L.H. Dubois, Ph.D. thesis, University of California, Berkeley, 1980, unpublished.
22. R.J. Koestner, M.A. Van Hove and G.A. Somorjai, Surf. Sci. 121 (1982) 321.
23. L.H. Dubois, D.G. Castner and G.A. Somorjai, J. Chem. Phys. 72 (1980) 5234.
24. R.J. Koestner, M.A. Van Hove and G.A. Somorjai, J. Phys. Chem. 87 (1983) 203.
25. E. Maslowsky, Jr., Vibrational Spectra of Organometallic Compounds, John Wiley, New York (1972).
26. Ref. 20, pg. 193.
27. This is a consequence of the fact that bond bending force constants are much smaller than bond stretching force constants.
28. F.M. Hoffmann and T.H. Upton, J. Phys. Chem. 88 (1984) 6209.
29. The question arises when considering the symmetry of an adsorbed species: "How much of the metal should be included?" Generally only the outermost layer is considered. However, if the adsorbate does "feel" the effects of the second layer, the adsorption symmetry will in some cases be lowered.

30. A nice introduction to the application of symmetry and group theory in vibrational spectroscopy has been given by: D.C. Harris and M.D. Bertolucci, Symmetry and Spectroscopy: An Introduction to Vibrational and Electronic Spectroscopy, Oxford, New York (1978); a more sophisticated treatment is given by: E.B. Wilson, Jr., J.C. Decius and P.C. Cross, Molecular Vibrations, McGraw-Hill, New York (1955).
31. T.R. Stengle and R.C. Taylor, *J. Mol. Spectrosc.* 34 (1970) 33.
32. E.O. Fischer, U. Schubert and H. Fischer, *Pure and Appl. Chem.* 50 (1978) 857; and references therein.
33. P.W. Sutton and L.F. Dahl, *J. Amer. Chem. Soc.* 89 (1967) 261.
34. B.E. Koel, B.E. Bent and G.A. Somorjai, *Surf. Sci.* 146 (1984) 211.
35. See Section 4.2.
36. One ethynidyne per four surface Rh atoms.
37. R.J. Koestner, Ph.D. thesis, University of California, Berkeley, 1982, unpublished.
38. C.M. Mate and G.A. Somorjai, *Surf. Sci.* 160 (1985) 542.
39. C.M. Mate, B.E. Bent and G.A. Somorjai, *J. Electron Spectrosc. and Rel. Phenom.* 39 (1986) 205.
40. R. Moret, E. Tronc, M. Huber and R. Comes, *Phil. Mag. B* 38 (1978) 105.
41. L.H. Dubois and G.A. Somorjai, ACS Symposium Series, A.T. Bell and M.L. Hair, eds. 137 (1980) 263.
42. J.E. Crowell and G.A. Somorjai, *App. Surf. Sci.* 19 (1984) 73.
43. M.A. Van Hove, R.J. Koestner, B.E. Bent, C.M. Mate, C.-T. Kao, G.S. Blackman and G.A. Somorjai, in preparation.

44. Ref. 20, pg. 98.
45. Ph. Avouris and J.E. Demuth, *Ann. Rev. Phys. Chem.* 35 (1984) 49.
46. L.H. Dubois, *J. Chem. Phys.* 77 (1982) 5228.
47. M.B. Lee, Q.Y. Yang and S.T. Ceyer, to be published.
48. J.R. Riter, Jr. and D.F. Eggers, Jr., *J. Chem. Phys.* 44 (1966) 745; Section 4.2.
49. J. Evans and G.S. McNulty, *J. Chem. Soc., Dalton Trans.* (1983) 639.
50. J.E. Demuth, *Surf. Sci.* 93 (1980) 282.
51. J.R. Durig, A.E. Sloan and J.D. Witt, *J. Phys. Chem.* 76 (1972) 3591.
52. Kinematic LEED calculations by A.L. Slavin, private communication.
53. M.W. Roberts and C.S. McKee, *Chemistry of the Metal-Gas Interface*, Oxford Univ., Oxford (1978).
54. J.A. Gates and L.L. Kesmodel, *Surf. Sci. Lett.* 120 (1982) L461; *Surf. Sci.* 124 (1983) 68.
55. M.M. Hills, J.E. Parmeter, C.B. Mullins and W.H. Weinberg, *J. Amer. Chem. Soc.* 108 (1986) 3554.
56. H. Ibach, *Proc. Int. Conf. Vibrations Adsorbed Layers*, Julich (1978) 64.
57. E.M. Stuve and R.J. Madix, *J. Phys. Chem.* 89 (1985) 105.
58. G.H. Hatzikos and R.I. Masel, to be published.
59. S. Lehwald and H. Ibach, *Surf. Sci.* 89 (1979) 425.
60. W. Eberhardt, S.G. Louie and E.W. Plummer, *Phys. Rev.* B28 (1983) 465; R.J. Behm, V. Penka, M.-G. Cattania, K. Christman and G. Ertl, *J. Chem. Phys.* 78 (1983) 7496; S.M. Foiles and M.S. Daw, *J. Vac. Sci. Technol.* A3 (1985) 1565.

61. J. Ushio, H. Nakatsuji and T. Yonezawa, *J. Amer. Chem. Soc.* 106 (1984) 5892.
62. T.V. Ashworth, J.A.K. Howard and F.G.A. Stone, *J. Chem. Soc., Dalton Trans.* (1980) 1609.
63. a) D.L. Davis, A.F. Dyke, A. Endes Felder, S.A.R. Knox, P.J. Naish, A.G. Orpen, D. Plaas and G.E. Taylor, *J. Organomet. Chem.* 198 (1980) C43; b) J. Evans and G.S. McNulty, *J. Chem. Soc., Dalton Trans.* (1984) 79.
64. L. Pauling, *The Nature of the Chemical Bond*, 3rd Edition, Cornell Univ., Ithaca (1960) 308.
65. A.J. Carty, B.F.G. Johnson, J. Lewis and J.R. Norton, *J. Chem. Soc., Chem. Commun.* (1972) 331.
66. T.M. Voyevodskaya, I.M. Pribytkova and Yu. A. Ustynyuk, *J. Organomet. Chem.* 37 (1972) 187.
67. G.A. Somorjai, *Chemistry in Two Dimensions*, Cornell University, Ithaca (1981) 135.
68. D.C. Miller and T.B. Brill, *Inorg. Chem.* 17 (1978) 240.
69. M.A. Beno, J.M. Williams, M. Tachikawa and E.L. Muetterties, *J. Amer. Chem. Soc.* 103 (1981) 1485.
70. A.J. Carty, S.A. McLaughlin and N.J. Taylor, *J. Amer. Chem. Soc.* 103 (1981) 2456.
71. G.V. Smith and J.R. Swoap, *J. Org. Chem.* 31 (1966) 3904.
72. R. Touroude, L. Hilaire and F.G. Gault, *J. Catal.* 32 (1974) 279.
73. R.J. Koestner, J.C. Frost, P.C. Stair, M.A. Van Hove and G.A. Somorjai, *Surf. Sci.* 116 (1982) 85.

74. K.M. Ogle, J.R. Creighton, S. Akhter and J.M. White, Surf. Sci. 169 (1986) 246.
75. N.R. Avery and N. Sheppard, Proc. R. Soc. Lond. A 405 (1986) 1.
76. S.M. Davis, Ph.D. thesis, University of California, Berkeley, 1981, unpublished.
77. F. Zaera and G.A. Somorjai, J. Phys. Chem. 89 (1985) 3211.
78. M.A. Van Hove, R.J. Koestner and G.A. Somorjai, J. Vac. Sci. Technol. 20 (1982) 886.
79. A. Goursot-Leray, M. Carles-Lorjou, G. Pouzard and H. Bodot, Spectrochim. Acta 29A (1973) 1497.
80. D. Seyferth, C.N. Rudie and J.S. Merola, J. Org. Chem. 162 (1978) 89.
81. See sections 4.2 and 5.1.
82. N. Sheppard, J. Electron Spectrosc. Related Phenom. 38 (1986) 175.
83. E.M. Stuve and R.J. Madix, J. Phys. Chem. 89 (1985) 3183.
84. J. Stohr, F. Sette and A.L. Johnson, Phys. Rev. Lett. 53 (1984) 1684.
85. J.A. Stroscio, S.R. Bare and W. Ho, Surf. Sci. 148 (1984) 499.
86. J.T. Yates, Jr., P.A. Thiel and W.H. Weinberg, Surf. Sci. 84 (1979) 427.
87. J.E. Demuth, IBM J. Res. Develop. 22 (1978) 265.
88. U. Seip, M.-C. Tsai, J. Koppers and G. Ertl, Surf. Sci. 147 (1984) 65.
89. B.A. Sexton, Surf. Sci. 94 (1980) 435.
90. J. Chatt and L.A. Duncanson, J. Chem. Soc. (1953) 2939; M.J.S. Dewar, Bull. Soc. Chim. Fr. 18 (1951) C79.

91. R.M. Badger, *J. Chem. Phys.* 2 (1934) 128.
92. R.A. Love, T.F. Koetzle, G.J.B. Williams, L.C. Andrews, and R. Bau, *Inorg. Chem.* 14 (1975) 2653.
93. J. Hiraishi, *Spectrochimica Acta* 25A (1969) 749.
94. C. Nyberg, C.G. Tengstal, S. Andersson and M.W. Holmes, *Chem. Phys. Lett.* 87 (1982) 87.
95. M.A. Chesters, G.S. McDougall, M.E. Pemble and N. Sheppard, *Appl. Surf. Sci.* 22/23 (1985) 369.
96. S. Lehwald, H. Ibach and H. Steininger, *Surf. Sci.* 117 (1982) 342.
97. W. Erley, A.M. Baro and H. Ibach, *Surf. Sci.* 120 (1982) 273.
98. M.A. Barteau, J.Q. Broughton and D. Menzel, *Appl. Surf. Sci.* 19 (1984) 92.
99. See ref. 20, pg. 298.
100. T. Shimanouchi, Tables of Molecular Vibrational Frequencies, Consolidated Vol. I NSRDS-NBS 39 (1972).
101. J.T. Neu and W.D. Gwinn, *J. Chem. Phys.* 18 (1950) 1642.
102. F. Zaera and G.A. Somorjai, *J. Phys. Chem.* 86 (1982) 3070.
103. S.M. Davis, F. Zaera and G.A. Somorjai, *J. Catal.* 77 (1982) 439.
104. B.E. Koel, J.E. Crowell, C.M. Mate and G.A. Somorjai, *J. Phys. Chem.* 88 (1984) 1988.
105. B.E. Koel, J.E. Crowell, B.E. Bent, C.M. Mate and G.A. Somorjai *J. Phys. Chem.* 90 (1986) 2949.
106. C.M. Mate and G.A. Somorjai, *Surf. Sci.* 160 (1985) 542.
107. D.M. Haaland, *Surf. Sci.* 111 (1981) 555.
108. D.G. Castner, B.A. Sexton and G.A. Somorjai, *Surf. Sci.* 71 (1978) 519.

109. M.W. Howard, S.F. Kettle, I.A. Oxton, D.B. Powell, N. Sheppard and P. Skinner, J. Chem. Soc., Faraday Trans. 2 77 (1981) 397.
110. I.A. Oxton, Spectrochim. Acta 38A (1982) 181.
111. C. Backx and R.F. Willis, Chem. Phys. Lett. 53 (1978) 471.
112. A.M. Baro and H. Ibach, J. Chem. Phys. 74 (1981) 4194.
113. J.E. Demuth and H. Ibach, Surf. Sci. 78 (1978) 1238.
114. L.L. Kesmodel, G.D. Waddill and J.A. Gates, Surf. Sci. 138 (1984) 464.
115. All 2-carbon or longer species bound to Pt(111) and Rh(111) have ν_{MC} frequencies less than 500 cm^{-1} regardless of whether the carbon chain is bound end-on or side-on to the surface.
116. E.M. Stuve, R.J. Madix and B.A. Sexton, Surf. Sci. 123 (1982) 491.
117. It is possible that the weak $p(2\times 2)$ LEED pattern for 0.5 L ethylene exposures is due to islands of the small amount of coadsorbed CO, although CO does not form this pattern on the clean Rh(100) surface.
118. A.B. Anderson, D.B. Kang and Y. Kim, J. Amer. Chem. Soc. 106 (1984) 6597.
119. D.B. Powell, J.G.V. Scott and N. Sheppard, Spectrochim. Acta A 28A (1972) 327.

CHAPTER 4

STOICHIOMETRIC REACTIONS OF UNSATURATED HYDROCARBONS WITH
TRANSITION METAL SURFACES: EXPERIMENTAL STUDIES ON
Rh(111), Rh(100) AND Pt(111)4.1 Thermal Fragmentation of Ethylene on Rh(111) and Rh(100) in the
Temperature Range of 80-800 K

4.1.1 Background. In Chapter 3, the identity and bonding of a number of hydrocarbon species on Rh(111), Rh(100) and Pt(111) were discussed. Chapter 4 now concentrates on the factors that control the formation and stability of these fragments and their interconversion. As mentioned in Chapter 1, many factors effect C-H and C-C bond breaking in adsorbed hydrocarbons. Two of these, temperature and metal surface structure, are investigated here in Section 4.1.

Temperature is an important factor in determining how hydrocarbons bind to transition metal surfaces, because the thermal decomposition of adsorbed hydrocarbons is kinetically controlled. Thermodynamically, the stable adsorption products for hydrocarbons on metals at room temperature are adsorbed carbon (usually bonding as a graphitic layer) and H₂ gas. Kinetics, however, dictates that this stable state is reached only high temperatures (500-1000 K). Below 500 K, a series of partially dehydrogenated fragments are formed that are stable in discrete temperature ranges [1].

The effects of metal surface structure on both the bonding and catalytic chemistry of hydrocarbons have not been as extensively studied as the effects of temperature. It has been found that the rates

and selectivities of some catalytic hydrocarbon reactions like isobutane and n-butane isomerization are effected by metal surface structure [2] while other catalytic reactions like n-hexane isomerization are "structure-insensitive" [3]. The same appears to be true for hydrocarbon bonding and thermal decomposition in UHV. For example, the bonding and thermal decomposition pathways for ethylene on Pd(111) [4] and Pd(100) [5] are substantially different, while benzene adsorption on these same surfaces [6] appears to be relatively structure insensitive.

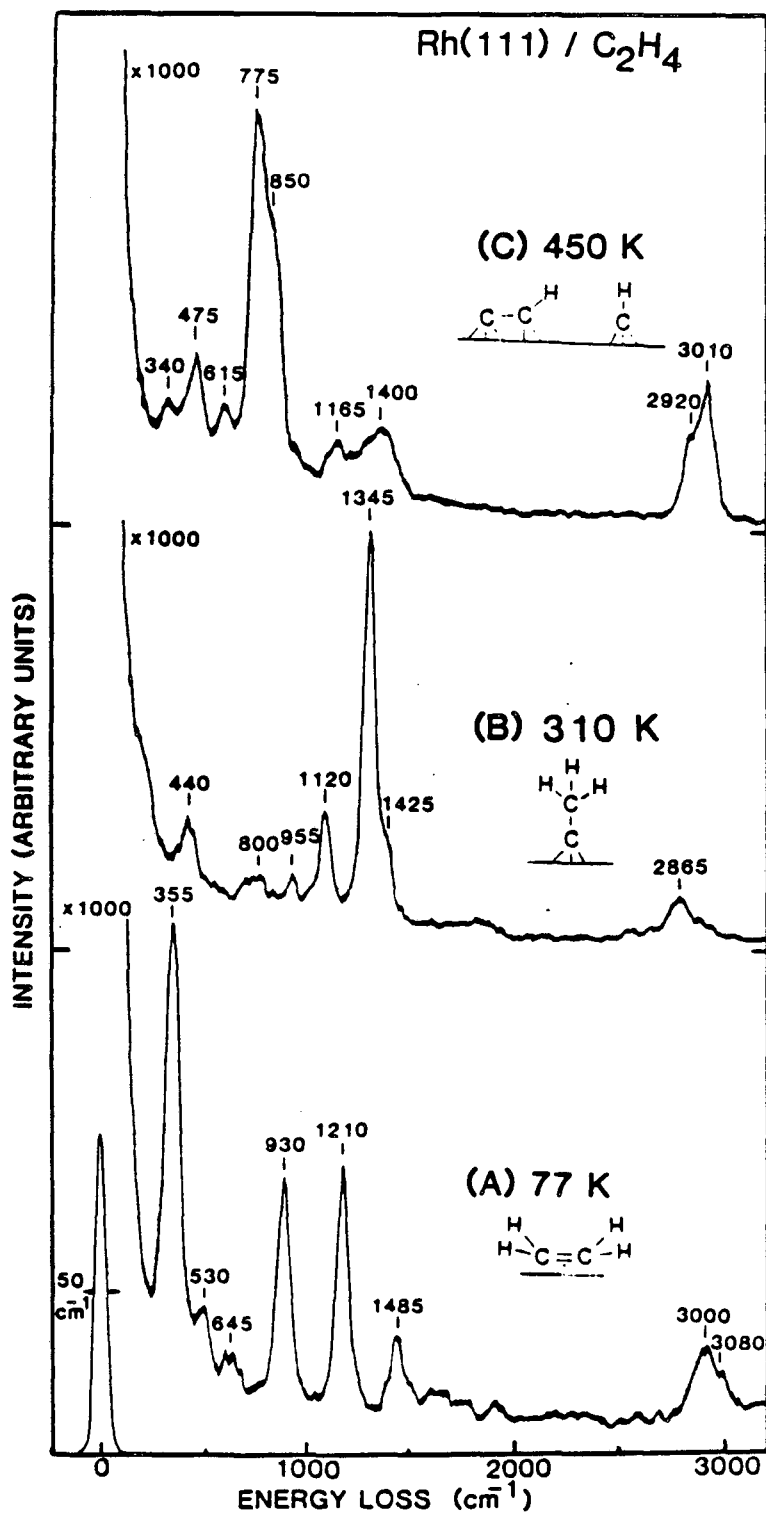
Here, studies of ethylene adsorption on Rh(111) and Rh(100) in the temperature range of 80-800 K are reported. As expected, a number of stable hydrocarbon fragments were isolated on both surfaces as a function of temperature. It was found that ethylene fragments to similar species on Rh(111) and Rh(100), unlike the structure sensitivity mentioned above for Pd(111) and Pd(100). However, an unexpected coverage dependence was observed on Rh(100). At low coverages on this surface, ethylene decomposes at room temperature directly to C_2H species, while at higher coverages, ethylidyne (CCH_3) species form. On Rh(111), ethylene decomposes to ethylidyne at room temperature, independent of surface coverage. A mechanism is proposed to explain the conversion of ethylene to ethylidyne.

4.1.2 Thermal Fragmentation of Ethylene on Rh(111). The thermal fragmentation of ethylene on Rh(111) is summarized in Fig. 4.1 which shows the HREEL spectra and corresponding surface species that form when ethylene is adsorbed at 77 K and annealed to indicated temperatures.

These spectra have all been assigned in Chapter 3. Molecularly adsorbed ethylene (Fig. 4.1A) is stable up to 200 K and bonds with its C-C bond approximately parallel to the surface. The C-C bond is stretched from 1.33 Å (gas phase) to about 1.4 Å upon adsorption (Section 3.4). At 200 K, ethylene converts to ethylidyne (Fig. 4.1B) which stands vertically in a 3-fold hollow site on the surface. The C-C bond is lengthened still further to 1.45 ± 0.1 Å, nearly single bond length [7]. Above 400 K, these CCH_3 species fall over on the surface to form C_2H and possibly CH species (Fig. 4.1C, Section 3.5), which in turn dehydrogenate and polymerize up to 800 K where C_x polymers remain on the surface. All of the adsorbed ethylene, except a small fraction which desorbs molecularly at high surface coverages, decomposes through this series of surface fragments.

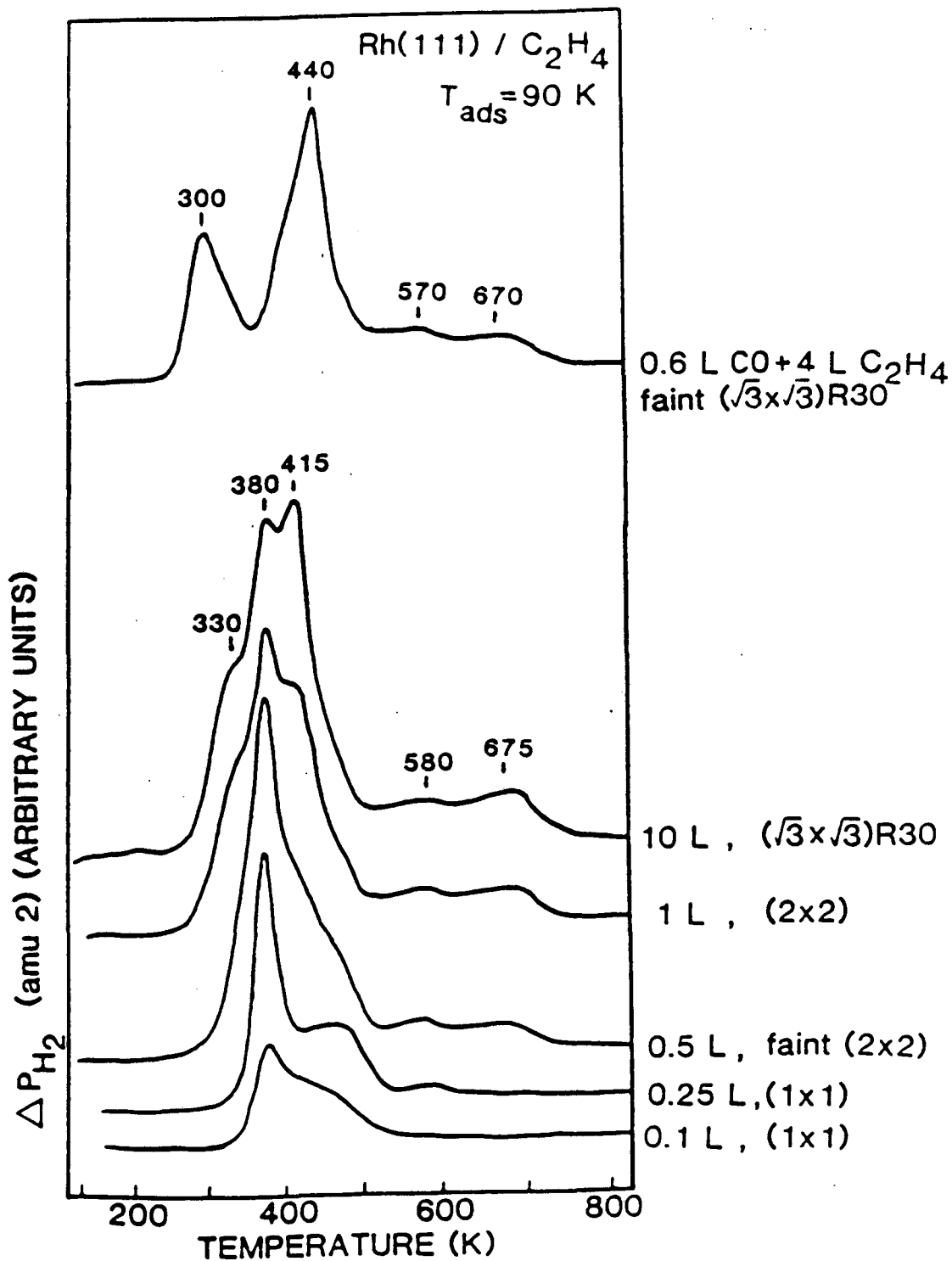
Before discussing the more complex ethylene chemistry on Rh(100), a brief comment on the H_2 TD spectra for ethylene on Rh(111) is needed, since these spectra (as shown below) provide a useful but potentially misleading fingerprint of the surface chemistry. The H_2 TD spectra for ethylene dehydrogenation on Rh(111) are shown in Fig. 4.2 as a function of ethylene coverage [8]. Also shown is the H_2 TDS for ethylene coadsorbed with 0.6 L of CO.

Without the surface HREEL spectra, these H_2 TD spectra would logically be interpreted as follows: "For 0.1 L exposures of ethylene, a surface species is formed which dehydrogenates at 380 K. Larger exposures produce additional peaks at 330 and 415 K, indicating that another hydrocarbon species is present." However, HREEL spectra show



XBL 8512-4941

Fig. 4.1 Specular HREEL vibrational spectra and proposed surface species for a saturation coverage of ethylene adsorbed on Rh(111) at: (A) 77 K, (B) 300 K and (C) 450 K. The spectra were taken at 77 K, 300 K and 300 K respectively.



XBL 866-2424A

Fig. 4.2 Hydrogen thermal desorption spectra from Rh(111) after the indicated ethylene exposures at 90 K and after exposure to 0.6 L CO + 4 L C₂H₄ at 100 K. The heating rates were 25 K/sec.

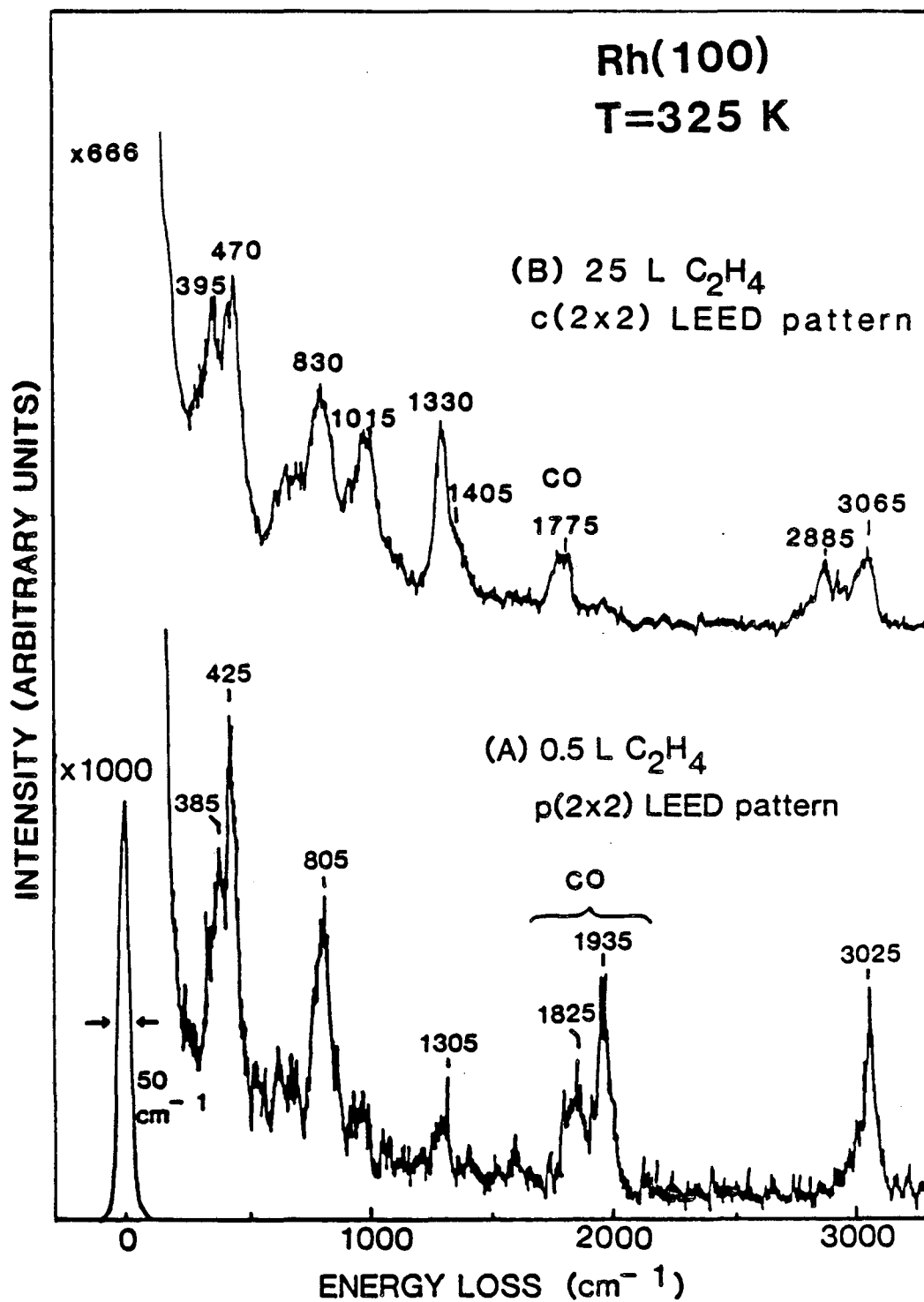
that this interpretation cannot be correct. As discussed above, HREELS shows that ethylene converts to ethylidyne (CCH_3) and surface hydrogen atoms at 200 K, regardless of the surface coverage. Therefore, the lowest temperature desorption peak in both the 0.1 L and 10 L spectra, despite being at different temperatures, must be due to desorption of surface hydrogen. The shift of this peak to lower temperature with increasing coverage is consistent with second order hydrogen desorption [9]. The further shift in this peak from 330 to 300 K when CO is coadsorbed (Fig. 4.2, top) may also be a coverage effect; however, this phenomenon is not well understood [10].

Coadsorption of CO with ethylene also causes the 380 and 415 K peaks to combine into a single peak at 440 K. The same merging together of peaks also occurs in the absence of CO when ethylene is adsorbed above 200 K (the ethylidyne formation temperature). The merged peak at 440 K is consistent with the ethylidyne decomposition temperature determined by HREELS. The reasons for the presence of two peaks at 380 and 415 K are not clear, but are related to the rapid heating rates in TDS. Similar phenomena in the H_2 TD spectra for ethylene on Ru(001) have been discussed [11].

The complexity of these Rh(111) TD spectra shows that while the H_2 TD spectra provide an easily obtainable fingerprint of the surface chemistry, the decomposition fragments on the surface could not have been predicted from these spectra.

4.1.3 Thermal Fragmentation of Ethylene on Rh(100). As on Rh(111), ethylene begins to decompose above 200 K on Rh(100). Up to $\theta_{\text{C}_2\text{H}_4} = 0.5$, ethylene dehydrogenates to C_2H species as discussed in Section 3.5. Figure 4.3A shows the HREEL spectrum for a p(2x2) overlayer of these C_2H species. When ethylene in excess of $\theta_{\text{C}_2\text{H}_4} = 0.5$ is adsorbed at room temperature, additional HREELS peaks grow in at 1015, 1330 and 2885 cm^{-1} until at saturation coverage the spectrum in Fig. 4.3B is produced. This spectrum is due to a mixture of C_2H and ethylidyne (CCH_3) species on the surface. The ethylidyne peaks were assigned by studies with coadsorbed CO as described in Section 3.2: $\nu_{\text{CC}} = 1015 \text{ cm}^{-1}$, $\delta_{\text{s}}(\text{CH}_3) = 1330 \text{ cm}^{-1}$ and $\nu_{\text{s}}(\text{CH}_3) = 2885 \text{ cm}^{-1}$.

It was also shown in these CO coadsorption studies that preadsorption of CO can completely block decomposition of ethylene to C_2H . By preadsorbing $\theta_{\text{CO}} = 0.5$ to form a c(2x2) structure, all subsequently adsorbed ethylene decomposes to ethylidyne. However, this effect is not specific to CO. Preliminary studies indicate that carbon and sulfur have similar effects on ethylene decomposition on Rh(100), blocking the decomposition to C_2H . Since all these adsorbates block decomposition to C_2H , and CO bonds in top and bridge sites on Rh(100) [12] while sulfur [13] and presumably carbon [14] and C_2H [15] bond in 4-fold hollow sites, decomposition of ethylene to C_2H must involve a small ensemble of sites rather than a specific site. Based on the fact that the coverage of these adsorbates must be $\theta_{\text{ads}} = 0.5$ before C_2H formation is completely blocked, the ensemble



XBL 8610-4102

Fig. 4.3 Specular HREEL spectra of a Rh(100) surface after exposure to (A) 0.5 L of ethylene and (B) 25 L of ethylene at 325 K. The surface species in (A) are C₂H while at saturation coverage in (B) there is a mixture of C₂H and CCH₃ species on the surface.

size is between 2 and 4 metal atoms. Further, since similar decomposition to C_2H is not observed on Rh(111) at room temperature, the ensemble requires at least 1 four-fold hollow site. It is not yet clear whether ethylidyne is an intermediate in C_2H formation and is only stable at high adsorbate coverages or whether two different decomposition pathways occur—one that produces C_2H at low coverage and another which produces CCH_3 at high coverage.

The thermal decomposition of C_2H and CCH_3 above room temperature on Rh(100) were studied independently by working at low surface coverages and with coadsorbed CO respectively. It was found that ethylidyne is stable up to 350 K, while C_2H is stable to 420 K. For C_2H , dehydrogenation occurs at 420–500 K without any identifiable surface fragments forming enroute to complete dehydrogenation. By contrast, ethylidyne dehydrogenates via at least two intermediate fragments.

HREEL spectra of ethylidyne (coadsorbed with CO) at 300 K and its decomposition products at 380 and 520 K are shown in Fig. 4.4. Both of the decomposition spectra are quite complex. However, by process of elimination, the spectrum at 380 K in Fig. 4.4B can be attributed predominately to CCH_2 species on the surface. Similar spectra have been reported and assigned to CCH_2 on Pt(111) [18] and Pd(111) [4]. A CCH_2 species is a logical decomposition product for an ethylidyne that "falls over" on the surface. Also, the poorly resolved bumps in Fig. 4.4B show reasonable agreement with the vibrational frequencies given adjacent to the figure for a CCH_2 ligand coordinated to three Os atoms [16]. Presumably an analogous tilted CCH_2 geometry would

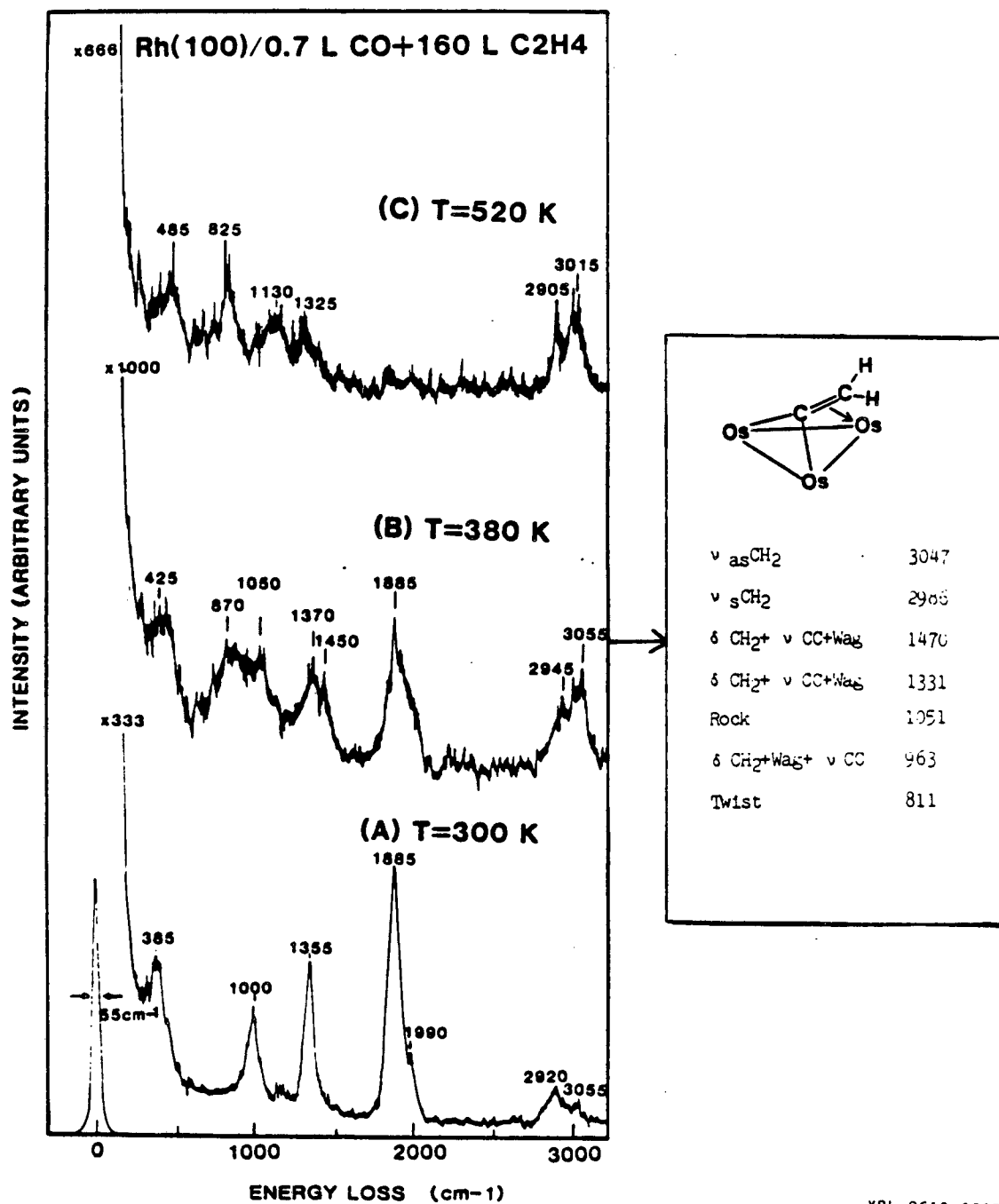


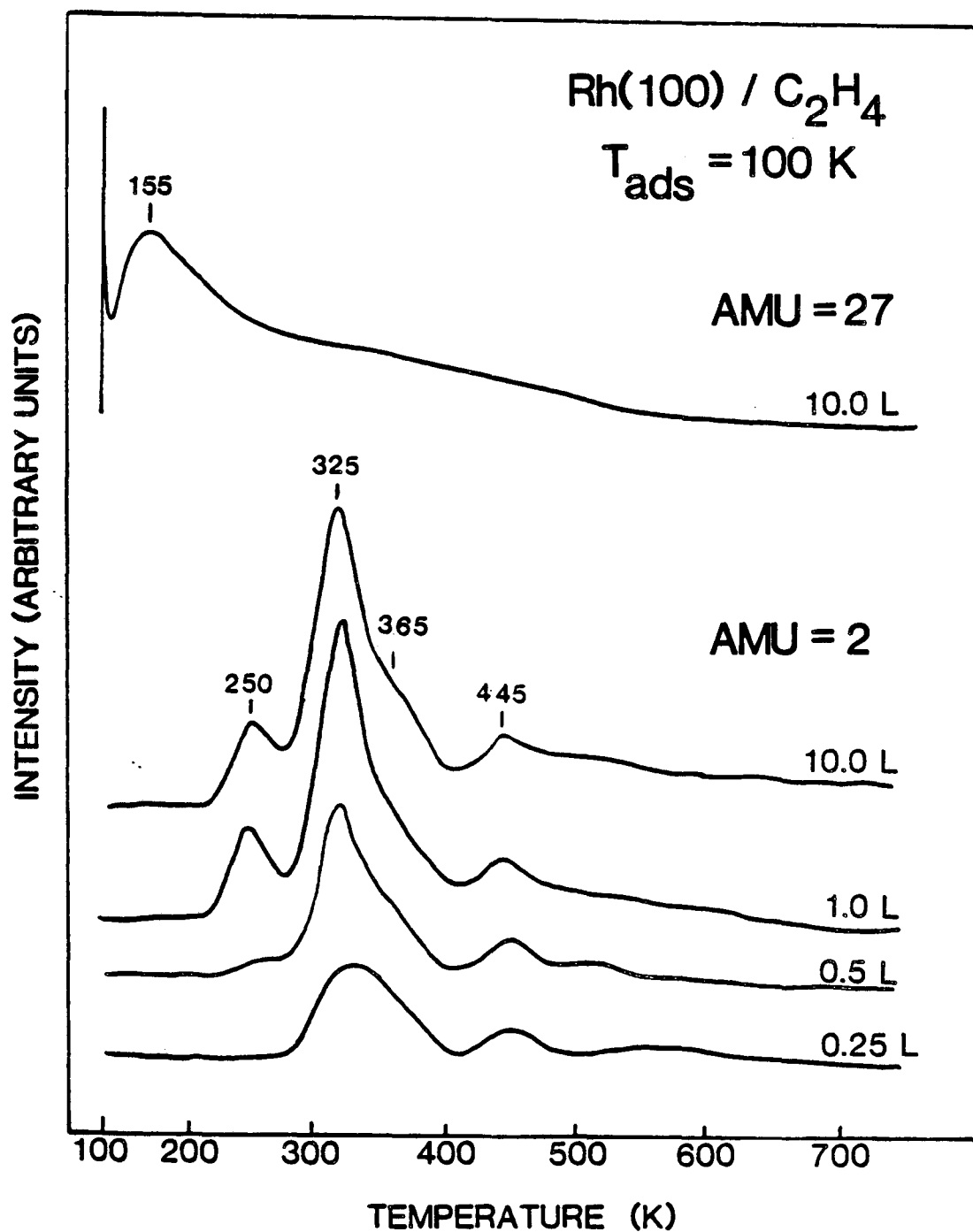
Fig. 4.4 Specular HREEL spectra of a Rh(100) surface after dosing 0.7 L of CO followed by 160 L of C₂H₄ at 300 K and annealing to the indicated temperatures. The surface species in (A) are CO and ethylidyne. These species decompose to the monolayer in (B) whose vibrational frequencies compare favorably with a CCH₂ organometallic ligand as shown. The spectrum for further dehydrogenation in (C) shows evidence for C₂H species.

also be possible in a four-fold hollow site [17]. The simultaneous presence of species like CH, CCH and CH₂ in addition to CCH₂ at 380 K on Rh(100) cannot be ruled out.

By 520 K (Fig. 4.4C) the peaks in the CH₂ scissors region (~1400 cm⁻¹) have greatly diminished, while the peak at 825 cm⁻¹ is characteristic of a C-H bending vibration. This spectrum is indicative of flat-lying C_xH species as discussed in Section 3.5.

Hydrogen thermal desorption spectra for ethylene on Rh(100) are shown in Fig. 4.5. Also shown is the mass 27 desorption from a saturation coverage of ethylene which, because of the low peak temperature (155 K) and broadness of the peak, is attributed to desorption from the Ta support wires. The 0.25 and 0.5 L H₂ TD spectra in Fig. 4.5 are consistent with C₂H formation and decomposition. The first peak at 300-400 K is due to desorption of surface hydrogen produced in formation of C₂H below room temperature. The 450 K peak is then a result of C₂H dehydrogenation. The integrated ratio of these 350 and 450 K peaks (2.8:1) is consistent with C₂H species within the ±10% uncertainty of TDS.

The higher exposure TDS in Fig. 4.5 are more complex because both CCH₃ and C₂H species form. It is interesting but not understood why a lower temperature H₂ desorption peak appears at 250 K for higher exposures in Fig. 4.5. Presumably both this 250 K peak and the 325 K peak are due to desorption of hydrogen bound to the Rh(100) surface. These peaks are absent for ethylene adsorptions at 300 K.



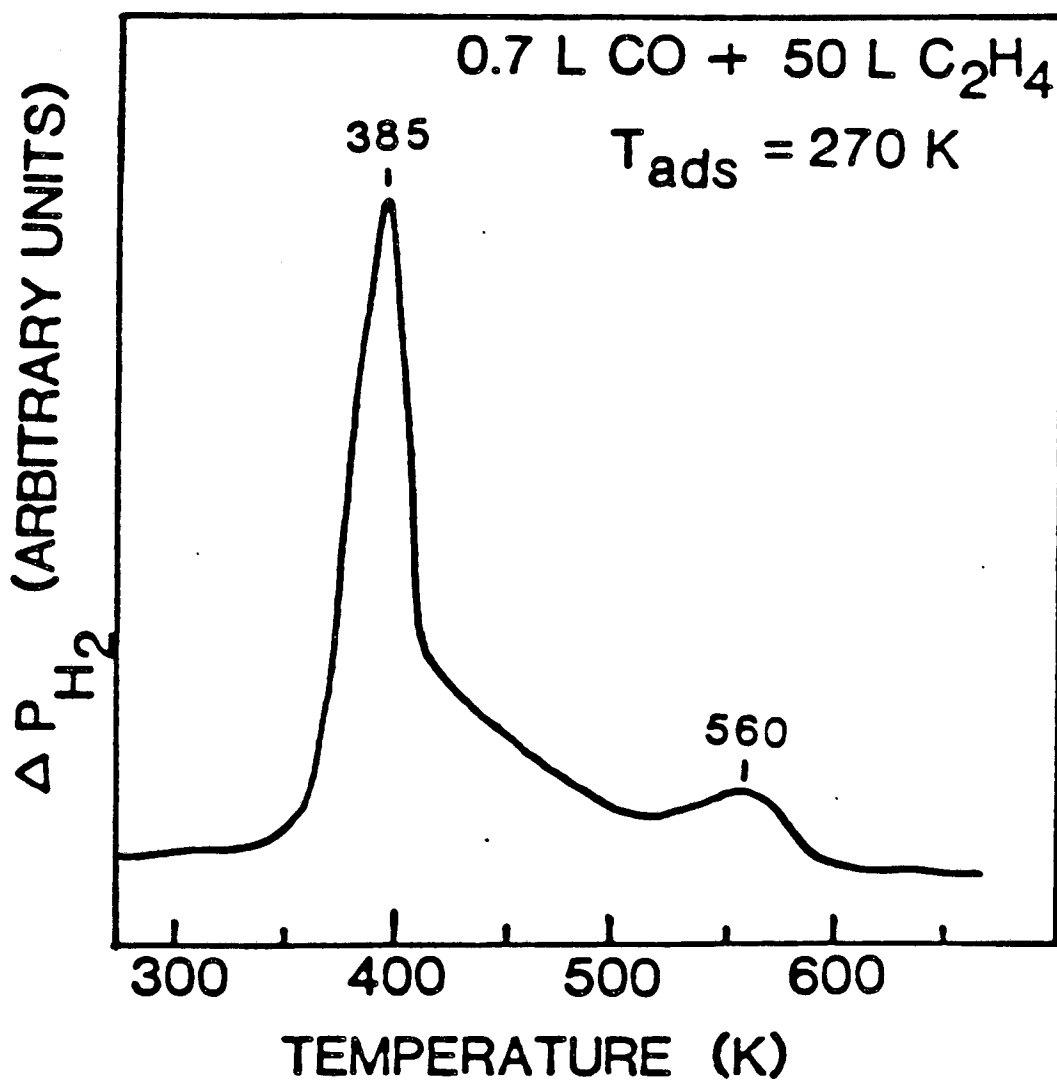
XBL 868-3199

Fig. 4.5 Thermal desorption spectra for ethylene adsorbed on Rh(100) at 100 K. The molecular ethylene desorption at 155 K may be from the support wires, since this peak is weak and broad. The heating rates were 17 K/sec.

The H_2 TDS peaks above 350 K in Fig. 4.5 are due to ethylidyne and C_2H dehydrogenation. The H_2 TDS for ethylidyne in the absence of C_2H and coadsorbed hydrogen is shown in Fig. 4.6. The 385 K peak results from conversion of CCH_3 to CCH_2 , while the shoulder between 400 and 500 K can be attributed to dehydrogenation of CCH_2 to CCH . The peaks at still higher temperature then represent dehydrogenation and polymerization of C_xH species.

The thermal fragmentation of ethylene on Rh(100) is summarized and compared to Rh(111) in Figure 4.7. Except for the CCH_2 species on Rh(100) and the CH species on Rh(111) (both of which require more studies for definitive identification), the decomposition products and temperatures on Rh(111) and Rh(100) are quite similar. The major difference between the (111) and (100) surfaces is the coverage dependence of the thermal decomposition products on Rh(100). The enhanced dehydrogenation observed at low coverages on the (100) surface can be correlated with the presence of 4-fold hollow sites and is eliminated for adsorbate coverages above $\theta_{ads} = 0.5$. This indicates that atoms surrounding the 4-fold hollow and possibly adjacent 4-fold hollow sites are required in order to form C_2H at room temperature.

4.1.4 Ethylene Thermal Fragmentation on Transition Metal Surfaces: Formation of Ethylidyne. Almost all the information reported to date on the identity of ethylene and its thermal decomposition fragments on transition metal surfaces has come from HREELS and TDS. Only ethylidyne on Pt(111) has been extensively studied by many other techniques [19]. Also, except for a few studies on the group 6 metals, almost all data

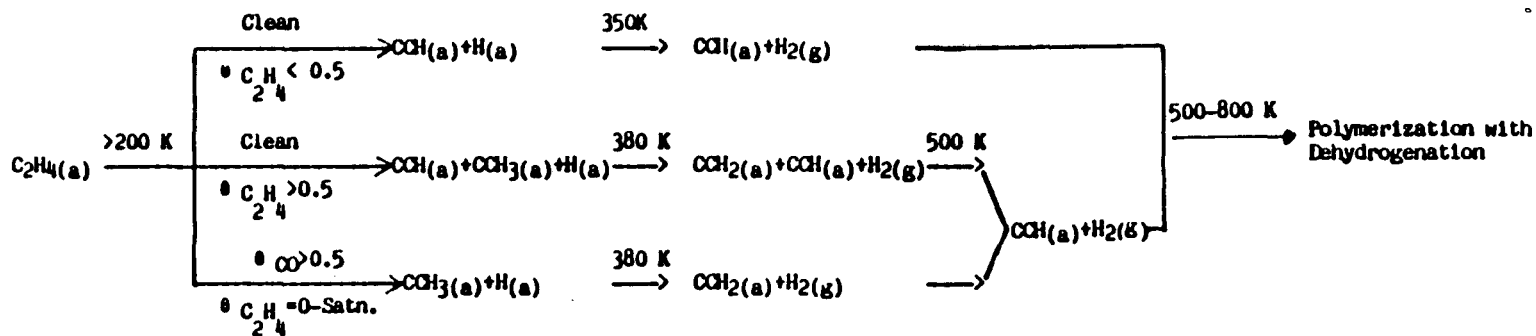


XBL 8610-4093

Fig. 4.6 Hydrogen thermal desorption spectra for ethylene adsorbed on a Rh(100) surface predosed with 0.7 L of CO at 270 K. The surface species at the adsorption temperature are ethylidyne and CO. The heating rate was 10 K/sec.

Thermal Chemistry of Ethylene and Ethylene Coadsorbed with CO on the Rh(100) & Rh(111) Surfaces:

(A) Rh(100)



(B) Rh(111)

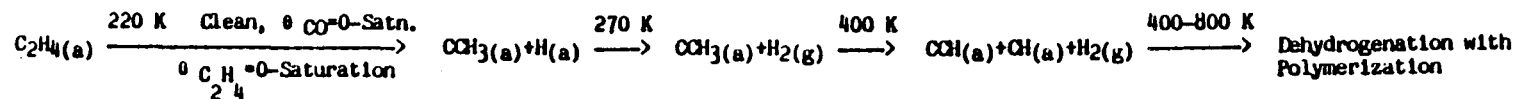


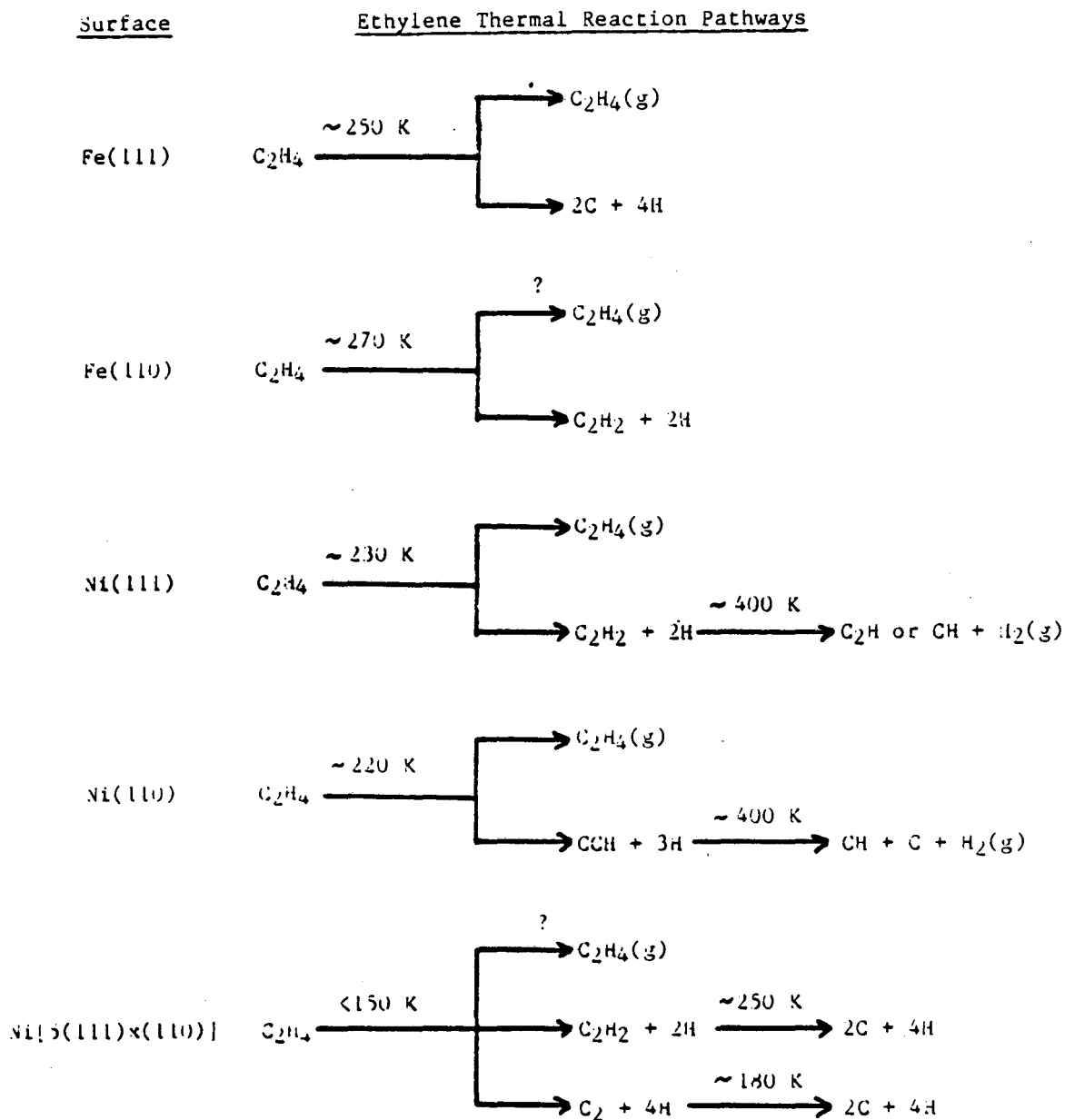
Fig. 4.7 Comparison of the surface fragments formed during ethylene thermal fragmentation on Rh(111) and Rh(100).

for ethylene fragmentation has been obtained for the groups 8-10 metal surfaces. Thus, only these metals will be discussed here.

Figures 4.8 and 4.9 show the thermal reaction pathways that have been identified for ethylene on the 3d and 4d/5d metal surfaces respectively. The metals are so-grouped because the 3d metal surfaces appear to have chemistry more similar to one another than to the 4d or 5d metal surfaces of the same group in the periodic table. For example, on all the 4d and 5d metal surfaces in Fig. 4.9 except Pd(100), at least one of the ethylene decomposition fragments is ethylidyne (CCH_3). None of the 3d metal surfaces in Fig. 4.8 form this species. Similar dichotomies between the 3d and 4d/5d metals also exist in molecular and solid state chemistry--for example in the formation of simple hydrated ions [25], the formation of high oxidation states [25], and the cohesive energies of the pure metals [26].

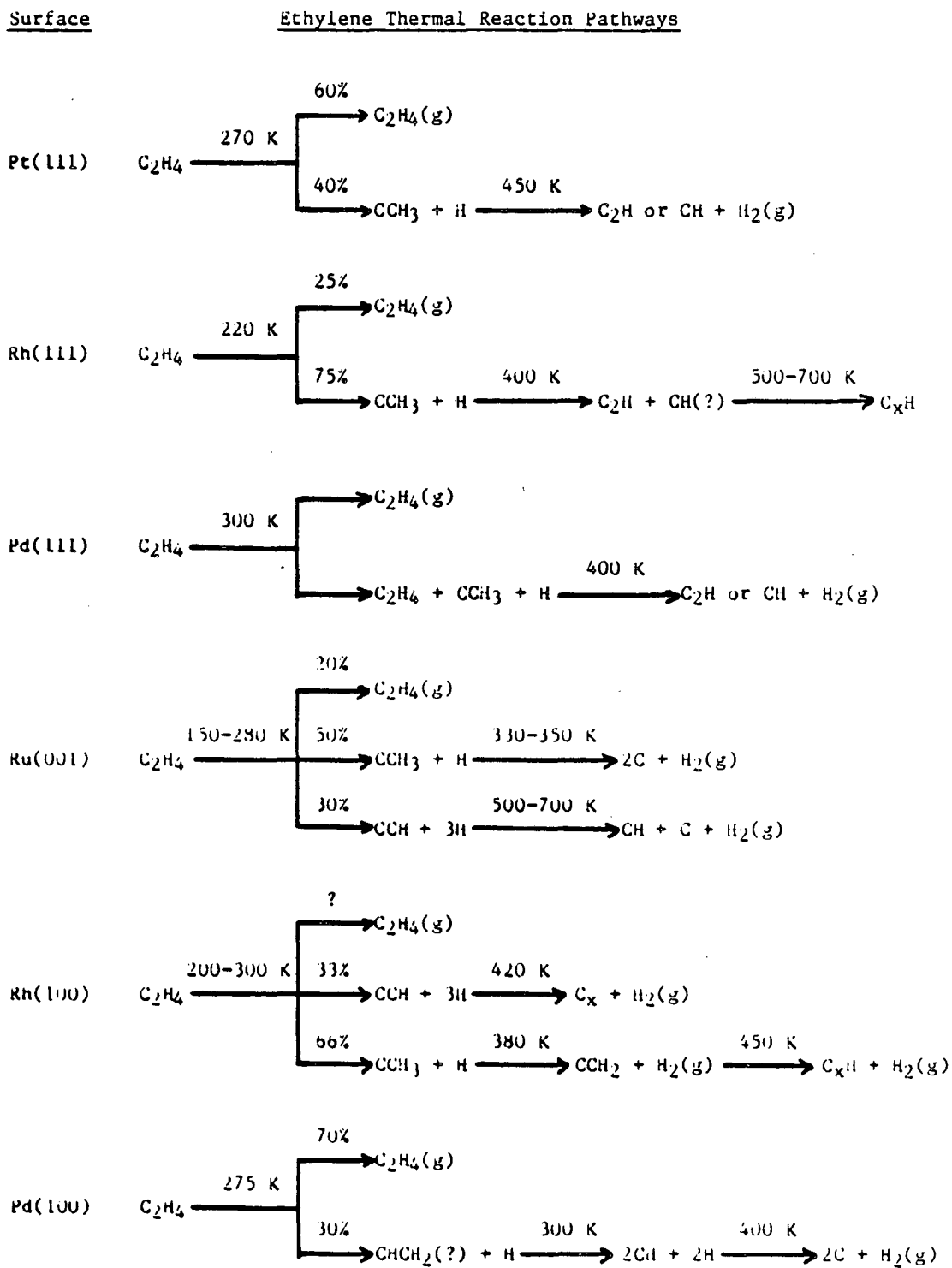
On both the 3d and 4d/5d metal surfaces (except possibly the highly corrugated Fe(111) surface), carbon-hydrogen bond breaking in ethylene occurs at lower temperature than carbon-carbon bond breaking. C-H bond breaking generally begins between 200 and 300 K, while C-C bond breaking (except on Fe(111) and stepped Ni[5(111)x(110)]) occurs above 300 K if at all.

Since C-H bond breaking occurs at a lower temperature than C-C bond breaking, it is generally assumed that ethylene decomposition is initiated by C-H bond cleavage. This is probably true for 3d metal surfaces, but not for the 4d and 5d metal surfaces which form ethylidyne. First, if dehydrogenation is favored, then HCCH_2 , HCCH ,



XBL 8610-4103

Fig. 4.8 Thermal reaction pathways determined by TDS and HREELS for ethylene on 3d metal surfaces. Question marks indicate that the reaction pathway or surface species is uncertain. References: Fe(111), [20]; Fe(110), [21]; Ni(111), [22]; Ni(110), [23]; Ni(11), [23]; Ni [5(111) x (110)], [22].



XBL 8610-4104

Fig. 4.9 Thermal reaction pathways determined by HREELS and TDS for ethylene adsorbed on 4d and 5d metal surfaces. Question marks indicate uncertain reaction pathways or surface species. References: Pt(111), [24]; Rh(111), [this work]; Pd(111), [4]; Ru(001), [11]; Rh(100), [this work]; Pd(100), [5].

CCH_2 , CCH , or C_2 are the expected decomposition products for ethylene on metal surfaces in the absence of C-C bond breaking. Indeed, these are the fragments observed on the 3d metal surfaces (Fig. 4.8) and on Pd(100) (Fig. 4.9). However, ethylidyne (CCH_3) species form on the vast majority of the 4d and 5d metal surfaces as shown in Fig. 4.9. Ethylidyne is also one of several decomposition products for acetylene on Rh(111) [28], Pd(111) [29] and Ru(001) [30] and for propylene, propadiene, and methylacetylene decomposition on Rh(111) [Section 4.3].

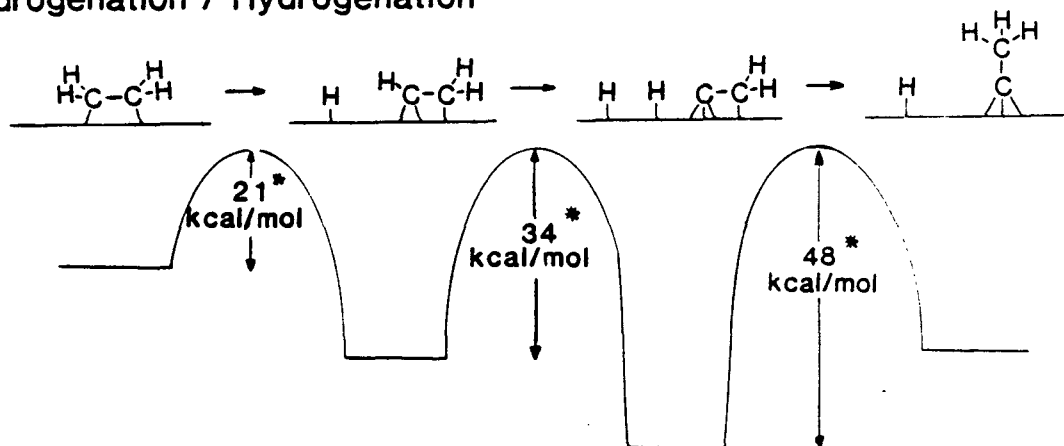
It is not obvious why ethylidyne should be such a ubiquitous and stable decomposition product on these 4d and 5d group 8-10 transition metal surfaces. One could imagine a mechanism where a 1,2 hydrogen shift above HCCH_2 or H_2CCH_2 in vacuum produced the methyl group, but the energy barrier for such a process is calculated to be quite high [31]. Further, studies of deuterium incorporation in the ethylidyne methyl group are not consistent with an intramolecular hydrogen shift [Section 4.2]. In particular, when 20 L of D_2 are adsorbed before and after 2 L of ethylene on Pt(111) at 310 K, three times as much deuterium is incorporated in the ethylidyne methyl group when the D_2 is adsorbed first. The reason some deuterium is found in the methyl group when D_2 is added second is because of H,D-exchange. The fact that substantially more deuterium is incorporated when D_2 is added first means that hydrogenation of some surface hydrocarbon species by surface hydrogen must occur in conversion of ethylene to ethylidyne.

Several groups [18,27,5] have proposed that ethylene conversion to ethylidyne is initiated by sequential dehydrogenation at one end of ethylene to produce CCH_2 plus 2H atoms ($CH_2CH_2 \rightarrow CHCH_2 + H \rightarrow CCH_2 + H + H$) followed by rehydrogenation at the other end to produce ethylidyne ($CCH_2 + 2H \rightarrow CCH_3 + H$). The energetics for such a dehydrogenation/hydrogenation mechanism of ethylidyne formation have been calculated by Kang and Anderson [27] using molecular orbital methods, and the results are shown in Fig. 4.10A. These energetics (which are consistent with other molecular orbital calculations for adsorbed hydrocarbon fragments on Pt(111) [32-34]) point out two problems with this dehydrogenation/hydrogenation mechanism. Not only is $CCH_2 + 2H$ calculated to be 18 kcal/mol more stable than $CCH_3 + H$, but the activation energy for this hydrogenation is calculated to be 48 kcal/mol (Fig. 4.10A), compared to the experimentally determined activation energy of 18 kcal/mol [35-37].

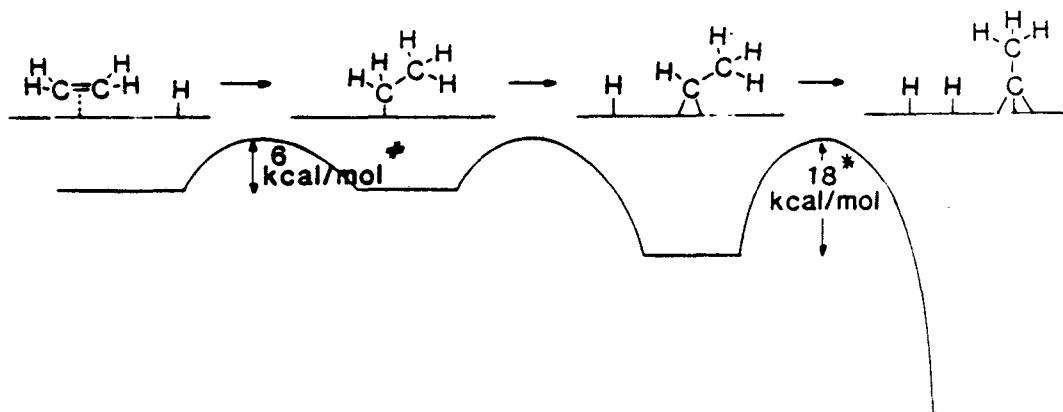
One possible explanation is that high surface hydrogen concentrations change the energetics of $CCH_2 + H \rightarrow CCH_3$, but this cannot account for conversion of ethylene to ethylidyne at low surface coverages. There is some experimental evidence that CCH_2 can be hydrogenated to CCH_3 in the conversion of acetylene to ethylidyne, but it is also true that this conversion appears to be much more difficult than conversion of ethylene to ethylidyne. For example, on Pt(111) the conversion of CCH_2 to CCH_3 involves heating 70 K above the ethylidyne formation temperature in 10^{-7} torr H_2 with filaments turned on near the surface to generate H atoms [18].

Proposed Mechanisms For Ethylidyne Formation

(A) Dehydrogenation / Hydrogenation



(B) Hydrogenation / Dehydrogenation



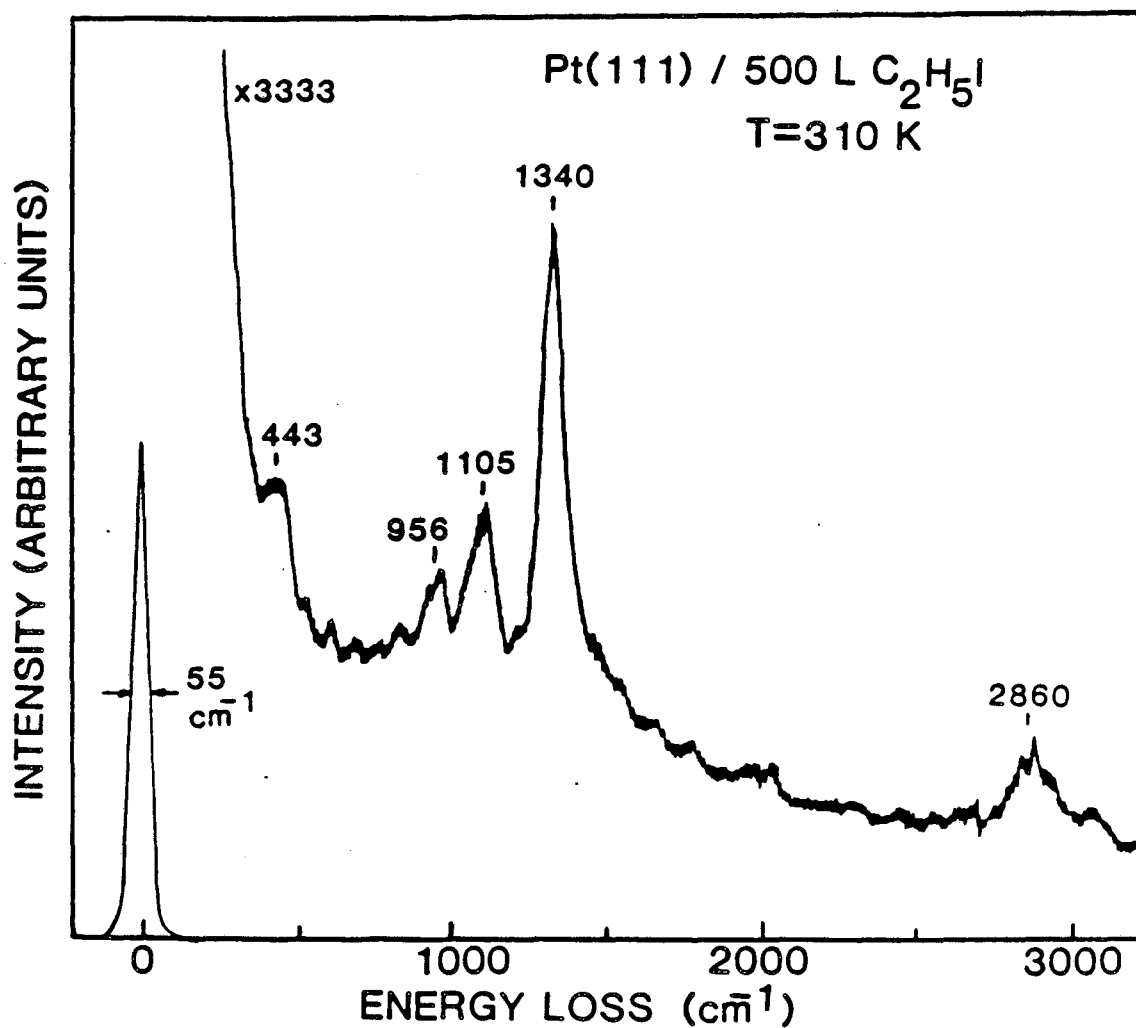
XBL 8512-4943

Fig. 4.10 Schematic representation of the surface intermediates and energetics for (A) the previously postulated dehydrogenation/hydrogenation mechanism and (B) the newly proposed hydrogenation/dehydrogenation mechanism for ethylidyne formation on transition metal surfaces. The energy levels and barrier heights are taken either from cluster molecular orbital calculations (* - ref. 27) or experimental results (# - ref. 37) as discussed in the text.

These puzzling aspects of ethylidyne formation can be resolved by considering a different mechanism for ethylidyne formation wherein C-H bond making rather than C-H bond breaking initiates the conversion of ethylene to ethylidyne. The projected and calculated energetics for this new hydrogenation/dehydrogenation mechanism are shown schematically in Fig. 4.10B. In this mechanism hydrogenation of ethylene to C_2H_5 initiates the conversion of ethylene to ethylidyne ($CH_2CH_3 \longrightarrow CHCH_3 + H \longrightarrow CCH_3 + 2H$) and avoids the CCH_2 thermodynamic sink. This mechanism was inspired by the experimental fact that ethylene, in the presence of surface hydrogen, can be hydrogenated to ethane at temperatures approximately equal to the ethylidyne formation temperatures on Rh(111) [this work] and Pt(111) [37]. The activation energy for production of ethane on Pt(111) was determined from TDS to be only 6 kcal/mol [37]. Presumably C_2H_5 is the intermediate in this reaction. It is estimated that the energy barrier for dehydrogenation at the α carbon of CH_2CH_3 to make $CHCH_3$ is small, since CH_2CH_3 will be floppy and able to achieve the necessary orientation [38] for C-H bond scission. The resulting ethylidene ($CHCH_3$) species is calculated to have a barrier of 18 kcal/mol towards formation of $CCH_3 + H$ [27], in fortuitously good agreement with the experimentally determined activation energy for ethylidyne formation on Pt(111) [35-37]. Further, recent considerations of orbital symmetry by Hatzikos and Masel [39] show that this hydrogenation/dehydrogenation mechanism is symmetry-allowed, while the $CCH_2 + H \longrightarrow CCH_3$ step in the dehydrogenation/hydrogenation mechanism is symmetry forbidden.

To summarize, the conversion of C_2H_4 to CCH_3 may be viewed as follows: A very small number of H atoms (from residual gas or produced by C_2H_4 decomposition at lower temperature at a small fraction of defect sites) hydrogenate some C_2H_4 to CH_2CH_3 with an activation energy of about 6 kcal/mol. This low activation energy may be the result of molecular C_2H_4 assuming a transient, weakly π -bound, and easily hydrogenated state as it diffuses across the surface. The resulting CH_2CH_3 species can either dehydrogenate at the β carbon to reform C_2H_4 , hydrogenate at the α carbon to form C_2H_6 , or sequentially dehydrogenate at the α carbon to form ethynylidyne. Whether or not ethynylidyne forms will depend on whether or not CH_2CH_3 forms more readily than ethylene dehydrogenates or surface hydrogen desorbs. The hydrogenation/dehydrogenation possibilities in C_2H_5 are reminiscent of analogous reaction probabilities calculated to explain the catalytic hydrogenation of and H,D exchange in C_2H_4 over a variety of metallic catalysts [40-42]. Note that the formation of CCH_3 generates surface hydrogen which can readily diffuse across the surface and initiate the decomposition of more ethylene to ethynylidyne.

In support of this hydrogenation/dehydrogenation mechanism, a Pt(111) surface was exposed to 500 L of C_2H_5I at 310 K. Comparison of the resulting surface vibrational spectrum shown in Fig. 4.11 with Fig. 4.1B shows that the surface species is ethynylidyne. Coadsorbed iodine atoms are also present, but they vibrate at low frequency and are not observed. It is plausible that the C-I bond (bond dissociation energy = 52 kcal/mol vs. 100 kcal/mol for the C-H bonds) breaks



XBL 866-2418

Fig. 4.11 Specular HREEL spectrum of a Pt(111) surface after exposure to 500 L of iodoethane at 310 K. The surface species are ethylidyne and coadsorbed I atoms.

first to form CH_2CH_3 , which then dehydrogenates as in Fig. 4.10B to form CCH_3 . As to why ethylene decomposes to ethynidyne on Pt(111), Pd(111) and Rh(111) when the molecular ethylene bonding on these surfaces is quite different, it may be that ethylene must assume a transient π -bound state in order to be hydrogenated to C_2H_5 and converted to ethynidyne. The bonding of this π -bond ethylene and of the resulting C_2H_5 to these surfaces may be quite similar.

It is interesting that in this mechanism the driving force for C_2H_4 decomposition to CCH_3 is the partial hydrogenation of C_2H_4 , and that the metals which form CCH_3 are good catalysts for the catalytic hydrogenation of ethylene to ethane. In fact, it was found in studies of catalytic ethylene hydrogenation over Pt(111) [43,44] and Rh(111) surfaces [45], that ethynidyne forms on the surface at room temperature even when the surfaces are exposed to 100 torr of hydrogen and 20 torr of ethylene and the hydrogen is added first. The 3d metal surfaces like Ni(111) and Fe(110) may dehydrogenate ethylene at a faster rate than that for hydrogenation, thus leading directly to fragments like acetylene and C_2H as shown in Fig. 4.8.

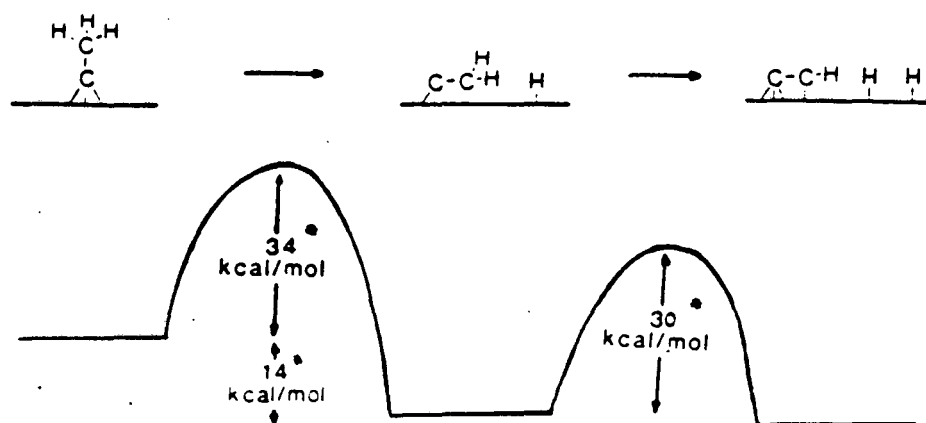
The Ru(001) and Rh(100) surfaces are particularly interesting cases in light of these two mechanistic possibilities, since both C_2H and CCH_3 can be formed by ethylene decomposition at room temperature on these surfaces (Fig. 4.9). For both surfaces the ratio of $\text{C}_2\text{H}/\text{CCH}_3$ is higher for low exposures of ethylene. On Rh(100) the ratio decreases from ∞ to ~ 2 with increasing exposure while on Ru(001) the ratio only decreases from about 1 to 0.6. Both cases can be rationalized by two

different mechanisms for ethylene decomposition -- one initiated by dehydrogenation and favored by larger ensembles of metal atoms at low surface coverages and the other initiated by hydrogenation and favored at high surface coverages where dehydrogenation is blocked.

An explanation for the higher temperature decomposition of ethynylidyne to C_2H on Rh(111) and Pt(111) and to CCH_2 on Rh(100) is afforded by the calculated energetics of Kang and Anderson [27]. As shown in Fig. 4.12 they find a barrier of 34 kcal/mol towards decomposition of CCH_3 to CCH_2 on Pt(111). This CCH_2 species, according to the calculations, then has enough internal energy to decompose to C_2H . The experimentally measured activation energy for ethynylidyne decomposition on Pt(111) is 22 kcal/mol [35].

In summary, all of the hydrogenation and dehydrogenation chemistry of ethylene on transition metal surfaces (in the absence of C-C bond breaking and forming) can be explained by the series of elementary hydrogenation/dehydrogenation steps shown in Fig. 4.13. It is postulated that intramolecular hydrogen shifts are not involved in the surface chemistry. All reaction steps in Fig. 4.13 are potentially reversible, but dehydrogenation is strongly favored for typical surface hydrogen coverages in UHV. The most highly reversible step is probably $C_2H_4 + H \longrightarrow C_2H_5$, which can explain the low temperature H,D-exchange observed in molecular ethylene on Pt(111) [37]. Further, it is proposed that this partial hydrogenation of C_2H_4 to C_2H_5 is the initiating step in the conversion of ethylene to ethynylidyne. The

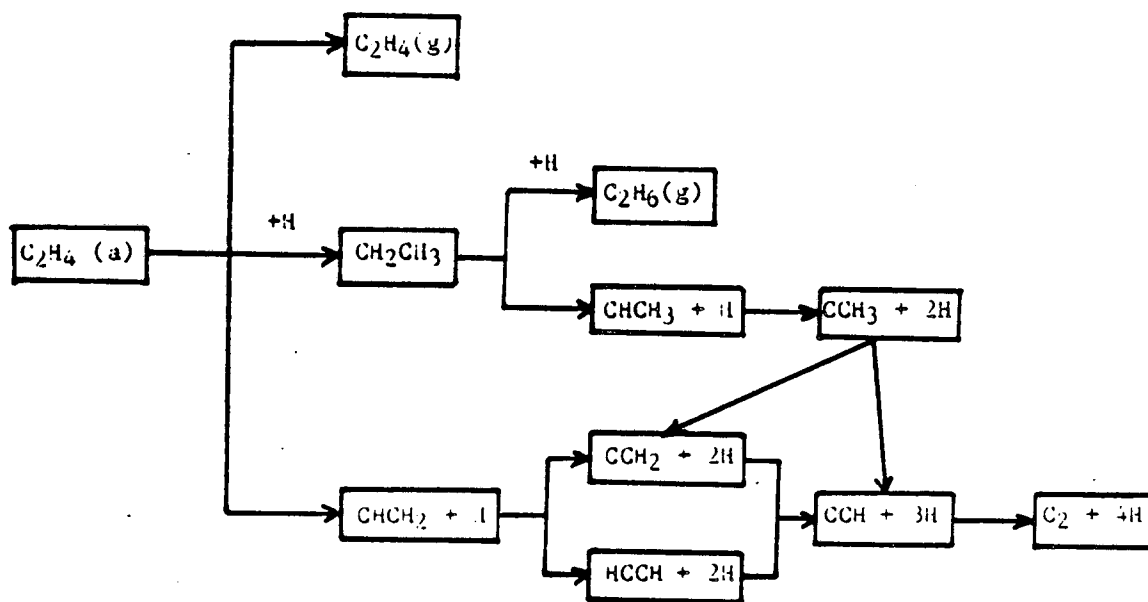
Proposed Surface Reaction Mechanism for Fragmentation of Ethylidyne (CCH_3) to Vinylidene (CCH_2) and Acetylide (CCH)



XBL 8610-4105

Fig. 4.12 Proposed mechanism for conversion of ethylidyne (CCH_3) to vinylidene (CCH_2) and acetylide (CCH). Energetics shown were calculated by molecular orbital methods for a Pt(111) slab [27].

Proposed Scheme For C-H Bond Chemistry of Ethylene on Transition Metal Surfaces



XBL 8610-4106

Fig. 4.13 Proposed scheme for ethylene fragmentation on transition metal surfaces in the absence of C-C bond breaking. All the elementary steps are either hydrogenation (reductive elimination) or dehydrogenation (oxidative addition) reactions.

absence of ethylidyne on 3d metal surfaces and on Rh(100) at low coverages is explained by decomposition pathways initiated by dehydrogenation.

4.2 Hydrogenation and H,D-exchange Studies of Ethylidyne on Pt(111) and Rh(111) in UHV and at 1 Atm Pressure

4.2.1 Background. An important function of the metallic component in hydrocarbon conversion reaction catalysts is to provide a source of reactive hydrogen atoms. Yet it is known that active hydrocarbon catalysts are covered with monolayer amounts of strongly-bound hydrocarbon species which inhibit hydrogen adsorption and dissociation [46]. Whether these carbonaceous deposits are an essential part of the catalyst or an unavoidable poison is not completely clear. An intriguing possibility is that these adsorbed hydrocarbons act as hydrogen storage agents, readily transferring hydrogen atoms to and from the surface [46]. There is also the possibility of direct hydrogen transfer from the carbonaceous deposit to reactive intermediates [47].

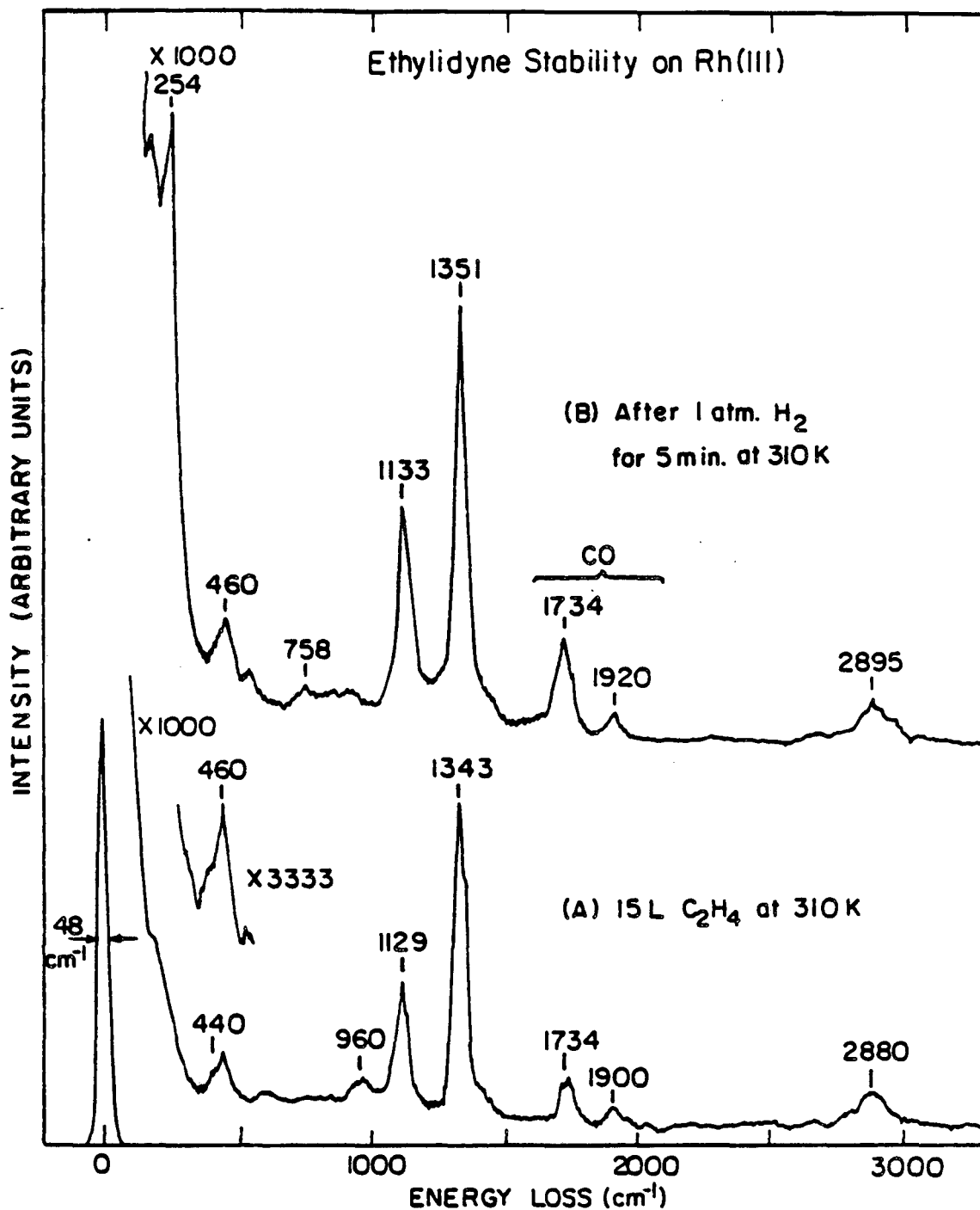
Hydrogen-deuterium exchange in adsorbed hydrocarbon species provides a means for studying the hydrogen transfer and storage capabilities of adsorbed hydrocarbons. Studies of H,D-exchange in the carbonaceous deposits on active Pt single crystal catalysts have been reported [46]. It was found that this process is indeed facile at the reaction temperature under atmospheric pressures of deuterium. However, in these studies it could not be determined whether some C-H bonds exchange more readily than others, since H_2 , HD and D_2 had to be thermally desorbed to detect exchange,

In this section, studies of the rate of H,D exchange in the methyl group of ethylidyne on Rh(111) and Pt(111) are reported. The H,D exchange was monitored by HREELS and TDS and was studied as a function

of temperature, ethylidyne coverage and deuterium pressure. It is found that deuterium atoms exchange with the methyl group hydrogens one at a time. The exchange rate is faster on Rh(111) than Pt(111). For saturation coverages of ethylidyne the exchange rate is slow and insensitive to deuterium pressure from 1×10^{-2} torr up to 1 atm. Exchange is rapid and extensive at subsaturation ethylidyne coverages. For Pt(111), the ethylidyne H,D exchange rate at room temperature is slower than the rate of H,D exchange previously reported for molecular ethylene below 270 K [37]. The differences are correlated to the relative rates of ethylene and ethylidyne hydrogenation.

4.2.2 Results and Interpretation. The results will be presented and interpreted in two parts. First control experiments on the structural stability of ethylidyne under 1 atm of hydrogen will be presented, and second, these experiments will be compared with the effects of deuterium. In each part the Rh(111) results will be presented first.

Ethylidyne + H₂. Figure 4.14 shows the effects of 1 atm of hydrogen on a monolayer of ethylidyne at room temperature on Rh(111). Figure 4.14A is the specular HREEL spectrum for a saturation coverage of ethylidyne on Rh(111) produced by adsorbing 15 L of ethylene at room temperature. This monolayer has the partially ordered LEED pattern characteristic of ethylidyne on Rh(111) [49]. Figure 4.14B shows the HREEL spectrum that results after this monolayer of ethylidyne is treated in the high pressure cell with 1 atm of H₂ for 5 min and then returned to the UHV chamber. The vibrational frequencies and relative peak intensities in this spectrum are, to within experimental



XBL 842-6616

Fig. 4.14 Specular HREEL spectra of a Rh(111) surface (A) saturated with ethynidyne under UHV conditions, and (B) following exposure of this monolayer to 1 atm of H_2 for 5 min. at 310 K. The fact that these spectra are virtually identical shows that ethynidyne monolayers are extremely stable towards rehydrogenation.

uncertainty, the same as before the high pressure hydrogen treatment. There is no evidence for decreased ethylidyne coverage as a result of rehydrogenation to ethylene or ethane. This means that any structural changes in ethylidyne under 1 atm of H_2 must be reversible.

Figure 4.14B also shows little contamination by other molecules that may coadsorb during high pressure gas exposure. On clean Rh(111), during 1 atm H_2 exposures, hydrocarbon contaminants from the HP cell loop adsorb dissociatively on the surface, giving broad, fingerprint HREELS peaks at about 800 and 1400 cm^{-1} . Similar features were also found in a recent study of surface structure following Fischer-Tropsch synthesis on Fe(110) and assigned to CH and CH_2 fragments [50].

Figure 4.14B shows no evidence for formation of such surface species in this case. Figure 4.14B also shows almost no change in the relative intensity of the contaminant CO (< 5% of a monolayer) peaks at 1938 and 1745 cm^{-1} , further evidence that the ethylidyne coverage does not change. There is a new feature at 254 cm^{-1} which may be due to contaminate sulfur atoms. (Unfortunately the AES was not operable at this point, so the presence of sulfur could not be confirmed.) The presence of sulfur atoms can also explain the formation of a $c(4 \times 2)$ LEED pattern during the hydrogen treatment, since a similar pattern was observed for CO coadsorbed with ethylidyne [49].

Ethylidyne monolayers on Pt(111) show similar stability to those on Rh(111) under 1 atm of H_2 at room temperature. HREEL spectra analogous to Fig. 4.14 showing effects of 1 atm hydrogen treatments at

310 K on ethylidyne have been published [44,51]. These Pt(111) spectra show slightly more contamination from hydrocarbons and CO after the high pressure hydrogen than the Rh(111) spectrum in Fig. 4.14B, indicating that ethylidyne is more easily hydrogenated and removed from the Pt(111) surface. Still the rate of removal is quite slow, $< 10^{-4}$ ethylidyne/Pt atom/s, as determined by previous carbon 14 labelling studies [52].

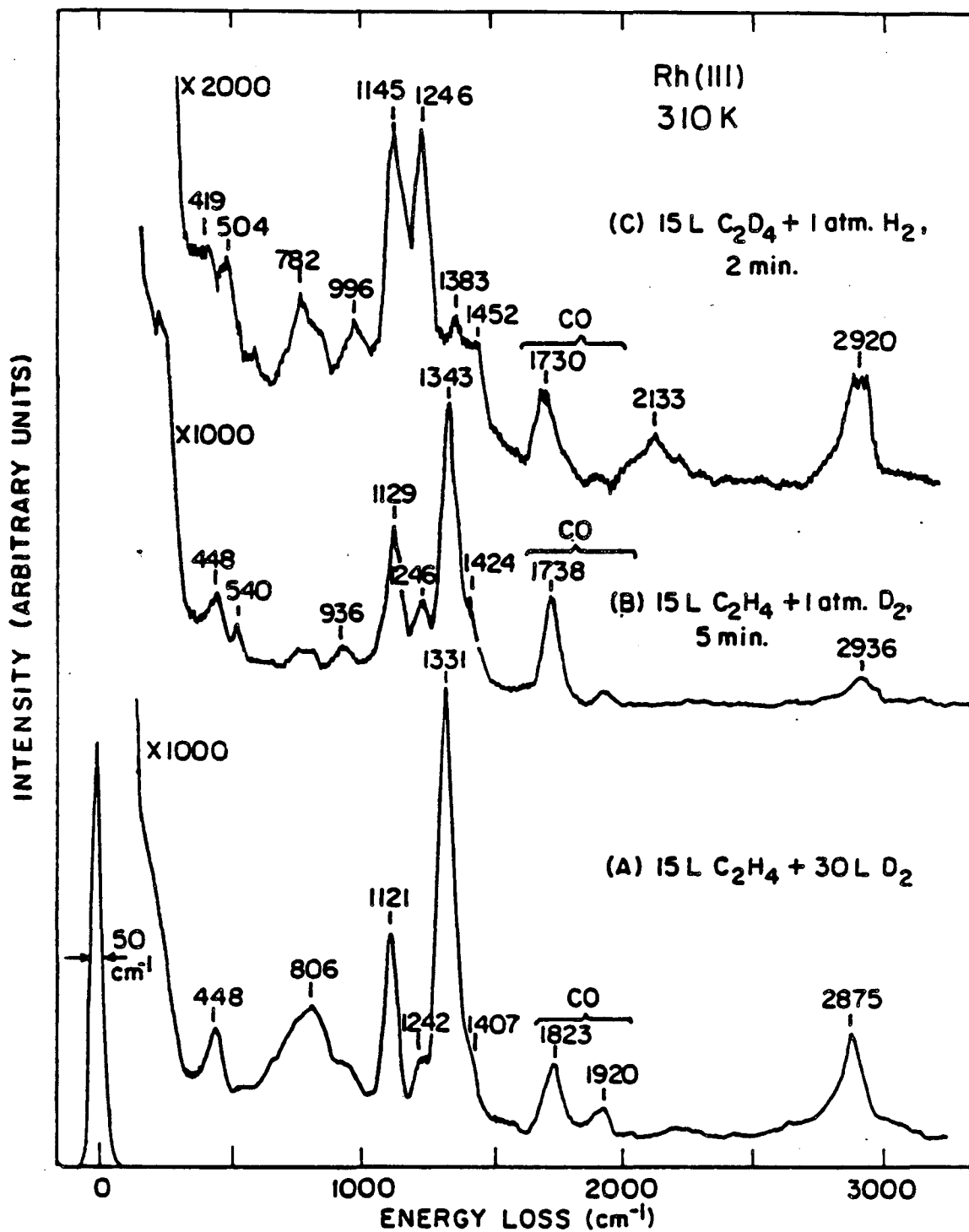
Previous TDS studies on Pt(111) have also shown that up to a quarter monolayer of hydrogen atoms, $\theta_H = 0.25$, can be coadsorbed with a saturation coverage of ethylidyne by using 1 atm of H_2 [37]. Since hydrogen can be adsorbed and dissociated under these conditions, the rehydrogenation and removal of ethylidyne must be kinetically prohibited because of the strong binding of ethylidyne to Pt(111). Presumably the same is also true on Rh(111) where ethylidyne shows similar bonding and a similar saturation packing density to Pt(111). Surface hydrogen atoms are not observed in the room temperature HREEL spectra on either Pt(111) and Rh(111) because the surface hydrogen residence time at this temperature is much less than the 20-30 min HREELS experiment. Furthermore, the Pt-H [53] and Rh-H [54] bonds are weak HREELS scatterers.

Ethylidyne + D_2 . Since the ethylidyne HREEL spectra showed no changes after 1 atm H_2 treatments, any changes after 1 atm of D_2 can be attributed to H,D-exchange. The HREEL spectra in Figs. 4.15A and 4.15B were taken of monolayers of CCH_3 on Rh(111) that were treated

with 30 L and 1 atm of D_2 respectively. In comparison with the ethynidyne HREEL spectra in Fig. 4.14 these spectra show two new peaks characteristic of methyl group H,D-exchange at ~ 1245 and $\sim 1410 \text{ cm}^{-1}$. (The 806 cm^{-1} peak in Fig 4.15A is due to contamination in the original CCH_3 monolayer.) Neither peak is present in the spectrum of CCD_3 (Fig. 3.3), so they must be the result of partial exchange. The rate of exchange is slow, since the $\delta_s CH_3$ mode at $\sim 1330 \text{ cm}^{-1}$ for CCH_3 is still quite intense. It is surprising that both 30 L and 1 atm of D_2 produce similar amounts of exchange.

The incorporation of hydrogen in deuterated ethynidyne was also investigated. Treatment of CCD_3 with 1 atm H_2 for 2 min. at 310 K, as shown in Fig. 4.15C, results in new peaks at 1246, 1300 - 1450, 2920, and a small increase in the peak at 780 cm^{-1} . The absence of a peak at 1340 cm^{-1} for the intense symmetric methyl deformation ($\delta_s CH_3$) mode shows there are also few completely exchanged methyl groups here.

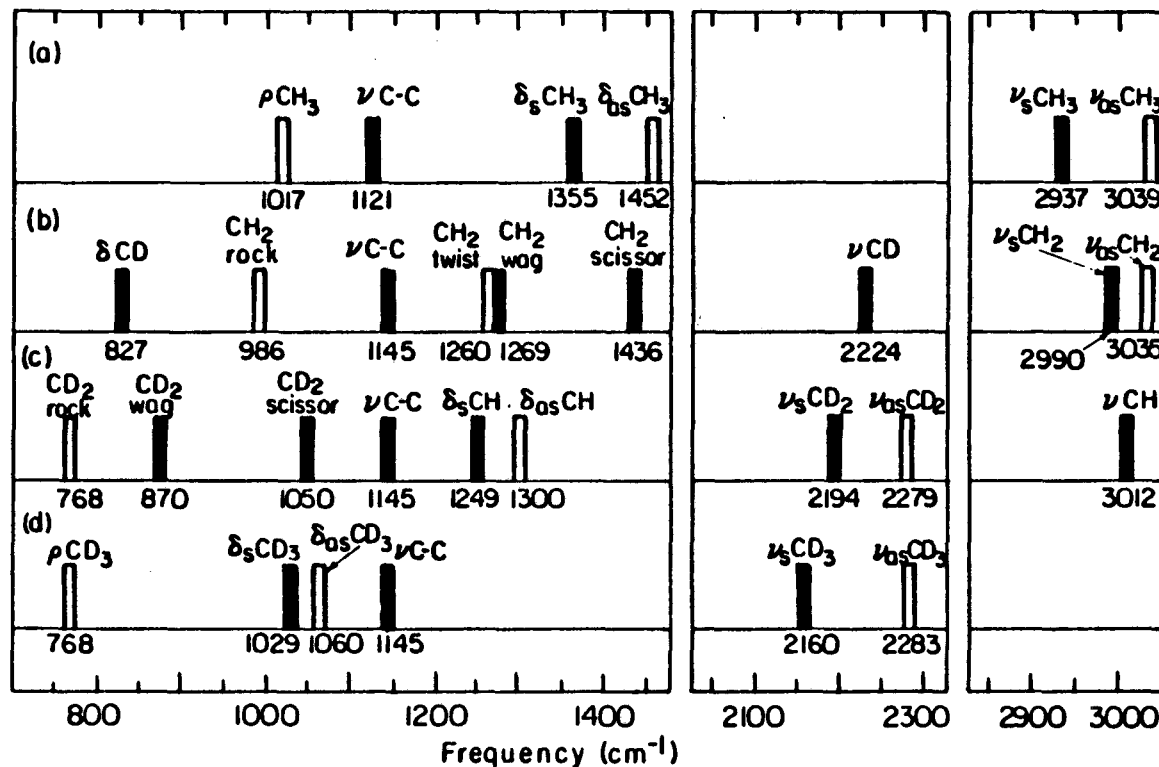
Peak assignments for the partially deuterated methyl groups were initially made [48] by comparison with variously deuterated methyl chlorides [55,56] whose peak frequencies and approximate mode descriptions are shown in Fig. 4.16. Here the ν_{C-Cl} modes have been replaced with expected C-C stretching frequencies of ethynidyne for comparison with HREEL spectra. The major effect of partial deuteration on the vibrational spectra is that the large percentage mass difference between H and D requires new approximate normal mode descriptions. As shown in Fig. 4.15, the methyl group modes for partially deuterated



XBL 842-6618

Fig. 4.15 Specular HREEL spectra of Rh(111) at 310 K showing the effects of (A) 30 L and (B) 1 atm of D₂ on CCH₃ and of (C) 1 atm H₂ on CCD₃. These spectra indicate partial H,D-exchange in the ethylidyne methyl group.

Methyl Group Modes in Variously Deuterated Methyl Chlorides



XBL 042-6629

Fig. 4.16 Methyl group vibrational frequencies and approximate mode descriptions in variously deuterated methyl chlorides. Shaded peaks are modes of A or A' symmetry (dipole-allowed), while unshaded peaks are modes of E or A'' symmetry (dipole-forbidden). C-Cl modes are replaced by approximate C-C stretching frequencies for direct comparison with ethylidyne. (A) CH₃Cl, (B) CDH₂Cl, (C) CD₂HCl, (D) CD₃Cl.

ethylidyne are now best described as a combination of $\text{CH}_2 + \text{CD}$ or $\text{CD}_2 + \text{CH}$ vibrations.

Another effect of partial deuteration is that the symmetry of ethylidyne is lowered from C_{3v} to C_s . This lower symmetry means that more vibrational modes are dipole active (compare the shaded bars in Fig. 4.16) and thus expected to have large scattering amplitudes in the specular direction. The HREEL spectra are further complicated by the presence of mixtures of variously deuterated ethylidyne on the surface; at a resolution of 50 cm^{-1} , dipole-active modes of the various CCH_xD_y species overlap as can be seen from the shaded bars in Fig. 4.16.

Using the vibrational frequencies from many HREEL spectra of variously deuterated ethylidyne mixtures formed by ethylidyne H,D-exchange, peak assignments have been made for the various CCH_xD_y species as shown in Table 4.1. The observed vibrational frequencies are also compared with those calculated in a normal coordinate analysis by Bruno Marchon [57] and show quite reasonable agreement. The most distinctive vibrational feature of both partially-exchanged species is a band at $\sim 1250 \text{ cm}^{-1}$. This frequency corresponds to a CH_2 wag for the monodeuterated species and to a CH in-plane bend for the dideuterated species. The monodeuterated ethylidyne is also uniquely characterized by a CH_2 scissors vibration at $1400 - 1430 \text{ cm}^{-1}$.

The effects of temperature and time on ethylidyne H,D exchange have also been studied. Some results from these studies are shown in

Table 4.1: Calculated^a and Observed^b Frequencies (cm⁻¹) for the Dipole-Allowed Vibrations in Variously Deuterated Ethylidyne [CCH_xD_y]

Modes	CCH ₃		CCD ₃		Modes	CCH ₂ D		Modes	CCHD ₂	
	Obs.	Calc.	Obs.	Calc.		Obs.	Calc.		Obs.	Calc.
ν_s CH ₃	2880	2888	2065	2088	ν_s CH ₂	2918	2903	ν_s CD ₂	2166	2122
δ_s CH ₃	1337	1355	988	1003	CH ₂ wag	1248	1256	γ CH	1239	1250
ν CC	1121	1166	1145	1176	ν CC	1125	1158	ν CC	1130	1161
ν_s Co-C	435	408	419	393	ν_s Co-C	435	399	ν_s Co-C	425	393
ν_{as} CH ₃	2920	2930	2178	2192	ν CD	2169	2158	ν CH	2952	2917
δ_{as} CH ₃	1420	1423	—	1027	CH ₂ scis.	1430	1403	CD ₂ scis.	1000	1021
ρ CH ₃	972	1009	769	822	δ CD	810	854	CD ₂ wag	784	881
ν_{as} Co-C	—	565	—	523	ν_{as} Co-C	—	541	ν_{as} Co-C	—	526

- a) Normal coordinate analysis by Bruno Marchon using force constants and geometry previously applied to Co₃(CCH₃)(CO)₉: Skinner, et al., ref. [59].
 b) An average of frequencies for spectra on Rh(111).

Fig. 4.17. Figure 4.17A (like Fig. 4.15B) shows the HREEL spectrum after 5 min of deuterium exchange at 1 atm pressure in a saturation coverage of CCH_3 at room temperature. Figure 4.17B shows the vibrational spectrum after the same monolayer is additionally treated with 1 atm D_2 for 2 min. at 350 K. Raising the temperature 40 K still does not cause any significant change in the total ethylidyne coverage (as monitored indirectly by CO adsorption), but increases the amount of exchange, as indicated by the growth of the 1246 and 1432 cm^{-1} peaks. Exposing this D and CCH_3 covered surface at 300 K to UHV for 36 hours results in additional exchange between the remaining adsorbed deuterium and partially exchanged ethylidyne, as shown in Fig. 4.17C.

It is difficult to quantitatively determine the amount of H,D exchange from the HREEL spectra even with the peaks assigned. The major problem is quantifying the dynamic dipoles perpendicular to the surface (which should be proportional to dipole scattering peak intensity) for the different adsorbates in the CCH_xD_y isotopic mixture. Because of differing dynamic dipole strengths and overlapping peaks, the peak heights do not change linearly with the concentration of the various molecules in a particular CCH_xD_y mixture. However, by assuming that the CH_2 wag dynamic dipole is equal to the CC stretch dynamic dipole [58], the exchange rate can be estimated. Comparing the intensity of the 1120 and 1246 cm^{-1} peaks (assumed to be all CH_2 wag for small amounts of exchange) in Fig. 4.17A, it is estimated that five minutes of 1 atm D_2 over CCH_3 incorporates 0.4 deuteriums/ethylidyne methyl group [60]. This value corresponds to methyl group H

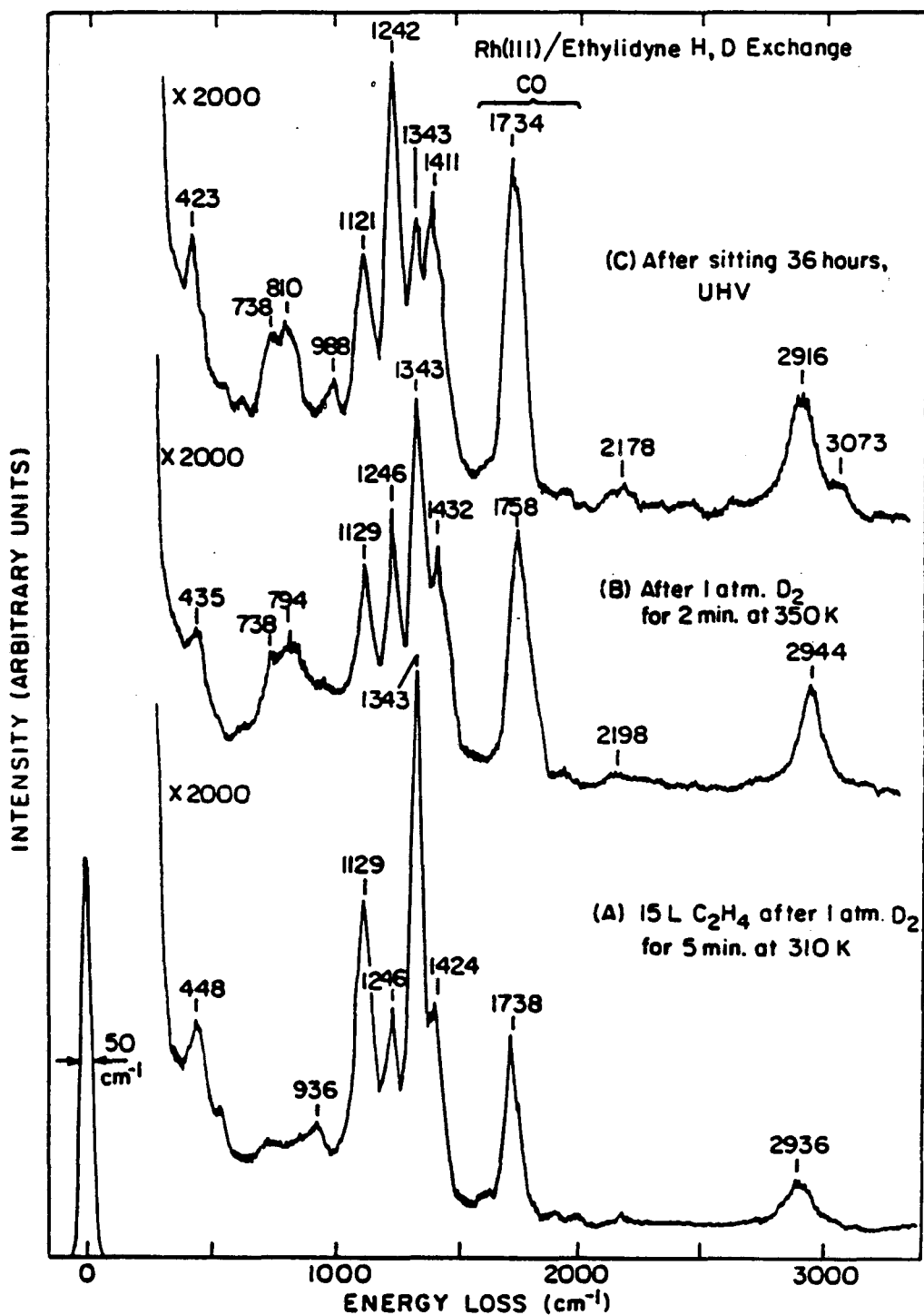


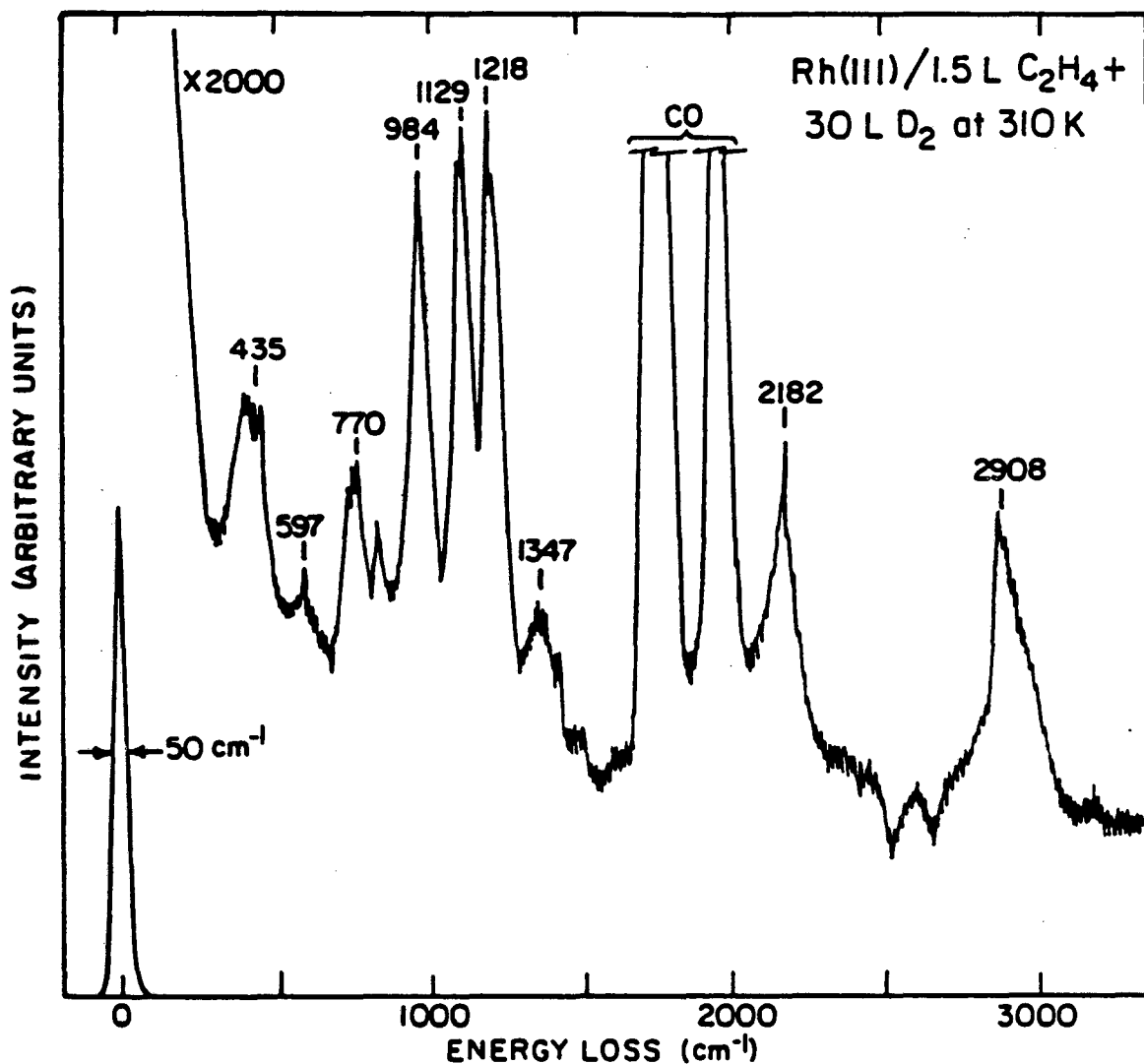
Fig. 4.17 Specular HREEL spectra of Rh(111) showing the effects of temperature and time on the extent of H,D-exchange in ethylidyne. The peaks at ~ 1245 and ~ 1420 cm^{-1} are characteristic of partially deuterated methyl groups. Under these conditions, almost no ethylidyne species have undergone complete exchange, and some species remain that have undergone no exchange.

replacement at a turnover rate of $< 10^{-3}$ /Rh atom/sec. This rate is faster than that for ethylidyne rehydrogenation but is still quite slow.

Subsaturation coverages of CCH₃ exchange much more rapidly. A HREEL spectrum after reaction of < 50 saturation coverage (1.5 L C₂H₄ exposure) CCH₃ with 30 L D₂ is shown in Fig. 4.18. The presence of the δ_s CD₃ peak at 984 cm⁻¹ and the nearly complete loss of the δ_s CH₃ peak at 1340 cm⁻¹ indicate complete exchange in some methyl groups. Some partially exchanged ethylidyne is still observed as evidenced by the 1218 cm⁻¹ peak.

The HREEL spectroscopy results for ethylidyne H,D exchange on Pt(111) are similar to Rh(111) and are not shown here. The major difference is that the room temperature exchange rate on Pt(111) is substantially slower than on Rh(111). The difference in rates approximately correlates with how far the reaction temperature is below the ethylidyne thermal decomposition temperature. For example, ethylidyne begins to decompose at ~ 400 K on Rh(111) and ~ 460 K on Pt(111). Similarly, the rate of H,D-exchange at 370 K on Pt(111) is comparable to the H,D-exchange rate on Rh(111) at 310 K.

The rates of ethylidyne H,D-exchange on Pt(111) under UHV conditions were determined by TDS for a number of temperatures and ethylidyne coverages. These rates are given in Table 4.2 along with the relative H₂, HD and D₂ peak areas from the TDS. All exchange reactions were carried out in the stoichiometric regime with a maximum incorporation of about one deuterium per ethylidyne. This means that



XBL842-6619

Fig. 4.18 Specular HREEL spectrum taken after a subsaturation coverage of ethylidyne was exposed to 30 L of D₂ at 310 K. All of the ethylidyne has undergone some H,D-exchange with a large fraction of the methyl groups having become completely deuterated.

Table 4.2: TDS Peak Areas and Calculated H,D-exchange Rates for Ethylidyne on Pt(111)

Experiment ^a	TDS Peak Areas ^b			Deuterium/Ethylidyne ^c	Exchange Rate ^d
	H ₂	HD	D ₂		
0.5L C ₂ H ₄ +20L D ₂ T = 310 K	2.6	0.23	1.4	1.1	2.8x10 ⁻³
1.0L C ₂ H ₄ +20L D ₂ T = 310 K	4.8	0.92	0	0.24	6.0x10 ⁻⁴
1.0L C ₂ H ₄ +20L D ₂ T = 380 K	2.3	1.9	0	0.68	1.7x10 ⁻³
2.0L C ₂ H ₄ +20L D ₂ T = 310 K	10.2	1.6	0	0.20	5.1x 10 ⁻⁴
20L D ₂ +1.0L C ₂ H ₄ T = 310 K	3.7	2.2	0.5	0.76	1.9x10 ⁻³

a) 20L D₂ added as 2x10⁻⁷ torr for 100 sec.

b) arbitrary units corrected for differing mass spectrometer sensitivities.

c) $3x[(1/2 HD+D_2)/(H_2+HD+D_2)]$.

d) number of exchanges/Pt atom/sec.

the rate of deuterium incorporation equals the H,D-exchange rate. All reactions were run by reacting the ethylidyne with 2×10^{-7} torr of deuterium for 100 sec, except in the experiment where the deuterium was added first.

More experiments are needed to determine the precision of these results and to draw definitive conclusions, but a few general trends are worth noting. The rates appear to be highly nonlinear with the coverage of ethylidyne, probably being limited in the 1 and 2 L ethylene cases by the rate of arrival of H_2 to the surface. (2 L of ethylene corresponds to 2/3 of saturation coverage of ethylidyne.) This is supported by the low activation energy for exchange of 3.5 kcal/mole determined from the 1 L ethylene experiments at 310 and 380 K. Also, the fact that three times more deuterium is incorporated in ethylidyne when the deuterium is added first is evidence against an intramolecular hydrogen shift during ethylidyne formation as discussed in Section 4.1. It should be noted that the ethylidyne surface coverage was not effected by the order of addition as confirmed by AES; however, more experiments are needed to delineate the effects of order of hydrogen and ethylene addition on the surface hydrogen coverage.

Ethylidyne H,D-Exchange Mechanism. The spectra in Fig. 4.15 and 4.17 with peaks assigned as in Table 4.1 can be used to show that deuterium atoms are incorporated in the CCH_3 methyl group one at a time. The most informative peaks are those at 1246 and 1430 cm^{-1} . The 1430 cm^{-1} peak is characteristic of the CH_2 scissor in CCH_2D . It is

the same intensity as the 1246 cm^{-1} CH_2 wag when deuterium exchange first begins, as seen in Figs. 4.15A,B and 4.16A,B. With continued exchange, the 1246 cm^{-1} peak grows in relative intensity (Fig. 4.17C). Since neither the 1246 nor 1430 cm^{-1} peak is present in CCH_3 or CCD_3 , the change in their relative intensities implies two partially-deuterated species. As CD_2H forms, the 1430 cm^{-1} CH_2 scissor has a smaller intensity relative to the 1246 cm^{-1} CH_2 wag peak which gains a contribution from the $\delta_s\text{CH}$ vibration in CCD_2H .

The presence of both CCH_2D and CCHD_2 and the gradual conversion of one to the other rules out an exchange mechanism wherein one molecule of D_2 always replaces two H atoms in the methyl group by a concerted exchange. The mechanism for the process here is single atom H,D-exchange. Furthermore, there is no evidence from the HREEL spectrum of complete methyl group deuteration by some rapid exchange process at selected sites after 5 - 10 min at 310 K under 1 atm D_2 . Similar conclusions were also reached in secondary ion mass spectroscopy (SIMS) studies of ethylidyne H,D-exchange on Pt(111) [61]. Thus, on both Pt(111) and Rh(111) the H,D-exchange process involves sequential, single-atom exchanges.

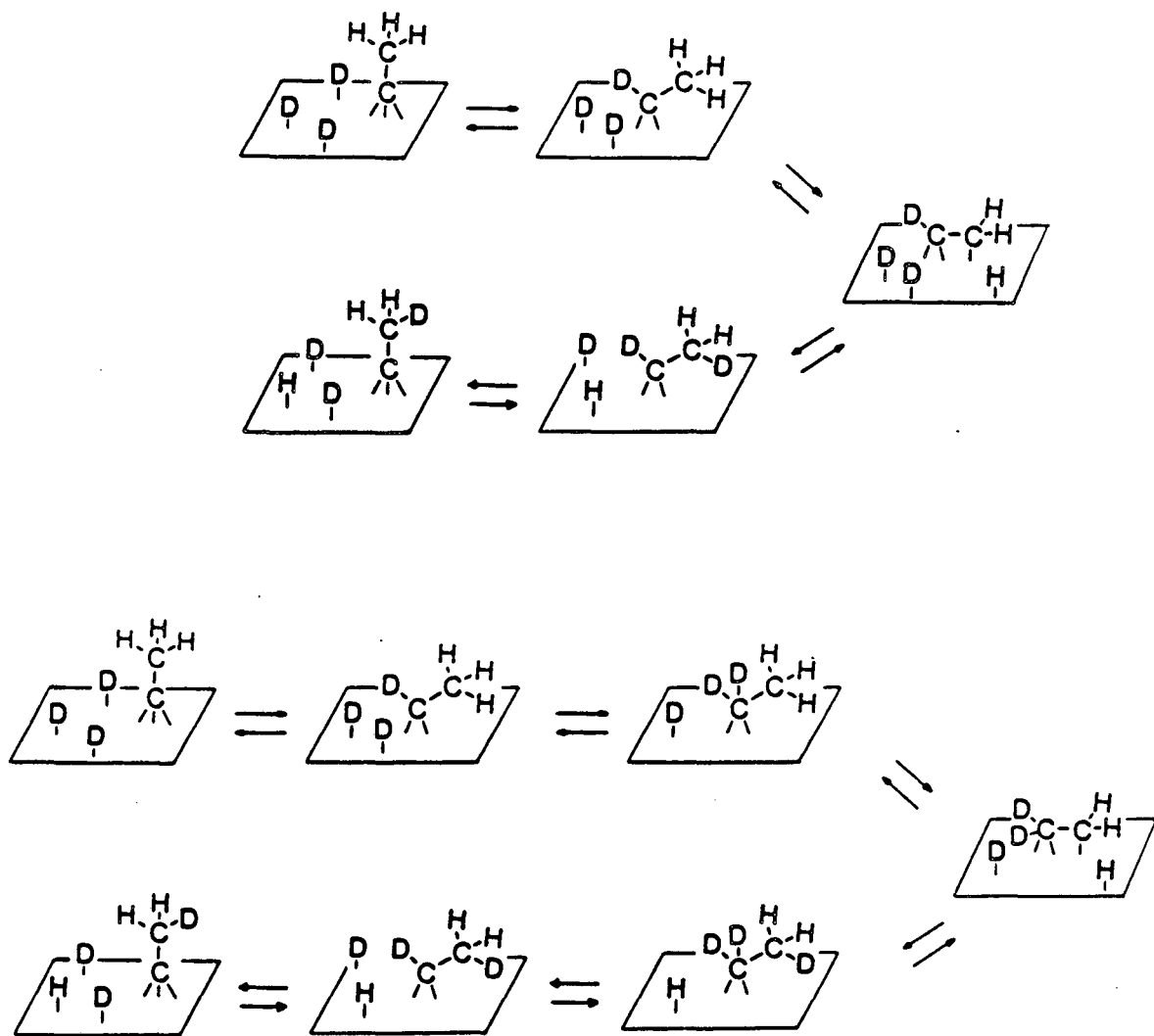
Three mechanisms have been suggested in the literature for ethylidyne H,D exchange--two based on the SIMS results on Pt(111) [61] and one based on the Rh(111) HREELS results discussed here [48]. In all three mechanisms the exchange is proposed to be initiated by hydrogen addition rather than abstraction for several good reasons: (1) exchange occurs at substantial rates over 100 K below the temperatures

for detectable ethylidyne dehydrogenation and (2) ethylidyne dehydrogenation appears to be irreversible. Addition-elimination mechanisms have also been proposed to explain benzene H,D-exchange on Pt(110) [62]. However, all three of the proposed ethylidyne H,D-exchange mechanisms involve intramolecular hydrogen shifts, which have been calculated to have high energy barriers [31].

Two reasonable pathways for ethylidyne H,D-exchange which are initiated by hydrogen addition and involve no intramolecular hydrogen shifts are shown in Fig. 4.19. These two pathways involve only elementary hydrogenation and dehydrogenation steps. Both pathways also involve the conversion of ethylidyne (CCH_3) to ethylidene (CHCH_3). A tilted ethylidene species brings the methyl group C-H bonds in close proximity with the surface so that the methyl group can dehydrogenate. The further hydrogenation of CHCH_3 to CH_2CH_3 in the lower pathway of Fig. 4.19 is shown as a possibility, since this mechanism is just the reverse of that proposed in Section 4.1 for the formation of ethylidyne. Further, the energetics shown for the ethylidyne formation mechanism in Fig. 4.10B make it obvious why ethylidyne H,D-exchange at 300 K on Pt(111) is much slower than H,D-exchange in molecular ethylene below 270 K. In both mechanisms the initiating step is hydrogenation, but the barrier for ethylene hydrogenation is only ~ 6 kcal/mol compared to ~ 30 kcal/mol for ethylidyne hydrogenation.

In summary, it has been shown that ethylidyne undergoes measurable H,D-exchange on Pt(111) and Rh(111) over 100 K below the ethylidyne decomposition temperatures on these surfaces. For saturation coverages

Proposed Mechanisms for Ethylidyne H,D-Exchange



XBL 8610-4164

Fig. 4.19 Proposed mechanisms for H,D-exchange in the ethylidyne methyl group. The energetics for most of the steps in these mechanisms on Pt(111) are shown schematically in Fig. 4.10B.

of ethynylidyne, the rate of exchange is slow at 310 K ($< 10^{-3}$ exchanges/metal atom/s) and insensitive to deuterium pressure from 10^{-7} torr up to 1 atm. Exchange is rapid and extensive for subsaturation coverages of ethynylidyne. It was shown by HREELS, that the H,D-exchange mechanism involves incorporation of deuterium atoms one at a time. Two mechanisms for this sequential H,D exchange were proposed which involve the partial hydrogenation of ethynylidyne to form ethynylidene (CHCH_2) as the rate-determining step.

4.3 Thermal Fragmentation of Propylene, Propadiene and Methylacetylene on Rh(111) in the Temperature Range of 80–800 K: Comparison to Pt(111)

4.3.1 Background. As mentioned in the introduction of this thesis, Pt and Rh, despite being neighbors in the periodic table, do significantly different hydrocarbon catalysis [63]. Consequently, it is of interest to compare the bonding and surface chemistry of hydrocarbons on isostructural Pt and Rh surfaces.

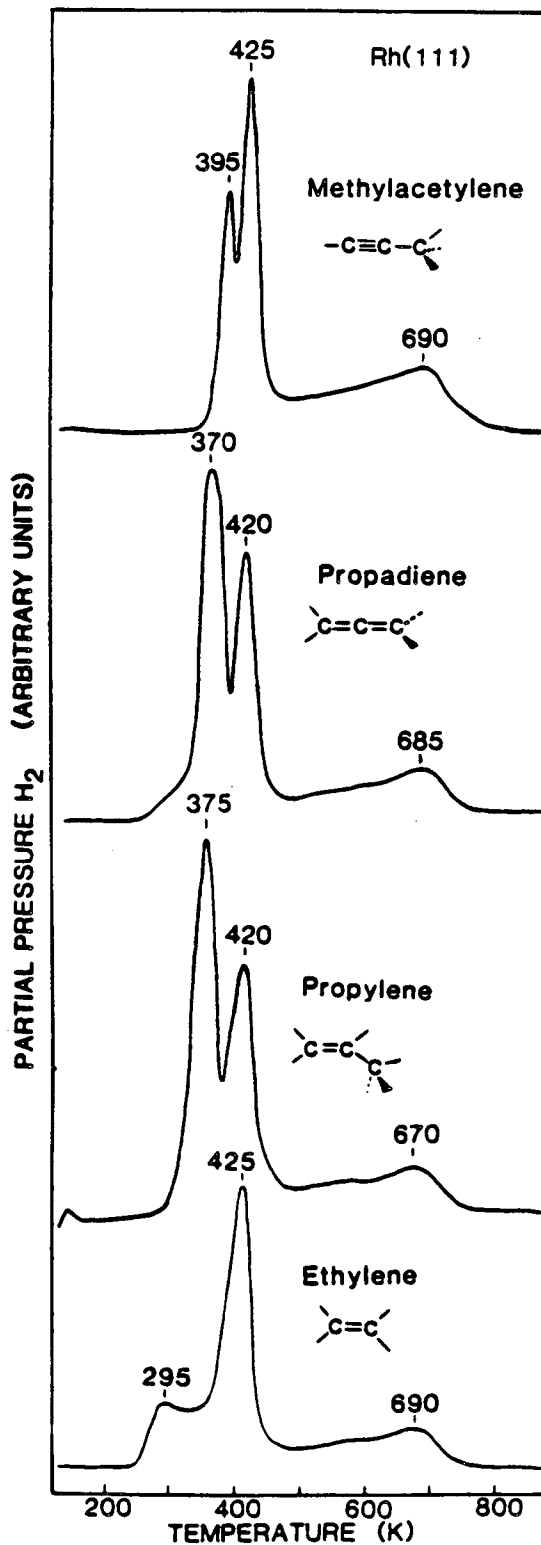
Only a few molecules have been extensively studied on both the Pt(111) and Rh(111) surfaces. For ethylene and benzene, the thermal chemistry on Rh(111) [64,65] is quite similar to Pt(111) [24,66] in that the same sequence of decomposition fragments are formed. This is consistent with the finding that Pt(111) and Rh(111) surfaces are equally good catalysts for the hydrogenation of ethylene to ethane [Chapter 5]. Despite this similar thermal chemistry, the molecular adsorption geometries of ethylene and benzene are somewhat different on these surfaces. Also, the decomposition temperatures for these two adsorbates are 50–100 K lower on Rh(111) than on Pt(111), consistent with Rh surfaces being the more active catalysts for hydrocarbon bond breaking reactions.

In this section, studies of the thermal fragmentation of propylene, propadiene, and methylacetylene on Rh(111) are reported and compared to similar studies on Pt(111). The major finding is that all three hydrocarbons undergo C–C bond breaking at 270 K on Rh(111) to form a mixture of ethynidyne and polymerized C_xH species. This chemistry,

unlike that for ethylene and benzene, is substantially different from Pt(111) where C-C bonds are not broken until above 450 K. Surface hydrogen atoms are implicated as an important factor in this low temperature C-C bond-breaking on Rh(111).

4.3.2 Results and Interpretation. Thermal Desorption Spectroscopy (TDS). Upon heating the rhodium crystal, H₂ gas is the primary desorption product from the (111) surface that has been covered with propylene, methylacetylene, or propadiene. Figure 4.20 shows the H₂ TD spectra for 10 Langmuir doses of methylacetylene, propadiene, and propylene adsorbed at 77 K on Rh(111). These are compared with the TD spectrum for ethylene adsorbed at 220 K. All the C₃ hydrocarbon desorption profiles have similar H₂ desorption peaks at ~ 380, ~420, and 500-800 K. Ethylene also has similar peaks above 400 K, but the lowest temperature peak is at ~ 300 K and is not as sharp.

There are several reasons for the similarities of the H₂ thermal desorption spectra for these four hydrocarbons. First, the work of Yates et al. [9] has shown that adsorbed hydrogen atoms desorb from a clean Rh(111) surface with TDS peak temperatures ranging from 390 K at low surface coverages down to 275 K at high surface coverages. Therefore, even though HREELS shows that ethylene, propylene, propadiene, and methylacetylene all decompose below room temperature, the adsorbed hydrogen atoms which result from this decomposition do not desorb until just above room temperature, resulting in the lowest temperature peak in the H₂ TD spectra shown in Fig. 4.20. It is not clear why surface hydrogen desorbs at lower temperature for the ethylene monolayer;



XBL 8512-4936

Fig. 4.20 H₂ thermal desorption spectra for ethylene, propylene, propadiene and methylacetylene decomposition on Rh(111). Propylene, propadiene and methylacetylene were adsorbed at 77 K, and ethylene was adsorbed at 220 K. The heating rates were 20 K/sec.

however, the first H_2 desorption peak shifts to 330–380 K like the C_3 hydrocarbons when ethylene is adsorbed at lower temperature [115].

Second, the similarity of the H_2 TDS peaks above 400 K suggests that these hydrocarbons have all decomposed by 400 K to similar hydrocarbon fragment(s). This is supported by HREELS results presented in Section 3.5, where it was noted that the long H_2 desorption tail from 500 to 800 K is characteristic of hydrocarbon decomposition to polymerized C_xH species Rh(111) [8,22].

Variation of the hydrocarbon coverage changed the appearance of the H_2 desorption spectra substantially. The coverage effects were studied for methylacetylene and propylene and are similar to those discussed for C_2H_4 adsorption on Rh(111) in Section 4.1. At low hydrocarbon coverages the H_2 TD peaks overlap and are poorly resolved. However, HREEL spectra show that the hydrocarbon fragments formed in the low coverage decompositions are the same as those for saturation coverages. The coverage effects in the TDS are probably mainly due to the shift of the surface hydrogen desorption peak to lower temperature with increasing surface hydrocarbon coverage.

In the case of propylene and methylacetylene, desorption of products other than H_2 was also checked. For methylacetylene, masses 2, 16, 27, 40 and 78 were monitored and, at all coverages, no masses other than mass 2 were detected. For propylene, masses 2, 16, 27, 28 and 42 were monitored; besides mass 2, only molecular propylene desorption (mass 42) was observed (at 200 K), and then only for coverages above

about 80% of saturation coverage. Analogous results have been found for ethylene on Rh(111) [Section 4.1].

Low-Energy Electron Diffraction (LEED). In Fig. 4.21 the LEED patterns observed for saturation coverages of the C_3 hydrocarbons are summarized and compared with those observed previously for C_2H_4 [Section 4.1] and C_2H_2 [8,28]. These LEED patterns turn out to be a convenient way to identify the different hydrocarbon monolayers produced in the C_3 hydrocarbon decomposition. As shown by the vertical solid or dashed lines in Fig. 4.21, the surface LEED pattern usually changes at the same temperature where the surface vibrational spectrum indicates a change in bonding on the surface. The LEED patterns in Fig. 4.21 are consistent with those reported previously [67-69], except that the $(2\sqrt{3} \times 2\sqrt{3})R30^\circ$ and $c(4 \times 2)$ LEED structures were produced here by coadsorption of CO as discussed in Sections 3.2 and 3.3. In Fig. 4.21, the coadsorption of CO is indicated by a "#".

Several observations about the LEED patterns summarized in Fig. 4.21, are noteworthy. First, propylene and propadiene do not form ordered monolayers at 77 K, but methylacetylene, like acetylene, orders into a $p(2 \times 2)$ overlayer. Second, propylene and propadiene do form $p(2 \times 2)$ patterns above 200 K, the temperature at which ethylene decomposes to form a $p(2 \times 2)$ ethylidyne (CCH_3) overlayer. These $p(2 \times 2)$ structures for all the C_3 hydrocarbons as well as for ethylidyne change to $c(4 \times 2)$ structures at ~ 270 K in the presence of coadsorbed CO.

LEED Patterns for C₂ and C₃ Hydrocarbons on Rh(111)

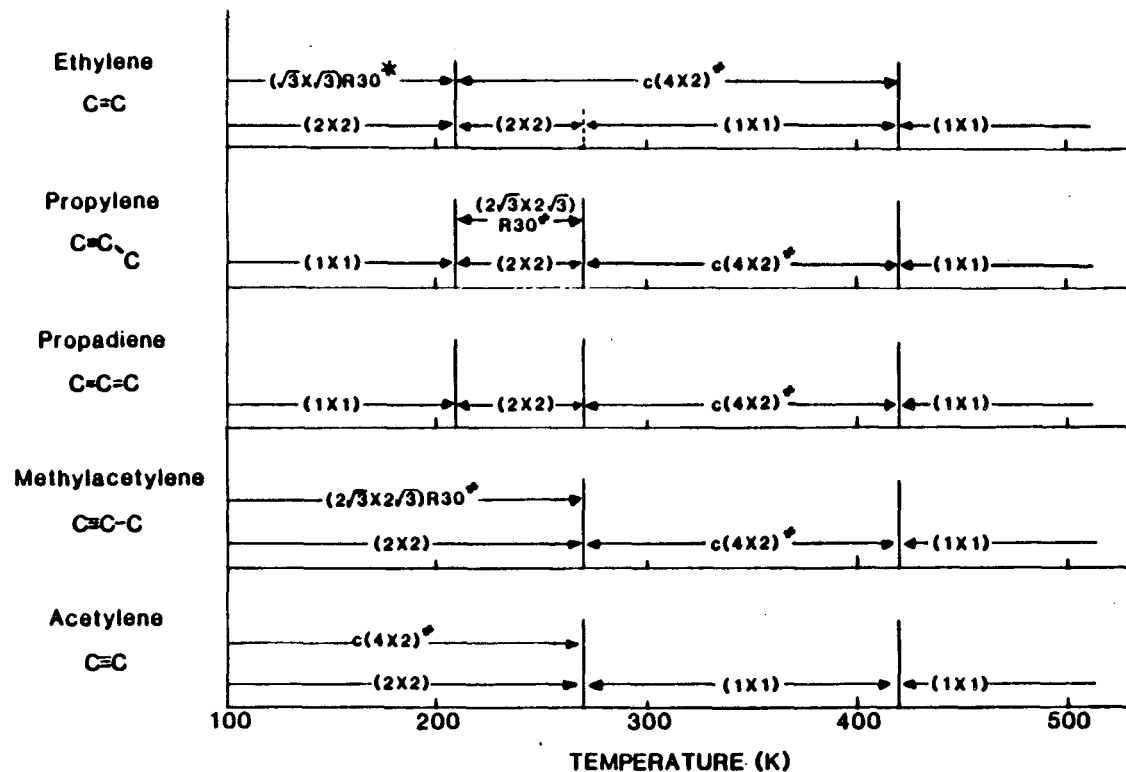


Fig. 4.21 LEED patterns observed for the adsorption and thermal decomposition of the C₂ and C₃ unsaturated hydrocarbons on Rh(111). Solid dividing lines indicate temperatures at which the HREEL spectrum changes. The dashed line indicates a change in LEED pattern as the surface hydrogen desorbs as H₂.

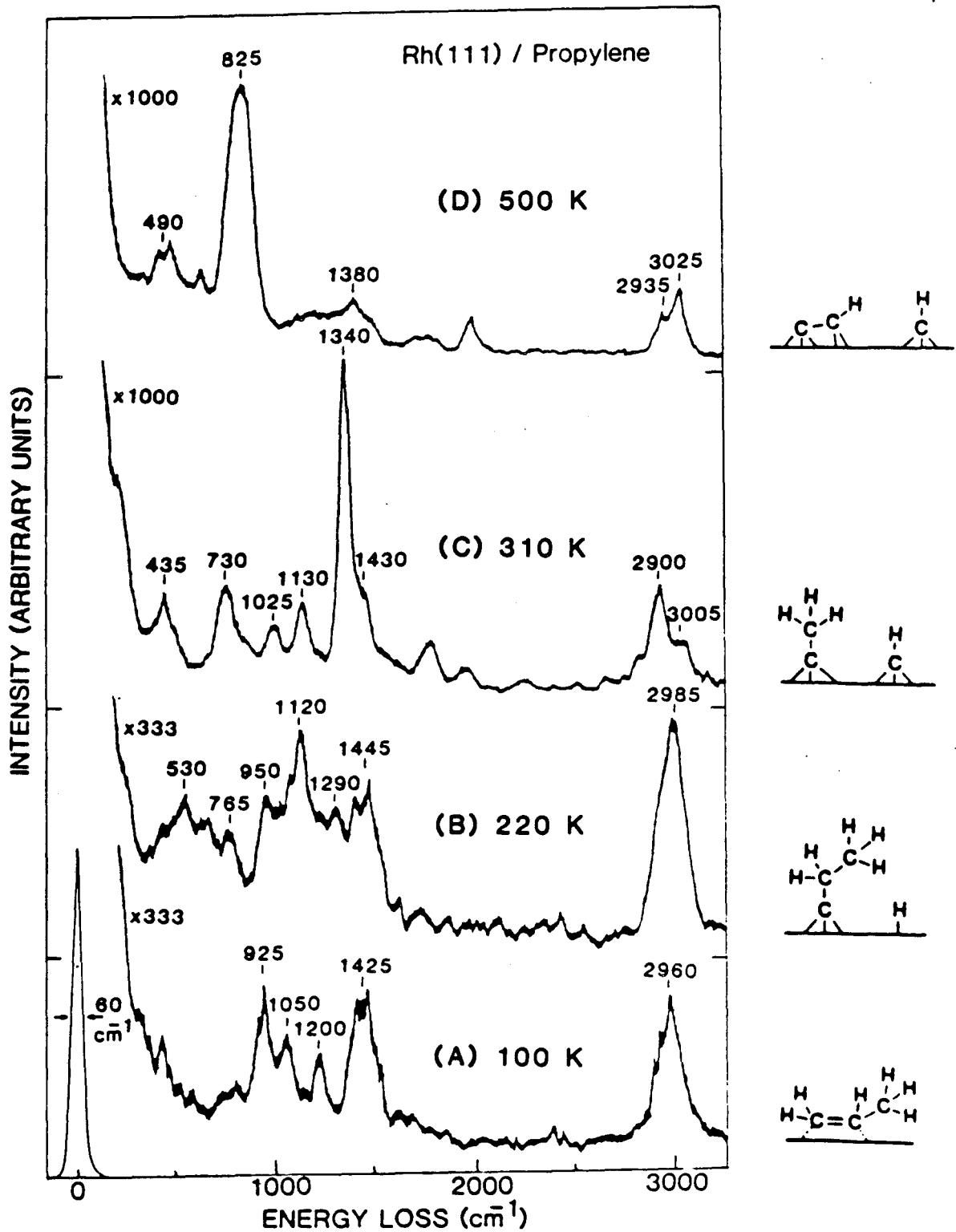
*) LEED pattern for $\theta(\text{C}_2\text{H}_4) = 1/3$. 25% of the C₂H₄ in this overlayer desorbs at 210 K to give $\theta(\text{C}_2\text{H}_4) = 1/4$.

#) LEED pattern formed by coadsorption of CO.

Above 420 K, all the C_3 hydrocarbons, like the C_2 hydrocarbons, form only (1x1) LEED patterns with some diffuse background intensity indicating that the hydrocarbon overlayer is disordered. This disordering temperature corresponds to the 420 K H_2 desorption peaks in the TD spectra of Fig. 4.20.

High-Resolution Electron Energy Loss Spectroscopy (HREELS). Surface vibrational spectra were taken by HREELS for all the ordered C_3 hydrocarbon monolayers listed in Fig. 4.21. The spectra were taken after momentarily warming a saturation coverage of the hydrocarbon to the temperature necessary to produce the hydrocarbon or hydrocarbon fragment monolayer. The temperature of the sample when the spectra were taken was either 77 K or room temperature.

a) Propylene Below 200 K. Figure 4.22 shows the vibrational spectra of a Rh(111) surface saturated with propylene at 77 K and after warming to the indicated temperatures. Also shown are the surface fragments responsible for these vibrational spectra. The vibrational spectrum below 200 K has many poorly resolved and overlapping peaks, making assignment of this spectrum difficult. Upon deuteration, the overlap of the bending modes between 900 and 1400 cm^{-1} becomes even more severe and does not aid in the assignment. Also, most of the vibrational normal modes of molecularly adsorbed propylene are dipole active because of the low symmetry of propylene and, consequently, can be observed in the specular direction.



XBL 862-578

Fig. 4.22 Surface vibrational spectra by HREELS in the specular direction of a saturation coverage of propylene adsorbed on Rh(111) at 100 K and warmed momentarily to the indicated temperatures.

Since chemisorbed ethylene on Rh(111) does not decompose until 200 K, and molecular propylene desorption is detected during TDS, it is reasonable to assume that propylene is molecularly adsorbed at 100 K. An approximate assignment of the 100 K propylene spectrum can be made by comparison to the frequencies of gas phase propylene [70] as follows: $2960 = \nu(\text{CH}_3) + \nu(\text{CH}_2) + \nu(\text{CH})$; $1425 = \delta_s(\text{CH}_3) + \text{CH}_2$ scissor; $1200 = \text{CH}_2$ wag or CH deformation; $1050 = \text{CH}_3$ rock; $925 = \nu(\text{CC}) + \text{CH}_2$ twist, rock.

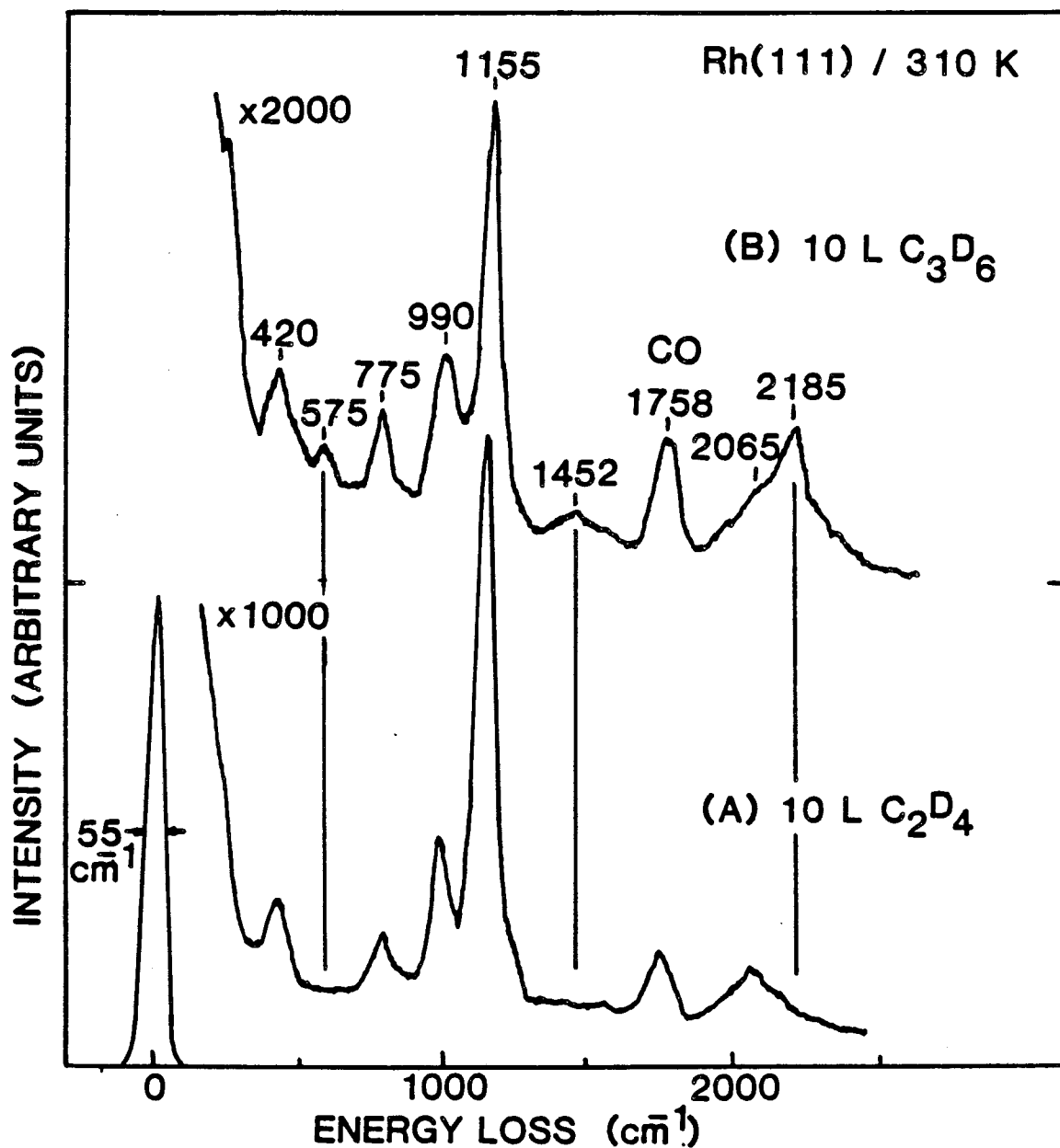
b) Propylene at 220 K. As was discussed in Section 3.3, chemisorbed propylene forms a (2x2) LEED structure on Rh(111) between 200 and 270 K. It was also shown there that the HREEL spectrum in Fig. 4.22B is consistent with propylidyne species. This assignment is supported by LEED [67] and SIMS [71] data. Unfortunately the TDS data here cannot be used to confirm the C_2H_5 stoichiometry as on Pt(111) [35], since propylidyne decomposes at 270 K which is below the temperature at which surface hydrogen desorbs.

c) Propylene at 300 K. Figure 4.22C shows the much simpler HREEL spectrum that results from annealing to 300 K. Several aspects of this vibrational spectrum suggest that C-C bonds have broken and that propylidyne has decomposed to ethylidyne plus C_xH fragments. First, the peak frequencies and relative intensities in the 300 K vibrational spectrum are quite similar to ethylidyne on Rh(111) [Fig. 3.3]. The only differences are extra peaks at 730 and 3005 cm^{-1} . This suggests that two species are produced from propylidyne by C-C bond breaking: ethylidyne and another hydrocarbon fragment.

Figures 4.23A and 4.23B compare the vibrational spectra of C_2D_4 and C_3D_6 adsorbed on Rh(111) at 300 K. The C_3D_6 -derived spectrum has all the peaks in the the C_2D_4 spectrum along with extra peaks 575, 1455, and 2185 cm^{-1} . The 575 and 2185 cm^{-1} peaks are due to C-D vibrations, since they correspond to the 730 and 3005 cm^{-1} peaks in the undeuterated spectrum shifted in frequency by factors of 1.27 and 1.37 respectively. The 1452 cm^{-1} peak is probably a C-C stretching mode, unshifted upon deuteration, and obscured by the C-H bends in Fig. 4.22C. The presence of this C-C bond, in addition to that in ethylidyne ($\nu_{CC} = 1155 \text{ cm}^{-1}$), indicates that the 1-carbon species produced when propylidyne converts to ethylidyne must polymerize.

These polymerized hydrocarbon fragments for decomposed propylene have the same spectral features as the high-temperature hydrocarbon spectra attributed to C_xH species and discussed in Section 3.5. The vibrational frequencies were assigned there by comparison to organometallic clusters as $\delta(CH) \approx 800$, $\nu(CH) \approx 3000$, and $\nu(CC) \approx 1400 \text{ cm}^{-1}$. Consistent with this polymerization interpretation, it was observed that the relative intensity and position of the 730 cm^{-1} (575 cm^{-1}) modes varies some, depending on whether the monolayer is formed by annealing from 77 to 300 K or by dosing propylene at 300 K.

The possibility that C-C bonds have not broken during propylene adsorption on Rh(111) at 300 K can be ruled out for two reasons. First, the C-C stretching frequencies at 1130 cm^{-1} in Fig. 4.22 and at 1155 cm^{-1} in Figure 4.23 are the same as for CCH_3 and CCD_3 ;



XBL 866-2415

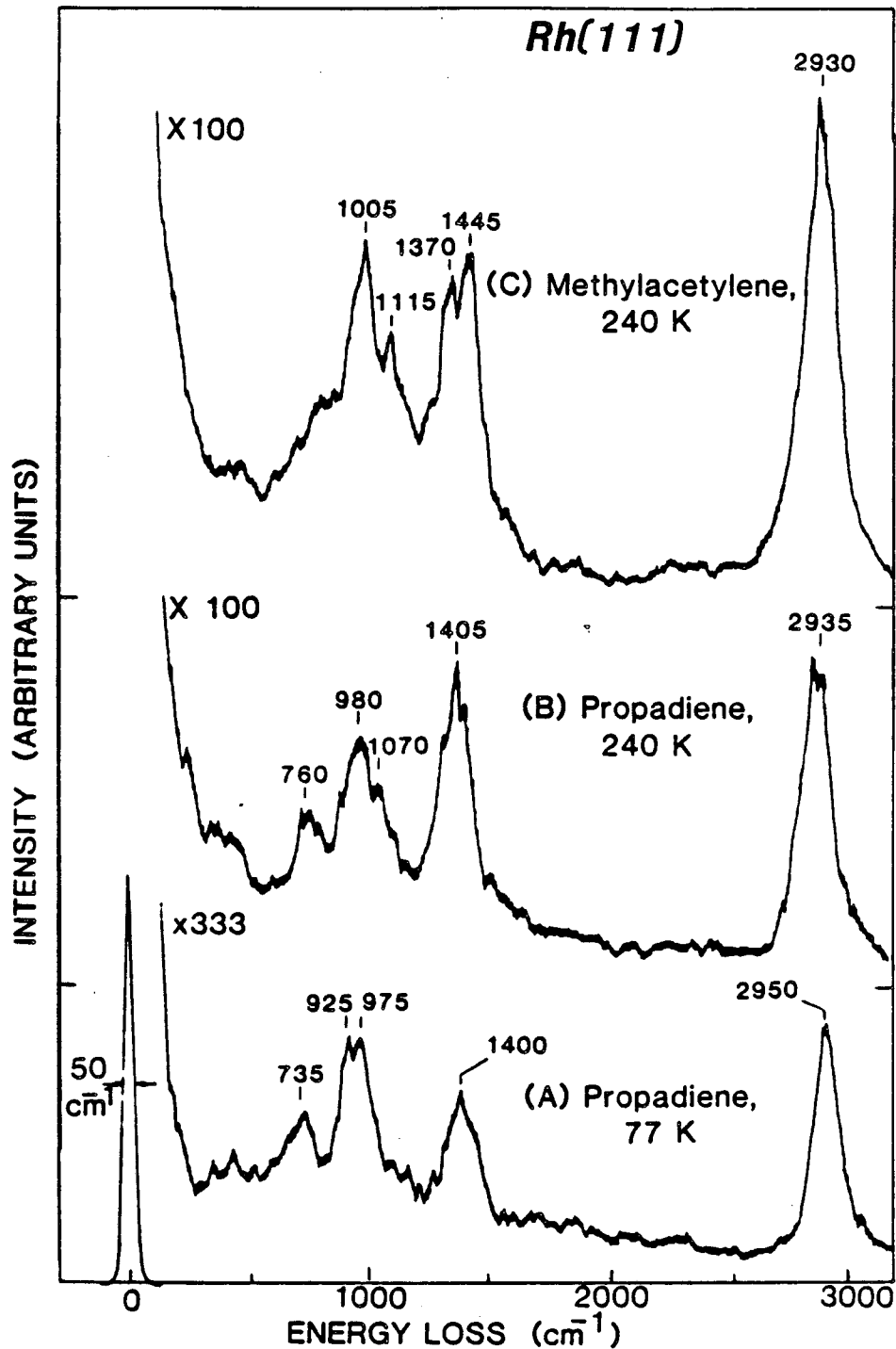
Fig. 4.23 Comparison of the specular HREEL spectra for room temperature decomposition of ethylene- d_4 and propylene- d_6 on Rh(111). The vertical lines indicate the spectral differences. The C_2D_4 fragment is ethylidyne (CCD_3) and the C_3D_6 fragments are CCD_3 and C_xD species.

it is highly unlikely that a 3-carbon species would have the same C-C stretching frequency.

Second, the intense 1340 cm^{-1} peak and weak shoulder at 1430 cm^{-1} are characteristic of δ_s and $\delta_{as}\text{CH}_3$ vibrations excited by dipole scattering for a methyl group with its symmetry axis close to the surface normal. Such a geometry would be highly unlikely for a C_3 hydrocarbon chain with nearly tetrahedral bond angles. Therefore, it is concluded that propylidyne decomposes at room temperature on Rh(111) by both C-H and C-C bond breaking to form ethylidyne and C_xH species.

d) Propylene Above 450 K. By annealing to 450 K, all vibrational features due to ethylidyne disappear. The subtle and gradual changes that occur in the HREEL spectra from 450 to 800 K are characteristic of hydrocarbons on Rh(111). Spectral features like those in 4.22D were discussed in Section 3.5 and attributed to partially hydrogenated polymeric carbon on the surface.

e) Methylacetylene and Propadiene. Assuming that propadiene and methylacetylene are molecularly adsorbed at 77 K, it was found by taking HREEL spectra as a function of temperature that propadiene, like propylene and ethylene, begins to decompose on Rh(111) at $\sim 200\text{ K}$, while methylacetylene, like acetylene, does not decompose until 270 K. Figures 4.24A and 4.24C show the vibrational spectra of propadiene at 100 K and methylacetylene at 240 K respectively. The methylacetylene monolayer is ordered in a $p(2 \times 2)$ LEED pattern while the propadiene monolayer is disordered. Figure 4.24B shows the HREEL spectrum of a propadiene monolayer annealed at 240 K to form a $p(2 \times 2)$ LEED structure.



XBL 866-2426

Fig. 4.24 Specular HREEL spectra for 10 L exposures of (A) propadiene at 77 K, (B) propadiene at 240 K, and (C) methylacetylene at 240 K on Rh(111). Propadiene begins to decompose at 210 K while methylacetylene does not decompose until 270 K on Rh(111).

The HREEL spectra for molecularly adsorbed propadiene and methylacetylene shown in Figs. 4.24A and 4.24C are interpreted by comparison to the gas phase infrared spectra for these molecules. These frequencies are given in Tables 4.3 and 4.4. Also included in Table 4.3 are the vibrational frequencies for 1,2,2,3-tetrachloropropane [72], which was chosen to mimic di- σ bonding of molecular propadiene to the surface. The vibrational frequencies for adsorbed propadiene and methylacetylene are substantially different from their gas phase values, indicating distortion of the chemisorbed molecules from their gas phase geometries. In particular, the CH stretching modes for both propadiene and methylacetylene shift to lower frequency upon adsorption. This is characteristic of rehybridization of the unsaturated C-C bonds from sp or sp^2 towards sp^3 and is consistent with the CH stretching frequencies given in Table 4.3 for 1,2,3-tetrachloropropane. The C-C stretching modes either shift down in frequency upon adsorption or are unobserved. Both situations are consistent with bonding geometries in which the unsaturated C-C bonds lie approximately parallel to the surface. Note, however, that if both C-C double bonds in propadiene lie parallel to the surface, then one of the hydrogens will point directly at the metal, if the gas phase orientation of the hydrogens with respect to the double bonds is maintained.

Warming propadiene monolayers above 200 K produces a $p(2 \times 2)$ LEED pattern and the HREEL spectrum in Fig. 4.24B. This transformation temperature is too high to be the result of desorption of multilayer propadiene, so the spectral differences between Fig. 4.24A and 4.24B

Table 4.3: Comparison of the vibrational frequencies for gas phase propadiene with those for propadiene adsorbed on Rh(111) and those for gaseous 1,2,2,3-tetrachloropropane

Mode ^a	Symmetry ^b	Vibrational Frequencies (cm ⁻¹)		
		CH ₂ CCH ₂ (g) ^c	CH ₂ CCH ₂ /Rh(111) ^d T = 77 K	CH ₂ ClCCl ₂ CH ₂ Cl(g) ^e
v _{as} (CH ₃)	e	3086		3020
v _s (CH ₂)	a ₁	3015	2950	2986
v _s (CH ₂)	b ₂	3007		
v(CC)	b ₂	1957		1076
v(CC)	a ₁	1073		998
			~ 1400	
CH ₂ scis	a ₁	1443		1423
CH ₂ scis	b ₂	1398		
CH ₂ rock	e	999	975	938
				884
CH ₂ twist	b ₁	865	925	1209
				1123
CH ₂ wag	e	841	735	938
				884
δ(CCC)	e	355		

- a) Approximate normal mode description for propadiene
 b) For gas phase propadiene
 c) Shimanouchi, ref. 55
 d) This work, Fig. 4.24A
 e) Dempster, Price and Sheppard, ref. 72

Table 4.4: Comparison of the vibrational frequencies for gas phase methylacetylene with those for molecularly adsorbed methylacetylene on Rh(111)

Mode ^a	Vibrational Frequencies (cm ⁻¹)		
	Symmetry ^b	HCCCHH ₃ (g) ^c	HCCCH ₃ /Rh(111) ^e T < 250 K
v(CH)	a ₁	3334	
v _{as} (CH ₃)	e	3008	2930
v _s (CH ₃)	a ₁	2918	
v(CC)	a ₁	2142	1115
v(CC)	a ₁	931	
δ _{as} (CH ₃)	e	1452	1445
δ _s (CH ₃)	a ₁	1381	1370
ρ(CH ₃)	e	10563	1005
δ(CH)	e	633	
δ(CCC)	e	328	

a) Approximate normal mode description for gas phase methylacetylene

b) For gas phase methylacetylene

c) Shimanouchi, ref. 55

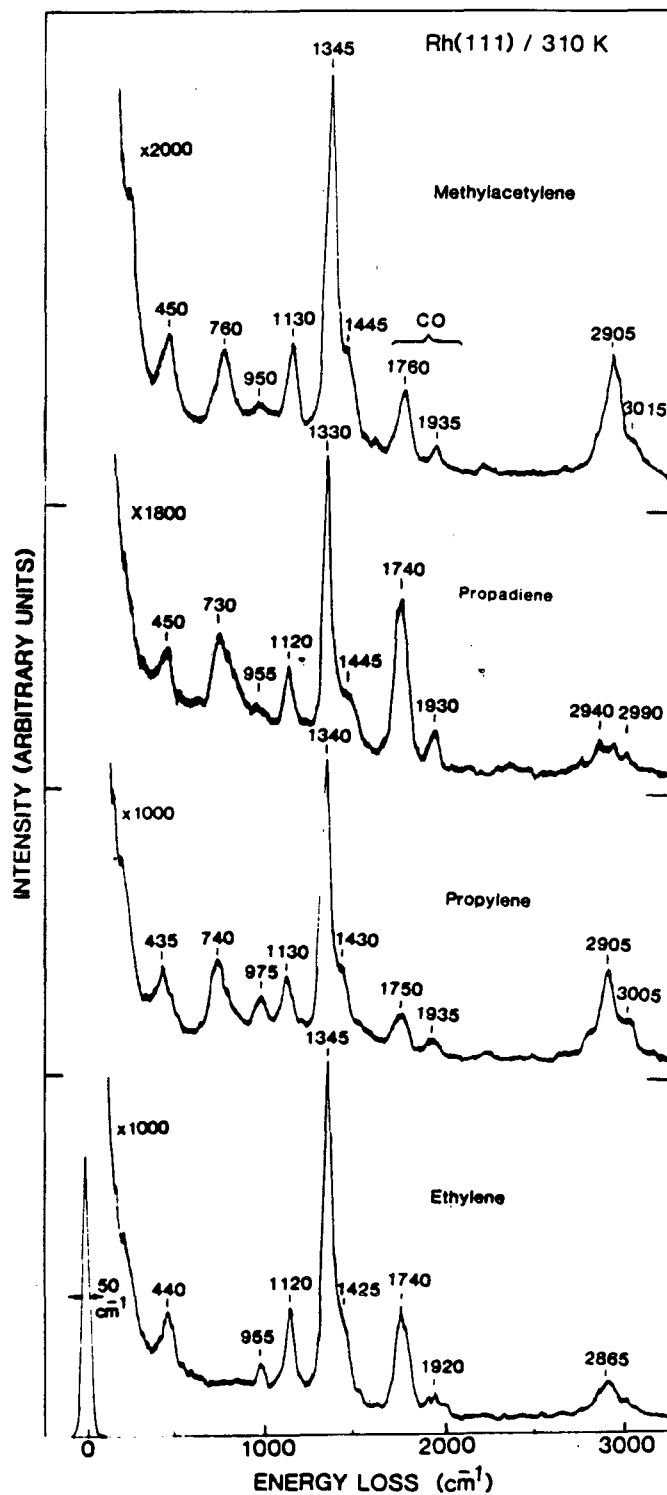
d) This work, Fig. 4.24C

are attributed to propadiene decomposition at 200 K. The main differences between the 77 and 240 K spectra are the broader peaks and the increased intensity of the modes at $\sim 1400 \text{ cm}^{-1}$ in the 240 K spectrum. This spectrum for decomposed propadiene (Fig. 4.24B) begins to resemble that for molecularly adsorbed methylacetylene in Fig. 4.24C. However, other species with methyl groups [$\delta_s(\text{CH}_3) \approx 1350 \text{ cm}^{-1}$, $\delta_{as}(\text{CH}_3) \approx 1450 \text{ cm}^{-1}$] like CCCH_3 or CCHCH_3 could also explain the enhanced intensity in the 1400 cm^{-1} region.

Above 270 K, the hydrocarbon monolayers formed by methylacetylene and propadiene adsorption are virtually identical to that formed by propylene adsorption. Figure 4.25 shows the vibrational spectra at 310 K for these hydrocarbon monolayers as well the one for an ethylidyne monolayer formed from ethylene adsorption. As noted in the previous interpretation of the propylene decomposition spectra, these spectra at 310 K are characteristic of ethylidyne and C_xH species.

f) Partially Deuterated Propylene and Methylacetylene. In order to gain more insight into which bonds break during the decomposition of propylene and methylacetylene, studies of partially deuterated propylene (CH_2CHCD_3) and methylacetylene (DCCCH_3) by TDS and HREELS were performed. The thermal desorption results are presented first.

The integrated areas for the entire TD spectrum and for the individual peaks for amu 2, 3, and 4 are given in Table 4.5. The absolute areas are normalized to the mass spectrometer sensitivity for H_2 using the sensitivity factors $S_{\text{H}_2}/S_{\text{D}_2} = 2.0$ and $S_{\text{H}_2}/S_{\text{HD}} = 1.5$. The $S_{\text{H}_2}/S_{\text{D}_2}$ factor was determined experimentally using H_2 and D_2 while the $S_{\text{H}_2}/S_{\text{HD}}$



LBL 361-75

Fig. 4.25 Comparison of the specular HREEL spectra for ethylene, propylene, propadiene, and methylacetylene adsorbed on Rh(111) at 310 K. The deuterated analogue of the propylene spectrum is shown in Fig. 4.23B. At 310 K, all the C_3 hydrocarbons have decomposed to the same fragments (CCH_3 and C_xH) on Rh(111).

Table 4.5: H₂, HD, and D₂ Desorption Peak Areas for C₃H₃D₃ and C₃H₃D Thermal Decomposition on Rh(111)

Dose	Area(s) Integrated ^θ	Absolute amounts (arb. units) ^Δ			Percentages			H:D Ratio*
		H ₂	HD	D ₂	H ₂	HD	D ₂	
6.0 L C ₃ H ₃ D ₃ propylene-3,3,3-d ₃	all peaks	5.6	8.4	7.5	26	39	35	H:D=1:1
	peak 1	3.8	3.3	1.2	45	40	15	H:D=2:1
	peak 2	1.3	3.0	3.2	18	40	42	H:D=1:2
	peak 3	0.4	2.1	3.1	8	37	55	H:D=1:3
6.0 L C ₃ H ₃ D methylacetylene-1-d ₁	all peaks	14.1	8.6	1.8	58	35	7	H:D=3:1
	peak 1	4.0	1.4	0.1	73	24	3	H:D=6:1
	peak 2	5.5	3.1	0.5	61	34	5	H:D=3:1
	peak 3	4.5	4.1	1.2	46	42	12	H:D=2:1

^θ Integrated areas of overlapping peaks were calculated by dropping a perpendicular from the minimum between the overlapping peaks to the baseline. Peak 1 = - 270-390K; Peak 2 = - 390-440K; Peak 3 = - 440-800K.

^Δ Amounts of HD and D₂ have been converted to the same units as H₂ using the sensitivity factors $S_{H_2}/S_{D_2} = 2.0$ and $S_{H_2}/S_{HD} = 1.5$ (see text). Arbitrary units are different for C₃H₃D₃ and C₃H₃D.

* The ratio of H to D atoms on the surface that would produce the indicated percentages of H₂, HD, and D₂.

factor was calculated by using the S_{H_2}/S_{D_2} factor and comparing the total desorption yields of H_2 , HD, and D_2 from saturation doses of CH_3CHCH_2 and CD_3CHCH_2 .

The H:D atom ratios for the individual peaks and for the complete TDS spectrum are given in the last column of Table 4.5. When all peaks are summed, the relative amounts of H and D correctly match the relative amounts in the parent hydrocarbons: 1:1 in $C_3H_3D_3$ and 3:1 in C_3H_3D . However, the individual peaks show quite different distributions, indicating that H,D-exchange does not completely scramble the H's and D's in the adsorbed hydrocarbon fragments. With complete scrambling, each peak in the TDS would have the same isotopic composition as the parent molecule.

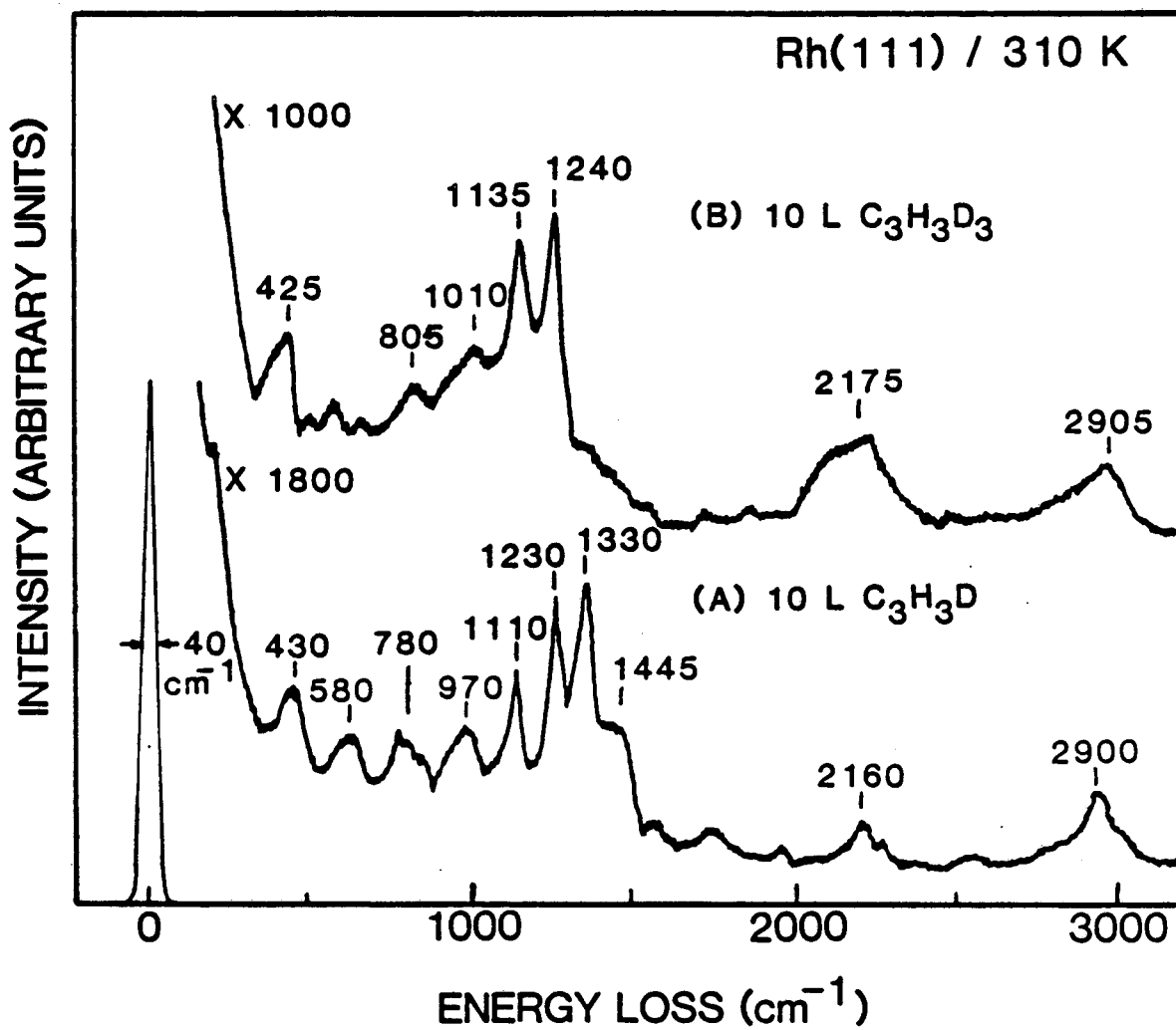
For $C_3H_3D_3$, the first peak has more hydrogen and the second and third peaks more deuterium than expected for random scrambling. Since the second and third TDS peaks result from decomposition of hydrocarbon fragments, their H:D ratios indicate the H:D stoichiometry in these fragments: $\sim 1:2$ and $\sim 1:3$ respectively [75]. For C_3H_3D , the isotopic composition of the first TDS peak corresponds to an H:D ratio on the surface of 6:1. This clearly implies that C-H bond breaking below room temperature occurs predominate in the methyl group. The hydrocarbon fragments that dehydrogenate to produce peak 2 have a stoichiometry H:D $\approx 3:1$, and the fragments responsible for peak 3 have an H:D stoichiometry of about 2:1.

It is interesting that for each of the H:D ratios given in the 1st column of Table 4.5, the relative amounts of H_2 , HD, and D_2 desorbing

are equal to the expected amounts for random recombinations of H and D atoms in a mixture of the indicated H:D composition. For example, a 3:1 mixture of 150 H atoms and 50 D atoms randomly assembled in pairs would produce H_2 , HD and D_2 in the relative amounts of 56:38:6. This distribution is nearly what is observed for each 3:1 ratio in Table 4.5 and implies that the H and D atoms equilibrate on the surface before desorbing.

As a result of H,D-exchange below 270 K and the inherently large number of vibrational frequencies for these polyatomics, the vibrational spectra below 270 K are too complex to assign and to determine whether the alkane, alkene, or alkyne C-H bonds break first. However, the simpler room temperature vibrational spectra of these decomposed molecules can be assigned. These spectra are due to partially deuterated ethylidyne and $C_xH(D)$ species and give further insight into which C-C bonds break first.

Figure 4.26 shows the vibrational spectra for saturation coverages of H_2CCHCD_3 and $DCCCH_3$ adsorbed on Rh(111) at 310 K. These spectra are assigned by comparison with the partially deuterated ethylidyne frequencies in Table 4.1 (Section 4.2) and the C_xH and C_xD frequencies in Section 3.5. For the methylacetylene decomposition (Fig. 4.26A), the peaks at 1330 ($\delta_s CH_3$) and 1110 (ν_{CC}) are characteristic of a CCH_3 species, while those at 1230 (CH_2 wag), and 1395 (CH_2 scissor) suggest a CCH_2D species. The 580 cm^{-1} peak (δ_{CD}) characterizes a C_xD fragment. There may be a δ_{CH} peak of a C_xH fragment in the $735\text{--}815\text{ cm}^{-1}$ feature, but this region also contains vibrations of the CCH_2D species. The



XBL 866-2414

Fig. 4.26 HREEL spectra for 10 L of DCCCH_3 and 10 L of CH_2CHCD_3 decomposed on Rh(111) at 310 K. The spectra are due to partially deuterated ethylidyne, C_xH and C_xD species.

predominant ethylidyne species are therefore CCH_3 and CCH_2D and the other predominant fragment is C_xD . This interpretation of the vibrational spectra is consistent with the TDS H:D stoichiometry of 3:1 in the 420 K ethylidyne decomposition peak (Table 4.3). The presence of CCH_3 species implies that the gas phase carbon-carbon triple bond is the C-C bond that breaks first on the surface.

In the room temperature HREEL spectrum of decomposed propylene-3,3,3- d_3 shown in Fig. 4.26B, the absence of the intense 1330 cm^{-1} ($\delta_s\text{CH}_3$) indicates that no detectable CCH_3 is formed. The presence of the 1240 cm^{-1} (δCH) peak and absence of a CH_2 scissor at $\sim 1400\text{ cm}^{-1}$ means that the majority species here is CCD_2H , consistent with the 1:2 = H:D TDS ratio for the 420 K decomposition peak (Table 4.3). There may also be a small amount of CCD_3 ($\delta_s\text{CD}_3 = 990\text{ cm}^{-1}$). This spectrum with an expanded intensity scale shows that the 805 cm^{-1} (δCH) peak predominates over the 595 cm^{-1} (δCD) peak, so the other fragment is mainly C_xH . The lack of CCH_3 and CCH_2D species suggest that it is the C-C bond closest to the surface that breaks when propylidyne decomposes. This assumes that the propylidyne still has most of the deuterium in its methyl group.

4.3.3 Discussion. In the previous section, the results for propylene, methylacetylene, and propadiene bonding and thermal decomposition on a Rh(111) single crystal surface were presented and discussed. The surface species that were identified as a function of temperature are summarized in Fig. 4.27 and compared to previous results for ethylene. Nearly 100% of the C_3 hydrocarbons molecularly adsorbed at 77 K on

Hydrocarbon Decomposition on Rh(111)

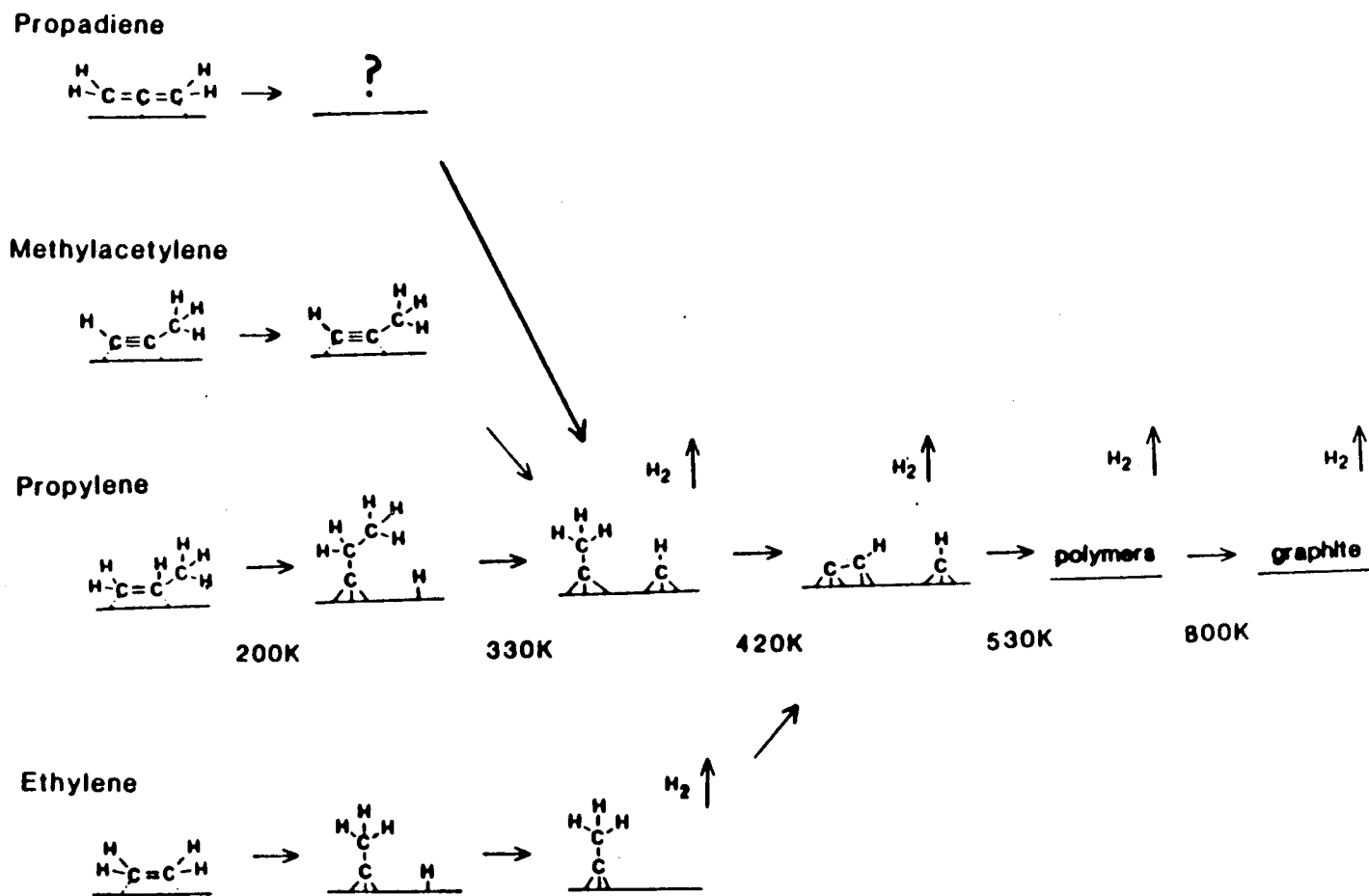


Fig. 4.27 Pathways for the thermal decomposition of ethylene, propylene, methylacetylene, and propadiene on Rh(111). These decomposition intermediates, determined by surface vibrational spectroscopy and thermal desorption studies, are stable in the indicated temperature ranges.

Rh(111) dehydrogenate. The only competing thermal chemistry is a small percentage of molecular desorption at high coverages. In this section, these results for Rh(111) are compared to those published for Pt(111), and the role of surface hydrogen atoms in the decomposition pathways is discussed.

Comparison of Propylene Decomposition on Pt(111) and Rh(111).

Propylene adsorbs molecularly on both Pt(111) and Rh(111) below 200 K. The vibrational spectra are, however, actually quite different and indicate different degrees of rehybridization and possibly different bonding sites. Judging from the frequency of the CH stretching modes [2925 cm^{-1} on Pt(111) [76] and 2960 cm^{-1} on Rh(111)], the gas phase propylene C-C double bond is more rehybridized towards sp^3 on Pt(111). Analogous differences in the bonding of ethylene to Rh(111) and Pt(111) at low temperature were noted in Section 3.4. Also, analogous to ethylene chemistry, more propylene desorbs molecularly from Pt(111) than from Rh(111).

On both Pt(111) and Rh(111), propylene decomposes to propylidyne. The temperatures at which CCH_2CH_3 forms [200 K on Rh(111) and 270 K on Pt(111)] are the same as the temperatures for C_2H_4 decomposition to CCH_3 on these surfaces. The HREEL spectra for CCH_2CH_3 on Pt(111) and Rh(111) are very similar, indicating similar bonding at 3-fold hollow sites. By contrast, molecular orbital calculations for propylene adsorption and decomposition on Pt(111) [31] have suggested that the first stable decomposition fragment would be a surface allyl (CH_2CHCH_2). Prob-

ably, this specie does not form because, as discussed for ethylene in Section 4.1, surface hydrogen influences the decomposition kinetics.

The propylidyne decomposition products on Rh(111) and Pt(111) are entirely different. This is the first major difference reported in the UHV chemistry of hydrocarbons on well-defined Pt and Rh surfaces. On Rh(111), propylidyne decomposes at 270 K by C-C bond breaking to give ethylidyne and C_xH species. On Pt(111), propylidyne does not decompose until above 400 K, and it produces an as yet unassigned HREEL spectrum [76]; however, no peaks in this spectrum can be attributed to ethylidyne.

Interestingly, above 500 K the propylene decomposition products on Pt(111) and Rh(111) are again the same. On both surfaces a mixture of CH and C_2H species forms at this temperature, and these species polymerize on both surfaces to graphitic carbon.

Methylacetylene decomposition also shows similar differences on Pt and Rh(111): methylacetylene bonds molecularly to both surfaces below 270 K, decomposes to very different fragments at room temperature, but forms C_xH fragments on both surfaces above 500 K [77].

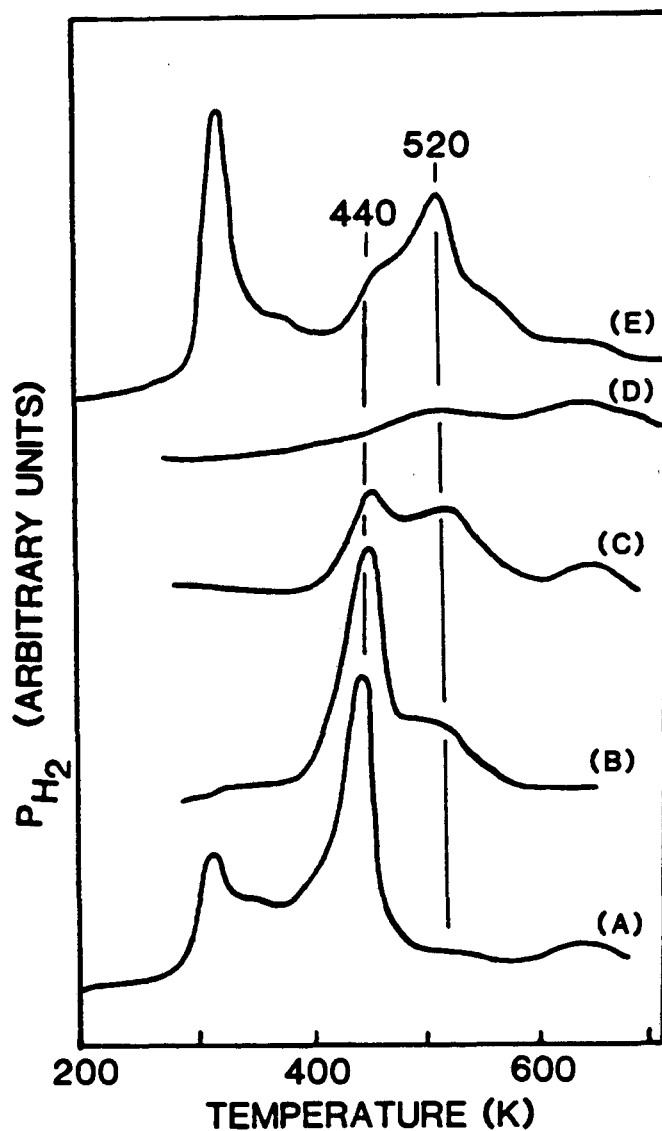
Role of Surface Hydrogen in Propylidyne Decomposition.

An important question is "Why does propylidyne decompose by different pathways on Pt(111) and Rh(111)?" In comparing the two decompositions, the most obvious difference at the decomposition temperature is the presence of surface hydrogen on Rh(111) and its absence on Pt(111). Possibly surface hydrogen is required in order for propylidyne to decompose to ethylidyne.

To test the effect of surface hydrogen on propylidyne decomposition, propylidyne was decomposed on Pt(111) in the presence of 5×10^{-4} torr H_2 [78]. The experiments were carried out in a chamber without HREEL spectroscopy, so the results were monitored by TDS and are shown in Fig. 4.28. Figures 4.28A and E show the TD spectra of saturation coverages of propylene and ethylene. The 440 K peak in the propylene spectrum is due to propylidyne decomposition, and the 520 K peak in the ethylene spectrum is due to ethylidyne decomposition. Heating propylene to 470 K in the presence of H_2 would enable ethylidyne to form, since it is still stable at this temperature. As shown in Figs. 4.28B and C, heating a propylidyne monolayer to 470 K or 480 K in 5×10^{-4} torr H_2 decreases the size of the propylidyne decomposition peak, and a new peak begins to form at the ethylidyne decomposition temperature. Both of these peaks are absent when a propylene monolayer is heated to 470 K in UHV as shown in Fig. 4.28D. This series of experiments supports the proposal that the decomposition of propylidyne to ethylidyne requires surface hydrogen.

The role of surface hydrogen in converting propylidyne to ethylidyne may be analogous to H,D-exchange in ethylidyne on Pt(111) and Rh(111) [Section 4.2]. H,D-exchange in ethylidyne on Rh(111), like the conversion of propylidyne to ethylidyne, is facile at room temperature, while on Pt(111) this exchange, like propylidyne decomposition, is immeasurably slow until temperatures above the hydrogen desorption temperature.

Pt(111)



XBL 866-2413

Fig. 4.28 H₂ thermal desorption spectra from Pt(111) for (A) propylene adsorbed at 200 K, (B) propylene adsorbed at 200 K and flashed to 470 K in 5×10^{-4} torr H₂, (C) propylene adsorbed at 200 K and flashed to 480 K in 5×10^{-4} torr H₂, (D) propylene adsorbed at 200 K and flashed to 470 K in UHV and (E) ethylene adsorbed at 200 K. Vertical lines indicate the decomposition temperatures of propylidyne (440 K) and ethylidyne (520 K). These spectra suggest that propylidyne may decompose to ethylidyne on Pt(111) when surface hydrogen is present.

Finally, a similarity between the reaction of methylacetylene with Rh(111) and with a cobalt complex in solution [79] is noted. The analogous reactions are shown in Fig. 4.29. Both in solution and on the surface the C-C triple bond in the alkyne is broken and two alkylidyne fragments are formed. In solution the two resulting alkylidynes bridge opposite faces of the trinuclear cobalt cluster, and on the surface the alkylidynes bond in two 3-fold hollow sites. Such an analogy between organometallic and surface chemistry is intriguing, since many similarities in the bonding of organic fragments in metal clusters and on metal surfaces have been previously noted.

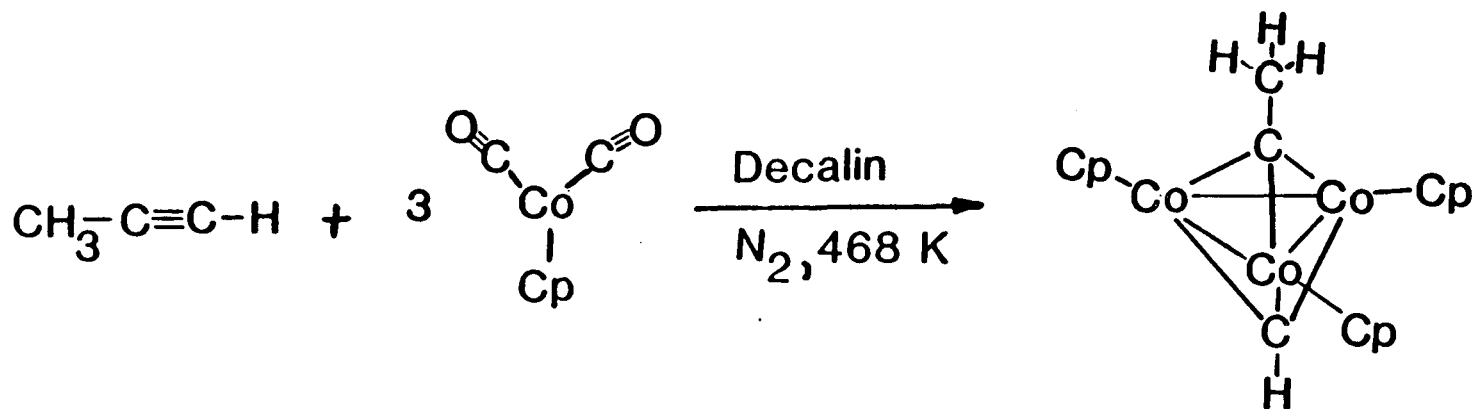
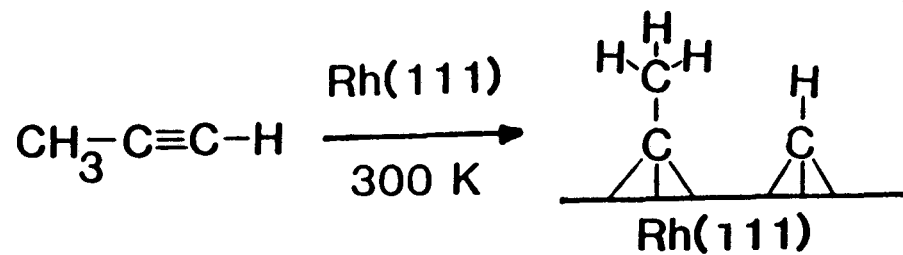


Fig. 4.29 The formal similarity between the reaction of methylacetylene with a Rh(111) single crystal surface in UHV and with a cobalt complex in solution. In both cases two alkylidyne species are produced, and each alkylidyne bonds to three metal atoms.

XBL 866-2412

4.4 Bonding and Reactivity of Unsaturated Hydrocarbons on Transition Metal Surfaces

4.4.1 Background. The previous sections in this thesis have detailed specific examples of the surface chemistry of unsaturated hydrocarbons. In this section the general trends in these case studies are discussed. These trends are then compared to well-established structures and reactions in organometallic chemistry in order to propose some principles for the bonding and reactivity of unsaturated hydrocarbons on transition metal surfaces. First, however, a brief look at the current status of surface chemistry is warranted.

Surface chemistry of the 1980's resembles in many ways organic and inorganic chemistry in the early 1900's and organometallic chemistry in the 1950's. In all these eras pure substances (organic molecules, inorganic and organometallic complexes, and now adsorbates on well-defined surfaces) were (are) being isolated and characterized with unprecedented rapidity, but with few principles to relate one structure to another. Recent tabulations of structure and spectroscopy data [82-85] attest to the rapidly growing data base in surface chemistry. In organic, inorganic and organometallic chemistry, many of these disconnected facts have since been unified in bonding principles (octet rule [80], effective atomic number rule [81],...) and reactivity patterns (nucleophilic substitution, oxidation/reduction, acid/base, ligand displacement,...).

Surface chemistry may be able to draw on these established structure and reactivity principles. Application of well-established

gas phase and solution chemistry to surfaces is, in fact, beginning to occur. For example, the structural analogy between metal carbonyls and the surface bonding of carbon monoxide is frequently noted [86]. Molecular reaction concepts like acid/base [87,88], nucleophilicity [89], oxidative addition [89-91], and ligand displacement [92] have also been applied to surfaces. Even molecular orbital theory, a chemists theory for molecules, is now being modified and applied to calculate energetics for adsorbates on metal cluster models of surfaces [31,34,93].

The objective of this section is not only to point out general trends in hydrocarbon surface bonding and reactivity but also to compare hydrocarbon/metal surface chemistry to that of hydrocarbon ligands in metal clusters. An important conclusion from this comparison is that the C-H bond chemistry of adsorbed hydrocarbons is appropriately described by the oxidative addition/reductive elimination formalism of organometallic chemistry. The discussion is divided in two parts: (1) structure and bonding and (2) C-H bond chemistry. Ethylene, acetylene and benzene and the groups 8-10 metal surfaces are used as examples, since these are the systems that have been most studied. However, the ideas proposed may be applicable to many other surface/adsorbate systems.

4.4.2 Structure and Bonding. Metal-carbon and carbon-carbon bond lengths have been determined for only a few hydrocarbon adsorbates. The adsorbed hydrocarbon bonding geometries which have been solved by low-energy electron diffraction include: ethylidyne on

Rh(111) [7] and Pt(111) [94], acetylene on Pt(111) [95], and benzene coadsorbed with CO on Rh(111) [96,97] and Pt(111) [98].

Many more hydrocarbon surface species whose structure is pending solution by surface crystallography have been identified by the combination of HREELS and TDS. A significant feature of nearly all the species so-identified is that the surface bonding appears to be quite similar to that of hydrocarbon ligands in organometallic clusters. These surface/cluster structure analogies are shown in Figs. 4.30 - 4.33. The C-C bond lengths and characteristic vibrational frequencies are also given where known.

The cluster/surface analogy for each of these ligands is discussed in the references given in the figure captions. Here, the effects on the bonding of changing the ligand, temperature, surface coverage, surface structure and metal atomic number are discussed. The molecular orbitals involved in the bonding are not explicitly considered, but for reference, the frontier molecular orbitals of these ligands can be found in the following sources: C₂H₂ [126], C₂H₄ [126], C₆H₆ [126], CCH₃ [34], CH [127], CCH₂ [34].

a) Ligand Effects. Molecular ligands (acetylene, ethylene and benzene) all bond to the surface through their unsaturated C-C bonds. The interaction with the surface rehybridizes the carbon atoms from sp/sp² towards sp³. This is evident from comparing in Figs. 4.30 - 4.32 the νCH_x and νCC frequencies for the adsorbed molecules to the gas phase values. Both of these modes shift to lower frequency upon adsorption, characteristic of rehybridization towards sp³. Consistent with

Structure			Vibrational Frequencies (cm^{-1})		
Surfaces	Proposed Surface Geometry	Cluster Analogue	Characteristic Dipole-Active Modes	Surface	Cluster
<u>Fe(110)</u> <u>Ni(111)</u> <u>Cu(111)</u> <u>Cu(110)</u>		$\sim 1.48 \text{ \AA}$ 	$\nu(\text{CC})$ $\nu_s(\text{CH})$	1402 3086	1307 2920
<u>Pd(111)</u> <u>Rh(111)</u> <u>Pd(110)</u> <u>Pt(111)</u> <u>Ni(110)</u> <u>Ru(001)</u>		$\sim 1.44 \text{ \AA}$ 	$\nu(\text{CC})$ $\nu_s(\text{CH})$	1301 2945	1260 2960
<u>Ni(100)</u> <u>Rh(100)</u> <u>Re(001)</u> <u>Pd(100)</u> <u>Fe(111)</u>		1.40 \AA 	$\nu(\text{CC})$ $\nu_s(\text{CH})$	1120 2805	1199 2993 ----- -----
<u>Pd(111)</u> <u>Rh(111)</u> <u>Ru(001)</u> <u>Pt(111)</u> <u>Ni(110)</u> <u>Ni(111)</u>		1.48 \AA 	$\nu(\text{CC})$ $\nu(\text{CH})$	1534 3157	1380 3020
<u>Rh(100)</u>		1.36 \AA 	$\nu(\text{CC})$ $\nu(\text{CH})$	----- -----	1305 3025
gas phase		1.2 \AA $\text{H}-\text{C}\equiv\text{C}-\text{H}$	$\nu(\text{CC})$ $\nu_s(\text{CH})$	----- -----	1974 3374

Fig. 4.30 The metal surface/cluster analogy for coordinated acetylene (C_2H_2) and acetylide (C_2H). The surface bonding geometries are proposed based on the HREEL vibrational frequencies and intensities. Underlined surfaces are expected to have similar bonding geometries to that shown. The other surfaces have similar HREEL spectra, but lack comparable coordination sites. References: 99-116 and those in Table 3.12.

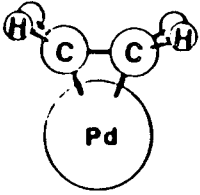
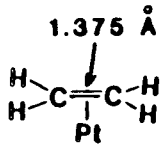
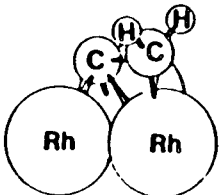
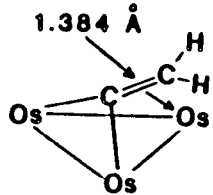
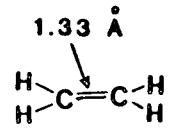
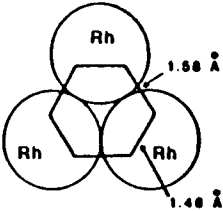
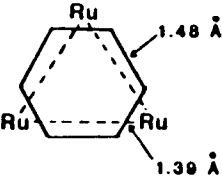
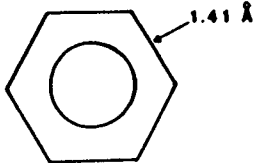
Structure			Vibrational Frequencies (cm^{-1})		
Surfaces	Proposed Surface Geometry	Cluster Analogue	Characteristic Dipole-Active Modes	Surface	Cluster
<u>Pd(111)</u> <u>Pd(110)</u>		1.375 \AA 	$\nu_s(\text{CH}_2)$ $\nu(\text{CC}) + \text{CH}_2 \text{ scissor}$	3000 1520	3031 1515
<u>Rh(111)</u> <u>Pt(111)</u> <u>Pd(111)</u> <u>Rh(100)</u>		1.384 \AA 	$\nu_s(\text{CH}_2)$ $\nu(\text{CC}) + \text{CH}_2 \text{ scis} + \text{CH}_2 \text{ wag}$	2945 1450	2986 1470
gas phase		1.33 \AA 	$\nu_s(\text{CH}_2)$ $\nu(\text{CC})$	3026 1623	

Fig. 4.31 The metal surface/cluster analogy for coordinated ethylene (C_2H_4) and vinylidene (CCH_2). Comments to Fig. 4.30 also apply here.

Molecular ethylene adsorption has been studied on many more surfaces than those shown (Section 3.4), but cluster analogues are lacking. References: those for Sections 3.4 and 4.1.

XBL 8610-4091

Structure			Vibrational Frequencies (cm^{-1})		
Surfaces	Proposed Surface Geometry	Cluster Analogue	Characteristic Dipole-Active Modes	Surface	Cluster
Rh(111) + CO Pt(111) Rh(111) Pd(111) Pd(100) Ni(111) Pt(110) Ni(100) Ni(110)			$\nu_s(\text{CH})$ $\gamma(\text{CH})$ $\nu(\text{CC})$	3000 776 1420	3098 817 { 1396 1373 }
gas phase			$\nu_s(\text{CH})$ $\gamma(\text{CH})$ $\nu(\text{CC})$	3059 670 1479	

XBL 8610-4092

Fig. 4.32 The metal surface/cluster analogy for coordinated benzene (C_6H_6).

The surface bonding geometry shown for Rh(111) + CO was solved by LEED [96,97]. In the absence of CO on Rh(111) or with CO on Pt(111) [98], benzene has been determined by LEED to bond in a bridge site. There is no known cluster analogue for this mode of coordination. References: 117-125.

Structure			Vibrational Frequencies (cm^{-1})		
Surfaces	Proposed Surface Geometry	Cluster Analogue	Characteristic Dipole-Active Modes	Surface	Cluster
<u>Rh(111)</u> <u>Pt(111)</u> <u>Pd(111)</u> <u>Ru(001)</u> <u>Rh(100)</u>			$\nu_s(\text{MC})$ $\nu(\text{CC})$ $\delta_s(\text{CH}_3)$ $\nu_s(\text{CH}_3)$	435 1121 1337 2860	401 1163 1356 2888
<u>Rh(111)</u> <u>Ru(001)</u> <u>W(110)</u>			$\nu_s(\text{MC})$ $\nu(\text{CH})$	~740 2930	715 3041
gas phase			$\nu(\text{CC})$ $\delta_s(\text{CH}_3)$ $\nu_s(\text{CH}_3)$	995 1379 2954	

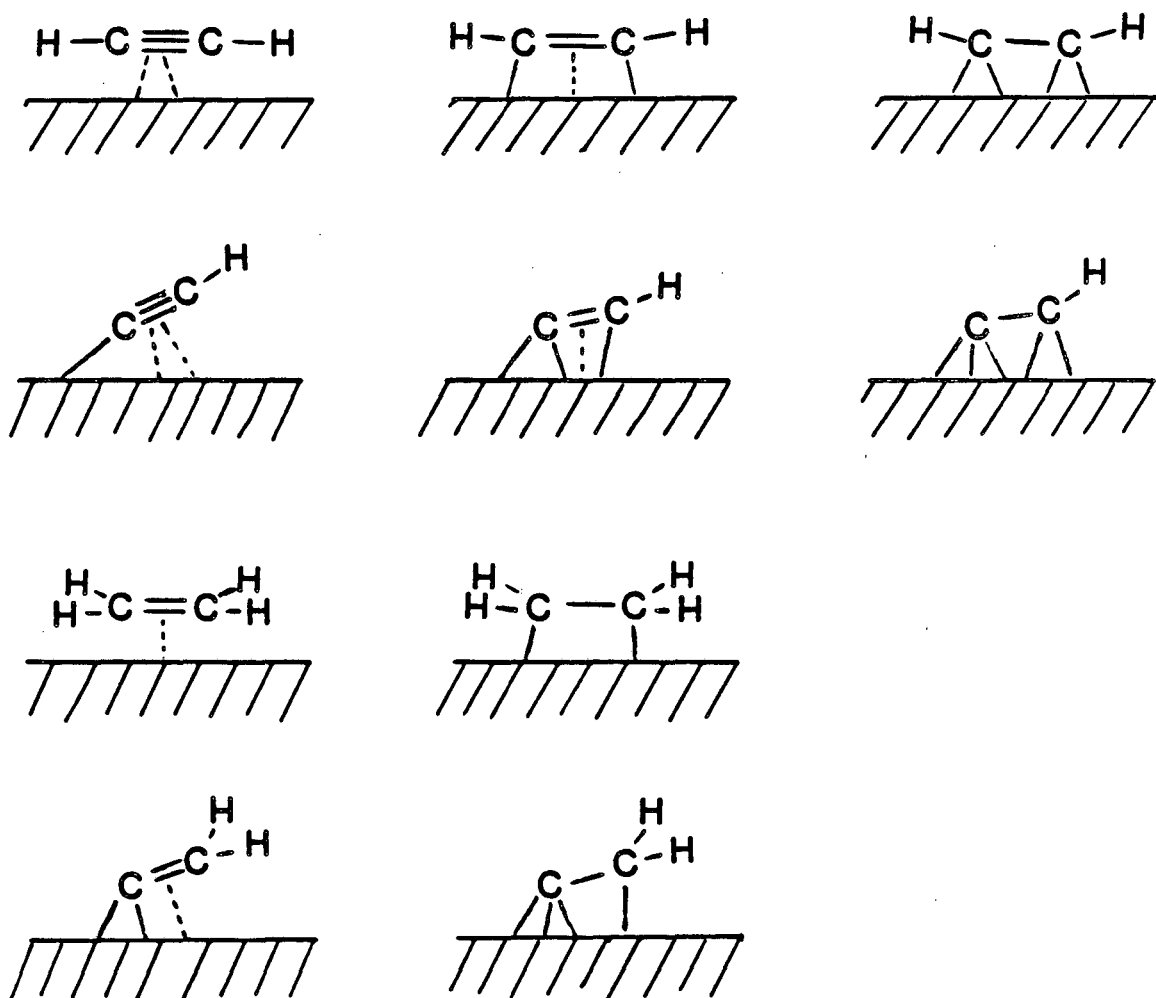
Fig. 4.33 The metal surface/cluster analogy of ethylidyne (CCH_3) and methylidyne (CH). Comments to Fig. 4.30 apply here also. The bonding geometries for ethylidyne on Pt(111) and Rh(111) have been determined by LEED.

this interpretation, the C-C bond lengths in adsorbed C_2H_4 and C_2H_2 on Pt(111) have been determined to lengthen by 0.16 and 0.25 Å respectively over their gas phase values [95]. The C-C bonds in adsorbed benzene also lengthen on Pt(111) [98] and Rh(111) [96,97], but not uniformly, giving rise to 2-fold or 3-fold symmetric distortions respectively of the π -ring.

Ethynylidyne (CCH_3) and methylidyne (CH) lack unsaturated C-C bonds, but are good ligands because of their radical character. They bond "standing up" on the surface and in clusters through the radical carbon. CCH_2 and CCH are radicals that also have unsaturated C-C bonds. Bonding to the surface through their radical ends promotes standing perpendicular to the surface, while coordination through the π bonds favors lying down. The actual configuration on the group 8-10 metals appears to be tilted. This judgement is based on the HREELS vibrational frequencies. As shown in Figs. 4.30 and 4.31, the shift down in the ν_{CH_x} and ν_{CC} frequencies compared to gas phase ethylene and acetylene is characteristic of rehybridization and bonding to the surface with the π -bond. This type of bonding is reminiscent of pyridine coordination to metal surfaces. Pyridine is known to σ -bond to metal surfaces through the nitrogen lone pair with its π -ring tilting varying amounts towards the surface depending on metal atomic number, temperature and surface coverage [129].

The notation for interaction between π -bonds and metals deserves comment. The varying degrees of interaction can be notated as shown in Fig. 4.34. The extremes are called π -bonding and di- σ bonding.

Notation for the Bonding Interaction Between π -bonds and Metal Atoms



XBL 8610-4115

Fig. 4.34 Types of notation for the bonding interaction between π -bonds and metal atoms or surfaces. Interaction with the surface is shown increasing from left to right.

Since the degree of bonding is often not clear, the π and di- σ bond notation are frequently used interchangeably.

b) Temperature Effects. The chemisorption bonding of the molecular hydrocarbons has been found in all but one case [130] to be independent of temperature down to 77K. Extended Huckel calculations, however, suggest that there is a small energy barrier to chemisorption, so that at still lower temperatures weakly (physisorbed) bonding to the surface can occur. There are conflicting reports as to whether benzene bonds in such a physisorbed state as high as 150 K on Pd(111) [130,131].

The bonding of CH, CCH₃, CCH and CCH₂ has been found to be temperature independent in the range of thermal stability. No change in the tilt angle of CCH and CCH₂ analogous to that for pyridine has yet been reported, but the studies are limited.

c) Surface Coverage Effects. No surface coverage effects for acetylene, benzene, CCH₃, CCH, CH, or CCH₂ surface bonding have been reported. Coverage dependent bonding of ethylene has been observed on Pd(110) [132], Pd(100) [5] and Rh(100) [134]. In these systems, more weakly bound species are adsorbed at high surface coverages.

d) Coadsorbate Effects. Coadsorption of hydrocarbon ligands with other adsorbates has only been studied in a few cases. Coadsorption of hydrogen or CO with ethynidyne changes the long range order on the surface without detectably affecting the local bonding of ethynidyne [135]. CO has been found to form ordered structures with a number of other hydrocarbons as well [136]. In all cases the vibrational

frequencies show almost no shift in the presence of CO. However, at least for benzene on Rh(111) [121] (and possibly on Rh(100) [137] and Pd(111) [138]), coadsorbed CO shifts the benzene adsorption site.

e) Surface Structure Effects For molecular adsorbates, the questions here are, "Does changing the surface structure change the adsorption site?", and if so, "Does the surface bonding change dramatically?". The existing data relevant to these questions are given in Table 4.6. While adsorption sites for these molecules are not well-established, coordination to more than one metal atom appears to predominate. Most of the HREELS results are for the fcc(111) and (100) surfaces. On these surfaces, ethylene and acetylene have dramatically different HREEL spectra, while the benzene HREEL spectrum shows little variation. For acetylene, the different bonding geometries are consistent with the multiple coordination geometries found for this ligand in organometallic clusters (Fig. 4.29). Similar multiple coordination modes for ethylene in clusters have not been reported, but are expected based on the structure sensitivity of the surface bonding. For benzene, the similarity of the HREEL spectra for different surface geometries is due either to (1) bonding in the same site (bridge), (2) insensitivity of the benzene bonding to different adsorption sites or (3) insensitivity of HREELS to the in-plane distortions of the benzene ring. The experimental evidence suggests that all three are at least partially true.

Table 4.6: Effects of Surface Structure on the Molecular Adsorption Geometries of C₆H₆, C₂H₂ and C₂H₄

<u>Molecule</u>	<u>Metal</u>	<u>Surfaces</u>	<u>Proposed Bonding Sites*</u>	<u>Bonding[#]</u>	<u>Refs.</u>
Benzene	Pd	(111), (100)	bridge, bridge	same	6
	Ni	(111), (110), (100)	-----	similar	118
	Pt	(111), (110)	bridge, ?	similar	62, 118a
	Rh	(111), (111)+CO	bridge, 3-fold	similar	121
Acetylene	Pd	(111), (110)	3-fold, ?	similar	111, 102
	Pd	(111), (100)	3-fold, 4-fold	different	111, 107
	Rh	(111), (100)	3-fold, 4-fold	different	115, 109
	Ni	(111), (110), (100)	bridge, ?, 4-fold	different	105, 113, 106
	Cu	(111), (110)	bridge, bridge	similar	102, 103
	Fe	(111), (110)	?, bridge	different	20, 104
Ethylene	Pd	(111), (110)	-----	similar	4, 132
	Pd	(111), (100)	-----	different	4, 5
	Ni	(111), (110)	-----	different	133, 23
	Rh	(111), (100)	-----	different	134

*) Proposal based on comparison to organometallic clusters, dynamical LEED calculations, or HREELS intensities.

#) Comparison based on the HREEL spectra.

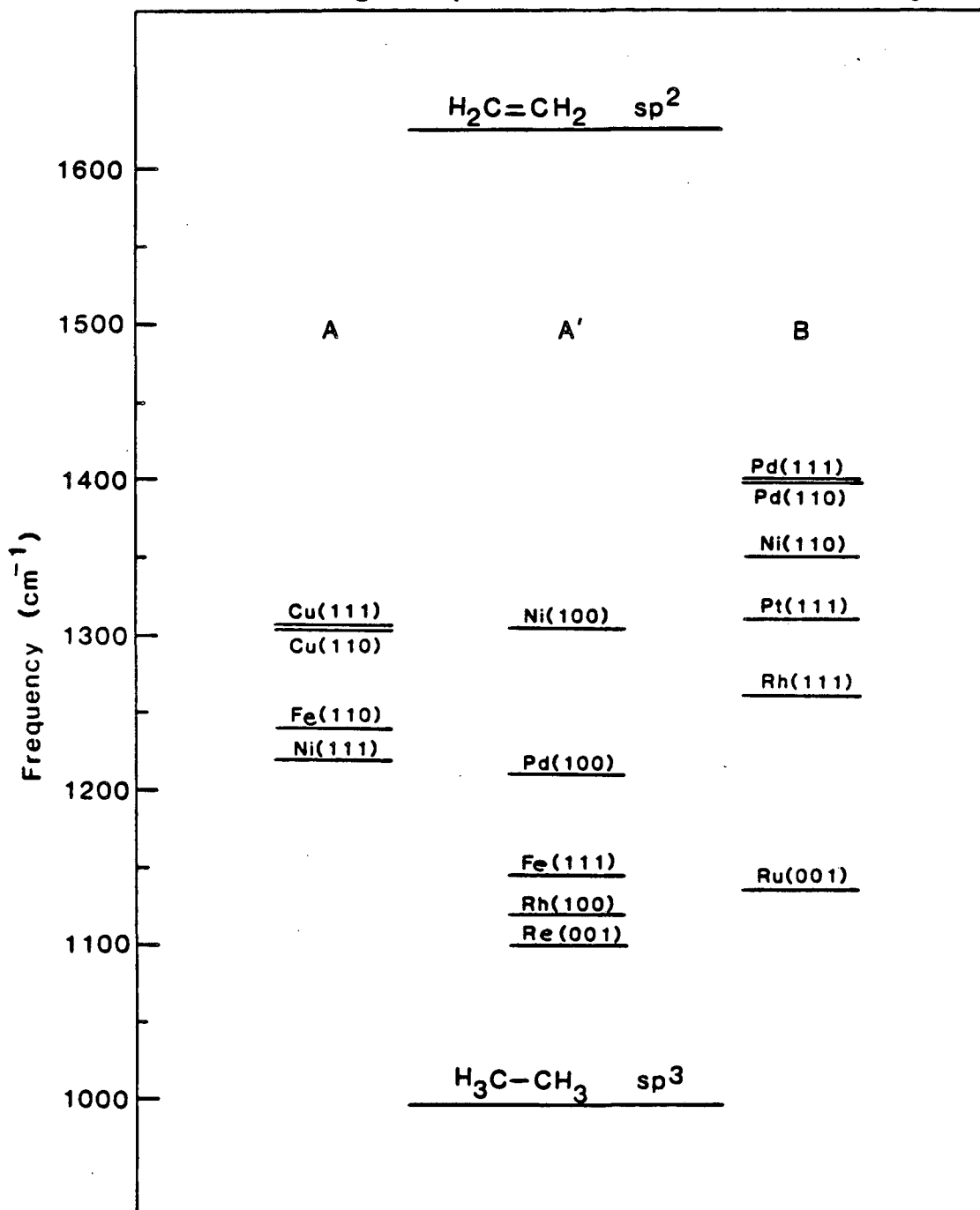
The hydrocarbon fragment ligands have been less-studied. For these ligands there is the additional question, "Can the fragment form on a surface with a particular geometry?" For example, it is significant that ethynidyne forms on Pd(111) [4] but not Pd(100) [5], while, formation of ethynidyne has been observed on both the Rh(111) and Rh(100) surfaces.

f) Atomic Number Effects. Comparison of the bonding in ligands on isostructural metal surfaces of different atomic number helps to distinguish the electronic and geometric aspects of surface chemical bonding. Parameters indicative of the degree of bonding of ethylene, acetylene, and benzene to transition metal surfaces are given in Table 3.9, Fig. 4.35 and Table 4.7 respectively. Comparison of the amounts of rehybridization on isostructural metal surfaces is, however, complicated by changes in the coordination geometry. For example, both ethylene and acetylene show dramatically different HREELS intensities on Rh(111) and Ni(111) suggesting that not only the rehybridization, but also the binding site is different on these isostructural surfaces.

Benzene, on the other hand, shows less structure-sensitivity in its adsorption bonding. In this case, atomic number effects are not masked by differences in bonding geometry. This is indicated by the $\nu(\text{CH})$ frequencies for adsorbed benzene in Table 4.7. The frequency differences between surfaces of the same metal are less than those between different metals.

A detailed explanation of the observed $\nu(\text{CH})$ trend in terms of the interaction between the benzene molecular orbitals and the metal surface

C-C Stretching Frequencies for Adsorbed Acetylene



XBL 8610-4107

Fig. 4.35 Values of the C-C stretching frequency for adsorbed acetylene. All frequencies indicate rehybridization to midway between C-C single and double bonds. Surfaces are grouped into types A, A' and B according to the classification of Sheppard [150].

Table 4.7: Effect of metal atomic number on the adsorbed benzene $\nu(\text{CH})$ frequency. For gas phase benzene, $\nu(\text{CH})$ is 670 cm^{-1} .

<u>Metal</u>	<u>Cohesive Energy*</u> (kcal/mol)	<u>Surface</u>	<u>Work Function#</u> (eV)	<u>$\nu(\text{CH})$</u> (cm^{-1})	<u>Ref.</u>
Ag	68	(111)	4.74	675	117
Pd	89.8	(111)	5.6	720	122
		(100)	5.45	720	122
Ni	102.4	(111)	5.35	730	118
		(110)	5.04	735	118c
		(100)	5.22	750	118b
Rh	132.5	(100)	5.15	760	137
		(111)	5.3	776	121
Pt	134.7	(111)	5.85	830	124

*) From Ref.26

#) From Refs. 140, 141

band structure is not presently possible [139]. However, it may be possible to empirically correlate the surface bonding with macroscopic parameters that reflect the electronic properties of the metal. Metal cohesive energies [130] and work functions [121b] are two such parameters cited in the literature (and listed in Table 4.7) to explain the $\nu(\text{CH})$ frequency shift in adsorbed benzene. Qualitatively, larger work functions and larger cohesive energies correlate with larger $\nu(\text{CH})$ shifts from gas phase benzene and presumably with stronger bonding to the surface. This is reasonable, since high cohesive energies (strong metal-metal bonds) might be expected to correlate with strong metal-carbon surface bonds while larger work functions can induce greater charge transfer between benzene and the metal, also leading to stronger metal-carbon bonds. Both of these parameters predict a large $\nu(\text{CH})$ shift for Pt(111) and a small one for Ag(111) as are observed. However, the cohesive energies more correctly predict the $\nu(\text{CH})$ for Pd(111) relative to Pt(111) [130] while the work functions more closely correlate the Rh(111) and Pt(111) shifts [121b]. Studies of benzene adsorption on high cohesive energy/low work function metals like tungsten are needed to determine the relative importance of these parameters in the surface bonding of benzene.

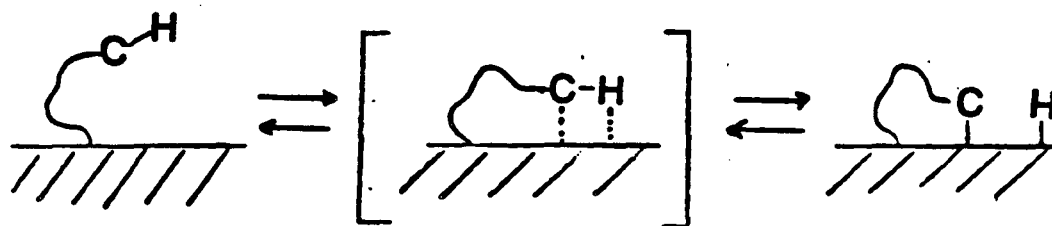
4.4.3 C-H Bond Chemistry. In the stoichiometric reactions of unsaturated hydrocarbons with groups 8-10 metal surfaces, C-H bonds are readily broken. Ethylene and acetylene begin to dehydrogenate at measurable rates between 200 and 300 K. These temperatures, assuming typical unimolecular decomposition preexponential factors of 10^{13} s^{-1} ,

correspond to activation energies of 8-15 kcal/mol. Since this value is much less than gas phase C-H bond dissociation energies of ~100 kcal/mol, this metal-assisted C-H bond breaking is called C-H activation [142].

The degree to which C-H bonds are activated depends on metal atomic number, surface roughness and the nature of the adsorbed C-H bond. Early transition metals, rough surfaces and surface fragments with the fewest metal-carbon bonds show the most C-H activation. These observations can be understood using elementary kinetic and thermodynamic considerations along with some established reactions in organometallic chemistry.

First, note that low activation energies for C-H bond breaking on surfaces are possible because metal-carbon, metal-hydrogen, and possibly carbon-carbon bonds form simultaneously with C-H bond breaking. Thermodynamics requires that at least two of these types of bonds be formed, since $E(\text{M-H}) \sim 60$ kcal/mol [63], $E(\text{M-C}) \sim 30-60$ kcal/mol [90] and $E(\text{C-C}) \sim 60$ kcal/mol (difference between C-C single and double bonds). If only one of these bonds forms, the minimum activation energy for C-H bond breaking would be at least 30 kcal/mol. Since the experimental activation energies are less, free radical chemistry can be ruled out as the mechanism for C-H bond breaking.

The simplest mechanism for elementary dehydrogenation that is thermodynamically favored and also well-established in organometallic chemistry is:

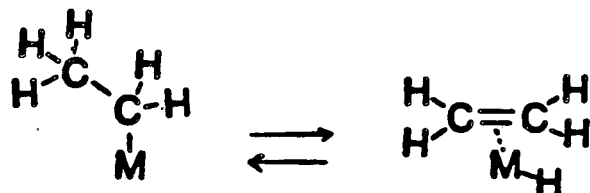


The overall process is called an oxidative addition, since the metal atom(s) formally donate(s) two electrons to form the metal-carbon and metal-hydrogen bonds [143]. The reverse process which results in C-H bond formation is called a reductive elimination. These types of reactions were first extensively applied to explain hydrocarbon surface chemistry by the late E.L. Muetterties [90-92].

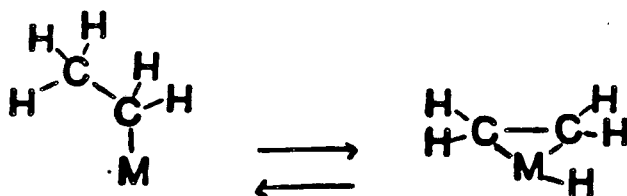
The term oxidative addition does not imply any mechanism or transition state as shown in brackets above. However, it appears likely, as concisely stated by Muetterties [90], that while "the geometric features of the oxidative addition reaction may comprise an initial linear M-H-C interaction, ultimate C-H bond cleavage requires a triangular M-H-C interaction." Such 3-center M-H-C interactions are observed in a number of stable organometallic complexes [90].

On surfaces it may be more appropriate to call the analogues of oxidative addition and reductive elimination simply C-H bond additions or eliminations (or maybe elementary dehydrogenations and hydrogenations), since the direction of net electron transfer is not clear. These alternative descriptions also avoid the following conflict. In

organometallic chemistry, conversion of an ethyl species to a coordinated ethylene:



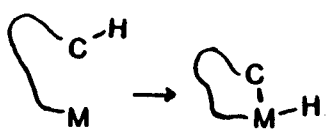
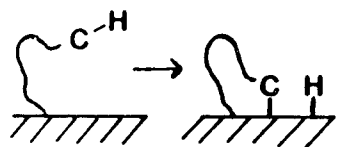
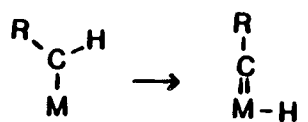
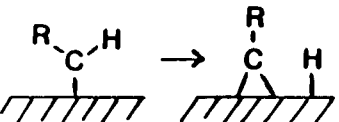
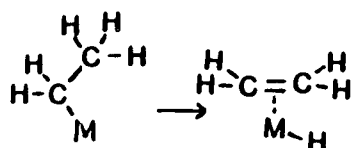
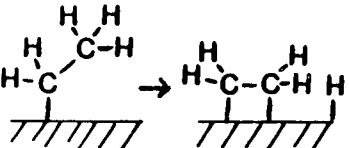
is called β -elimination rather than oxidative addition, since the metal is not formally oxidized when ethylene assumes π coordination. However, on many metal surfaces ethylene coordination may be more accurately described by "di- σ " bonding, in which case the process can clearly be viewed as an oxidative addition:



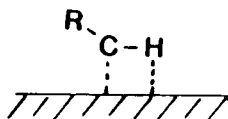
Further, since both oxidative addition and β -elimination presumably have similar triangular M-H-C transition states, it seems to me unfortunate that one is called elimination (of H from the hydrocarbon) and the other addition (of the C-H bond to the metal). These processes are compared in Fig 4.36 to possible surface analogues, all of which are simply called additions or dehydrogenations.

This issue also raises another question: "When should the π -bond and when should the di- σ bond notation in Fig. 4.34 be used?" In principle it doesn't matter as long as one realizes that they are both

Organometallic Nomenclature and Proposed Surface Nomenclature For C-H Bond-Breaking Reactions

<u>Organometallic Process</u>	<u>Name</u>	<u>Surface Analogue</u>	<u>Proposed Names</u>
	oxidative addition		addition or dehydrogenation
	α -elimination		addition or dehydrogenation
	β -elimination		addition or dehydrogenation

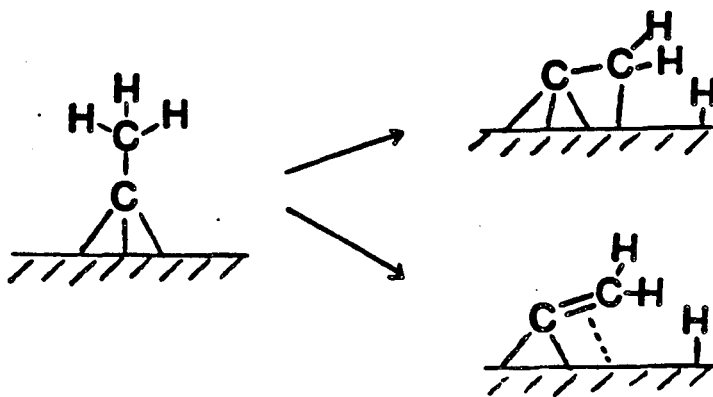
Presumed Transition State Configuration



XBL 8610-4114

Fig. 4.36 Comparison of existing organometallic nomenclature and proposed surface nomenclature for three types of C-H bond-breaking reactions. Also shown as the type of transition state which is generally presumed for these related reactions.

approximate descriptions of the same situation. However, the di- σ notation more clearly implicates formation of metal-carbon and metal-hydrogen bonds in the C-H bond breaking transition state. For example, the decomposition of CCH_3 to CCH_2 on $\text{Rh}(100)$ can be notated two ways:



The upper notation suggests (correctly, I believe) that CCH_3 falls over and dehydrogenates through a triangular M-H-C transition state, while the lower notation gives the impression that the methyl hydrogen "jumps" to the surface followed by a tilting of the resulting vinyl species.

An implication of this C-H bond addition mechanism is that the rate of C-H bond breaking will depend strongly on the proximity of the C-H bond to the metal atom or metal surface. Muetterties has noted examples of hydrocarbon surface chemistry supporting this proximal effect [90] and several other experimental results deserve mention here.

First, there is generally ~ 600 K between the temperature at which C-H bonds begin to break and complete complete dehydrogenation (Section 3.5). Differences in C-H bond energies cannot begin to account for this enormous variation in the C-H bond breaking rate. The

proximal effect can, however, account for the large variations in both the activation energy and the preexponential factors that are observed. For example, the activation energy for α C-H bond breaking in HCCH_3 is calculated to be only 60% of that for β CH bond breaking in CCH_3 [27]. This difference parallels the difference in the frequency of the bending vibrational coordinate needed to bring the C-H bond near the metal surface—a low frequency metal-carbon bend in HCCH_3 vs the higher frequency $\nu(\text{CH}_3)$ mode in CCH_3 :



Further, the near zero activation energy for dissociation of the 104 kcal/mol H-H bond compared to the 10-30 kcal/mole barrier for breaking C-H bonds is no doubt partially a result of the H-H bond having no hindrance towards orienting parallel to the surface.

The preexponential factors for some "unimolecular" dehydrogenations also suggest a geometrically demanding transition state which might be expected for a triangular M-H-C interaction. The experimentally-determined values of 10^9 for ethynyl decomposition on Pt(111) [35] and for methanol decomposition on Ni (100) [144] are 10^4 lower than expected for unimolecular decomposition, indicating a large entropy of activation.

Up to this point, addition of C-H bonds to metal surfaces has been stressed. There is also experimental evidence for the reverse, elimination reaction. Such a hydrogenation reaction is implicated, for example, by the formation of methane in ethanol decomposition on Ni(111) [145], methane formation in acetaldehyde decomposition on Pt[6(111) x (100)] [146], ethylene hydrogenation to ethane with co-adsorbed D₂ on Pt(111) [37] and Rh(111) [Section 3.4], and ethylidyne H,D-exchange on Pt(111) and Rh(111) [Section 4.2]. Some other C-H bond forming reactions like that in the conversion of ethylene to ethylidyne have been postulated to occur by hydrogen shifts. However, as mentioned in sections 4.1 and 4.2, intramolecular H shifts have been calculated to be of higher energy than a two-step pathway where H is transferred from one carbon of the adsorbate to another via the surface [31].

Thus, it is asserted that the surface C-H bond chemistry of hydrocarbons involves only simple addition (dehydrogenation) and elimination (hydrogenation) reactions of C-H bonds on the metal surface. Further, an important criterion for C-H bond addition is that the C-H bond be oriented in the transition state so that both metal carbon and metal hydrogen bonds can begin forming.

These simple ideas are useful in rationalizing and relating many observations from both stoichiometric surface chemistry and heterogeneous catalysis. For example, the C-H bond chemistry observed for ethylene on transition metal surfaces can be nicely summarized (as shown in Fig. 4.13 and discussed in Section 4.1) by a series of

addition and elimination reactions. The importance of surface H atoms in UHV chemistry [147] and catalysis [148,149] can be rationalized to a large extent by simple elimination (hydrogenation) reactions.

Further, the C-H bond proximity to the metal surface can account for the effects of adsorbate and metal structure on the C-H bond breaking rate. For example, the facile dehydrogenation of the α C-H bonds in CH_2CH_3 vs. the β C-H bonds in CCH_3 [Section 4.1] and the enhanced reactivity of step and kink sites on surfaces for dehydrogenation [90] may both be due to geometrical effects. Another implication is that adsorbate structure can directly indicate reactivity. That is, those C-H bonds closest to the surface react fastest. Note, however, that correlation of surface reactivity to gas phase geometries is only indirect, since the structure of unsaturated hydrocarbons changes substantially upon adsorption.

These geometric arguments are most useful for comparing the reactivity of different hydrocarbons on various surfaces of a given metal. Comparison of different metals requires consideration of electronic factors. These effects can be indirectly considered in the model above by taking into account the effects of M-C and M-H bond strengths on the activation energy for C-H bond breaking. For example, the stronger M-H and M-C bonds for the early transition metals can explain why C-H bonds are more readily broken on these surfaces. Hopefully the equivalent of a Lewis dot picture of surface valency can eventually be developed so that electronic effects on C-H (and C-C) bond breaking can be directly considered.

REFERENCES

1. G.A. Somorjai and B.E. Bent, *Progr. in Colloid and Polymer Sci.* 70 (1985) 38.
2. S.M. Davis, F. Zaera and G.A. Somorjai, *J. Am. Chem. Soc.* 104 (1982) 7453, and references therein.
3. S.M. Davis, F. Zaera and G.A. Somorjai, *J. Catal.* 85 (1984) 206, and references therein.
4. J.A. Gates and L.L. Kesmodel, *Surf. Sci.* 124 (1983) 68.
5. E.M. Stuve and R.J. Madix, *J. Phys. Chem.* 89 (1985) 105.
6. L.L. Kesmodel, *Phys. Rev. Lett.* 53 (1984) 1001; G.D. Waddill and L.L. Kesmodel, *Phys. Rev.* B31 (1985) 4940.
7. R.J. Koestner, M.A. Van Hove and G.A. Somorjai, *Surf. Sci.* 121 (1982) 321.
8. Spectra at saturation coverage have been published: L.H. Dubois, D.G. Castner and G.A. Somorjai, *J. Chem. Phys.* 72 (1980) 5234.
9. J.T. Yates, Jr., P.A. Thiel and W.H. Weinberg, *Surf. Sci.* 84 (1979) 427.
10. J.T. Yates, Jr. and T.E. Madey, *J. Chem. Phys.* 54 (1971) 4969; D.W. Goodman, J.T. Yates, Jr. and T.E. Madey, *Surf. Sci. Lett.* 93 (1980) L135; B.E. Koel, D.E. Peebles and J.M. White, *Surf. Sci. Lett.* 107 (1981) L367; Y. Kim, H.C. Peebles and J.M. White, *Surf. Sci.* 114 (1982) 363.
11. M.M. Hills, J.E. Parmeter, C.B. Mullins and W.H. Weinberg, *J. Amer. Chem. Soc.* 108 (1986) 3554.

12. L.H. Dubois, J. Chem Phys. 77 (1982) 5228.
13. S. Hengrasmee, P.R. Watson, D.C. Frost, and K.A.R. Mitchell, Surf. Sci. 87 (1979) L249.
14. The vibrational frequency of carbon atoms on Rh(100) of 555 cm^{-1} is almost exactly a factor of $(32/12)^{1/2}$ higher than that for sulfur (313 cm^{-1}). This is what is expected in the harmonic oscillator approximation based on the differences in mass assuming that the bonding of these adsorbates on the surface is the same. Therefore, since sulfur bonds in a 4-fold hollow [13], carbon presumably does too.
15. See Section 3.5
16. J. Evans and G.S. McNulty, J. Chem. Soc. Dalton Trans (1983) 639; vibrational frequencies are also given in this reference for a CCH_2 species standing vertically in a diruthenium cluster; these frequencies are substantially different from those for the tilted ligand in Fig. 4.4B.
17. C_2H species are known to have tilted geometries in both 3-fold and 4-fold coordination geometries [Fig. 3.39] as well as similar vibrational frequencies on (111) and (100) surfaces (Table 3.12).
18. H. Ibach and S. Lehwald, J. Vac. Sci. Technol. 15 (1978) 407; the ethylidyne (CCH_3) spectra in this paper are improperly attributed to ethylidene (CHCH_3).
19. See Section 3.1
20. U. Seip, M.-C. Tsai, J. Kupperts and G. Ertl., Surf. Sci. 147 (1984) 65.

21. W. Erley, A.M. Baro and H. Ibach, Surf. Sci. 120 (1982) 273.
22. S. Lehwald and H. Ibach, Surf. Sci. 89 (1979) 425.
23. J.A. Stroscio, S.R. Bare and W. Ho, Surf. Sci. 148 (1984) 499.
24. H. Steininger, H. Ibach and S. Lehwald, Surf. Sci. 117 (1982) 341.
25. A.F. Wells, Structural Inorganic Chemistry, 3rd edition, London, Oxford University Press (1962) 907.
26. C. Kittel, Introduction to Solid State Physics, 5th edition, N.Y., John Wiley (1976) 74.
27. D.B. Kang and A.B. Anderson, Surf. Sci. 155 (1985) 639.
28. C.-T. Kao, C.M. Mate, B.E. Bent and G.A. Somorjai, in preparation.
29. L.L. Kesmodel, G.D. Waddill and J.A. Gates, Surf. Sci. 138 (1984) 464.
30. J.E. Parameter, M.M. Hills and W.H. Weinberg, J. Am. Chem. Soc. 108 (1986) 3563.
31. A.B. Anderson, D.B. Kang and Y. Kim, J. Am. Chem. Soc. 106 (1984) 6597.
32. A. Gavezzotti and M. Simonetta, J. Mol. Structure 107 (1984) 75; Surf. Sci. 99 (1980) 453.
33. C. Minot, M.A. Van Hove and G.A. Somorjai, Surf. Sci. 127 (1982) 441.
34. J. Silvestre and R. Hoffmann, Langmuir 1 (1985) 621.
35. M. Salmeron and G.A. Somorjai, J. Phys. Chem. 80 (1982) 341.
36. J.R. Creighton and J.M. White, Surf. Sci. 129 (1983) 327.
37. D. Godbey, F. Zaera, R. Yeates and G.A. Somorjai, Surf. Sci. 167 (1986) 150.

38. E.L. Muetterties, Chem. Soc. Rev. 11 (1982) 283.
39. G.H. Hatzikos and R.I. Masel, to be published.
40. C. Kemball, J. Chem. Soc. (1956) 735.
41. G.C. Bond, J.J. Philipson, P.B. Wells and J.M. Winterbottom, Trans. Faraday Soc. 60 (1964) 1847.
42. J.R. Anderson and B.G. Baker, Chapter 8 in Chemisorption and Reactions on Metallic Films, Vol. II, J.R. Anderson, ed., Academic Press: N.Y. (1971).
43. F. Zaera and G.A. Somorjai, J. Am. Chem. Soc. 106 (1984) 2288.
44. A. Wieckowski, S. Rosasco, G. Salaita, A. Hubbard, B.E. Bent, F. Zaera and G.A. Somorjai, J. Am. Chem. Soc. 107 (1985) 5910.
45. See Chapter 5.
46. S.M. Davis, F. Zaera and G.A. Somorjai, J. Catal. 77 (1982) 439, and references therein.
47. S.J. Thomson and G.J. Webb, J. Chem. Soc., Chem. Commun. (1976) 526.
48. B.E. Koel, B.E. Bent and G.A. Somorjai, Surf. Sci. 146 (1984) 211; the H,D-exchange mechanism proposed in this paper has been revised and is shown in Fig. 4.19.
49. See Section 3.2.
50. W. Erley, P.H. McBreen and H. Ibach, J. Catal. 84 (1983) 229.
51. F. Zaera, Ph.D. Thesis, University of California, Berkeley (1984) unpublished.
52. S.M. Davis, F. Zaera, B.E. Gordon and G.A. Somorjai, J. Catal. 92 (1985) 240.
53. A.M. Baro, H. Ibach and H.D. Bruchmann, Surf. Sci. 88 (1979) 384.
54. C.M. Mate and G.A. Somorjai, submitted.

55. T. Shimanouchi, Tables of Molecular Vibration Frequencies, Consolidated Volume I, NSRDS-NBS 39 (1972) 51.
56. J.R. Ritter and D.F. Eggers, J. Chem. Phys. 44 (1966) 745.
57. Bruno Marchon, unpublished calculations.
58. These modes are both reported to be of medium intensity in ref. 59.
59. P. Skinner, M.L. Howard, I.A. Oxton, S.F.A. Kettle, D.B. Powell and N. Sheppard, J. Chem. Soc. Faraday Trans. II 77 (1981) 1203.
60. The only complication is that the $\delta_s(\text{CH}_3)$ peak, whose intensity decreases with deuteration, is not symmetrically placed between the 1246 and 1440 cm^{-1} peaks. Its decrease in intensity will contribute some to the changes in the 1246 cm^{-1} and 1440 cm^{-1} relative intensities.
61. J.R. Creighton, K.M. Ogle and J.M. White, Surf. Sci. 138 (1984) L137.
62. M. Surman, S. R. Bare, P. Hofmann and D.A. King, Surf. Sci. 126 (1983) 349.
63. G.A. Somorjai, Chemistry in Two Dimensions: Surfaces, Cornell Univ. Press, Ithaca (1981).
64. Section 4.1.
65. B.E. Koel, J.E. Crowell, C.M. Mate and G.A. Somorjai, J. Phys. Chem. 88 (1984) 1988; C.M. Mate and G.A. Somorjai, Surf. Sci. 160 (1985) 542.
66. S. Lehwald, H. Ibach and J.E. Demuth, Surf. Sci. 78 (1978) 577; M.-C. Tsai and E.L. Muetterties, J. Am. Chem. Soc. 104 (1982) 2534.

67. R.J. Koestner, M.A. Van Hove and G.A. Somorjai, *J. Phys. Chem.* 87 (1983) 203.
68. M.A. Van Hove, R.J. Koestner and G.A. Somorjai, *J. Vac. Sci. Technol.* 20(3) (1982) 886.
69. R.J. Koestner, J.C. Frost, P.C. Stair, M.A. Van Hove and G.A. Somorjai, *Surf. Sci.* 116 (1982) 85.
70. L.M. Sverdlov, M.A. Kovner and E.P. Krainov, *Vibrational Spectra of Polyatomic Molecules*, Wiley: New York, 1974.
71. K.M. Ogle, J.R. Creighton, S. Akhter, and J.M. White, *Surf. Sci.* 169 (1986) 246.
72. A.B. Dempster, K. Price and N. Sheppard, *Spectrochimica Acta* 27A (1971) 1579.
73. S. Palfi, W. Lisowski, M. Smutek and S. Cerny, *J. Catal.* 88 (1984) 300.
74. C.E. Anson, B.T. Keiller, I.A. Oxton, D.B. Powell and N. Sheppard, *J. Chem. Soc., Chem. Commun.* (1983) 470.
75. This assumes that all hydrogens in the fragment are equivalent, which is reasonable, since the surface fragments at these temperatures are CCH_3 and C_xH as discussed in Section 3.3.
76. N.R. Avery and N. Sheppard, *Proc. Roy. Soc. Lond. A* 405 (1986) 1.
77. B.E. Bent, unpublished data.
78. These experiments were performed by D. Godbey.
79. J.R. Fritch and K.P.C. Vollhardt, *Angew. Chem.*, 92 (1980) 570; *Angew. Chem. Intern. Ed. Engl.* 19 (1980) 559.

80. G.N. Lewis, Valence and The Structure of Atoms and Molecules, J.J. Little and Ives: New York (1923).
81. N.V. Sidgwick, The Electronic Theory of Valency, Cornell Univ. Press: Ithaca (1927).
82. P.A. Thiry, J. Electron Spectrosc. and Related Phenom. 39 (1986) 273; 30 (1983) 261.
83. J. Darville, J. Electron Spectrosc. and Related Phenom. 39 (1986) 311.
84. D.G. Walmsley and J.L. Tomlin, Progr. in Surf. Sci. 18 (1985) 247.
85. J.B. Pendry and M.A. Van Hove, Surface Crystallography Information Service, in preparation.
86. T.T. Nguyen and N. Sheppard in "Advances in Infrared and Raman Spectroscopy Vol. 5", R.E. Hester and R.H.J. Clark, eds., Heyden: London (1978).
87. P.C. Stair, J. Am. Chem. Soc. 104 (1982) 4044.
88. M.A. Barteau and R.J. Madix, Surface. Sci. 120 (1982) 262.
89. N.D.S. Canning and R.J. Madix, J. Phys. Chem. 88 (1984) 2437.
90. E.L. Muetterties, Chem. Soc. Rev. 11 (1982) 283.
91. E.L. Muetterties in "Reactivity of Metal-Metal Bonds", ACS Symposium Series No. 155, M.H. Chisholm, ed. (1981) 273.
92. E.L. Muetterties, Angew. Chem. Int. Ed. Engl. 17 (1978) 545.
93. R. Hoffmann, S.D. Wijeyesekera and S.-S. Sung, Pure and Appl. Chem. in press.
94. L.L. Kesmodel, L.H. Dubois and G.A. Somorjai, J. Chem. Phys. 70 (1979) 2180.

95. L.L. Kesmodel, P.C. Stair, R.C. Baetzold and G.A. Somorjai, *Phys. Rev. Lett.* 36 (1976) 1316; the C-C bond length could not be determined, but has been subsequently determined by NEXAFS: J. Stohr, F. Sette and A.L. Johnson, *Phys. Rev. Lett.* 53 (1984) 1684.
96. M.A. Van Hove, R.F. Lin, and G.A. Somorjai, *J. Am. Chem. Soc.*, 108 (1986) 2532.
97. R.F. Lin, G.S. Blackman, M.A. Van Hove and G.A. Somorjai, to be submitted.
98. D.F. Ogletree, M.A. Van Hove and G.A. Somorjai, to be published.
99. C₂H₂/Co₂: Y. Iwashita, F. Tamura and A. Nakamura, *Inorg. Chem.* 8 (1969) 79; C₂H₂/clusters: E. Sappa, A. Tiripicchio, P. Braunstein, *Chem. Rev.* 83 (1983) 203.
100. C₂H₂/Os₃: C.E. Anson, B.T. Keiller, I.A. Oxton, D.B. Powell and N. Sheppard, *J. Chem. Soc. Chem. Commun.* (1983) 470.
101. C₂H₂/Co₄: G. Gervasio, R. Rossetti and P.L. Stanghettini, *Organomet.* 4 (1985) 1612; C₂R₂/Ir₄: P.F. Heveldt, B.F.G. Johnson, J. Lewis, P.R. Raithby and G.M. Sheldrick, *J. Chem Soc. Chem. Commun.* (1978) 340.
102. C₂H₂/Cu(111): B.J. Bandy, M.A. Chesters, M.E. Pemble, G.S. McDougall and N. Sheppard, *Surf. Sci.* 139 (1984) 87.
103. C₂H₂/Cu(110): N.R. Avery, *J. Am. Chem. Soc.* 107 (1985) 6711.
104. C₂H₂/Fe(110): ref. 21.
105. C₂H₂/Ni(111): ref. 22; J.C. Bertolini and J. Rousseau, *Surf. Sci.* 83 (1979) 531; H. Ibach and S. Lehwald, *J. Vac. Sci. Technol.* 18 (1981) 625; J.E. Demuth and H. Ibach, *Surf. Sci.* 85 (1979) 365.

106. $C_2H_2/Ni(100)$: N.J. DiNardo, J.E. Demuth and Ph. Avouris, Phys. Rev. B 27 (1983) 5832; N.J. DiNardo, J.E. Demuth and Ph. Avouris, J. Vac. Sci. Technol. A 1 (1983) 1244.
107. $C_2H_2/Pd(100)$: L.L. Kesmodel, J. Chem. Phys. 79 (1983) 4646.
108. $C_2H_2/Fe(111)$: ref. 20.
109. $C_2H_2/Rh(100)$: C.T. Kao, B.E. Bent and G.A. Somorjai, to be published.
110. $C_2H_2/Re(001)$: J. Bertolini, B. Tardy and R. Dueros, C.R. Acad. Sc. Paris 298 (1984) 107.
111. $C_2H_2/Pd(111)$: J.A. Gates and L.L. Kesmodel, Surf. Sci. 124 (1983) 68; J. Chem. Phys. 76 (1982) 4218.
112. $C_2H_2/Pd(110)$: ref. 102.
113. $C_2H_2/Ni(110)$: ref. 102; ref. 23.
114. $C_2H_2/Pt(111)$: H. Ibach and S. Lehwald, J. Vac. Sci. Technol. 15 (1978) 407; H. Ibach, H. Hopster and B. Sexton, Appl. Phys. 14 (1977) 21.
115. $C_2H_2/Rh(111)$: L.H. Dubois, D.G. Castner and G.A. Somorjai, J. Chem. Phys. 72 (1980) 5234; C.T. Kao, C.M. Mate, B.E. Bent and G.A. Somorjai, in preparation.
116. $C_2H_2/Ru(001)$: J.E. Parameter, M.M. Hills and W.H. Weinberg, J. Am. Chem. Soc. 108 (1986) 3563.
117. $C_6H_6/Ag(111)$: Ph. Avouris and J.E. Demuth, J. Chem. Phys. 75 (1981) 4783.

118. $C_6H_6/Ni(111)$: S. Lehwald, H. Ibach and J.E. Demuth, Surf. Sci. 78 (1978) 577; J.C. Bertolini and J. Rousseau. Surf. Sci. 89 (1979) 467; J.C. Bertolini, J. Massardier and B. Tardy, J. Chim. Phys. 78 (1981) 939.
119. $C_6H_6/Ni(110)$: ref. 118c.
120. $C_6H_6/Ni(100)$: ref. 118b.
121. $C_6H_6/Rh(111)$: C.M. Mate and G.A. Somorjai, Surf. Sci. 160 (1985) 542; B.E. Koel, J.E. Crowell, C.M. Mate and G.A. Somorjai, J. Phys. Chem. 88 (1984) 1988.
122. $C_6H_6/Pd(111)$, Pd(100): ref.6.
123. $C_6H_6/Pt(110)$: ref. 62.
124. $C_6H_6/Pt(111)$: ref. 118a.
125. C_6H_6/Ru_6 , C_6H_6/Os_3 : M.P. Gomez-Sal, B.F.G. Johnson, J. Lewis, P.R. Raithby and A.H. Wright, J. Chem. Soc., Chem. Commun. (1985) 1682.
126. W.L. Jorgensen and L. Salem, The Organic Chemist's Book of Orbitals, Academic Press: N.Y. (1973).
127. J. Ushio, H. Nakatsuji and T. Yonezawa, J. Am. Chem. Soc. 106 (1984) 5892.
128. E. Shustorovich, Surf. Sci. Rep. 6 (1986) 1.
129. J.E. Demuth, Ph. Avouris and D. Schmeisser, J. Electron Spectrosc. 29 (1983) 163, and references therein.
130. V.H. Grassian and E.L. Muettterties, J. Phys. Chem., in press.
131. L.L. Kesmodel, Chem. Phys. Lett. 128 (1986) 208.

132. M.A. Chesters, G.S. McDougall, M.E. Pemble and N. Sheppard, Appl. Surf. Sci. 22/23 (1985) 369.
133. S. Lehwald and H. Ibach, Surf. Sci. 89 (1979) 425.
134. See section 3.4.
135. See section 3.2.
136. C.M. Mate, B.E. Bent and G.A. Somorjai, J. Electron Spectrosc. and Rel. Phenom. 39 (1986) 205.
137. B.E. Bent, C.T. Kao, A.L. Slavin and G.A. Somorjai, to be published.
138. H. Ohtani, B.E. Bent, C.M. Mate and G.A. Somorjai, to be published.
139. Surface band structures are not readily available and the nature of metal-carbon bonding is not well-understood.
140. H.B. Michaelson, J. Appl. Phys. 48 (1977) 4731.
141. H.A.C.M. Hendrickx, A. Hoek and B.E. Nieuwenhuys, Surf. Sci. 135 (1983) 81.
142. A.H. Janowicz and R.G. Bergman, J. Am. Chem. Soc. 105 (1983) 3929, and references therein.
143. J.P. Collman and L.S. Hegeudus, Principles and Applications of Organotransition Metal Chemistry, University Science Books, Mill Valley (1980).
144. R.B. Hall, A.M. DeSantolo and S.J. Bare, Surf. Sci. 161 (1985) L533.
145. S.M. Gates, J.N. Russell, Jr. and J.T. Yates, Jr., Surf. Sci. 171 (1986) 111.

146. R.W. McCabe, C.L. DiMaggio and R.J. Madix, J. Phys. Chem. 89 (1985) 854.
147. See Sections 4.1 - 4.3.
148. Z. Paal, ed. Hydrogen in Catalysis - Theoretical and Practical Aspects, Marcel Dekker, in press.
149. N. Yoshida, N. Matsumoto and Shozo Kishimoto, J. Catal. 92 (1985) 177.
150. N. Sheppard, J. Electron Spectrosc. and Related Phenom. 38 (1986) 175.

CHAPTER 5

SURFACE SCIENCE STUDIES OF ETHYLENE HYDROGENATION

5.1 Catalytic Hydrogenation of Ethylene Over Pt(111) and Rh(111)Single Crystal Surfaces

5.1.1 Background. The previous two chapters of this thesis have detailed studies identifying adsorbed hydrocarbon species and determining their stoichiometric reactivity. In this chapter, studies utilizing the high pressure/low pressure capability of the experimental apparatus to study catalytic ethylene hydrogenation are reported. The high pressure cell (see Section 2.3) allows ethylene hydrogenation reactions to be carried out at atmospheric pressure over clean Rh(111) and Pt(111) single crystal surfaces followed by transfer to ultra-high vacuum (UHV) (without exposure to the ambient) for surface analysis by low-energy electron diffraction (LEED), thermal desorption spectroscopy (TDS), Auger electron spectroscopy (AES) and high-resolution electron energy loss spectroscopy (HREELS). In this way, the adsorbate structure on the active catalyst can be determined. Restarting the catalytic reaction over these adsorbed species with isotopically labelled reactants permits the role of the adsorbed species in the catalytic reaction to be studied.

Ethylene hydrogenation was chosen for two reasons. First, the kinetics for the reaction over single crystals can be compared to extensive studies over metallic films, foils, wires, and plates. Second, the adsorbed monolayer that forms during the catalytic reaction can be compared to the species already identified for ethylene adsorption in UHV.

Several good reviews have been written about hydrogenation reactions in general [1], hydrogenation over metallic catalysts [2,3], and ethylene hydrogenation over metallic catalysts [4]. The mechanistic details of this stoichiometrically simple reaction are still not understood because of the mechanistic sensitivity to catalyst pretreatments and reaction conditions. However, a number of general statements about this reaction can be made.

First, ethylene hydrogenation to ethane is both facile and selective at room temperature in the presence of transition metal surfaces. Groups 8-10 metals are the most active hydrogenation catalysts among the pure metals [5,6]. Studies with deuterium show that hydrogenation is accompanied by H,D-exchange in both the reactant deuterium and ethylene [4]. The hydrogenation kinetics are generally 1st order in hydrogen pressure, 0 or negative order in ethylene, and independent of the product ethane. When ethylene hydrogenation is studied by different experimentalists using different forms of catalysts, measured activation energies can range from 4-20 kcal/mol [4], even for the same metal; when a single experimentalist studies the same form of catalyst, all metals show similar activation energies for hydrogenation and the rate variation between metals is due to differences in preexponential factors [5,7].

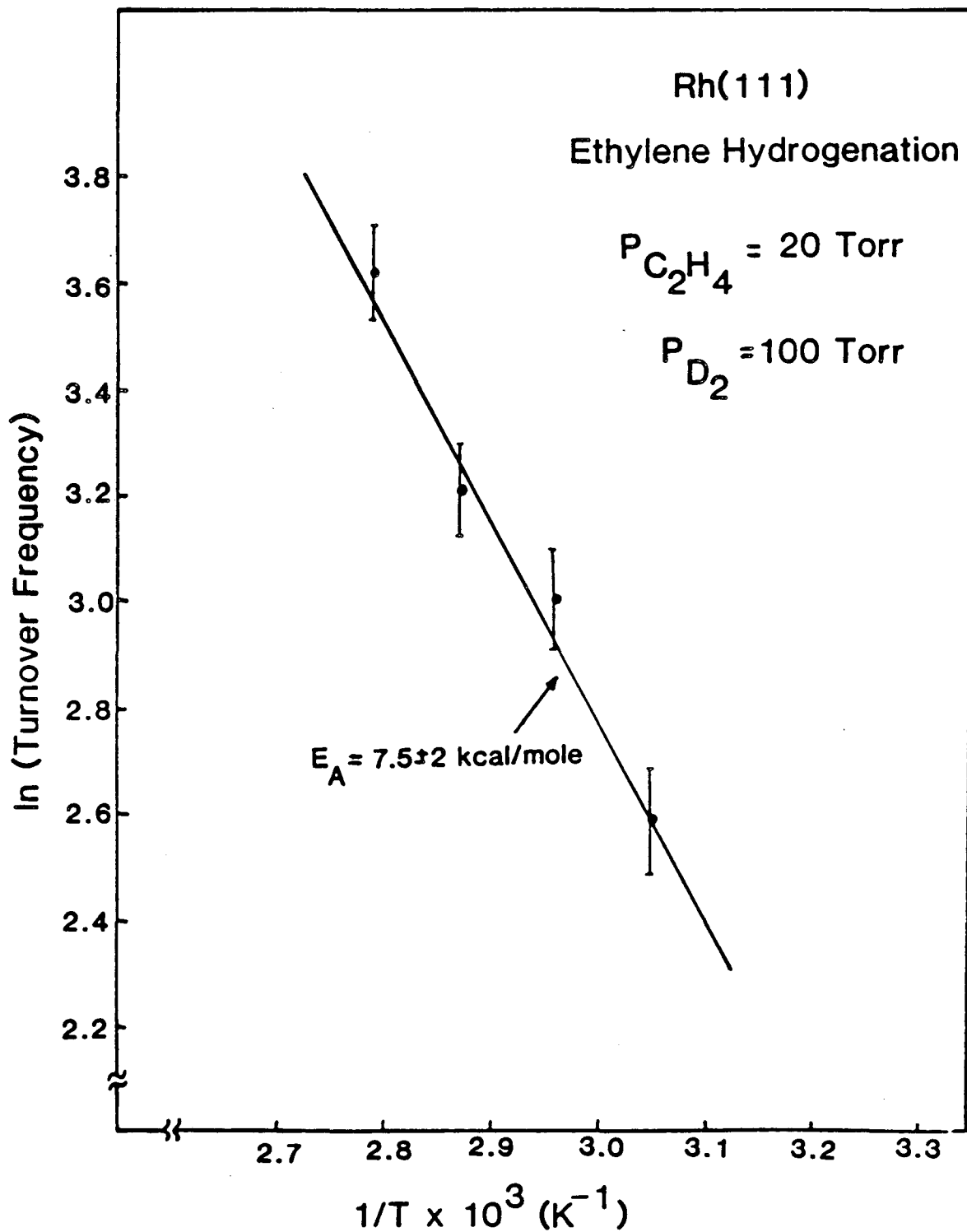
A significant observation by Horiuti and Miyahara in their review of ethylene hydrogenation over metallic catalysts [8] was that, while the form of the metal catalyst has little effect on hydrogenation

activity, catalyst preparation can have dramatic effects. This observation is particularly interesting, since active hydrogenation catalysts are covered with strongly bound hydrocarbon species [4] whose bonding to the surface could be dramatically altered by catalyst pretreatments. The experimental results here support this hypothesis.

In this section, studies of the structure and role of the adsorbed monolayer on Pt(111) and Rh(111) surfaces during ethylene hydrogenation are presented. The effects of catalyst pretreatments are detailed in Section 5.2. The results for Rh(111) are emphasized, since many of the analogous results for Pt(111) have already been published [9,10,23]

5.1.2 Results and Interpretation. Kinetics. The rate of ethylene hydrogenation over Rh(111) surfaces was measured from 300–390 K with 20 torr of ethylene and 20–100 torr of H₂ or D₂. The rates were reproducible to ±15%. It was found that the presence of any carbon monoxide in the reaction mixture (CO was a contaminant in the H₂) severely poisoned the reaction below 360 K. Figure 5.1 shows an Arrhenius plot for four hydrogenation reactions with 20 torr of ethylene and 100 torr of D₂ from 300 to 360 K in the absence of contaminating CO. The measured activation energy is 7.5 ± 2 kcal/mol. The dependence of the hydrogenation rate on reactant pressures was not determined, but the rate does increase with increasing hydrogen pressure.

This limited kinetic data for ethylene hydrogenation over Rh(111) is compared with extensive studies over Pt(111) [9] and with published results for high-surface-area Rh catalysts [17,18] in Table 5.1. Rh(111) surfaces appear to be good models for hydrogenation catalysts,



XBL 8610-4108

Fig. 5.1 Arrhenius plot of $\ln(\text{rate})$ vs $1/T$ for ethylene hydrogenation over Rh(111) from 300 to 360 K.

Table 5.1: Kinetic Parameters For Ethylene Hydrogenation Over Platinum And Rhodium Catalysts

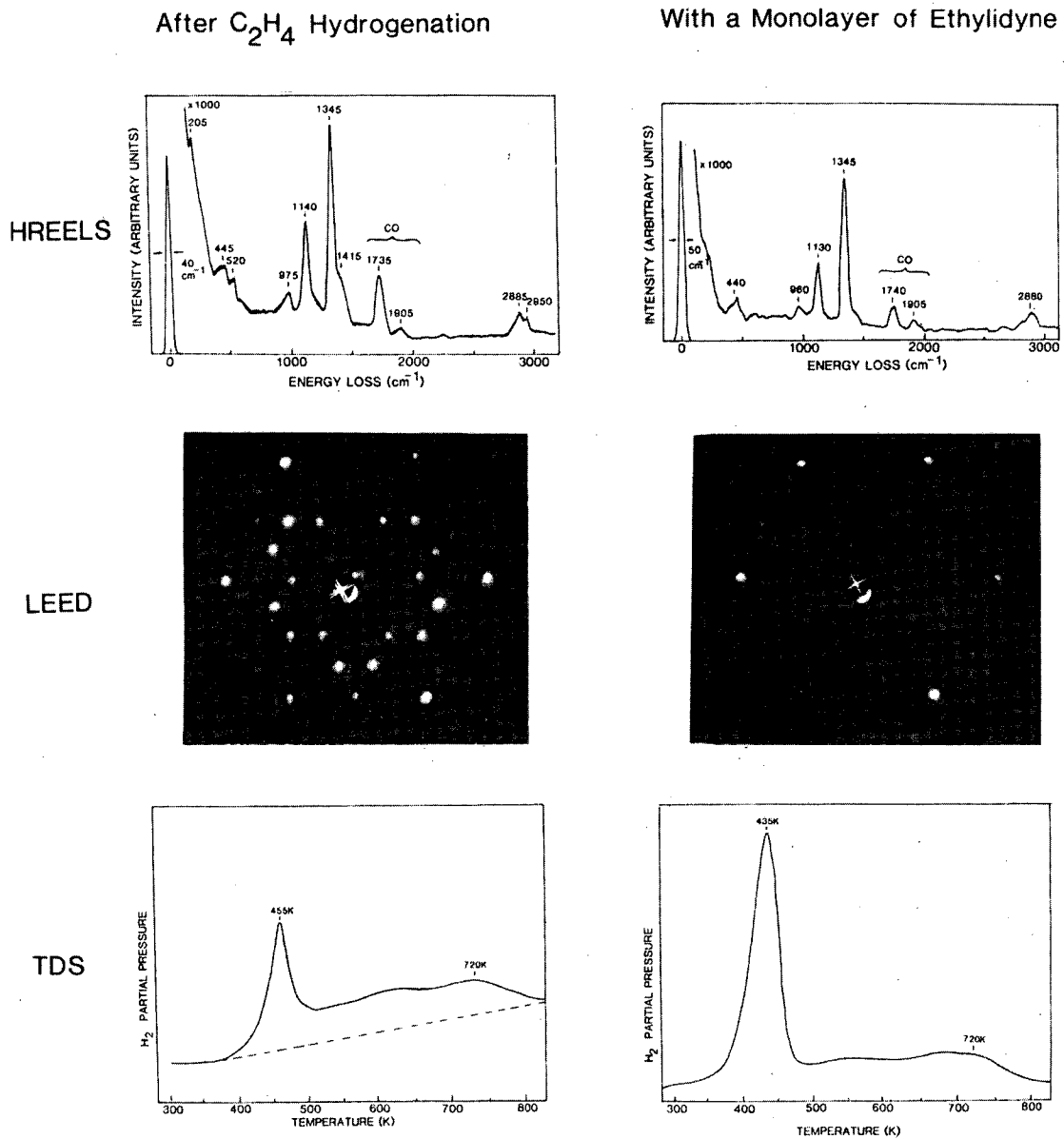
Catalyst	Reaction Temp. (K)	Order in Ethylene	Order in Hydrogen	E _A (kcal/mole)	Authors
Platinized Foil	275 - 350	-0.8	1.3	10	Farkas, Farkas 1938 [11]
Pt Foil	345 - 400	---	---	4.5	Rienacker, Muller Burmann 1943 [12]
Pt Wire	< 500	-.5	1.2	20	Kazanskii, Strunin 1960 [13]
1%Pt/Al ₂ O ₃	255 - 325	-.5	1.2	9.9	Bond 1956 [14]
Pt/SiO ₂	----	.25	.77	8.4	Schuit, Reijen 1958 [15]
.05% Pt/SiO ₂	320 - 365	0	.5	16	Sinfelt 1964 [16]
Pt(111)	300 - 370	-.6	1.31	10.8	Zaera, Somorjai 1984 [9]
Rh/Al ₂ O ₃	255 -380	0	1	12±2	Bond, et al 1966 [17]
Rh Evaporated Film	150 - 170	---	- -	7	Kenball 1956 [18]
Rh(111)	300 - 370	---	> 0	7.5±2	Bent, Somorjai 1986 [this work]

since the measured activation energy for Rh(111) is equivalent to that measured for Rh films [18]. A more extensive comparison between the kinetic parameters for Pt(111) and those for high surface area Pt catalysts also shows a close correspondence [9]. The absolute rates over Rh(111) are comparable to those found for Pt(111).

Adsorbed Monolayer Structure. Auger electron spectra of either Pt(111) or Rh(111) surfaces after pumping out the reaction mixtures and returning the single crystal catalysts to UHV show that the surface has about half a monolayer of carbon (one carbon per two metal atoms) and sometimes a fraction of a monolayer of contaminant sulfur. Nearly 100% of this carbon is partially hydrogenated and, as shown below, exists on the surface as ethylidyne (CCH_3) species. Figures 5.2 and 5.3 compare the surface HREEL spectra, LEED patterns and thermal desorption spectra for Rh(111) and Pt(111) after ethylene hydrogenation with the analogous fingerprints for ethylidyne. The Rh(111) results are discussed first.

The HREEL spectra in Fig. 5.2 definitively show that ethylidyne species cover the Rh(111) surface after hydrogenation. The spectrum after reaction is nearly identical to that for a saturation coverage of ethylidyne and shows characteristic $\nu(\text{CC})$ (1140 cm^{-1}), $\delta_s(\text{CH}_3)$ (1345 cm^{-1}), and $\nu_s(\text{CH}_3)$ (2885 cm^{-1}) vibrational frequencies and intensities. The only differences between the ethylidyne and after-reaction vibrational spectra are: (1) slightly more coadsorbed carbon monoxide ($\nu(\text{CO}) = 1735, 1905 \text{ cm}^{-1}$) after reaction, (2) a small, unidentified peak near 520 cm^{-1} and (3) a shoulder, possibly due to sulfur atoms,

Rh(111) Surface:



XBB 850-9415

Fig. 5.2 Evidence for the presence of ethylidyne (CCH₃) on the Rh(111) surface after ethylene hydrogenation at atmospheric pressure over this surface. High-resolution electron energy loss spectroscopy (HREELS), low-energy electron diffraction (LEED), and thermal desorption spectroscopy (TDS) data for ethylidyne are compared with the results of these techniques on Rh(111) after catalytic ethylene hydrogenation and transfer of the crystal to UHV. The differences in the LEED patterns are due to coadsorbed CO on the surface after reaction.

EVIDENCE FOR THE PRESENCE OF ETHYLIDYNE AFTER
ATMOSPHERIC HYDROGENATION OF ETHYLENE OVER Pt (111)

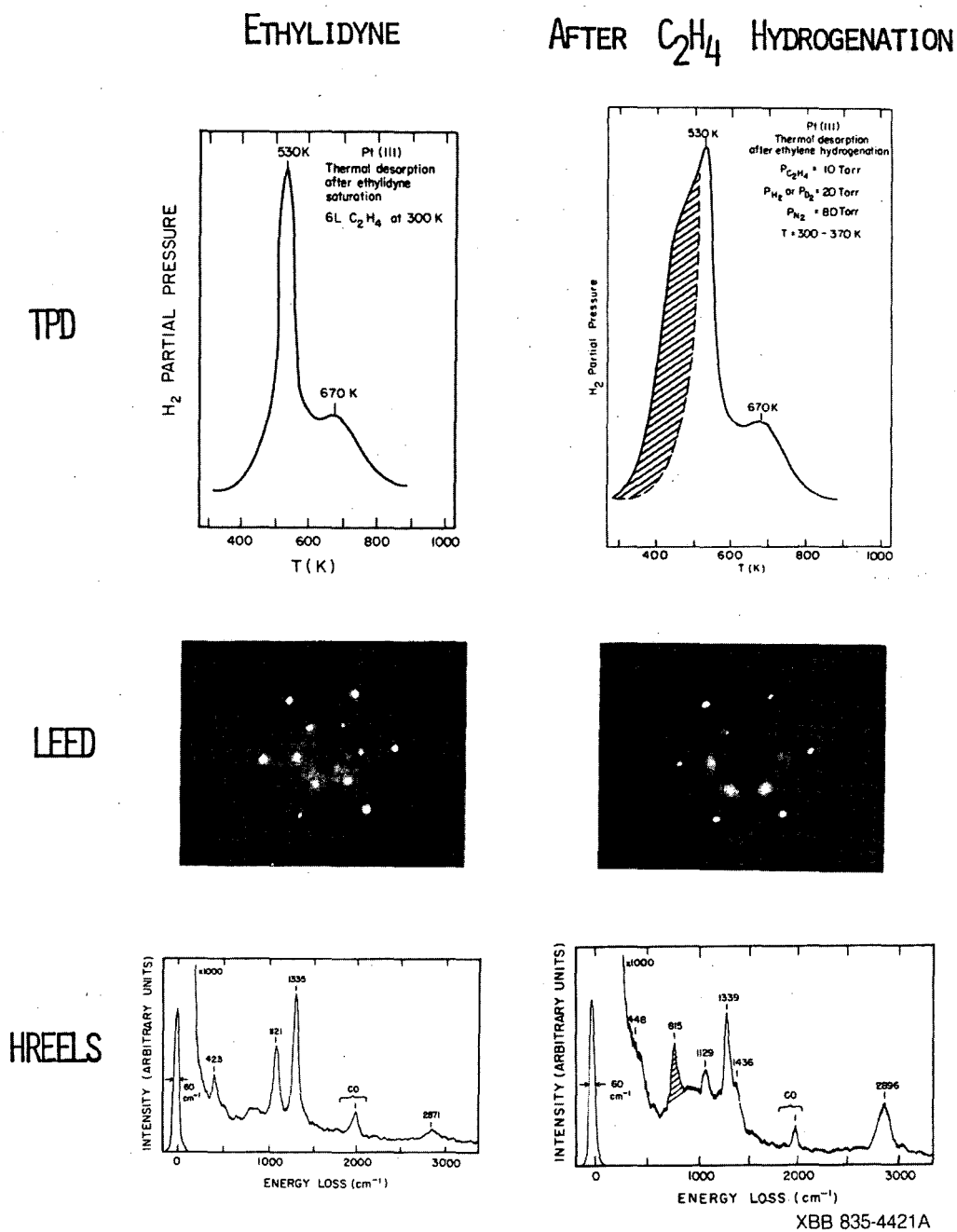


Fig. 5.3 Evidence for the presence of ethylidyne on Pt(111) after catalytic ethylene hydrogenation at atmospheric pressure. The results are analogous to those in Fig. 5.2. The shaded regions in the TD and HREEL spectra are due to another hydrocarbon fragment that is coadsorbed with ethylidyne. These shaded peaks are absent after some reactions.

at 205 cm^{-1} . The surface LEED pattern after reaction, as shown in Fig. 5.2, is different from that for an ethylidyne monolayer at 300 K, but is characteristic of a monolayer of ethylidyne coadsorbed with some CO as was discussed in Section 3.2.

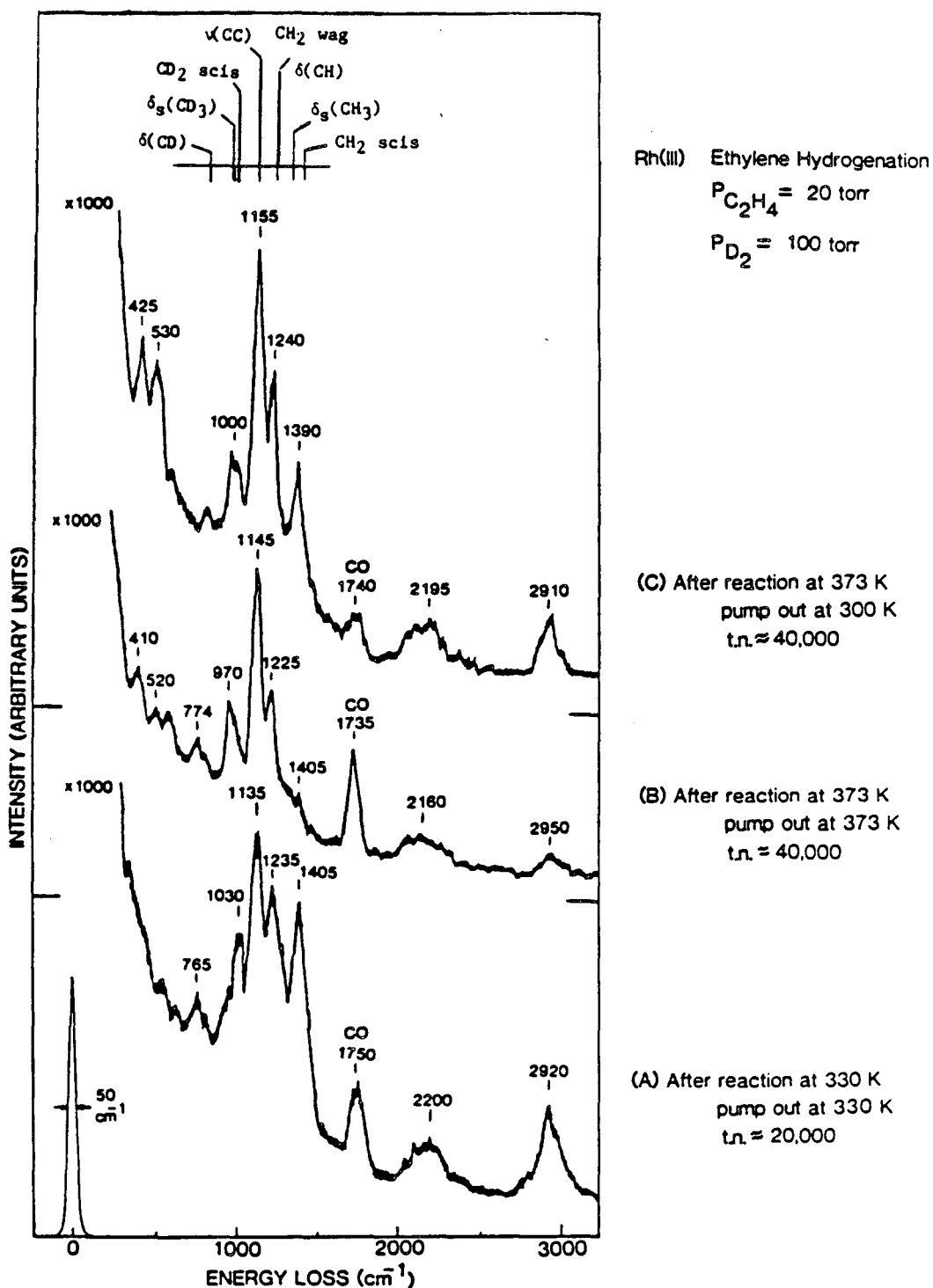
The H_2 TD spectra shown in Fig. 5.2 for Rh(111) after reaction and for Rh(111) saturated with ethylidyne in UHV are similar except for a smoothly increasing H_2 background that comes from the Ta supports after the catalytic reaction. The 430 K H_2 thermal desorption peak results from decomposition of ethylidyne to C_xH species [Section 3.5]. These C_xH species then dehydrogenate from 500–800 K giving the broad, high-temperature H_2 desorption. Hydrogen bound directly to the Rh(111) surface during the catalytic reaction desorbs at room temperature [20] during pumping out the reaction mixture and is not observed in the thermal desorption.

The results for Pt(111) in Fig. 5.3 are analogous to those for Rh(111), except that the shaded regions in the HREEL and TD spectra are due to some hydrocarbon fragment in addition to ethylidyne. The identity of this species cannot be determined from these data, but molecular ethylene can be ruled out as a possibility [21]. Note also that small amounts of coadsorbed CO on Pt(111) do not affect the (2x2) ethylidyne LEED pattern. This may be a consequence of the fact that ethylidyne bonds to fcc hollow sites on Pt(111) and to hcp hollow sites on Rh(111) [Section 3.1].

Saturation coverages of ethylidyne species are present on Pt(111) and Rh(111) surfaces after ethylene hydrogenations for all reaction and

evacuation temperatures between 300 and 390 K. However, the exchange of the methyl group hydrogens with surface H atoms changes with reaction and evacuation temperatures. This exchange is illustrated for Rh(111) in Fig. 5.4 which shows HREEL spectra after hydrogenation reactions with deuterium. These spectra, taken for different reaction and evacuation temperatures, are due to partially deuterated ethylidyne species; they were assigned as indicated on the spectra using the vibrational frequencies predicted by normal coordinate analysis and given in Table 4.1. The predominant surface species are: CCH_2D and CCHD_2 after reaction and evacuation at 330 K, CCD_3 after reaction and evacuation at 373 K, and $\text{CCD}_3 + \text{CCD}_2\text{H}$ after reaction at 373 K and evacuation at 300 K. This shows that while ethylidyne remains on the surface after all reactions between 300 and 390 K, the amount of deuterium incorporated in the methyl group increases with both higher reaction and higher evacuation temperatures.

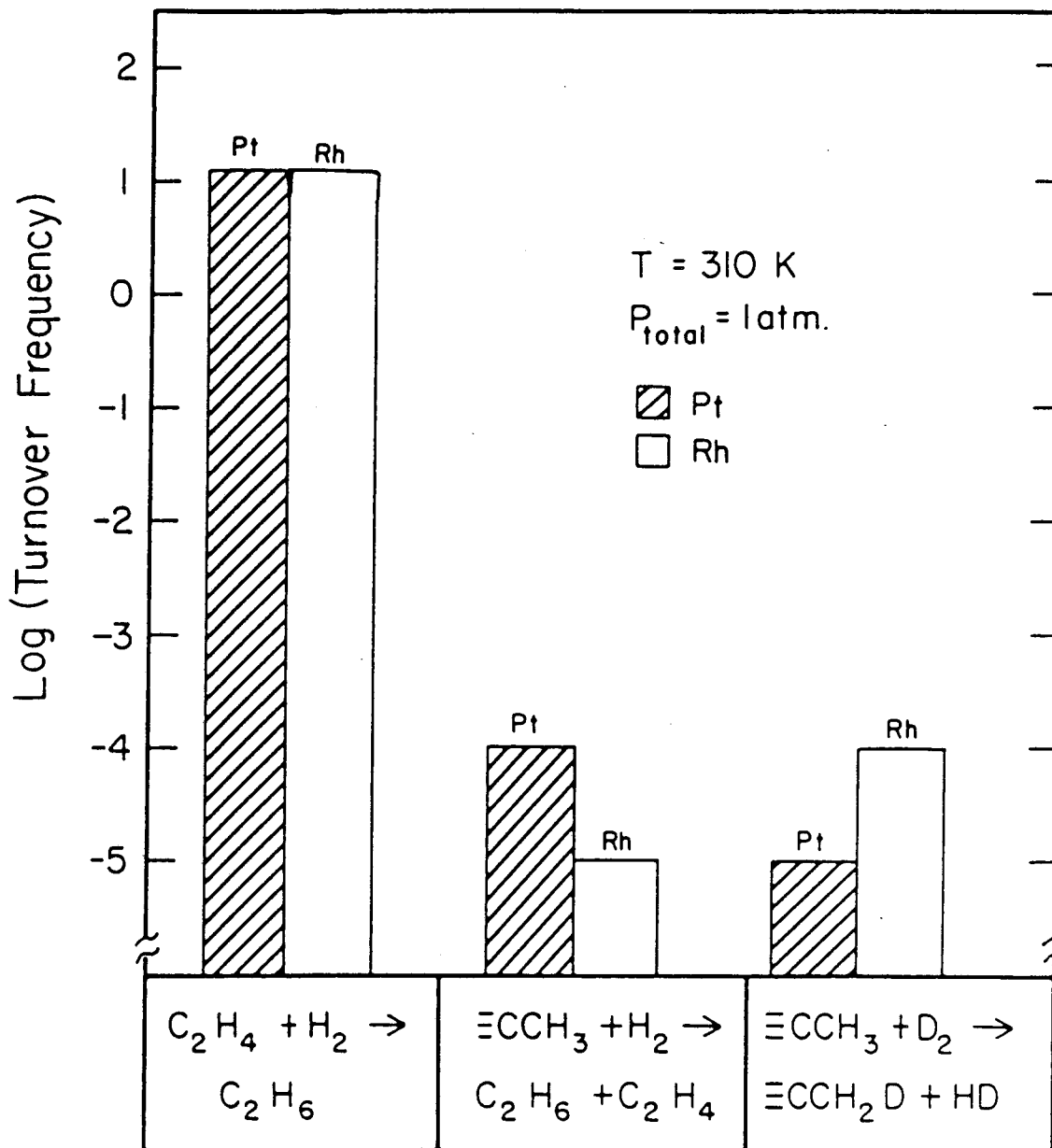
Role of the Adsorbed Monolayer. The first question that must be answered about catalyst monolayer structure determined after evacuation of the reactants is, "Does the transfer to UHV change the structure of the active, steady state catalyst?" This can be determined by restart reactions and isotope labelling. For ethylene hydrogenation it was found that preadsorption of a saturation coverage of ethylidyne (one ethylidyne/4 surface metal atoms) does not affect the hydrogenation rates to within the $\pm 15\%$ uncertainty in the rates. Further, as shown in Fig. 5.5, the rates of ethylidyne hydrogenation and removal from the surface and the rates of H,D exchange in the ethylidyne methyl



XBL 8610-4116

Fig. 5.4 Effects of reaction and evacuation temperature on the H,D-exchange in the ethylidyne species which remain after catalytic hydrogenation of C_2H_4 with D_2 . These HREEL spectra show that the amount of exchange in the methyl group increases with increasing reaction and evacuation temperature.

Comparison of Hydrogenation Rates
over Pt(III) and Rh(III) Single-Crystal Surfaces



XBL 846-2487

Fig. 5.5 Comparison of the rates of catalytic ethylene hydrogenation, ethylidyne rehydrogenation and ethylidyne H,D-exchange over Pt(III) and Rh(III). These rates show that ethylidyne cannot be an intermediate in the catalytic hydrogenation of ethylene at room temperature.

group on both Pt(111) [10] and Rh(111) [Section 4.2] are 10^4 - 10^6 times slower than the catalytic ethylene hydrogenation rate. In fact, a saturation coverage of CCH_3 is so stable, that such a monolayer can be exposed to an atmosphere of air without appreciable degradation. These results show that (1) any structural changes during transfer of the working catalyst to UHV must be reversible and (2) the strongly bound carbon (existing as ethylidyne in UHV) is not a hydrogenation intermediate but instead is a part of the catalyst.

To confirm these results, an ethylene hydrogenation was run with 20 torr C_2H_4 and 100 torr H_2 over a Rh(111) surface presaturated in UHV with CCD_3 . After running the hydrogenation to a turnover number of 500 (500 ethane molecules produced per surface Rh atom) at 300 K, the HREEL spectrum shown in Fig. 5.6 was obtained. This spectrum, like those in Fig. 5.4, was assigned as indicated using the calculated frequencies given in Table 4.1 for variously deuterated ethylidynes. The predominant adsorbed species are CCHD_2 , CCH_2D and CCH_3 . The presence of deuterium in the ethylidyne species after 500 turnovers confirms that ethylidyne is not the predominant hydrogenation intermediate at this temperature and that the methyl group hydrogens are not involved in the predominant reaction mechanism.

The effect of ethylidyne on hydrogen and ethylene adsorption on the surface was also determined. Published TD spectra have shown that while a monolayer of ethylidyne on Pt(111) hinders hydrogen adsorption, up to a quarter monolayer of hydrogen can be adsorbed and dissociated between the ethylidynes at 1 atm pressure [22,23]. This is consistent

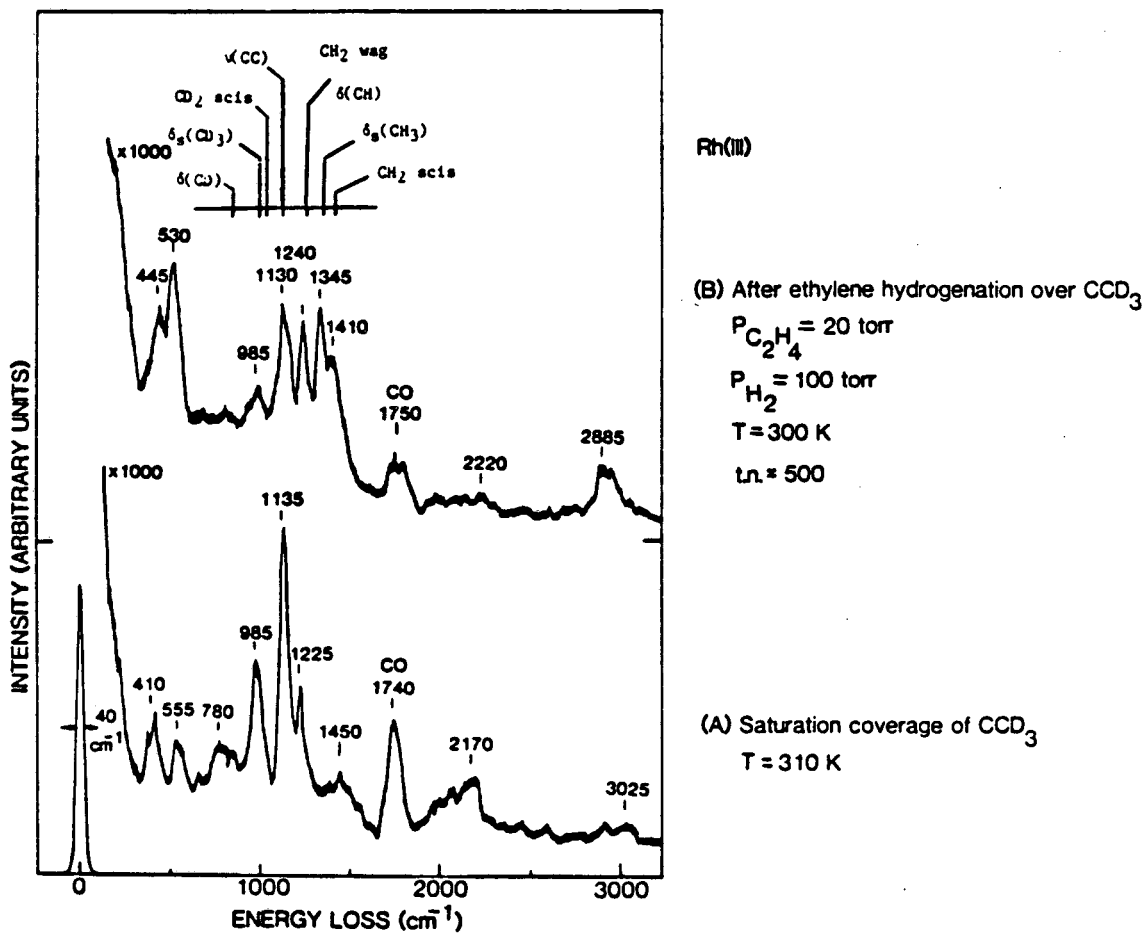


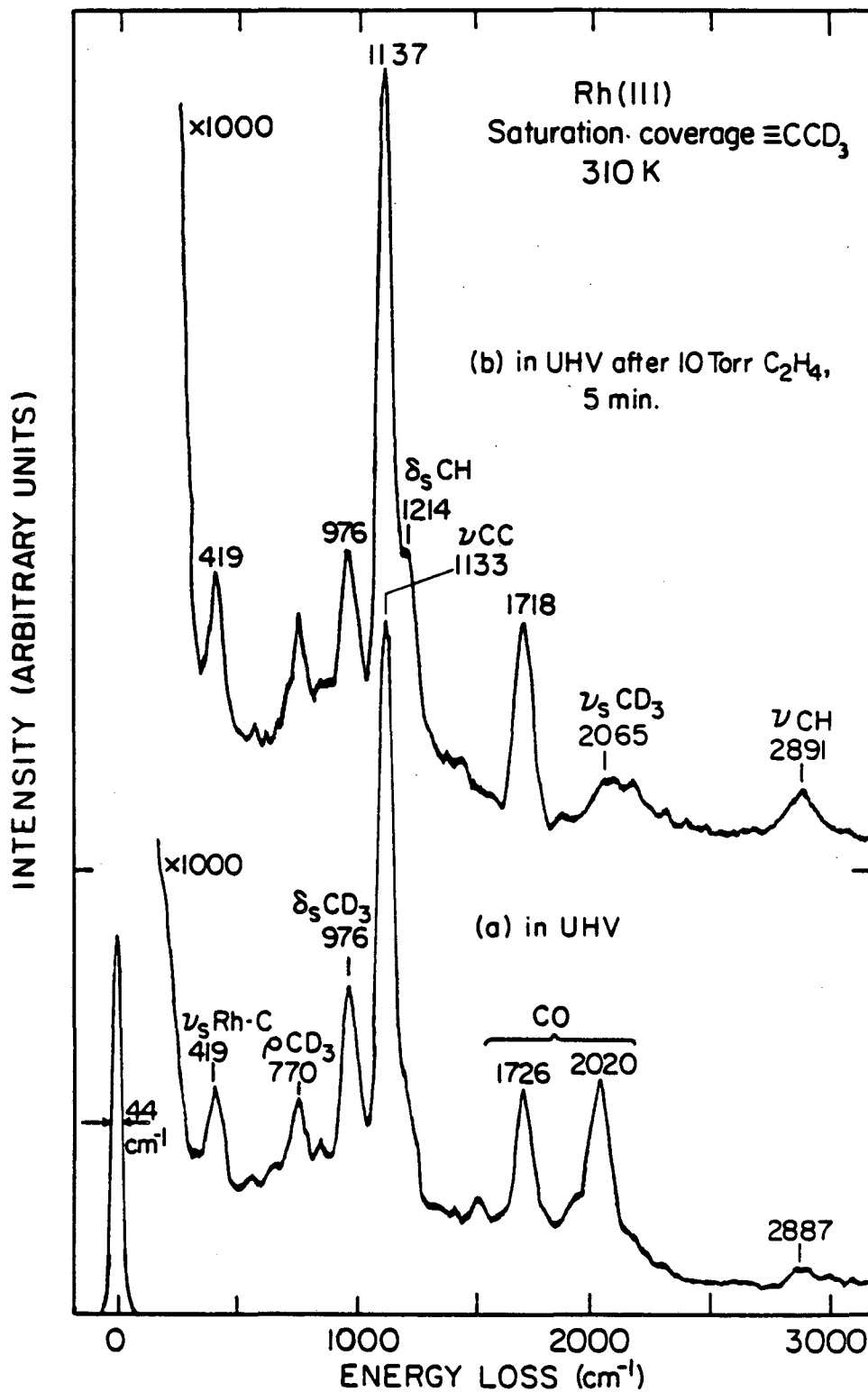
Fig. 5.6 HREEL spectra of a Rh(111) surface (A) saturated with CCD_3 and (B) after catalytic ethylene hydrogenation over this monolayer to a turnover number of 500. The presence of deuterium in the surface monolayer after reaction confirms that ethylidyne is not a hydrogenation intermediate.

XBL 8610-4089

with the amount of vacant space between the methyl groups in the (2x2) structure. However, HREELS and TDS experiments show that ethylene can only be physisorbed on Pt(111) and Rh(111) surfaces covered with ethylidyne. Figure 5.7 shows the Rh(111) HREEL spectra for a CCD_3 monolayer before and after treatment with 20 torr of C_2H_4 . There is no evidence for either CCH_3 ($\delta_s(\text{CH}_3) = 1330 \text{ cm}^{-1}$) or molecularly adsorbed C_2H_4 (CH_2 "wag" $\cong 980 \text{ cm}^{-1}$, CH_2 "scissor" $\cong 1430 \text{ cm}^{-1}$). This shows not only that C_2H_4 must be weakly adsorbed, but also that gas phase ethylene cannot displace adsorbed ethylidyne. The low heat of adsorption of ethylene on top of ethylidyne was confirmed for both Rh(111) and Pt(111) by exposing saturation coverages of ethylidyne in UHV to 20 L of C_2H_4 at 100 K; no molecular ethylene was detected in a subsequent TDS. This observation places an upper limit on the heat of adsorption of ethylene on top of ethylidyne at about 10 kcal/mol.

5.1.3 Discussion. These results for Pt(111) and Rh(111) support and clarify many of the observations made over the last 35 years about the surface composition of evaporated metallic film catalysts. Evaporated films, pioneered by Otto Beeck in the 1950's, have proven to be the cleanest and most reproducible surfaces prepared outside of UHV. Using these films as catalysts, it was found by a number of groups that:

- (1) Ethylene dissociates when adsorbed at room temperature on clean metal films of Pt [24], Ir [25], and Ni [5,7,26], as evidenced by the "self-hydrogenation" of ethylene to produce ethane.



XBL846-7108

Fig. 5.7 HREEL spectra of (A) a CCD_3 monolayer on Rh(111) and (B) the monolayer that remains after treatment with 10 torr of C_2H_4 for 5 min. These spectra show that no more ethylidyne can be adsorbed in a saturation monolayer of ethylidyne using atmospheric pressures of ethylene and that ethylidyne is not displaced by ethylene.

- (2) The stoichiometry of the dissociatively adsorbed ethylene varies depending on the metal, temperature of adsorption, and amount of evacuation. Stoichiometries of $C_2H_{3.6-3.9}$ on Ir at 373 K [25] and $C_2H_{0.8}$ on Ni at 300 K [5] have been reported.
- (3) The coverage of dissociatively adsorbed ethylene is 15% of the number of surface atoms on Pt [24] and Ir [25] assuming that H atoms adsorb at 100% coverage.
- (4) Dissociatively adsorbed ethylene during ethylene hydrogenation was inferred from mass balance studies over Ni films [27].
- (5) Preadsorption of ethylene had little effect on the hydrogenation rates over Pt and Rh films, but did decrease the hydrogenation rate over Ni and severely poisoned Ta and W [7].
- (6) The rate at which dissociatively adsorbed ethylene is hydrogenated from the catalyst surface is slower than the catalytic hydrogenation rate for Rh [5,28] and Pt [24,28] films.
- (7) Adsorbed ethylene hinders, but does not prevent, H_2/D_2 exchange over Ni surfaces [29].

These observations are consistent with the more detailed spectroscopic results here on the presence and stability of ethylidyne on active Pt(111) and Rh(111) catalysts.

Recent spectroscopic studies show that ethylidyne also forms on high surface area metallic catalysts. NMR studies of Pt particles supported on alumina show that ethylene adsorbs at room temperature to form ethylidyne [30]. FTIR spectroscopy of supported Pt, Pd, Rh, and Ru particles exposed to ethylene shows that ethylidyne forms on these

surfaces as well [31-33]; H-D-exchange in ethylidyne was detected on the supported Pd surface [31].

The question arises whether these ethylidyne species are an unavoidable poison or do they play some peripheral role in the ethylene hydrogenation mechanism. One possibility, which cannot be ruled out, is that a small percentage of sites not covered with ethylidyne and not spectroscopically detectable do all the catalysis. The major arguments against this possibility are the reported structure insensitivity of hydrogenations [34] and statistical mechanical calculations showing that the number of active sites/cm² on ethylene hydrogenation catalysts is $\sim 10^{15}$ [39]. Since surface atomic densities are also $\sim 10^{15}$ atoms/cm² this suggests that the entire surface is catalytically active.

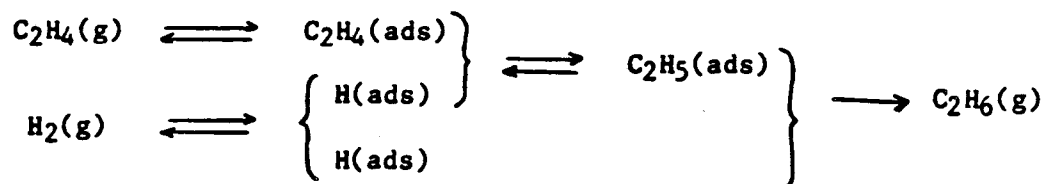
Reaction over the entire surface was assumed in previous discussions of the role of ethylidyne in ethylene hydrogenation over Pt(111) [9,10]. It was also assumed in these discussions that ethylene could not reach the surface (for example by diffusion of ethylidyne species) to react directly with surface H atoms. Inspired by the suggestion of Thomson and Webb that the hydrogen for ethylene hydrogenation may come from a C-H bond rather than a metal-hydrogen bond [40], it was proposed [9,10] that surface hydrogen is transferred up to ethylene adsorbed in a second layer on top of ethylidyne via ethylidene (CHCH₃) species (Fig. 5.12 in Section 5.2). There is no direct evidence for ethylidene, but such a species has been previously proposed on Pt(111) [55,22] and Rh(111) [56] to explain the observed surface chemistry of

ethylene and ethylidyne. The attractive features of this second layer hydrogenation mechanism are that it can explain:

- (1) the observation that ethylidyne species block ethylene adsorption directly on the metal surface but ethylene can still be catalytically hydrogenated in the presence of saturation coverages of ethylidyne.
- (2) why the measured activation energies for ethylene hydrogenation directly on Pt(111) surfaces in UHV [22] and at Pt electrodes free of carbonaceous deposits in solution [10] are ~5 kcal/mol lower than for Pt(111) single crystals covered with ethylidyne [9].
- (3) the pressure dependences of the hydrogenation kinetics which are consistent with this type of Eley-Rideal mechanism [5].

Such a 2nd layer mechanism does not, however, explain why the measured activation energy over Rh(111) is 1-5 kcal/mol lower than for Pt(111). Also, this second layer mechanism was originally drawn as a concerted reaction between gas phase ethylene and two ethylidene species [10]. Both the observed H,D exchange in ethylene [9] and the large separation between two such ethylidenes on the surface, suggest that the reaction cannot be concerted. However, sequential addition in a second layer generates a gas phase C₂H₅ radical. Simple bond energy arguments show that this process is probably >15 kcal/mol endothermic — 50% larger than the measured activation energy. Thus, it appears that partial hydrogenation of ethylene to C₂H₅ (either by surface hydrogen or hydrogen in a C-H bond) can only be thermodynamically favored if the ethyl radical can bond to the surface.

Based on these simple arguments, the most logical ethylene hydrogenation mechanism is still that proposed by Horiuti and Polanyi in 1934 [41]:



The results here for Pt(111) and Rh(111) suggest that an adsorbed C_2H_5 species is either very sterically crowded between ethynyl species or that it bonds at small percentage of defect sites on the surface. These points are considered in more detail in Section 5.2.

5.2 Effects of Surface Modification on Catalytic Ethylene Hydrogenation Over Rh(111) Surfaces

5.2.1 Background. One way to determine the roles that the metal surface and the adsorbed carbonaceous overlayer play in ethylene hydrogenation is to alter them in a controlled fashion and observe the effects on the reaction kinetics. For example it was shown in the previous section that clean and ethylene-pretreated Rh(111) and Pt(111) surfaces have the same hydrogenation kinetics. This is because ethylidyne species form on the surface in both cases. In this section, studies of the effects of surface sputtering, CO adsorption, and adsorption of C_xH species on ethylene hydrogenation over Rh(111) are reported.

5.2.2 Results and Interpretation. a) Surface Sputtering. To determine whether a specific type of surface site is required for catalysis, the reaction rates for annealed and sputtered Rh(111) surfaces were compared. A Rh(111) surface was sputtered for 30 min with a 1 kV Ar^+ ion beam (6 μ A current to ground) so that LEED showed large, diffuse spots. Ethylene hydrogenation at 368 K over this surface gave rates approximately the same as for an annealed Rh(111) surface. Also, like the annealed surface, the surface species after reaction (as determined by HREELS) were ethylidyne. This result suggests that the ethylene hydrogenation rate and mechanism are not sensitive to metal structure.

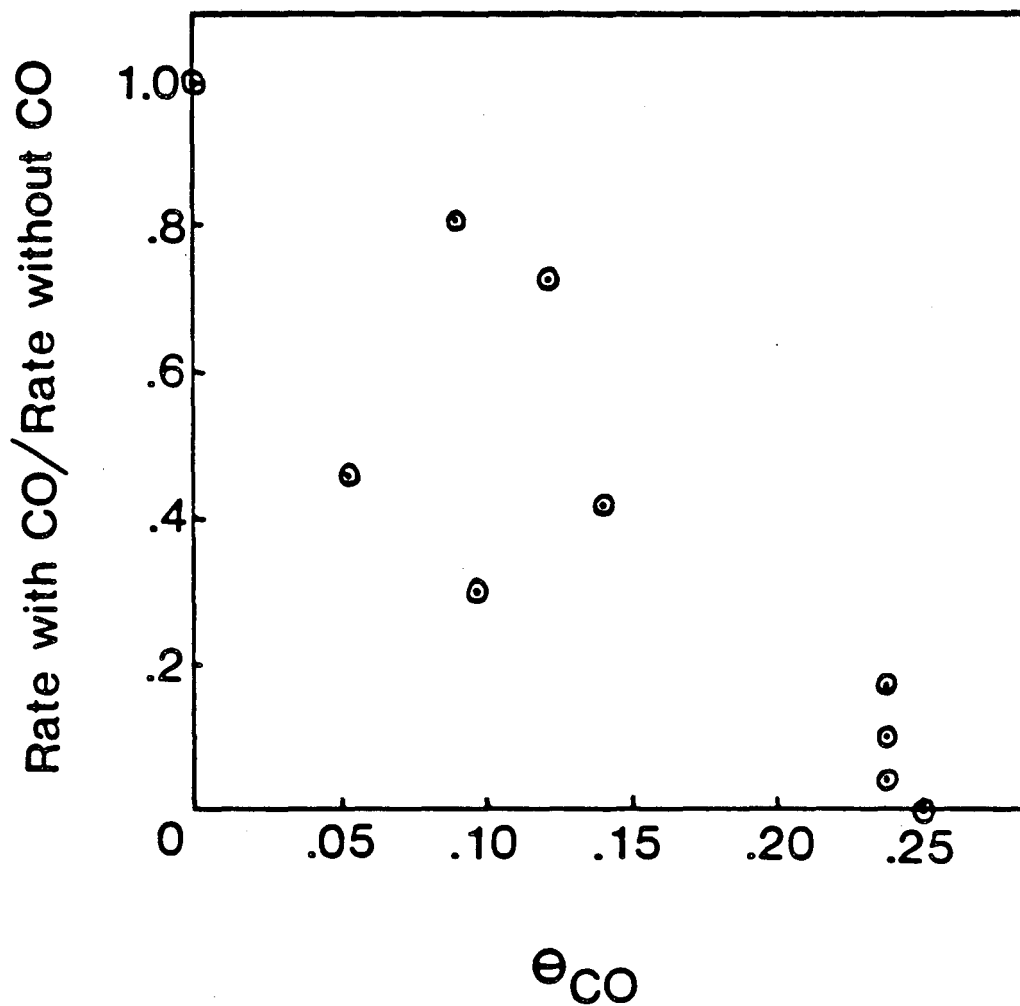
However, recent ethylene hydrogenation studies over a Rh foil [42] gave turnover frequencies a factor of 25 higher than found here for

Rh(111). Also, structure sensitivity has been reported for hydrogenations of a number of larger alkenes [35-38, 43]. Work is in progress with stepped and kinked Rh single crystal surfaces to test the structure insensitivity of ethylene hydrogenation.

b) CO Adsorption. As mentioned in Section 5.1, trace amounts of CO poison ethylene hydrogenation over Rh(111). HREEL vibrational spectra after poisoned reactions showed, in addition to ethylidyne, carbon monoxide bound to the surface with a predominant CO stretching frequency at $\sim 1825 \text{ cm}^{-1}$ and a much smaller peak at $\sim 1950 \text{ cm}^{-1}$. This CO coadsorbed with ethylidyne also results in a $c(4 \times 2)$ LEED pattern for the post reaction monolayer.

As discussed in Section 3.2 (Fig. 3.10), the amount of coadsorbed CO can be determined from the HREEL spectrum by comparing the νCO peak height with the $\delta_s(\text{CH}_3)$ peak height. Figure 5.8 shows the correlation between CO surface coverage determined by this means and the ethylene hydrogenation rate normalized to the rate at 0 coverage of coadsorbed CO. Because of the scatter in the data, which probably results from changes in the amount of coadsorbed CO during evacuation of the reactants, it is not possible to determine a functional dependence of the reaction rate on CO coverage. However, if only a small fraction of the surface sites were catalytically active, the correlation between CO coverage and reaction rate would probably be highly nonlinear, with a sharp decrease in rate near either $\theta_{\text{CO}} = 0$ or 0.25. This is not the case, so it can be inferred that the majority of sites poisoned by CO are active in ethylene hydrogenation.

Correlation of CO Coverage and
Ethylene Hydrogenation Rate
Over Rh(111)



XBL 8610-4109

Fig. 5.8 Correlation of the rate of ethylene hydrogenation with the surface coverage of carbon monoxide after reaction. The scatter in the data may be due to adsorption or desorption of CO during evacuation of the reaction mixture.

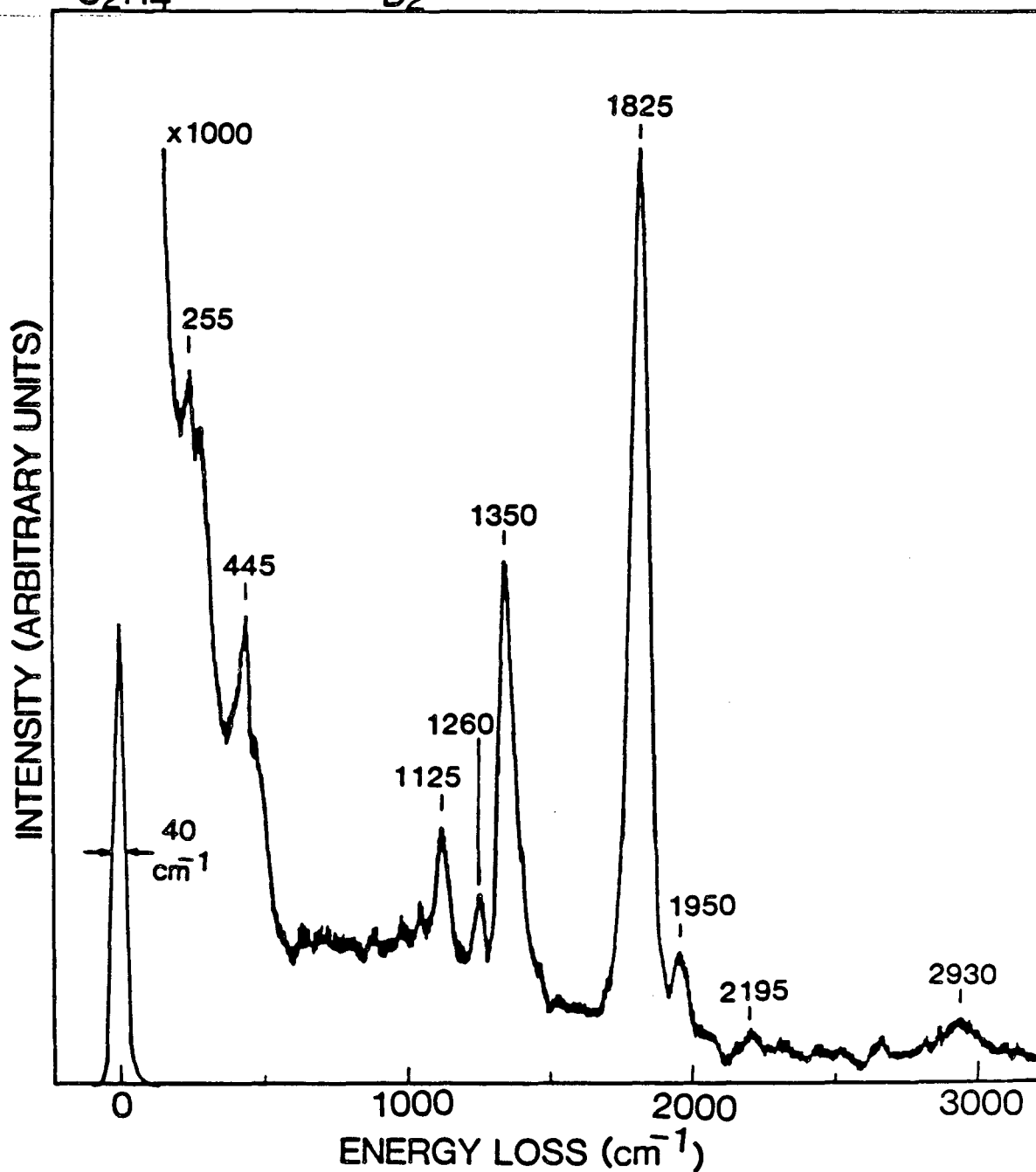
The poisoning effect of CO can be understood knowing the structure of the $c(4 \times 2)$ ethylidyne + CO monolayer. A top view of this densely packed structure is shown in Fig. 3.15. There is no room for H_2 adsorption and dissociation, a presumed prerequisite for ethylene hydrogenation. The role of the interstitial sites between ethylidyne species for hydrogen dissociation was tested by prepoisoning a Rh(111) surface with a $c(4 \times 2)$ monolayer of CO and ethylidyne. In a subsequent hydrogenation with 20 torr of ethylene and 100 torr of deuterium, no ethane was detected after 55 min at 318 K. The HREEL spectrum after reaction is shown in Fig. 5.9. All peaks are either due to ethylidyne or to CO except for the small peak at 1260 cm^{-1} due to a small amount of CCH_2D or $CCHD_2$. The lack of substantial H,D exchange in the methyl group (which occurs in the absence of CO (Fig. 5.4)) is evidence that D_2 is not dissociated in this monolayer.

c) Adsorption of Hydrocarbon Fragments. The effect of hydrocarbon species other than ethylidyne on ethylene hydrogenation was investigated by pretreating Rh(111) surfaces with ethylene above 500 K. Two series of experiments were performed with 20 torr C_2H_4 and 100 torr of H_2 ; the kinetic data and the surface vibrational spectra are shown in Fig. 5.10. First, the Rh (111) surface was pretreated with 30 L of C_2H_4 at 500 K in UHV to give a saturation coverage of C_xH species [Section 3.5], having the surface vibrational spectrum shown in Fig. 5.10A. A steady state hydrogenation rate was then established at 300 K over this surface and the catalyst heated sequentially to 318, 328 and 338 K to establish steady state rates at each temperature as shown in Fig. 5.10.

Rh(III)

After ethylene hydrogenation at 318 K completely poisoned
by preadsorption of an ethylidyne CO monolayer

$P_{C_2H_4} = 20$ torr $P_{D_2} = 100$ torr

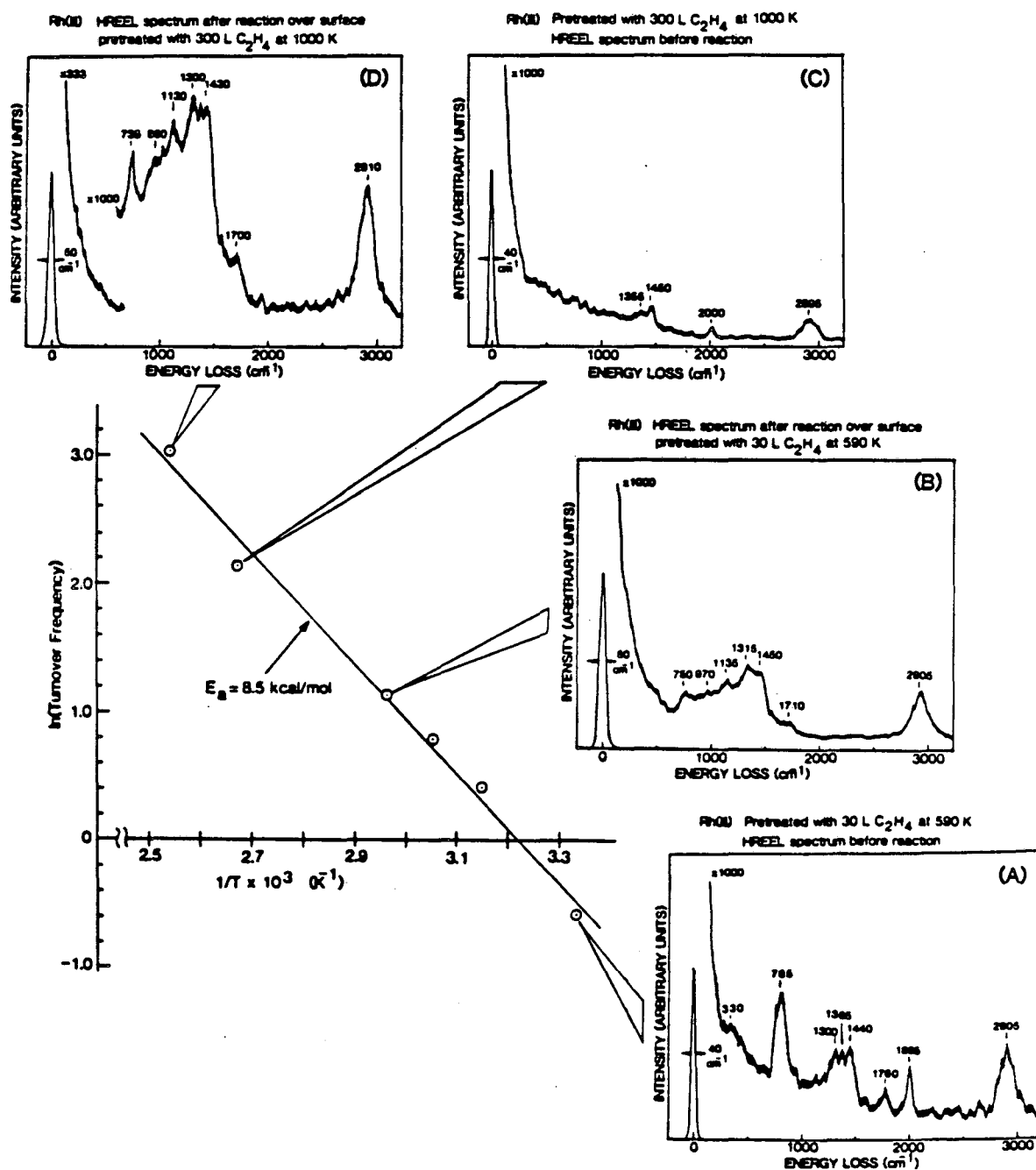


XBL 8610-4110

Fig. 5.9 HREEL spectrum showing the suppression in ethylidyne H,D-exchange during an ethylene hydrogenation poisoned by coadsorbed CO. This spectrum should be compared to that in Fig. 5.4A where almost no CO is coadsorbed.

Ethylene Hydrogenation Over Hydrocarbon Fragments on Rh(III)

$$P_{C_2H_4} = 20 \text{ torr} \quad P_{H_2} = 100 \text{ torr}$$



XBL 8610-4111

Fig. 5.10 Arrhenius plot and HREEL spectra for ethylene hydrogenation over C_xH and C_x fragments on Rh(III). HREEL spectra (A) and (C) are for the C_xH and C_x monolayers before reaction at the indicated temperatures. Spectra (B) and (D) were taken after establishing the indicated rates. Preadsorption of C_x or C_xH species results in similar kinetics and similar HREEL spectra after reaction.

The total conversion of ethylene to ethane in this sequence was 3%. The surface vibrational spectrum after reaction at 338 K is shown in Fig. 5.10B. The Rh (111) surface was then cleaned and pretreated with 300 L of C_2H_4 at 1000 K to give a saturation coverage of C_x species [Section 3.5], having the surface vibrational spectrum shown in Fig. 5.10C. After measuring the steady state hydrogenation rates first at 393 K and then at 413 K as shown in Fig. 5.10, the surface vibrational spectrum was again taken and is shown in Fig. 5.10D.

The most notable effects of the pretreatments are that (1) the hydrogenation rates decrease by 60% compared to clean or ethylidyne precovered Rh(111) surfaces, (2) the activation energy to within experimental uncertainty is unchanged, (3) ethylidyne is not reformed on the surface under reaction conditions below 400 K, (4) pretreatments with C_x or C_xH species give the same hydrogenation kinetics, and (5) both C_x and C_xH pretreated surfaces have similar, complex vibrational spectra after ethylene hydrogenation. The identity of the surface species remaining after ethylene hydrogenation over this partially hydrogenated carbon cannot be determined from the poorly resolved HREELS peaks. However, from the CH_x stretching frequencies at $\sim 2900\text{ cm}^{-1}$, the hydrocarbon fragments appear to be saturated. Also, based on the vibrational frequencies near 1400 cm^{-1} , some CH_2 groups (possibly in polymeric chains) are likely. There is no evidence for molecularly adsorbed ethylene; π -bonded ethylene generally has an intense CH_2 "wag" frequency near 950 cm^{-1} [Table 3.5].

Rh(111) surfaces can be even more severely poisoned by adsorbing 500 L of ethylene at 1100 K to form a graphitic overlayer. This surface gave hydrogenation rates that were a factor of 10–15 lower than for initially clean Rh(111) surfaces. Interestingly, the surface vibrational spectrum after reaction was similar to that found for the C_x and C_xH monolayers after reaction [Figs. 5.10B and D]; however the peaks for the graphitized surface were a factor of 5 less intense relative to the elastic peak. This decrease, in intensity, which roughly correlates with the rate decrease suggests that only that fraction of the surface covered by these hydrocarbon species is catalytically active; the majority of the surface is graphitized and inactive.

The observation that these hydrocarbon monolayers derived from C_x or C_xH species are less active than ethylidyne monolayers in ethylene hydrogenation can explain the "optimum temperature" for ethylene hydrogenation over Rh(111). As shown in the Arrhenius plot of Fig. 5.11, the ethylene hydrogenation rate for 20 torr of ethylene and 20 torr of hydrogen begins to decrease above 430 K. This optimum temperature is approximate, because the rates above 400 K are not steady state—they show a steady decrease with time. Such an optimum temperature is frequently reported for metallic ethylene hydrogenation catalysts [4,44,45].

In this case, the optimum temperature correlates with a change in the adsorbed monolayer structure on the Rh (111) catalyst. The HREEL spectrum after reaction above the optimum temperature is shown in Fig. 5.11B. There is little of the intense ethylidyne $\delta_s(CH_3)$ peak

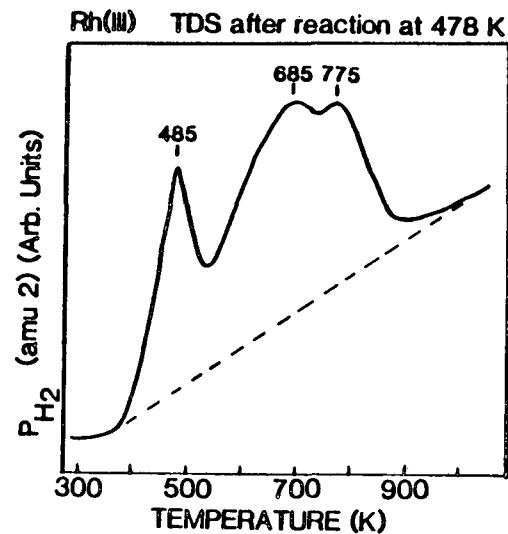
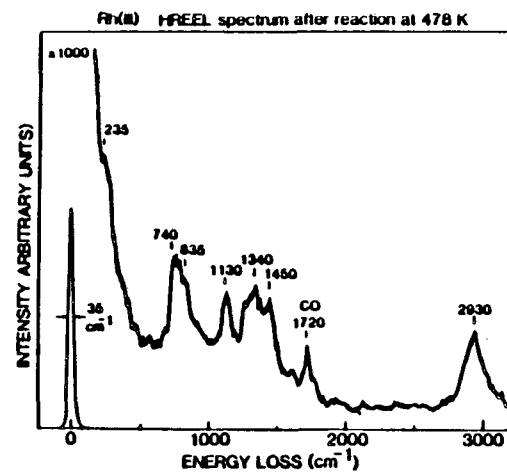
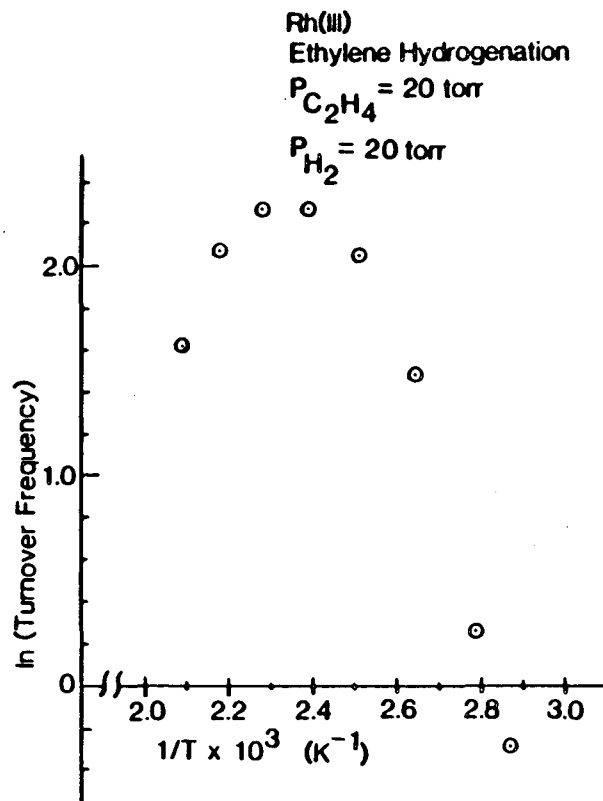


Fig. 5.11 Arrhenius plot showing the optimum temperature for ethylene hydrogenation over Rh(111) using 20 torr of ethylene and 20 torr of hydrogen. Also shown are the HREEL and TD spectra after the reaction at 475 K. Ethylidyne is no longer the predominant surface species after reaction above the optimum temperature. XBL 8610-4096

(1340 cm^{-1}). This species would be expected to form on any bare metal surface during cooling of the reaction mixture even if it is not stable above 430 K. Instead, the HREEL spectrum resembles those after reaction at lower temperature over surfaces prepoisoned by C_x and C_xH species (Fig. 5.10B and D). The H_2 TD spectrum taken after the HREEL spectrum in Fig. 5.11B is shown in Fig. 5.11C. It shows a much larger peak at (500 to 800 K) relative to the ethylidyne decomposition peak (485 K) and is also quite similar to the H_2 TD spectrum taken after hydrogenations prepoisoned by C_x species.

5.2.3 Discussion. The poisoning of ethylene hydrogenation by adsorbed CO, C_xH species and graphitic carbon can be attributed to blocking of hydrogen dissociation. In the case of CO, the blocking of hydrogen dissociation is inferred from the lack of H,D-exchange in surface ethylidyne during ethylene hydrogenations. In the case of preadsorbed C_xH fragments, the hydrogenation rate decreases without a change in the activation energy, also suggesting a decrease in the concentration of surface H atoms. (Note that ethylene hydrogenation is generally first order in P_{H_2} and zero or negative order in $P_{C_2H_4}$.) Comparison of the structure of CCH_3 with C_xH species shows why H_2 dissociation can be inhibited more by a C_xH monolayer. Ethylidyne stands up on the surface while C_xH species lie down [Section 3.5], blocking more surface sites. These conclusions are in accord with previous studies on the poisoning by carbonaceous layers of single crystal Pt catalysts used in hydrocarbon cracking and reforming reactions [46,47].

These conclusions are also consistent with the idea that the major requirement of hydrogenation catalysts is the ability to dissociate H_2 . For example, gold and metal oxide surfaces do not readily dissociate H_2 or hydrogenate ethylene. But on both surfaces, hydrogenation can occur if there is a source of H atoms. In the case of oxides, hydrogenation by hydrogen atom spillover from a neighboring noble metal surface is a well-documented phenomenon [48-50], while for gold it has been shown that cyclohexene can be hydrogenated by H atoms diffused through a Pd thimble [51]. The availability of H atoms appears to limit the hydrogenation rate to a large extent [4].

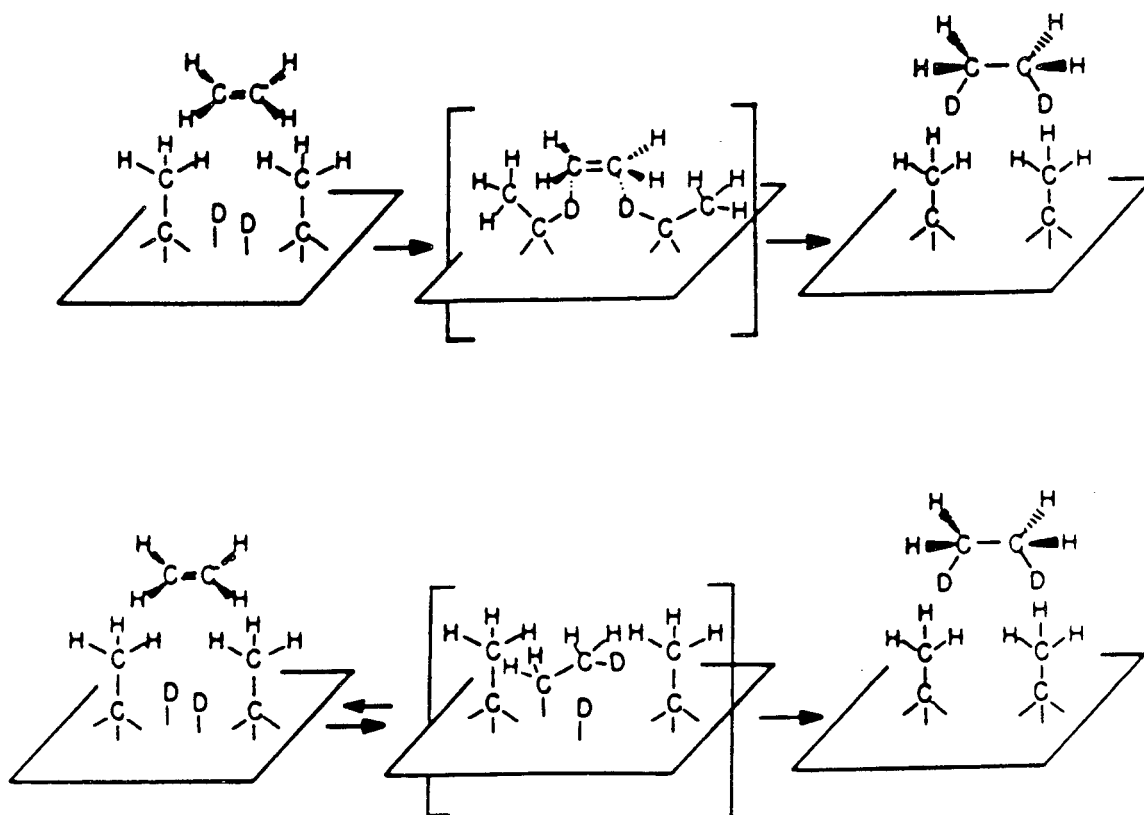
In this respect, ethylidyne poisons ethylene hydrogenation by hindering hydrogen adsorption and dissociation [22]. However, if ethylidyne is not present on Rh(111) and Pt(111), some other strongly adsorbed monolayer must be present to prevent ethylidyne formation. Forming an irreversibly adsorbed layer of ethylidyne species may be desirable, since saturation coverages of CCH_3 still allow a quarter monolayer of hydrogen to dissociate [22], and yet the methyl group shadows the surface and prevents poisons larger than CO from adsorbing. This can explain why Rh and Pt are better ethylene hydrogenation catalysts than Ni [5]. Studies of ethylene adsorption on Ni(111) in UHV [52] show that ethylene and its decomposition fragments lie down on the surface rather than standing up like ethylidyne does on Pt(111) and Rh(111).

How the actual hydrogenation of ethylene occurs cannot be determined from these data. However, published hydrogenation studies with

deuterium show that on most catalysts hydrogenation is accompanied by H,D-exchange. This observation implicates a sequential hydrogenation mechanism. Further, as mentioned in the previous section, bond energy arguments show that the intermediate CH_2CH_3 species in a sequential hydrogenation must be bound to the surface. Since such an adsorbed ethyl species is proposed to be the intermediate in ethylidyne formation [Section 4.1] this species must adsorb at a site where it cannot dehydrogenate to ethylidyne. Possibly high coverages of ethylidyne will permit some CH_2CH_3 to form in the interstices, but the rate of α -dehydrogenation to ethylidyne will now be slower than the rate of β -dehydrogenation back to ethylene or the rate of α -hydrogenation to ethane. (There may be cases where the rate of α -hydrogenation is greater than the rate of α -dehydrogenation even in the absence of a high coverage of adsorbed hydrocarbon fragments [53,54].)

Such a sequential Horiuti/Polanyi hydrogenation mechanism in the presence of ethylidyne is shown in Fig. 5.12 along with the concerted mechanism previously proposed [see discussion in Section 5.1]. The ethylidyne on the catalyst in this mechanism acts like a shade tree on the surface: it protects the surface from poisons and prohibits CH_2CH_3 decomposition to more ethylidyne while providing ample room between and beneath the methyl groups for hydrogen dissociation. There is also the intriguing possibility that the diffusion of the ethylidyne species on the surface to provide room for CH_2CH_3 formation may be responsible for the measured activation energies in ethylene hydrogenation. The role of ethylidyne or of some partially hydrogenated species

Proposed Mechanisms for Ethylene Hydrogenation Over Platinum Metals



XBL 8610-4163

Fig. 5.12 Proposed mechanisms for steady state ethylene hydrogenation over Pt(111) and Rh(111) surfaces between 300 and 400 K. These mechanisms are consistent with but not proven by the data presented in Chapter 5. It is assumed in proposing these mechanisms that the hydrogenation occurs over the entire surface. The second layer mechanism is discussed in Section 5.1 and references 9-10, while the Horiuti-Polanyi type mechanism is discussed in Section 5.2.

like ethylidene (CHCH_3) in the hydrogenation steps (as in a Thomson/ Webb-type mechanism [40]) is still not clear. Studies of butene and cyclohexene hydrogenation with deuterium over flat, stepped and kinked Rh surfaces are planned to address this point as well as the structure sensitivity, the stereochemistry, and the rate-determining step of the hydrogenation.

REFERENCES

1. R.L. Augustine, "Organic Functional Group Hydrogenation," *Catal. Rev. - Sci. Eng.* 13 (1976) 285.
2. P.N. Rylander, Catalytic Hydrogenation Over Platinum Metals, Academic: New York (1967).
3. J.R. Anderson and B.G. Baker, "Adsorption, Kinetics and Surface Structure in Catalysis," Chapter 7 in Chemisorption and Reactions on Metallic Films, Vol. II, J.R. Anderson, ed., Academic: New York (1971).
4. J. Horiuti and K. Miyahara, "Hydrogenation of Ethylene on Metallic Catalysts," NSRDS-NBS-13 (1969).
5. O. Beeck, *Discuss. Faraday Soc.* 8 (1950) 118.
6. G.C.A. Schuit, *Discuss. Faraday Soc.* 8 (1950) 126, 205.
7. O. Beeck, *Rev. Mod. Phys.* 17 (1945) 61.
8. Ref. 4, pg. 8.
9. F. Zaera and G.A. Somorjai, *J. Am. Chem. Soc.* 106 (194) 2288.
10. A. Wieckowski, S.D. Rosasco, G.N. Salaita, A. Hubbard, B.E. Bent, F. Zaera, D. Godbey and G.A. Somorjai, *J. Am. Chem. Soc.* 107 (1985) 5910.
11. A. Farkas and L. Farkas, *J. Am. Chem. Soc.* 60 (1938) 22.
12. G. Rienacker, E. Muller and R. Burmann, *Z. Anorg. Allgem. Chem.* 251 (1943) 55.
13. V.B. Kazanskii and V.P. Strunin, *Kinetika i Kataliz* 1 (1960) 553.
14. G.C. Bond, *Trans. Faraday Soc.* 52 (1956) 1235.
15. G.C.A. Schuit and L.L. Van Reijen, *Advances in Catalysis* 10 (1958) 298.

16. J.H. Sinfelt, J. Phys. Chem. 68 (1964) 856.
17. G.C. Bond, J.J. Phillipson, P.B. Wells and J.M. Winterbottom, Trans. Faraday Soc. 62 (1966) 443.
18. C. Kemball, J. Chem. Soc. 146 (1956) 735.
19. This assumes that the catalysis occurs over the entire surface. Reaction at only the 1-5% of defect sites cannot be discounted.
20. J.T. Yates, Jr., P.A. Thiel and W.H. Weinberg, Surf. Sci. 84 (1979) 427.
21. Molecular ethylene vibrational spectra show no intense peaks below 850 cm^{-1} (see Table 3.5).
22. D. Godbey, F. Zaera, R. Yeates and G.A. Somorjai, Surf. Sci. 167 (1986) 150.
23. F. Zaera, Ph.D. Thesis, University of California, Berkeley (1984) unpublished.
24. S.J. Stephens, J. Phys. Chem. 63 (1959) 512.
25. R.W. Roberts, J. Phys. Chem. 67 (1963) 2035.
26. G.I. Jenkins and E.K. Rideal, J. Chem. Soc. (1955) 2490, 2496.
27. K. Miyahara, J. Res. Inst. Catalysis, Hokkaido Univ. 14 (1966) 134.
28. D. Cormack, S.J. Thomson and G. Webb, J. Catal. 5 (1966) 224.
29. G.H. Twigg and E.K. Rideal, Proc. Roy. Soc. London A 171 (1939) 55.
30. P.-K. Wang, C.P. Slichter and J.H. Sinfelt, J. Phys. Chem. 89 (1985) 3606.
31. T.P. Beebe, M.R. Albert and J.T. Yates, Jr., J. Catal. 96 (1985) 1;
T.P. Beebe and J.T. Yates, Jr., Surf. Sci. 173 (1986) L606.

32. B.J. Bandy, M.A. Chesters, D.I. James, G.S. McDougall, M.E. Pemble and N. Sheppard, *Phil. Trans. Roy. Soc. Lond.* A318 (1986) 141;
N. Sheppard, D.J. James, A. Lesiunas and J.D. Prentice, *Commun. Dept. Chem. (Bulg. Acad. Sci.)* 17 (1984) 95.
33. T.P. Beebe, Jr. and J.T. Yates, Jr., to be published.
34. M. Boudart, *J. Mol. Catal.* 30 (1985) 27, and references therein.
A number of studies, however, show that hydrogenations can be structure-sensitive [35-38].
35. S. Siegel, J. Outlaw, Jr. and N. Garti, *J. Catal.* 52 (1978) 102.
36. M.J. Ledoux, *Nour. Chim.* 2 (1978) 9.
37. R.L. Augustine and R.W. Wagner, *J. Catal.* 80 (1983) 358.
38. F. Notheisz, M. Bartok, D. Ostgard and G.V. Smith, *J. Catal.* 101 (1986) 212.
39. J. Horiuti, K. Miyahara and I. Toyoshima, *J. Res. Inst. Catalysis, Hokkaido Univ.* 11 (1966) 59.
40. S.J. Thomson and G.J. Webb, *J. Chem. Soc., Chem. Commun.* (1976) 526.
41. J. Horiuti and M. Polanyi, *Trans. Faraday Soc.* 30 (1934) 1164.
42. K. Williams, M. Levin and G.A. Somorjai, unpublished results.
43. J.G. Ulan, W.F. Maier and D.A. Smith, submitted for publication.
44. K. Miyahara, S. Teratani and A. Tsumura, *J. Res. Inst. Catalysis, Hokkaido Univ.* 12 (1965) 98.
45. S. Sato and K. Miyahara, *J. Res. Inst. Catalysis, Hokkaido Univ.* 13 (1965) 10.
46. S.M. Davis, F. Zaera and G.A. Somorjai, *J. Catal.* 77 (1982) 439.

47. S.M. Davis, Ph.D. Thesis, University of California, Berkeley (1981) unpublished.
48. G.M. Pajonk, S.J. Teichner and J.E. Germain, eds., Spillover of Adsorbed Species, Elsevier: Amsterdam (1983).
49. R.B. Levy and M. Boudart, *J. Catal.* 32 (1974) 304.
50. P.A. Sermon and G.C. Bond, *Catal. Rev.* 8 (1973) 211.
51. B.J. Wood and H. Wise, *J. Catal.* 5 (1966) 135.
52. S. Lehwald and H. Ibach, *Surf. Sci.* 89 (1979) 425.
53. T.P. Beebe, Jr. and J.T. Yates, Jr., *J. Am. Chem. Soc.* 108 (1986) 663.
54. T. Hattori and R.L. Burwell, Jr., *J. Phys. Chem.* 83 (1979) 241;
R.L. Burwell, *Langmuir* 2 (1986) 2.
55. M. Salmeron and G.A. Somorjai, *J. Phys. Chem.* 86 (1982) 341.
56. B.E. Koel, B.E. Bent and G.A. Somorjai, *Surf. Sci.* 146 (1984) 211.

This report was done with support from the Department of Energy. Any conclusions or opinions expressed in this report represent solely those of the author(s) and not necessarily those of The Regents of the University of California, the Lawrence Berkeley Laboratory or the Department of Energy.

Reference to a company or product name does not imply approval or recommendation of the product by the University of California or the U.S. Department of Energy to the exclusion of others that may be suitable.

*LAWRENCE BERKELEY LABORATORY
TECHNICAL INFORMATION DEPARTMENT
UNIVERSITY OF CALIFORNIA
BERKELEY, CALIFORNIA 94720*